HIGH PERFORMANCE BIO-BASED THERMOSETS FOR COMPOSITES AND COATINGS

A Dissertation
Submitted to the Graduate Faculty
of the
North Dakota State University
of Agriculture and Applied Science

By

Adlina Ambeg Paramarta

In Partial Fulfillment of the Requirements
for the Degree of
DOCTOR OF PHILOSOPHY

Major Department:
Coatings and Polymeric Materials

November 2016

Fargo, North Dakota

North Dakota State University
Graduate School

Title

High Performance Bio-based Thermosets for Composites and Coatings

By

Adlina Ambeg Paramarta

The Supervisory Committee certifies that this *disquisition* complies with North

Dakota State University's regulations and meets the accepted standards for the

degree of

DOCTOR OF PHILOSOPHY

SUPERVISORY COMMITTEE:

Dean C. Webster

Chair

Chad A. Ulven

Dante Battocchi

Kevin D. McCaul

Approved:

11-08-2016	Dean C. Webster
Date	Department Chair

ABSTRACT

In the recent decade, there has been increasing interest in using renewable feedstocks as chemical commodities for composites and coatings application. Vegetable oils are promising renewable resources due to their wide availability with affordable cost. In fact, the utilization of vegetable oils to produce composite and coatings products has been around for centuries; linseed oil was widely used for wide variety of paints. However, due to its chemical structure, the application of vegetable oils for high-performance materials is limited; and thus chemical modification is necessary. One of the modification approaches is by substituting the glycerol core in the triglycerides with sucrose to form sucrose esters of vegetable oil fatty acids, in which this resin possesses a higher number of functional group per molecule and a more rigid core.

In this research, thermosets of highly functionalized sucrose esters of vegetable oils were developed. Two crosslinking methods of epoxidized surcrose soyate (ESS) resins were explored: direct polymerization with anhydride moieties for composite applications and Michael-addition reaction of acrylated-epoxidized sucrose soyate (AESS) for coatings applications. In the first project, it was shown that the reaction kinetics, thermal and mechanical properties of the materials can be tuned by varying the molar ratio between the epoxide and anhydride, plus the type and amount of catalyst. Furthermore, the toughness properties of the ESS-based thermosets can be improved by changing the type of anhydride crosslinkers and incorporating secondary phase rubbers. Then, in the second system, the epoxy functionality in the ESS was converted into acrylate group, which then crosslinked with amine groups through the Michael-addition reaction to produce coatings systems. The high number of functional groups and the fast reactivity of the crosslinker results in coatings that can be cured at ambient temperature, yet still possess moderately high glass transition temperatures.

ACKNOWLEDGEMENTS

I am extremely thankful to everyone who has given me incredible amount of support and encouragement throughout my education, and I am truly blessed to have amazing individuals to surround me as I pursued my goal of obtaining a PhD. in Coatings and Polymeric Materials.

First of all, my deep appreciation goes to my research advisor, Dr. Dean Webster. It is a tremendous experience to have work with him and be his student for the past 8 years. I could never forget the day when I decided to come to his office and asked whether I could join his research group. And without any hesitation, he welcomed me to work under his supervision even though I was still a freshman. From that first day until now, he keeps believing in me and my potential to be successful. The journey has not always been smooth ride, yet he always has the confidence in me and keep motivating me to try my best.

I would like to thank my committee member, Dr. Chad Ulven, Dr. Kevin McCaul, and Dr. Dante Battocchi for their assistance, guidance, advice and contribution in this dissertation. I am also very appreciative of the support given by many of the Department of Coatings and Polymeric Materials professors including Dr. Stuart Croll, Dr. Gordon Bierwagen, and Dr. Victoria Gelling. Not only that they have provided me a colorful insight to the coatings field, but also offered me emotional support during this tough graduate school journey.

Then, I must thank all of my family in Indonesia and past graduate students and postdoctoral research in the Department of Coatings and Polymeric Materials. There have been definitely bumpy roads in this graduate school journey, and in those times, thinking of all of you gives me the motivation to keep working hard and not giving up. Special thanks go to Stacy Sommer, T.J. Nelson, Xiao Pan, and Bobby Jo Merten for being excellent role models, giving me plenty of wise advice, and encouraging me to pursue my dream career.

I also appreciate the help provided by collaborators in the Department of Mechanical Engineer, Chris Taylor and Rob Sailer, and in the Electron Microscopy Laboratory, Scott Payne and Jayma Moore. Additionally, I would like to acknowledge the great work of my undergraduate and high school researchers in helping me to conduct this project, AliReza Rahimi, Myungkeun Oh, and Ruiying Feng.

I could not have completed this graduate school journey without Zack Stephanchick being next to me in every step of the way. His infinite love, wisdom, patience, and laughter have definitely been the source of my strength. I could not be more excited to begin the next chapter of my life with such an amazing person.

DEDICATION

I dedicate my dissertation to my incredible, amazing, wonderful parents, Susilo Hambeg Poromarto and

Yuni Etty Armawati. I am eternally grateful for your endless love, care, support and encouragement; I

would not be where I am today without your lifetime of hard-work and dedication to your children's

education. To my father, thank you for bringing our family to Fargo and letting us pursue our American

dream. To my mother, thank you for your patience and sacrifice for our family; I can't imagine how tough

it is for you to be 10,000 miles away from your loved ones while we are pursuing our education.

TABLE OF CONTENTS

LIST OF TABLES

LIST OF FIGURES

LIST OF SCHEMES

CHAPTER 1. GENERAL INTRODUCTION

1.1.   Future sustainability

Due to uncertainty in the supply and cost of petrochemicals and greater awareness of future sustainability in the recent decades, more and more research has been dedicated to the development of materials from renewable resources. The challenges to this "green" movement are to produce materials that will be economically feasible and have comparable properties to the current technology. Some of the renewable resources that have been explored include vegetable oils, polysaccharides (cellulose, starch, chitin), sugars, wood (tannins, lignin, cardanol), and others [1-9]. Among this list, vegetable oils are the most commonly used renewable resource in the chemical industry due to its abundancy, low cost and potential degradability. Furthermore, historically, the use of vegetable oils for a chemical commodity is not a new idea. Vegetable oils have been used widely in artists' and other paints, varnishes, and as a component of linoleum due to its ability to form a film. The application of these vegetable oils in coatings still exists today, and the use of vegetable oils has been broadened into more fields such as biofuels, lubricants, surfactants, and structural composites.

1.2.   Chemistry of vegetable oils

Vegetable oils are triglycerides or glycerol esters of fatty acid, and a representative chemical structure is shown in Figure 1.1. These fatty acids tend to have long carbon chain with 16 – 22 carbons, and have variations in the degree of unsaturation as well as the presence of additional functional groups. The number of unsaturated groups in the fatty acids can range from 1 – 3, and the configuration can be in either the conjugated or non-conjugated position. The most typical fatty acids found in many vegetable oils include palmitic, stearic, oleic, linoleic, and linolenic acid. Fatty acids with functional group other than unsaturation such as ricinoleic acid (containing a hydroxyl functional group) or vernolic acid (containing an epoxy functional group) are quite uncommon, and can only be found in certain plant sources.
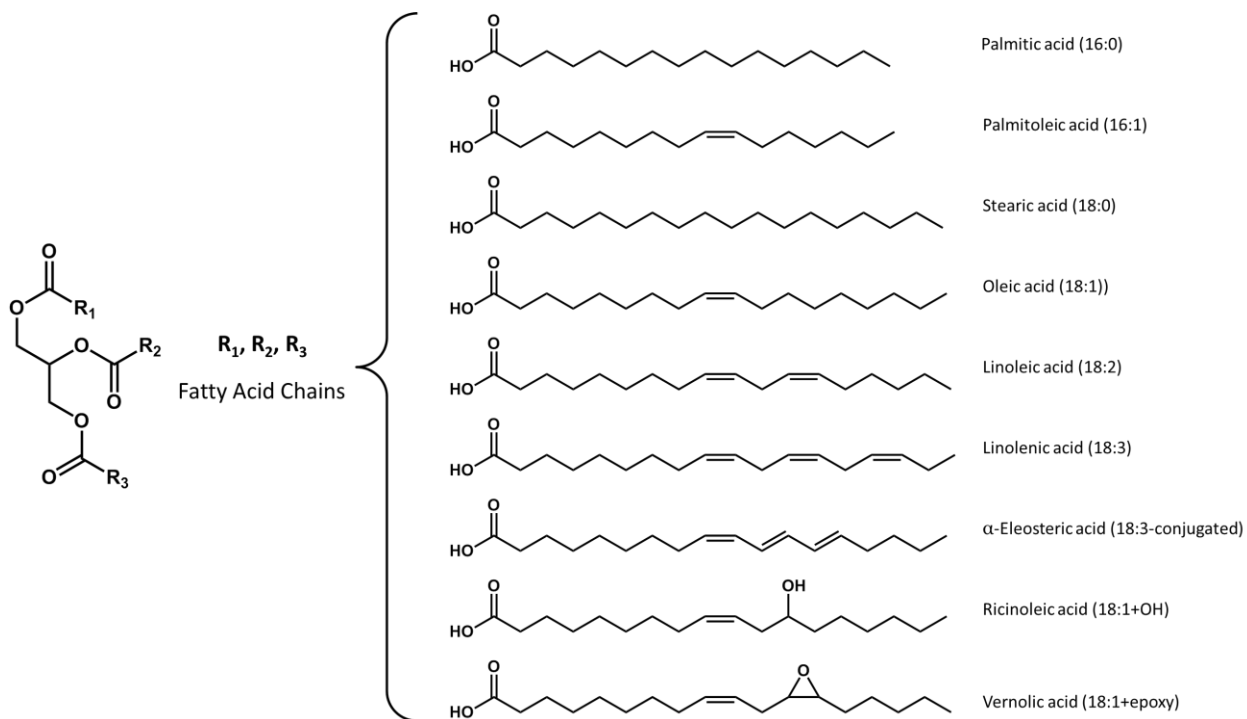
Figure 1.1. Representative chemical structure of vegetable oil

The types and amounts of fatty acids found in vegetable oils are dependent on the plant source, crop season and location, and growing conditions. The fatty acid composition of commonly used vegetable oils is summarized in Table 1.1. In addition, Table 1 also lists the average number of double bonds and iodine value. The iodine value is defined as the amount of iodine in milligrams needed to saturate the double bonds in 100 gram of oil; thus the iodine value is proportionally related to the average number of double bonds in the oil. The iodine value (IV) of a vegetable oil is often correlated with the "drying" behavior of vegetable oil, or its ability to form a dry film: oils with IV value > 140 are classified to be drying oils, oils with IV values of 125 - 140 are classified as semi-drying oils, and oils with IV values < 125 are classified as non-drying. The "drying" of an oil is a result of polymerization of the fatty acids due to the unsaturated groups through an autoxidation process. Literature articles describing the detailed reaction scheme of the autoxidation process of plant oils have been widely published [10-12]. The autoxidation rate of an oil depends on the number of double bonds, the conjugation of double bonds, and geometrical arrangement; the rate is faster for higher amounts of double bonds and in non-conjugated oils, the *cis-* configuration.

Table 1.1. Typical fatty acid compositions of vegetable oils [13]

| Vegetable oil | Fatty Acids | | | | | Other | Ave. Double bonds | Iodine value |
	Palmitic (16:0)	Stearic (18:0)	Oleic (18:1)	Linoleic (18:2)	Linolenic (18:3)			
Palm	42.8	4.2	40.5	10.1	-	-	1.7	44 – 58
Olive	13.7	2.5	71.1	10.0	0.6	-	2.8	75 – 94
Castor	1	1	5	1	2	Ricinoleic (90%)	3.0	85 – 88
Soybean	11.0	4.0	23.4	53.3	7.8	-	4.6	117 – 143
Sunflower	5.2	2.7	37.2	53.8	1.0		4.7	110 – 143
Safflower	7.0	4.0	13.0	75.0	1.0	-	5.0	140 – 150
Linseed	5.5	3.5	19.1	15.3	56.6	-	6.6	168 – 204

The polymerization of vegetable oils through the autoxidation reaction can be a slow process despite the addition of transition metal catalysts commonly called "driers." The process continues for a long time, and may ultimately result in brittle films. Chemical modifications of vegetable oils are often carried out to provide other reactive functional groups that can be used to polymerize the oils with different mechanisms. One of the popular modifications is the epoxidation of the unsaturation, which then provides access to many crosslinking technologies such as homo-polymerization, acid/anhydride curing and further functionalization to introduce other functional groups (e.g. polyol, meth(acrylate), and cyclic carbonate). Furthermore, epoxidized vegetable oils can also be used as additives such as plasticizers, stabilizers and lubricants [14-16].

1.3. Epoxidation method of vegetable oil

The epoxidation of unsaturated fatty acids materials has been reported since the 1940s. Findley et al. epoxidized various types of oils (i.e. lard, olive, peanut, cottonseed, soybean, linseed, castor, etc.) by using peracetic acid in acetic acid solution [17]. This epoxidation process is still widely used today, and also commonly known as the Prilezhaev reaction. Scheme 1.1 illustrated the epoxidation reaction scheme [18, 19]. In general, the epoxidation of unsaturation follows these steps:

1. Formation of peracids from reaction of hydrogen peroxide with the corresponding acid, either formic or acetic acid, in the presence of strong catalyst in the aqueous phase;

2. Transfer of peracid from the aqueous phase to the oil phase;

3. Reaction between peracid and unsaturation in the oil phase through a "Butterfly Mechanism" where oxygen is added and the proton is shifted simultaneously, thus producing epoxides and organic acid;

4. Undesired side reactions include degradation of the epoxide ring in the oil phase and oil-aqueous interface due to reaction with acidic proton (acid catalyst, carboxylic acid, peracids), water and hydrogen peroxide; the reaction mechanism is illustrated in Scheme 1.2;

5. Transfer of organic acids phase to aqueous phase.

The kinetics of this epoxidation reaction has been studied using a variety of vegetable oils such as soybean oil, sunflower oil, corn oil, rubber seed oil, cottonseed oil, and many more [20-24].

Step 1: Peracetic acid formation

Step 2: Oxirane formation
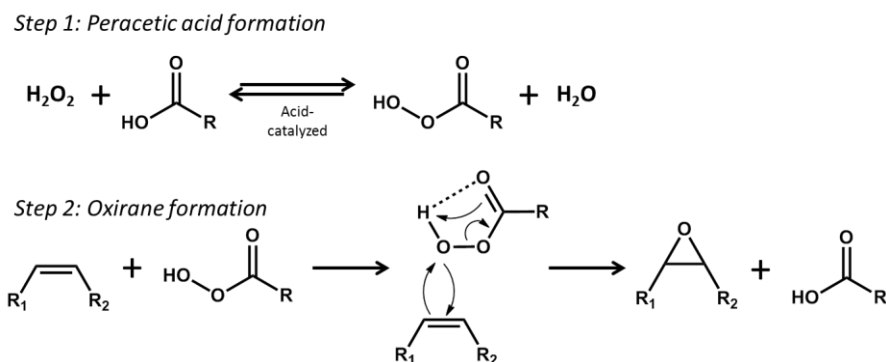
Scheme 1.1. Epoxidation of unsaturation through Prilazhaev reaction
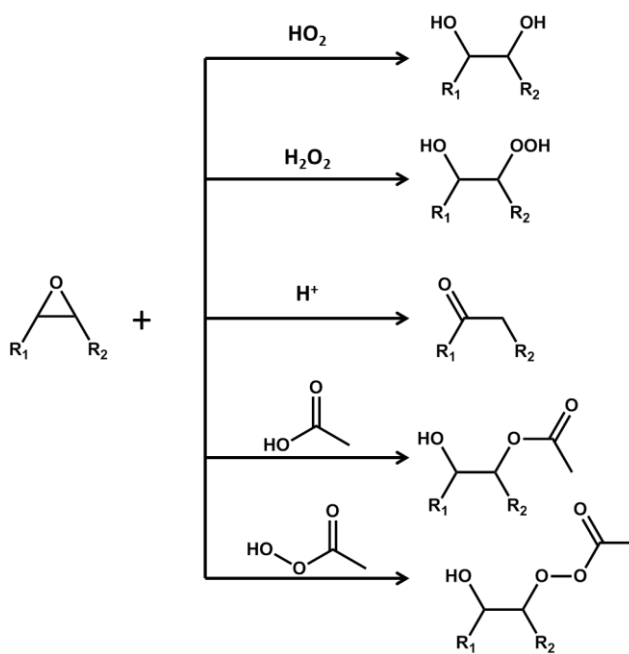
Scheme 1.2. Oxirane degradation

4

The epoxidation kinetics through the Prilazhaev reaction has been shown to be dependent on reaction parameters such as reaction temperature, type and loading amount of carboxylic acid, type and loading amount of acid catalyst, molar ratio of hydrogen peroxide to unsaturation, stirring speed, and feeding system. It is important to optimize the reaction parameter in order to achieve the highest epoxide conversion with a minimal reaction time and oxirane degradation. Many researchers found that high epoxide conversion, up to 80%, may be obtained with moderate reaction temperature (40-60 °C), sulfuric acid as catalyst, acetic acid as peracid source and vigorous stirring speed to maximize the transfer of reactants between the organic and aqueous phase [20, 23, 24]. Furthermore, a biphasic reaction model of the epoxidation of soybean oil with H_2O_2 in a fed-batch reactor has been successfully established by Santacesaria et al [21].

The use of strong mineral acids such as sulphuric, phosphoric or nitric acid often results in many drawbacks such as poor selectivity to epoxidized product, challenging isolation process, corrosion issues on the reactor and safety concerns on handling the materials. One of the improvements being made involves substituting the strong mineral acids with an ion-exchange resin as the peracid formation catalyst. The most commonly used acidic ion-exchange resin (AIER) is Amberlite IR 120 Na^+ or H^+, which is a gel type, strongly acidic cation exchange resin of the sulfonated polystyrene type. Since this AEIR catalyst comes in solid beads, and is insoluble, an easy separation becomes more feasible than conventional homogenous catalysts and chemical handling becomes safer. Furthermore, AIER can be re-used up to 4 times without compromising the oxirane conversion value [25]. Similar to the conventional epoxidation process, the reaction kinetics as a function of reaction parameters has been studied extensively using many vegetable oils [25-29].

Many studies have been dedicated to examining the effect of reaction parameters such as stirring speed, hydrogen peroxide-to-double bond molar ratio, acetic acid-to-double bond molar ratio, reaction temperature, catalyst loading and particle size. Similar to the acid-catalyzed reaction, increasing the molar ratio of hydrogen peroxide or acetic acid to double bond will increase the reaction rate, yet also can increase the oxirane degradation at the same time. Using AIER as a catalyst, high oxirane conversion may be obtained at shorter amount of time and higher reaction temperature compared to a conventional acid-catalyzed system. However, it was also found that in two separate studies using two different

vegetable oils, Goud et al. and Petrovic et al. observed the correlation between the reaction temperature and the types of acids used [26, 30]. They observed that at lower temperature ($\approx$40°C), peroxoformic acid was found to be more efficient than peroxoacetic with double the epoxidation rate constant. However, at higher temperature (>60°C), there is no difference between the two peroxo acids. Furthermore, Petrovic suggested the reaction kinetics of unsaturation epoxidation using AIER catalyst was found be first-order with respect to double bond concentration, yet deviation was observed at higher temperature and higher conversion [30].

When AEIR is used as a catalyst, the epoxidation process mechanism entails many sub-steps such as reactant's diffusion into catalyst pores, reactant's adsorption on the catalyst surface, reaction at the catalyst surface, and desorption of the products off the catalyst surface. In a study of epoxidation of jatropha oil, Goud et al. observed that the catalytic reaction of the peracid formation was characterized by the adsorption of the acid on the catalyst site, and the irreversible surface reaction was the overall rate-determining step [26]. However, surprisingly, the particle size of the AEIR (>599 µm vs <64 µm) did not make a significant difference, where the ratio of the initial reaction rates was practically the same [31]. This result is contradictory to observations made by Campnaella and Baltanas. They found that at the same catalyst loading, decreasing the particle size can reduce the reaction time and slightly improve the conversion [28]. However, decreasing the particle size of the AIER catalyst also resulted in a higher amount of epoxy degradation [29].

Another reported epoxidation method is through an enzymatic process, where lipase was used to catalyze the conversion of fatty acids with hydrogen peroxides to peroxy fatty acids, which then converts unsaturation into epoxide through the Prilezhaev mechanism [32-35]. This epoxidation method eliminates the use of strong acid (either as catalyst for peracid source), and thus is thought to be a greener process. One of the most common lipase used for catalyzing this peracid formation is *Candida Antarctica*, which is also capable of catalyzing perhydrolysis or reaction of carboxylic aid esters with hydrogen peroxide to form percarboxylic acids; the reaction mechanism is shown in Scheme 1.3. With this epoxidation reaction, unfortunately, the resulting product contains a mixture of tri-, di-, and mono-glycerides of epoxidized fatty acids, and the separation process can be very challenging. To minimize the amount of mono- and diglyceride epoxy, Rüsch gen Klaas and Warwel added 5% molar ratio of free fatty acids

related to the unsaturation [36]. They observed that the hydroxyl group perhydrolysis by-products are re-esterified immediately by the excess of free fatty acids. Lu et al. further observed that the type of fatty acids used in the epoxidation of soybean oil methyl esters affects the oxirane conversion value [37].
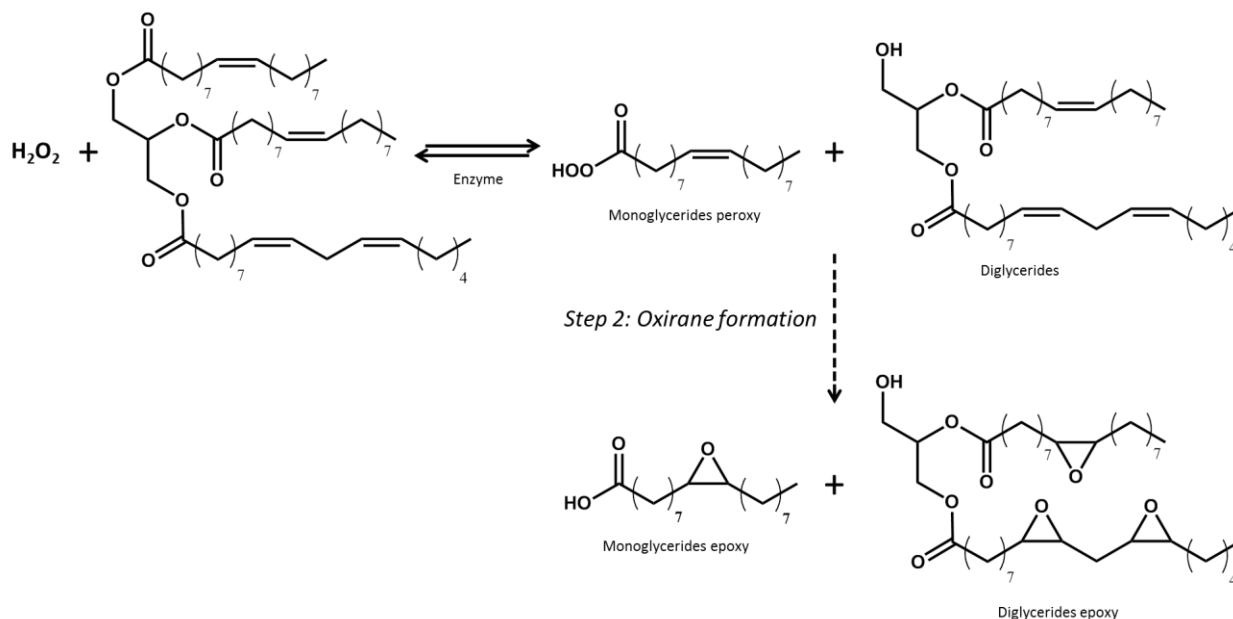
Scheme 1.3. Epoxidation of unsaturation through enzymatic reaction

The kinetics of chemo-enzymatic epoxidation of vegetable oils has been carried out by many researchers. One of the important parameters determining the chemo-enzymatic epoxidation rate is the lipase activity and stability. Hilker et al. observed that the activity and stability of the enzyme depends on the reaction temperature and H_2O_2 concentration [38]. They suggested that no enzyme deactivation may be obtained by carrying out the reaction at <60 °C and using >50% aqueous H_2O_2 concentration. Furthermore, in another study, Orellana-Coca conducted simultaneous esterification and epoxidation of oleic acid to produce alkyl epoxy stearates [39]. They found out that the type of alcohol used in the esterification affected the rate and yield of epoxidation; the use of iso-propanol enhanced the epoxidation rate, while the use of ethanol decreased the rate due to deactivation of enzyme.

1.4.   Crosslinking routes of epoxidized vegetable oil (EVO)

The most common crosslinking route for epoxy functional groups is through reaction with amine groups. However, for EVO system, this crosslinking method has been shown to be a less efficient curing compared to acid/anhydride curing. First, EVO contains internal epoxy groups, and therefore they are less reactive compared to a terminal epoxy. This low reactivity leads to low polymerization efficiency

when crosslinked with amine hardeners. Second, there is a de-esterification of the fatty acid chain

through ester-aminolysis reaction with amide and alcohol as a by-product; the reaction is illustrated in

Scheme 1.4.

$$R_1—COOR_2 \ + \ R_3—NH_2 \ \longrightarrow \ R_1 \overset{O}{\underset{\underset{H}{N}}{\|}} R_3 \ + \ R_4—OH$$
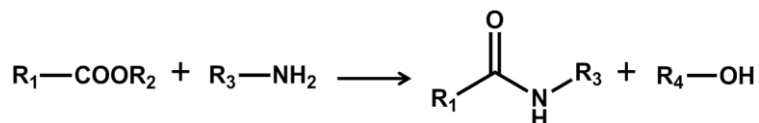
Scheme 1.4. Ester aminolysis

1.4.1. Homo-polymerization

The epoxy functional group in the EVO can be reacted with itself in the presence of a cationic or

anionic initiator. Anionic polymerization of epoxides is possible through ring opening of the epoxides

using metal hydroxides, alkoxides, oxides, amides, and metal alkyls. Using this method of

polymerization, polymer molecular weights, end chain, and polydispersity index may be precisely

controlled. However, there has been no published literature describing anionic polymerization of EVO. In

contrast, cationic polymerization of epoxides with the addition of super acids catalyst has been widely

used for EVO curing. Due to high reactivity of the super acids, the catalysts are often added as latent

complexes, which are inert under ambient temperature and release active species upon external

stimulation such as heating or photo-irradiation. Most commonly used latent catalysts in EVO cationic

polymerization include boron trihalides-derivatives and hexafluoroantimonate onium salts; chemical

structure of the catalyst is shown in Figure 1.2.

Thermal Latent Catalysts

N-benzylpyrazinium
hexafluoroantimonate
(BPH)

SbF_6^-

N-benzylquinolium
hexafluoroantimonate
(BQH)

SbF_6^-

Photo-initiated Latent Catalyst

$$Ar_3S^+ \ PF_6^- \ \xrightarrow{hv} \ Ar_2S^+ \ (SbF_6^-) \ + \ Ar^{\cdot}$$

$$\downarrow HY$$

$$Ar_2S \ + \ Y^{\cdot} \ + \ H^+(SbF_6^-)$$

Super Acids
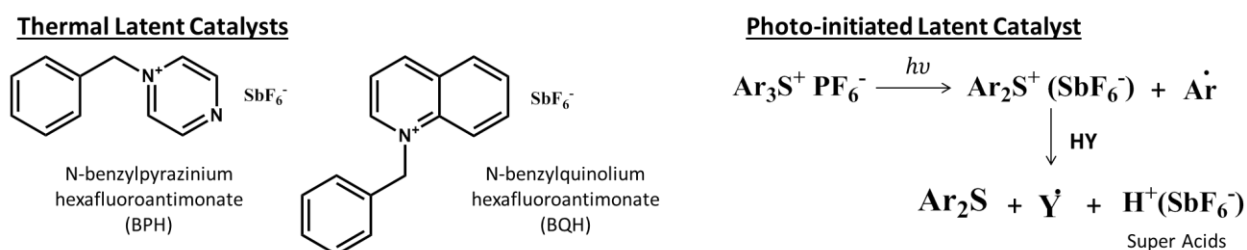
Figure 1.2. Chemical structure of cationic initiator

The reaction mechanism for the EVO cationic polymerization is shown in Scheme 1.5. First, the

latent catalyst is activated through thermal heating or photo-irradiation to produce super acids. This

strong acid then reacts with an epoxide to form an oxonium ion. Propagation of occurs by nucleophilic

attack of the epoxides toward the oxonium ion. The presence of hydroxyl groups or moisture in the

reaction may enhance the polymerization rate by reducing the activation energy and shifting the reaction toward activated monomer mechanism; with this mechanism, the hydroxyl group has higher nucleophilicity than the epoxides. However, the presence of hydroxyl groups can also act as chain transfer agents, and too much of it may result in difficulty to achieve high molecular weight polymer.
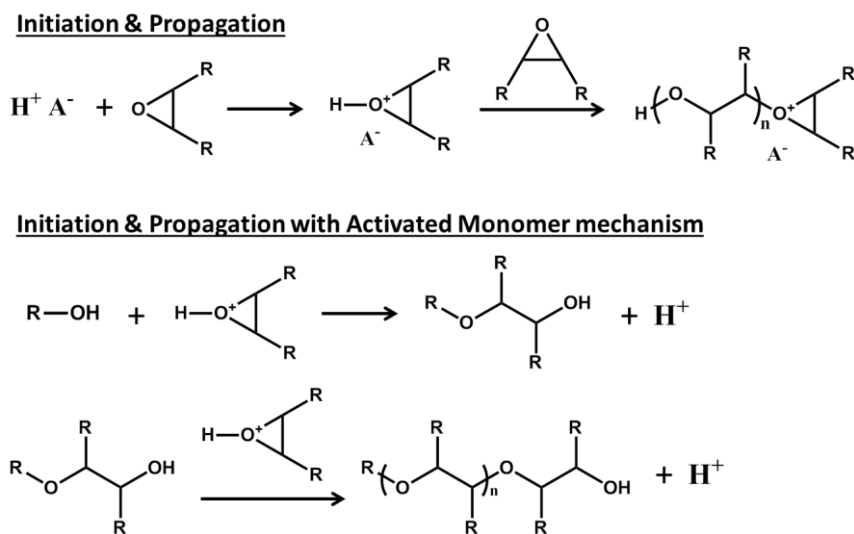
Scheme 1.5. Reaction mechanism of EVO cationic polymerization

The structure-property relationships and reaction kinetics of EVO cationic polymerization have been studied by many researchers. Using thermal latent catalyst, n-benzylpyrazaninium hexafluoroantiomante (BPH), Park et al. compared the thermoset properties of epoxidized soybean oil (ESO) and epoxidized castor oil (ECO) [40]. These EVO have different epoxide number per molecule and backbone structures: ESO has higher epoxide number (4.6 vs. 2.8), and ECO contains secondary hydroxyl groups in its backbone. Due to the dissimilarities between the two EVOs, ESO thermosets were observed to have lower glass transition temperature (T_g) values, yet higher crosslink density. Higher intermolecular interaction in the ECO thermoset was predicted to contribute to its high T_g value. The effect of photo-initiators in the cationic polymerization of EVO has been studied by Chakrapani et al [41]. They compared the induction time of diaryliodonium photo-initiators with different anionic groups: SbF_6^-, AsF_6^-, and PF_6^-. Through monitoring the infrared absorption of epoxy group (830 and 1160 cm^{-1}), they observed the photo-polymerization rate decreases in the order $SbF_6^- > AsF_6^- >$ and PF_6^-. They suggested that this observation was contributed to the nucleophilicity of the anion and its relative stability towards ion splitting reactions.

1.4.2. Acid/anhydride curing

Acid/anhydride curing of epoxides is a crosslinking mechanism for EVO. The reaction kinetics and mechanism of anhydride-cured epoxy are known to be complex due to many simultaneous reactions, and depends heavily on the type of catalyst used in the formulation. Even though the addition of catalyst in the formulation is not needed to initiate the reaction, it is often added to ensure efficient polymerization. The type of catalyst that is often used to accelerate epoxy-anhydride curing includes alcohols, tertiary amines, quaternary onium salts, and metal salts and chelates. The reaction mechanism for uncatalyzed and catalyzed process is shown in Scheme 1.6.

For a non-catalyzed system, the reaction is possible due to the presence of hydroxyl groups in the formulation, which can either come from hydroxyls attached to the epoxy resin or anhydride crosslinker, impurities in the raw materials, or the presence of small carboxylic acid groups from the hydrolysis of the acid anhydride crosslinker. These hydroxyl groups are able to ring open either epoxy or anhydride to form a mono-ester and carboxylic acid end group, which can then further react with either epoxy or anhydride. In contrast, for a catalyzed system, the catalyst is able to ring open the epoxy or anhydride through nucleophilic attack and form a zwitterionic carboxylate and/or alkoxide anion. This anion then becomes an active end group and propagates the polyester chain. For either mechanism, it has been widely known that the addition of epoxy and anhydride occurs in an alternating fashion. Homopolymerization of epoxy is a possible side reaction, and this reaction rate has been found to be higher with uncatalyzed systems [42, 43].

Uncatalyzed reaction
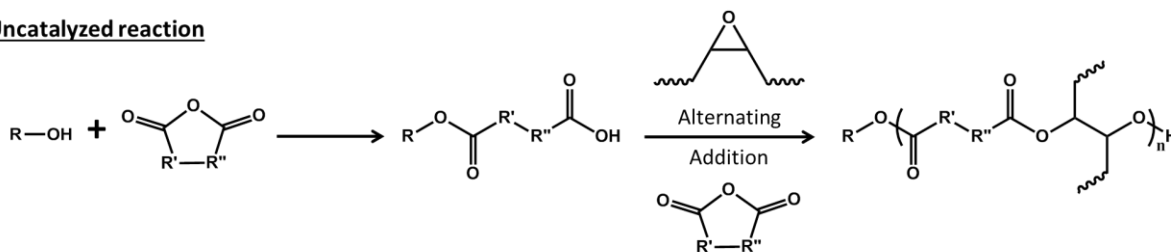
Catalyzed reaction
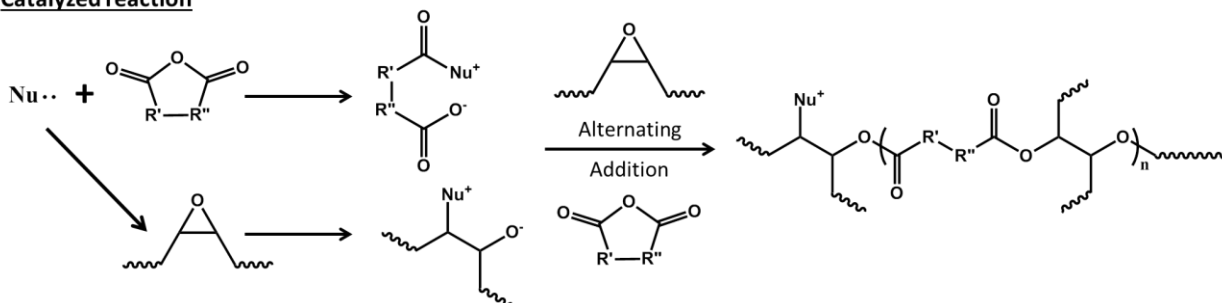
Scheme 1.6. Reaction mechanism for acid/anhydride curing

Structure-property relationships studies of acid/anhydride-cured EVO thermosets have been widely published. Boquillon et al. investigated the effect of catalyst and anhydride structure on the reaction kinetics and mechanical properties of the thermoset based on epoxidized linseed oil [44]. They found that imidazole catalyst shows a higher extent of conversion of anhydrides and increased material stiffness. In addition, they suggested that steric hindrance in an anhydride crosslinker such as methyl-endomethylene tetrahydrophthalic anhydride (METH) results in thermoset system with lower crosslink density. Furthermore, the presence of dangling ends and free anhydride in the network was observed when the anhydride-to-epoxy molar ratio was higher than 0.8. In another study, Gerbasee et al. investigated the thermoset properties of anhydride-cured epoxidized soybean oil by varying the type of anhydride, anhydride-to-epoxy molar ratio, and epoxy group content [45]. They suggested that thermosets with higher T_g may be obtained by using anhydride crosslinkers with rigid structures such as phthalic, maleic anhydride, higher anhydride-to-epoxy molar ratio up to the threshold ratio, and higher epoxy group amount.

1.4.3. Other curing

In addition to epoxy homo-polymerization and anhydride crosslinking, the epoxy groups can also be easily converted into other functionalities, such as polyol, acrylate, (meth)acrylate, which then can provide other crosslinking methods (Scheme 1.7). Polyol functionalities in the EVO can be obtained by

reacting the epoxides with alcohols. With the hydroxyl functionalities, the EVO thermoset can then be

reacted with isocyanate groups to form polyurethanes. A literature review of vegetable oil polyurethanes

has been published by Desroches et al. [46]. Acrylate acid can also reacted with the epoxide groups in

an EVO. The acrylate group contains terminal double bond groups which can then be polymerized

through free radical reactions or be reacted with nucleophilic moieties (i.e. amine, acetoacetate), through

Michael-addition reaction [47].

Hydroxylation reaction

Acrylation reaction
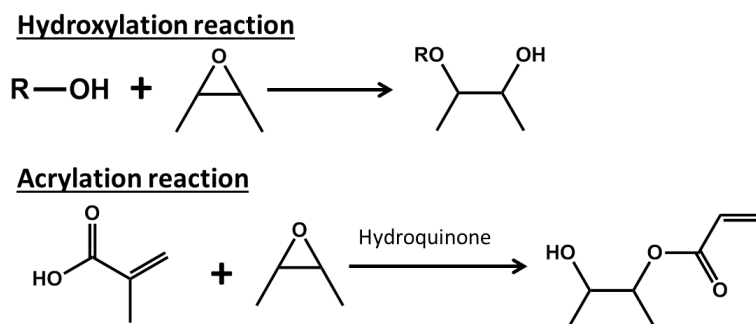
Scheme 1.7. Reaction mechanism of epoxides ring opening using acid/alcohol

1.5.   Improving the mechanical properties of EVO-based thermoset

Due to the long linear alkyl chain of the fatty acids, thermoset materials based on EVO tend to be

rubbery and have relatively low glass transition temperatures. In order to increase its mechanical

strength, the most commonly taken approach includes blending EVO with petrochemical-based epoxy

resin such as diglycidyl ether bisphenol-A or –F (DGEBA or DGEBF) resin or chemically-modifying the

chemical structure.

1.5.1. EVO blends with petrochemical-based epoxy resin

Creating a blend of EVO with petrochemical-based epoxy resins such as DGEBA and DGEBF is

advantageous from two perspectives. By combining the rigid aromatic structure of the DGEBA or DGEBF

resin and the flexible aliphatic structure of the EVO, improvement in toughness properties and easy

formulation processability can be expected. However, caution also must be taken in determining the

blend ratio of the two resins, so that optimum impact toughness properties can be achieved without

compromising the yield strength of the materials. Furthermore, the large difference in the reactivity of the

terminal epoxy in the DGEBA or DGEBF and the internal epoxy in the EVO may result in phase

separation and incomplete curing, which lead to inferior thermoset properties. A thorough literature review of EVO blends with petrochemical-based resin has been reported by Tan and Wang [48, 49].

Altuna et al. studied the impact of EVO substitution in an anhydride-cured DGEBA thermoset, where they varied the concentration of the EVO from 0-100% by wt [50]. Figure 1.3 shows the tan delta curves, impact properties and compression properties of the thermosets as a function of EVO concentration. In general, increasing the EVO content resulted in thermosets with lower enthalpy of polymerization, glass transition temperature, and compression strength. The optimum set of properties that were able to be achieved at 40% wt. EVO substitution where significant improvement in the impact properties was observed with only slight decrease in the other mechanical properties. Based on the scanning electron microscopy (SEM) imaging, they suggested that the improvement in the impact properties was a result of the phase separation of the EVO and DGEBA thermoset.
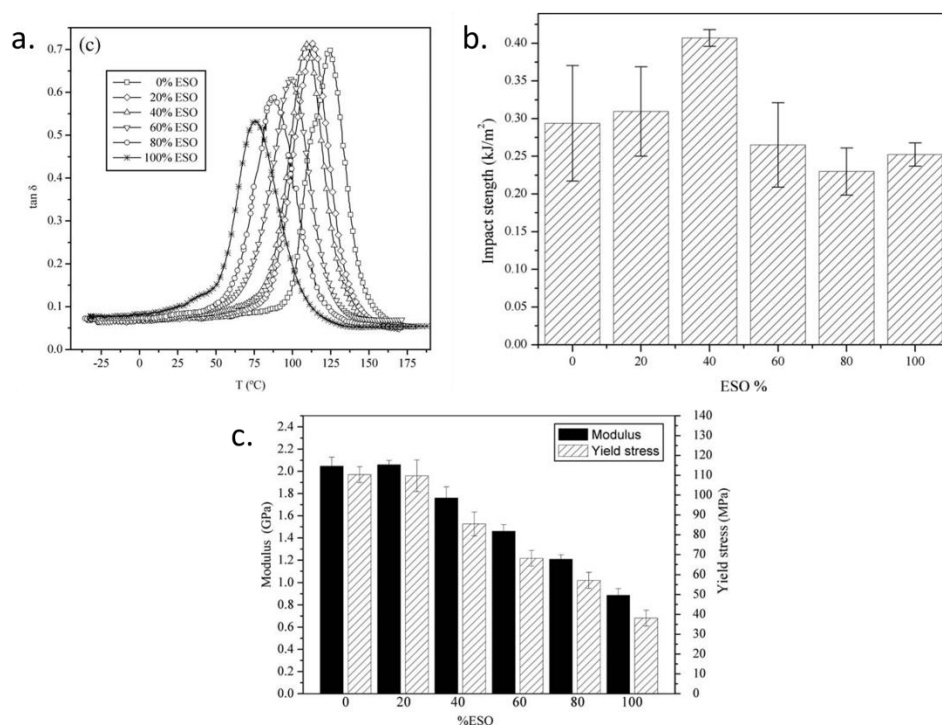
Figure 1.3. Mechanical properties of the EVO-DGEBA blends as a function of EVO concentration: a. tan delta curves, b. Impact strength, c. Compression modulus and yield stress (The images were reproduced from Reference [50])

1.5.2. Chemically modified EVO and/or epoxy resin based on vegetable oil

Another method to enhance the mechanical properties of EVO-based thermosets is by modifying the chemical structure to have a stiffer polymer backbone. Chisholm et. al. developed a high molecular

weight poly-vinylether polymer based on soybean oil fatty acids ester; the synthesis route is illustrated in Scheme 1.8 [51]. Using a similar approach to conventional vegetable oils, the unsaturation in the fatty acids was then converted into epoxy groups. The number of fatty acids chain (and oxiranes) in the polymer can be controlled by adjusting the molecular weight of the polymer. In addition, further functionalization of the polymer or customized polymer backbone is possible through co-polymerization of the 2-(vinyloxy)ethyl soyate with other unsaturated monomers such as butadiene, cyclohexyl vinyl ether, maleic anhydride, and many more. Due to an increased number of functional groups per molecule, anhydride-cured epoxy copolymerization was shown to have faster curing kinetics compared to soybean oil-based system. Furthermore, the storage modulus of the coatings thermoset was shown to have one order of magnitude higher than its soybean oil-based counterparts.
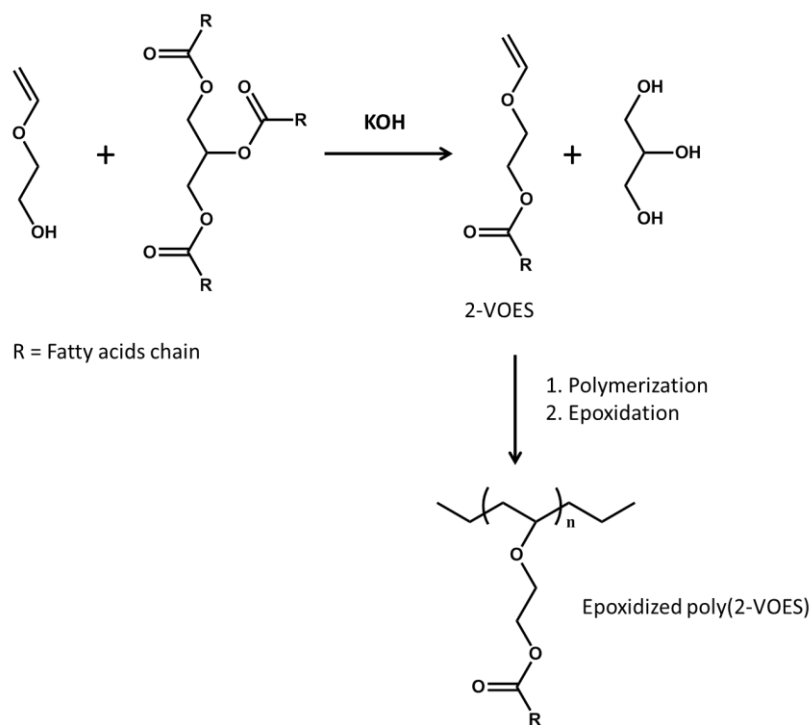
Scheme 1.8. Synthesis of poly-epoxides based on 2-(vinyloxy)ethyl soyate

In another study, Huang et al. developed a di-glycidyl or triglycidyl esters monomer (DGEC21 and TGEC22, respectively) based on tung oil fatty acid. This dimer/trimer fatty acids system was derived from Diels-Alder addition of methyl-eleostearate (major component of tung oil) with acrylic acid and fumaric acid, as shown in Scheme 1.9. When cured with nadic-methyl anhydride, the thermoset system was shown to have comparable strength, modulus and T_g to diglycidyl ether bisphenol A-epoxy system. This

performance was attributed to the high reactivity of its terminal epoxy group, cyclic structure, and shorter

aliphatic segment between the epoxy groups in the backbone.
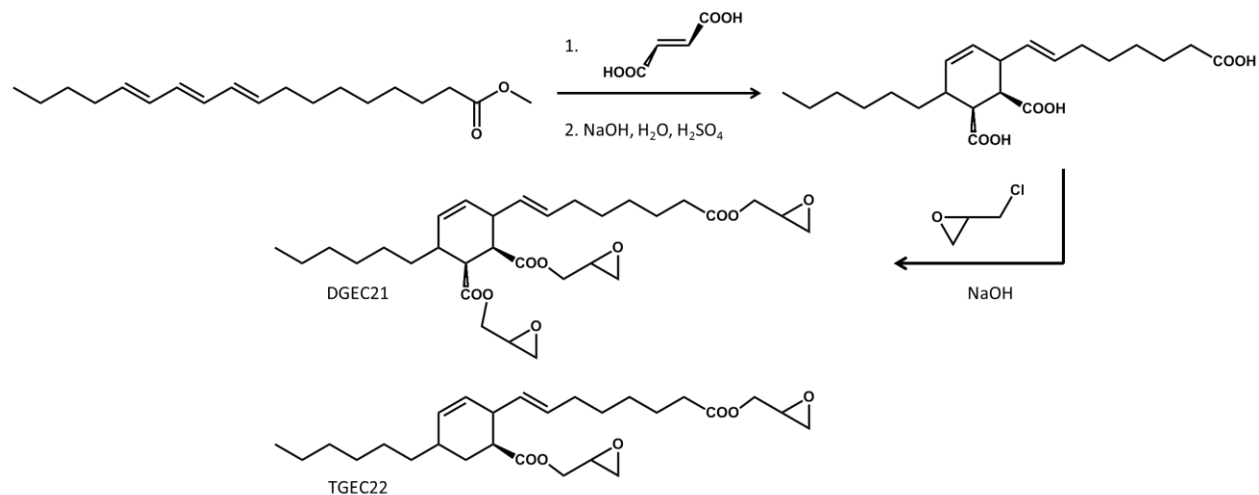
Scheme 1.9. Synthesis of di/tri-glycidyl esters derived from tung oil fatty acids

1.6.   Epoxidized Sucrose Soyate (ESS) resin

Another type of molecule invented as the result of derivatization of vegetable oil is sucrose esters

of fatty acids. Efficient synthesis of highly substituted sucrose ester was optimized by Proctor and

Gamble in the 1960s and they marketed for a fat substitute under the name of Olestra . The

representative structure of this molecule is illustrated in Figure 1.4. A variety of sucrose ester of fatty

acids resins can be obtained with the selection of different vegetable oils or fatty acid methyl esters,

degree of esterification, and hydrogenation of unsaturation. Unlike triglycerides of fatty acids, sucrose

esters of fatty acids can have up to eight fatty acids attached to its core molecule, resulting in larger

molecular size. Due to its larger size, human or bacterial enzymes in the digestive track cannot break

down the molecule, and thus it is not absorbed in the intestinal wall to any appreciable extent. The

potential use for Olestra as "fat-free" oil in the food market includes its application as frying oil,

margarines, and food additives in snacks and cookies. Unfortunately, after 30 years process of acquiring

FDA approval and estimated $500 million in product development, the application of Olestra in the food

market was not as successful as originally thought off due to reported gastrointestinal side effects

concern from small fractions of consumers [52].
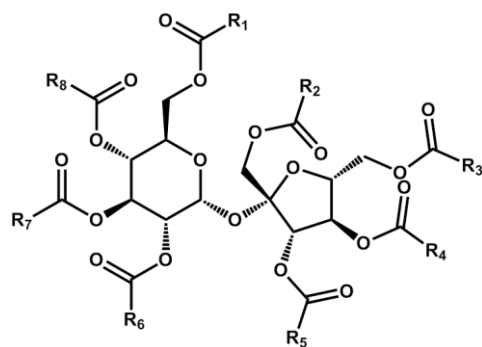
Figure 1.4. General structure of sucrose ester of fatty acids

Fortunately, the application of sucrose polyester is not only limited to food market. Proctor and Gamble also commercialized sucrose ester as Sefose® for coatings and paint industry and as Sisterna® for cosmetics and personal care industry. In 2009, Sefose® based alkyd coatings called Chempol® MPS was awarded with Presidential Green Chemistry Challenge Award for paint formulations that contains 50% less volatile organic content (VOC) solvents and higher renewable content, while not compromising the performance such as application flow, dry time, scrub resistance and solvent resistance [53, 54]. The benefits of using Sefose® in the alkyd resin is attributed to the low viscosity of the resin due to the compact, star-like structure which minimizes intermolecular interactions and the unsaturation functionality in the resin which provides auto-oxidative crosslinking technology.

An epoxy resin based on Sefose® resin has been developed by Webster et al., and is named epoxidized sucrose ester (ESE) [55-57]; the representative chemical structure is shown in Figure 1.5. This resin is obtained by converting the unsaturation in the Sefose® into epoxy groups through the Prilazhaev reaction using acidic ion exchange resin as catalyst. Since invented in the late 2000s, many crosslinking routes using ESE resins have been explored. Epoxy homopolymerization of ESE has been studied using cationic UV and thermal-cured method [58, 59]. Then, structure-property of polyester thermoset from acid/anhydride crosslinked ESE has also been well-studied [9, 60-64]. The conversion of the epoxy groups into methacrylated and acrylated group has been explored to provide external unsaturation, which then can be cured thermally and via UV-radiation [65-67]. Furthermore, polyol-ESE derivatives can be cured with polyisocyanates or melamine-formaldehyde [68-70]. These thermosetting polymers have been shown to have comparable properties to petrochemical-based counterparts. This performance is attributed to its high number of functional groups and sucrose core. When soybean oil fatty acids was

used, ESE have up to 8 fatty acids chains attached its sucrose core, thus would have up to 12 epoxy groups per molecule [64]. In comparison soybean oils only contain 3 fatty acid chains or an average of 4.5 functional groups per molecule. Furthermore, the improvement in the properties of the ESS thermosets was attributed to the rigidity of the sucrose core. In a study comparing the properties of anhydride-cured epoxy thermoset using ESS and tripentaerythritol-based epoxy-- 2 epoxy resins with same number of functionalities yet different core molecule – the ESS-based thermoset was shown to have higher tensile strength and Young's modulus. The application of the ESS-based thermoset system can range into coatings, composites, adhesives, printing inks, and many more [67, 71-74].
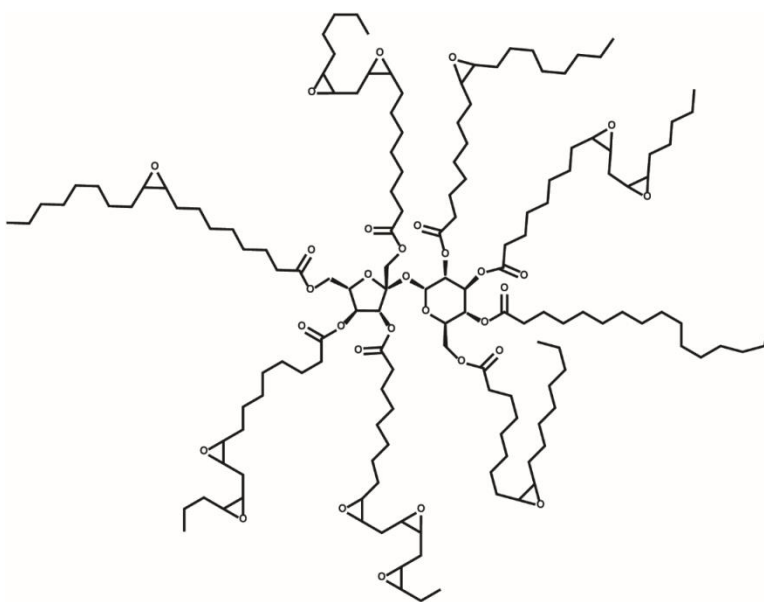
Figure 1.5. Epoxidized sucrose soyate (ESS) chemical structure; the resin has an average of 12 epoxy functional groups per molecule

1.7.   Conclusion

The interest in the development of high performance materials derived from natural resources has gained popularity due to greater awareness of future sustainability and uncertainty in supply and cost of petrochemicals. The abundance and relatively low cost of vegetable oils make them an industrially attractive and feasible feedstock to be explored as chemical commodity. The conversion of unsaturation in the vegetable oil fatty acids in to epoxy functionality has opened up routes to many crosslinking technologies to form thermosetting polymers. To meet the high performance requirements for structural materials, chemical modification of the vegetable oils and addition of rigid molecules in the thermoset formulation has been explored. Despite this improvement, vegetable-oil based thermosets still tend to be

softer than petrochemical-based materials or otherwise the bio-based content in the final product is compromised. The breakthrough of sucrose ester as chemical building block has shown tremendous promise in creating a thermoset polymer that has comparable properties to the currently existing petrochemical-based counterpart. The work described in this dissertation is devoted to the further exploration of the use of epoxidized sucrose soyate as an alternative to petrochemical feedstock in resins and thermosetting materials for composite and coatings application.

1.8.   References

[1]   R. Auvergne, S. Caillol, G. David, B. Boutevin, J.-P. Pascault, Biobased Thermosetting Epoxy: Present and Future, Chemical Reviews, 114 (2013) 1082-1115.

[2]   Y.H. Kim, E.S. An, S.Y. Park, B.K. Song, Enzymatic epoxidation and polymerization of cardanol obtained from a renewable resource and curing of epoxide-containing polycardanol, Journal of Molecular Catalysis B: Enzymatic, 45 (2007) 39-44.

[3]   C. Aouf, C. Le Guernevé, S. Caillol, H. Fulcrand, Study of the O-glycidylation of natural phenolic compounds. The relationship between the phenolic structure and the reaction mechanism, Tetrahedron, 69 (2013) 1345-1353.

[4]   W.O.S. Doherty, P. Mousavioun, C.M. Fellows, Value-adding to cellulosic ethanol: Lignin polymers, Industrial Crops and Products, 33 (2011) 259-276.

[5]   C.I. Simionescu, V. Rusan, M.M. Macoveanu, G. Cazacu, R. Lipsa, C. Vasile, A. Stoleriu, A. Ioanid, Lignin/epoxy composites, Composites Science and Technology, 48 (1993) 317-323.

[6]   Y. Takada, K. Shinbo, Y. Someya, M. Shibata, Preparation and properties of bio-based epoxy montomorillonite nanocomposites derived from polyglycerol polyglycidyl ether and ε-polylysine, Journal of Applied Polymer Science, 113 (2009) 479-484.

[7]   M. Shibata, K. Nakai, Preparation and properties of biocomposites composed of bio-based epoxy resin, tannic acid, and microfibrillated cellulose, Journal of Polymer Science Part B: Polymer Physics, 48 (2010) 425-433.

[8]   J.O. Metzger, Fats and oils as renewable feedstock for chemistry, European Journal of Lipid Science and Technology, 111 (2009) 865-876.

[9]   X. Pan, P. Sengupta, D.C. Webster, High biobased content epoxy-anhydride thermosets from epoxidized sucrose ester of fatty acids, Biomacromolecules, 12 (2011) 2416-2428.

[10]   M.H. Brodnitz, Autoxidation of saturated fatty acids. A review, Journal of Agricultural and Food Chemistry, 16 (1968) 994-999.

[11]   S.M.P. Meneghetti, R.F. de Souza, A.L. Monteiro, M.O. de Souza, Substitution of lead catalysts by zirconium in the oxidative polymerization of linseed oil, Progress in Organic Coatings, 33 (1998) 219-224.

[12]   M.D. Soucek, T. Khattab, J. Wu, Review of autoxidation and driers, Progress in Organic Coatings, 73 (2012) 435-454.

[13]   Y. Xia, R.C. Larock, Vegetable oil-based polymeric materials: synthesis, properties, and applications, Green Chemistry, 12 (2010) 1893-1909.

[14]   J. Karger-Kocsis, S. Grishchuk, L. Sorochynska, M.Z. Rong, Curing, gelling, thermomechanical, and thermal decomposition behaviors of anhydride-cured epoxy (DGEBA)/epoxidized soybean oil compositions, Polymer Engineering & Science, 54 (2014) 747-755.

[15]   S.G. Tan, W.S. Chow, Thermal Properties, Fracture Toughness and Water Absorption of Epoxy-Palm Oil Blends, Polymer-Plastics Technology and Engineering, 49 (2010) 900-907.

[16]   A. Adhvaryu, S.Z. Erhan, Epoxidized soybean oil as a potential source of high-temperature lubricants, Industrial Crops and Products, 15 (2002) 247-254.

[17]   T.W. Findley, D. Swern, J.T. Scanlan, Epoxidation of Unsaturated Fatty Materials with Peracetic Acid in Glacial Acetic Acid Solution, Journal of the American Chemical Society, 67 (1945) 412-414.

[18]   E. Prilezhaeva, Reaktsiya Prilezhaeva. Elektrofil'noe okislenie (Prilezhaev Reaction. Electrophilic Oxidation), in, Moscow: Nauka, 1974.

[19]   V.G. Dryuk, The mechanism of epoxidation of olefins by peracids, Tetrahedron, 32 (1976) 2855-2866.

[20]   A. Campanella, C. Fontanini, M.A. Baltanás, High yield epoxidation of fatty acid methyl esters with performic acid generated in situ, Chemical Engineering Journal, 144 (2008) 466-475.

[21]   E. Santacesaria, R. Tesser, M. Di Serio, R. Turco, V. Russo, D. Verde, A biphasic model describing soybean oil epoxidation with H2O2 in a fed-batch reactor, Chemical Engineering Journal, 173 (2011) 198-209.

[22]   F.E. Okieimen, O.I. Bakare, C.O. Okieimen, Studies on the epoxidation of rubber seed oil, Industrial Crops and Products, 15 (2002) 139-144.

[23]   S. Dinda, A.V. Patwardhan, V.V. Goud, N.C. Pradhan, Epoxidation of cottonseed oil by aqueous hydrogen peroxide catalysed by liquid inorganic acids, Bioresource Technology, 99 (2008) 3737-3744.

[24]   C. Cai, H. Dai, R. Chen, C. Su, X. Xu, S. Zhang, L. Yang, Studies on the kinetics of in situ epoxidation of vegetable oils, European Journal of Lipid Science and Technology, 110 (2008) 341-346.

[25]   R. Mungroo, N.C. Pradhan, V.V. Goud, A.K. Dalai, Epoxidation of Canola Oil with Hydrogen Peroxide Catalyzed by Acidic Ion Exchange Resin, Journal of the American Oil Chemists' Society, 85 (2008) 887-896.

[26]   V.V. Goud, A.V. Patwardhan, S. Dinda, N.C. Pradhan, Kinetics of epoxidation of jatropha oil with peroxyacetic and peroxyformic acid catalysed by acidic ion exchange resin, Chemical Engineering Science, 62 (2007) 4065-4076.

[27]   S. Dinda, V.V. Goud, A.V. Patwardhan, N.C. Pradhan, Selective epoxidation of natural triglycerides using acidic ion exchange resin as catalyst, Asia-Pacific Journal of Chemical Engineering, 6 (2011) 870-878.

[28]   A. Campanella, M.A. Baltanás, Degradation of the oxirane ring of epoxidized vegetable oils with solvated acetic acid using cation-exchange resins, European Journal of Lipid Science and Technology, 106 (2004) 524-530.

[29]   A. Campanella, M.A. Baltanás, Degradation of the oxirane ring of epoxidized vegetable oils with hydrogen peroxide using an ion exchange resin, Catalysis Today, 107–108 (2005) 208-214.

[30]   Z.S. Petrović, A. Zlatanić, C.C. Lava, S. Sinadinović-Fišer, Epoxidation of soybean oil in toluene with peroxoacetic and peroxoformic acids — kinetics and side reactions, European Journal of Lipid Science and Technology, 104 (2002) 293-299.

[31]   V.V. Goud, A.V. Patwardhan, S. Dinda, N.C. Pradhan, Epoxidation of karanja (Pongamia glabra) oil catalysed by acidic ion exchange resin, European Journal of Lipid Science and Technology, 109 (2007) 575-584.

[32]   T. Vlček, Z.S. Petrović, Optimization of the chemoenzymatic epoxidation of soybean oil, Journal of the American Oil Chemists' Society, 83 (2006) 247-252.

[33]   F.d.A. Corrêa, F.K. Sutili, L.S.M. Miranda, S.G.F. Leite, R.O.M.A. De Souza, I.C.R. Leal, Epoxidation of oleic acid catalyzed by PSCI-Amano lipase optimized by experimental design, Journal of Molecular Catalysis B: Enzymatic, 81 (2012) 7-11.

[34]   G.J. Piazza, T.A. Foglia, A. Nuñez, Optimizing reaction parameters for the enzymatic synthesis of epoxidized oleic acid with oat seed peroxygenase, Journal of the American Oil Chemists' Society, 78 (2001) 589-592.

[35]   J.M.R. da Silva, M.d.G. Nascimento, Chemoenzymatic epoxidation of citronellol catalyzed by lipases, Process Biochemistry, 47 (2012) 517-522.

[36]   M. Rüsch gen. Klaas, S. Warwel, Complete and partial epoxidation of plant oils by lipase-catalyzed perhydrolysis1, Industrial Crops and Products, 9 (1999) 125-132.

[37]   H. Lu, S. Sun, Y. Bi, G. Yang, R. Ma, H. Yang, Enzymatic epoxidation of soybean oil methyl esters in the presence of free fatty acids, European Journal of Lipid Science and Technology, 112 (2010) 1101-1105.

[38]   I. Hilker, D. Bothe, J. Prüss, H.J. Warnecke, Chemo-enzymatic epoxidation of unsaturated plant oils, Chemical Engineering Science, 56 (2001) 427-432.

[39]   C. Orellana-Coca, J.M. Billakanti, B. Mattiasson, R. Hatti-Kaul, Lipase mediated simultaneous esterification and epoxidation of oleic acid for the production of alkylepoxystearates, Journal of Molecular Catalysis B: Enzymatic, 44 (2007) 1033-137.

[40]   S.-J. Park, F.-L. Jin, J.-R. Lee, Synthesis and Thermal Properties of Epoxidized Vegetable Oil, Macromolecular Rapid Communications, 25 (2004) 724-727.

[41]   S. Chakrapani, J.V. Crivello†, Synthesis and Photoinitiated Cationic Polymerization of Epoxidized Castor Oil and Its Derivatives, Journal of Macromolecular Science, Part A, 35 (1998) 691-710.

[42]   R.F. Fischer, Polyesters from epoxides and anhydrides, Industrial and Engineering Chemistry, 52 (1960) 321-323.

[43]   E.C. Dearborn, R.M. Fuoss, A.K. MacKenzie, R.G. Shepherd, Epoxy resins from bis-, tris-, and tetrakisglycidyl etheres, Industrial and Engineering Chemistry, 45 (1953) 2715-2721.

[44]   N. Boquillon, C. Fringant, Polymer networks derived from curing of epoxidised linseed oil: influence of different catalysts and anhydride hardeners, Polymer, 41 (2000) 8603-8613.

[45]   A.E. Gerbase, C.L. Petzhold, A.P.O. Costa, Dynamic mechanical and thermal behavior of epoxy resins based on soybean oil, Journal of the American Oil Chemists' Society, 79 (2002) 797-802.

[46]   M. Desroches, M. Escouvois, R. Auvergne, S. Caillol, B. Boutevin, From Vegetable Oils to Polyurethanes: Synthetic Routes to Polyols and Main Industrial Products, Polymer Reviews, 52 (2012) 38-79.

[47]   J.L. Scala, R.P. Wool, The effect of fatty acid composition on the acrylation kinetics of epoxidized triacylglycerols, Journal of the American Oil Chemists' Society, 79 (2002) 59-63.

[48]   S.G. Tan, W.S. Chow, Biobased Epoxidized Vegetable Oils and Its Greener Epoxy Blends: A Review, Polymer-Plastics Technology and Engineering, 49 (2010) 1581-1590.

[49]   R. Wang, T. Schuman, CHAPTER 9 Towards Green: A Review of Recent Developments in Bio-renewable Epoxy Resins from Vegetable Oils, in: Green Materials from Plant Oils, The Royal Society of Chemistry, 2015, pp. 202-241.

[50]   F.I. Altuna, L.H. Espósito, R.A. Ruseckaite, P.M. Stefani, Thermal and mechanical properties of anhydride-cured epoxy resins with different contents of biobased epoxidized soybean oil, Journal of Applied Polymer Science, 120 (2011) 789-798.

[51]   S. Alam, H. Kalita, A. Jayasooriya, S. Samanta, J. Bahr, A. Chernykh, M. Weisz, B.J. Chisholm, 2-(Vinyloxy)ethyl soyate as a versatile platform chemical for coatings: An overview, European Journal of Lipid Science and Technology, 116 (2014) 2-15.

[52]   M. Nestle, The Selling of Olestra, Public Health Reports (1974-), 113 (1998) 508-520.

[53]   D.R. Eslinger, D.A. Ryer, N. Rogers, R.S. Berger, D.J. Back, Resin and Paint Coating Compositions Comprising Highly Esterified Polyol Polyesters with Two or More Pairs of Conjugated Double Bonds, in: United States Patent Office, US, 2010.

[54] Chempol® MPS Resins and Sefose® Sucrose Esters Enable High-Performance Low-VOC Alkyd Paints and Coatings, in: Presidential Green Chemistry Challenge: 2009 Designing Greener Chemicals Award, US Environmental Protection Agency, 2009.

[55] D.C. Webster, P.P. Sengupta, Z. Chen, X. Pan, A. Paramarta, Highly functional epoxidized resins and coatings, in: United States Patent Office, NDSU Research Foundation, US, 2015.

[56] X. Pan, P. Sengupta, D.C. Webster, Novel biobased epoxy compounds: epoxidized sucrose esters of fatty acids, Green Chemistry, 13 (2011) 965-975.

[57] E.M. Monono, D.C. Webster, D.P. Wiesenborn, Pilot scale (10 kg) production and characterization of epoxidized sucrose soyate, Industrial Crops and Products, 74 (2015) 987-997.

[58] P.P. Sengupta, X. Pan, T.J. Nelson, A. Paramarta, D.C. Webster, Cationic UV curing characteristics of epoxidized sucrose esters, in: American Coatings Society National Meeting, PMSE, 2010, pp. 888-889.

[59] T. Nelson, T. Galhenage, D. Webster, Catalyzed crosslinking of highly functional biobased epoxy resins, J Coat Technol Res, 10 (2013) 589-600.

[60] C.S. Kovash, E. Pavlacky, S. Selvakumar, M.P. Sibi, D.C. Webster, Thermoset Coatings from Epoxidized Sucrose Soyate and Blocked, Bio-Based Dicarboxylic Acids, ChemSusChem, 7 (2014) 2289-2294.

[61] S. Ma, D.C. Webster, Naturally Occurring Acids as Cross-Linkers To Yield VOC-Free, High-Performance, Fully Bio-Based, Degradable Thermosets, Macromolecules, 48 (2015) 7127-7137.

[62] S. Ma, D.C. Webster, F. Jabeen, Hard and Flexible, Degradable Thermosets from Renewable Bioresources with the Assistance of Water and Ethanol, Macromolecules, 49 (2016) 3780-3788.

[63] A. Paramarta, D.C. Webster, Bio-based high performance epoxy-anhydride thermosets for structural composites: The effect of composition variables, Reactive and Functional Polymers, 105 (2016) 140-149.

[64] X. Pan, D.C. Webster, Impact of Structure and Functionality of Core Polyol in Highly Functional Biobased Epoxy Resins, Macromolecular Rapid Communications, 32 (2011) 1324-1330.

[65] A. Paramarta, X. Pan, D.C. Webster, Highly functional acrylated biobased resin system for uv-curable coatings, Radtech Report, (2013) 26-32.

[66]   J. Yan, D.C. Webster, Thermosets from highly functional methacrylated epoxidized sucrose soyate, Green Materials, 2 (2014) 132-143.

[67]   A. Amiri, A. Yu, D. Webster, C. Ulven, Bio-Based Resin Reinforced with Flax Fiber as Thermorheologically Complex Materials, Polymers, 8 (2016) 153.

[68]   X. Pan, D.C. Webster, New Biobased High Functionality Polyols and Their Use in Polyurethane Coatings, ChemSusChem, 5 (2012) 419-429.

[69]   T.J. Nelson, L. Bultema, N. Eidenschink, D.C. Webster, Bio-Based High Functionality Polyols and Their Use in 1K Polyurethane Coatings, Journal of Renewable Materials, 1 (2013) 141-153.

[70]   T. Nelson, B. Masaki, Z. Morseth, D. Webster, Highly functional biobased polyols and their use in melamine–formaldehyde coatings, J Coat Technol Res, 10 (2013) 757-767.

[71]   N. Hosseini, S. Javid, A. Amiri, C. Ulven, D.C. Webster, G. Karami, Micromechanical viscoelastic analysis of flax fiber reinforced bio-based polyurethane composites, Journal of Renewable Materials, 3 (2015) 205-2015.

[72]   N. Hosseini, C.A. Ulven, F. Azarmi, D.C. Webster, T.J. Nelson, Utilization of Flax Fibers and Glass Fibers in a Bio-Based Resin, in: ASME 2014 International Mechanical Engineering Congress and Exposition, The American Society of Mechanical Engineers, Montreal, Quebec, Canada, 2014.

[73]   N. Hosseini, D.C. Webster, C. Ulven, Advanced biocomposite from highly functional methacrylated epoxidized sucrose soyate (MAESS) resin derived from vegetable oil and fiberglass fabric for composite applications, European Polymer Journal, 79 (2016) 63-71.

[74]   Taylor, T. Krosbakken, C.A. Ulven, A. Paramarta, D.C. Webster, Structural quality biocomposites of treated flax fiber with epoxidized sucrose soyate resin, in: International Conference on Composite Materials, Montreal, Canada, 2013.

CHAPTER 2. CURING KINETICS OF BIO-BASED ANHYDRIDE THERMOSETS WITH ZINC CATALYST

2.1.   Abstract

The kinetics of curing of epoxidized sucrose soyate with a cycloaliphatic anhydride was studied using differential scanning calorimetry. Epoxidized sucrose soyate (ESS), a novel bio-based resin with high epoxy functionality, can be used to produce thermoset polymers for structural applications. ESS was crosslinked with methyl hexahydrophthalic anhydride using a zinc-based catalyst. Differential scanning calorimetry (DSC) studies indicated that the reaction kinetics was influenced by the formulation variables, i.e. anhydride-to-epoxy molar ratio and catalyst amount. Multiple exothermic peaks suggest the presence of several different reaction mechanisms of the epoxy-anhydride reaction using metal complex catalyst, based on the formulation variables. All of the reaction rate data can be fitted into both n-th order and autocatalytic kinetic models. Based on the value of reaction order in the n-th order and autocatalytic kinetic model, the curing process is more dominated by non-autocatalytic reaction and less controlled by the autocatalytic process. This kinetic model observation suggested that the presence of hydroxyl groups or carboxylic acid pendant chains in the ESS molecule or as the product of side reactions did not auto-catalyze the reaction, and the reaction is initiated solely from the metal complex.

2.2.   Introduction

In the recent decade, there has been increasing interest in replacing petrochemical-based materials with bio-based materials [1, 2]. This interest is mainly influenced by two factors: the rising and unstable cost of petrochemicals and a greater awareness of future sustainability. The challenges to this "green" movement are to produce materials from renewable resources that will be both economically feasible and have comparable properties to current technology. Some efforts have been made by partially substituting petrochemical products with chemicals derived from vegetable oils. However, this technology results in a low bio-based content of the final product. Since thermosets or crosslinked polymers are used in numerous high performance applications such as matrix resins for composites, structural adhesives, and coatings, significant research efforts are underway to develop bio-based thermosets derived from vegetable oils or chemicals derived from lignin [3-13]. However, obtaining

materials having the performance that meets or exceeds the requirements for these demanding

applications has been challenging.

Recently, Webster et al. has developed a novel bio-based epoxy resin, namely epoxidized

sucrose soyate (ESS), shown in Figure 2.1 [14]. When crosslinked, this epoxy resin has been shown to

have properties comparable to its petrochemical-based counterpart [15-19]. The ESS-based thermoset is

an improvement over epoxidized soybean oil (ESO); ESS has more epoxy functional groups per molecule

and in addition its sucrose core provides rigidity to the thermoset [20]. Anhydride-cured thermosets

based on ESS have been shown to be good candidates to be a matrix resin for structural composite

materials [15, 21]. In order to be able to achieve the best possible properties, it is important to

understand the effect of composition variables of the matrix resin itself on the curing kinetics and

thermoset properties.
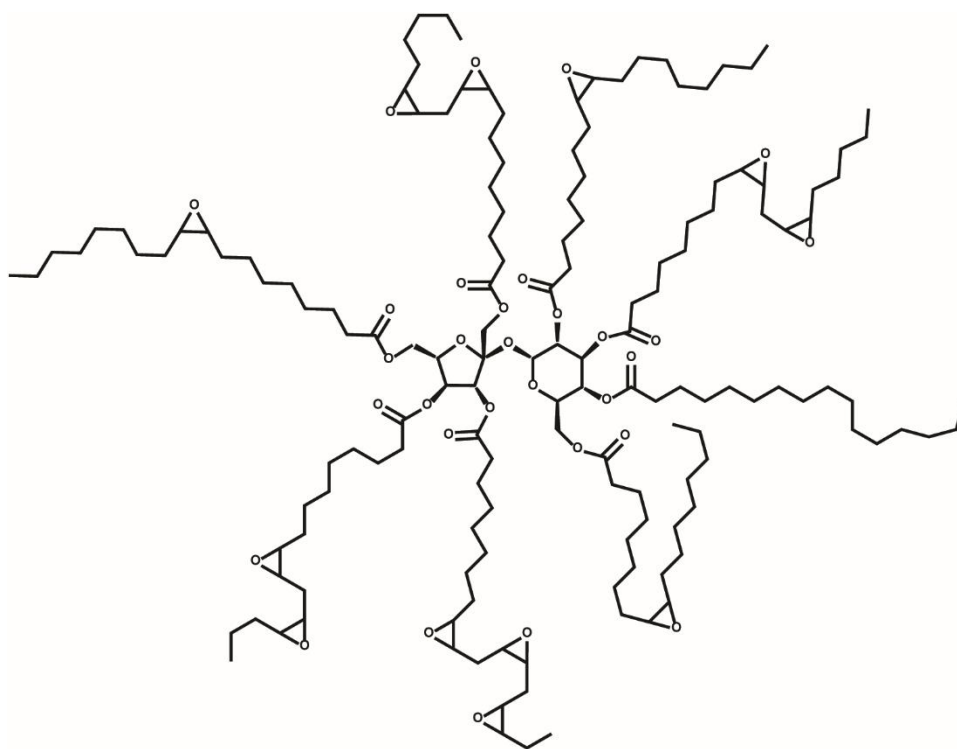
Figure 2.1. Epoxidized sucrose soyate (ESS) chemical structure; the resin has an average of 12 epoxy functional groups per molecule.

The epoxy-anhydride curing reaction may be catalyzed with alcohols, tertiary amines, quaternary

ammonium or phosphonium salts, or metal salts and chelates. The reaction mechanism for epoxy-

anhydride curing is known to be very complex, and depends heavily on the type of catalyst used in the

formulation. Scheme 2.1 shows the reaction mechanism for an uncatalyzed system. The reaction is feasible due to the presence of a hydroxyl group attached to either the epoxy resin or impurities present in the raw materials, or the presence of a small amount of carboxylic acid groups from the hydrolysis of the acid anhydride crosslinker [22-25]. This hydroxyl group is able to ring open the cyclic anhydride to form a mono-ester and carboxylic acid end group, which then can further react to form polyester. Along with this mechanism, many scientists believe that homo-polymerization of epoxy occurs as a side reaction.
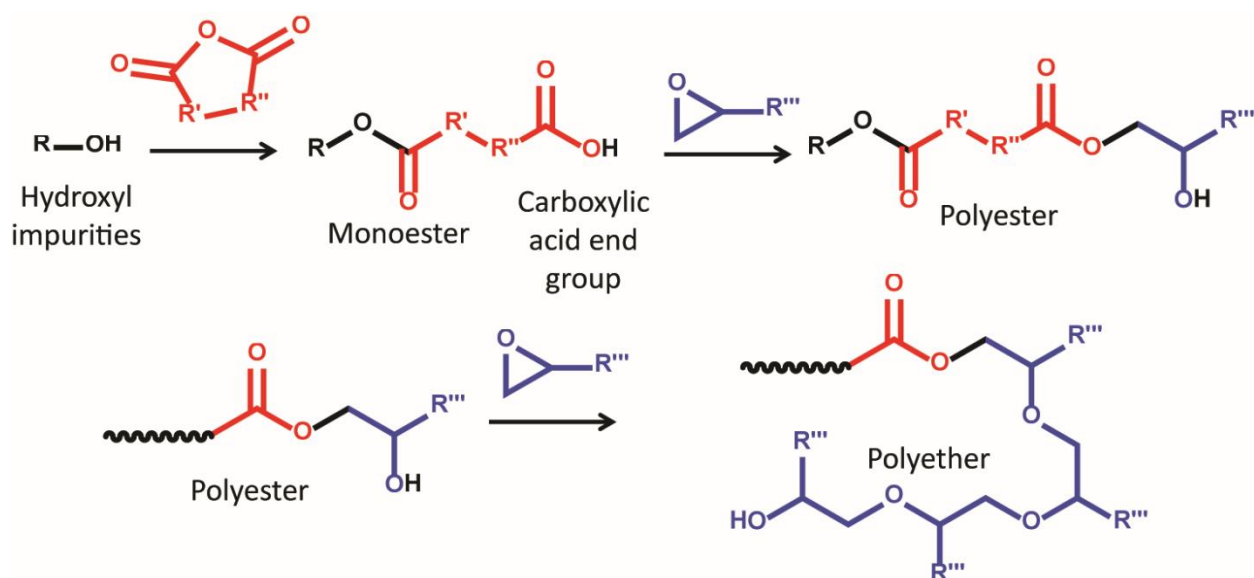
Scheme 2.1. Uncatalyzed polymerization of anhydride and epoxy

For comparison, Scheme 2.2 shows the reaction mechanism when a catalyst is used for the epoxy-anhydride polymerization. The initial ring opening of cyclic anhydride/epoxy occurs from nucleophilic attack of the catalyst, i.e. tertiary amine, amidine, quaternary onium salt, or metal salts, to form a zwitterionic carboxylate and/or alkoxide anion [26]. The carboxylate and alkoxide anion then becomes the active end group and propagates the polyester chain. Within this mechanism, there is a debate as to whether an active hydrogen atom, i.e. acid/alcohol, should be present in the copolymerization process; the hydrogen-bonded complex is thought to have enough reactivity to ring open the cyclic anhydride/epoxy [27-29]. However, depending on the type of acid/alcohol used, the formation of a hydroxyl/carboxylic acid end group is possible. These functional groups can then catalyze the reaction, as shown in Scheme 2.1.
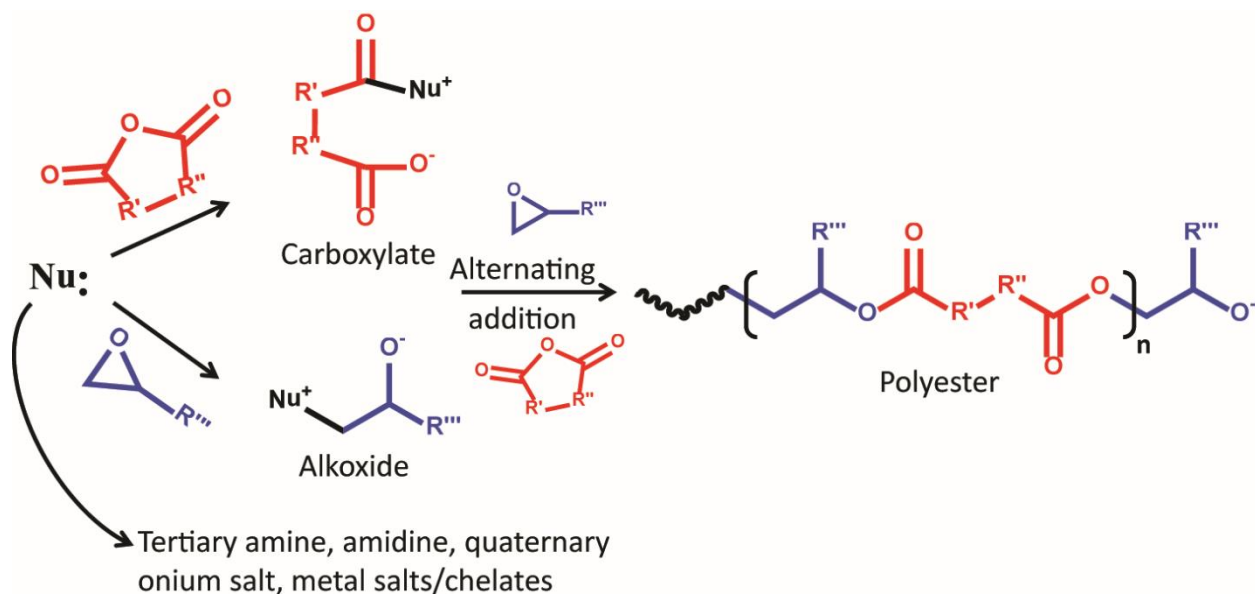
Scheme 2.2. Catalyzed polymerization of anhydride and epoxy

Organometallic compounds have been used as epoxy-anhydride catalysts since the 1950s, mainly for electronic applications [30]. The most common ligand used for these catalysts is acetylacetonate [31-37]. Metal chelates are also capable of catalyzing epoxy homopolymerization; interestingly, there are more articles reporting the metal catalysis of epoxy homopolymerization than for the epoxy-anhydride copolymerization. The final product properties of the thermoset polymer can be affected by the choice of metal, ligand, and anion type. A review article regarding the use of metal chelates as epoxy resin modifiers has been published by Hamerton et al. [38]. They summarized catalysis by coordination compounds with different ligands: amino, acetylacetonate, imidazole, imidazolium, phthalocyanine, and Schiff's base. The use of metal coordination compounds as epoxy cure accelerators can modify the cure profile and improve storage stability.

This paper focuses on a study of the curing kinetics of a novel highly functional bio-based epoxy-anhydride resin system to understand the effects of the composition variables. The variables studied are the anhydride-to-epoxy molar ratio and the amount of catalyst. Differential scanning calorimetry (DSC) is a convenient and rapid tool for obtaining kinetic information on the curing process. The kinetic parameters such as activation energy, reaction orders, and pre-exponential order are calculated based on different kinetic models. These values may help to understand the reaction mechanism of ESS and anhydride curing.

2.3.   Experimental

2.3.1.   Materials, polymer composition, and cure procedure

Epoxidized sucrose soyate (ESS) was synthesized from sucrose soyate through the Prilezhaev reaction mechanism; the details of the synthesis reaction is presented in literature [14, 39]. ESS has an equivalent weight of 250 g/mol, determined by hydrogen bromide titration. The crosslinker used in this study was methyl hexahydrophthalic anhydride (MHHPA), provided by Dixie Chemicals. To catalyze the epoxy-anhydride reaction, a zinc-complex catalyst (CXC-1765® provided by King Industries) was added to the formulation.

Nine formulations with different anhydride-to-epoxy (AE) molar ratios and catalyst amounts were prepared; the detailed amounts are listed in Table 2.1. To prepare the formulations, ESS resin and MHHPA crosslinker were first mixed at 50 °C for 1 hour. Then, the catalyst was added gradually to the mixture over a 1-hour period.

Table 2.1. Polymer compositions

Sample #	AE Molar Ratio	AE Weight Ratio	Catalyst (% wt. total)
S1	0.50	0.32	2
S2	0.75	0.48	2
S3	1.00	0.65	2
S4	0.50	0.32	5
S5	0.75	0.48	5
S6	1.00	0.65	5
S7	0.50	0.32	8
S8	0.75	0.48	8
S9	1.00	0.65	8

2.3.2.   Weight loss measurement by thermogravimetric analysis

Thermogravimetric analysis was used to study the volatilization of raw materials and formulation mixtures as they were being heated. The TGA experiment was conducted using a Q500 by TA Instruments, and the sample size used in the experiment was 30-50 mg. Two TGA experiments were conducted: dynamic and isothermal scans. During the dynamic scans, the samples were heated from room temperature to 600 °C at a rate of 10 °C/min. For the isothermal scan experiments, the samples were heated from room temperature to 120 °C at a rate of 10 °C/min, and then the temperature was held

isothermally at 120 °C for 2 hours. During both dynamic and isothermal scans, the samples were purged with air at 60 mL/min flow rate, while the TGA balance was purged with nitrogen at 40 mL/min flow rate.

2.3.3.   Curing kinetics by differential scanning calorimetry

2.3.3.1. DSC experiment

The kinetic parameters of the curing process were obtained by performing differential scanning calorimetry (DSC) experiments, using a DSC Q1000 by TA Instruments. Non-isothermal scans of 10 mg samples were conducted at different heating rates (1, 2.5, 5 and 10 °C/min) from 25 to 250 °C under a nitrogen atmosphere.

2.3.3.2. Reaction kinetic analysis

Calculation of kinetic parameters by DSC assumes that the measured heat flow (dH/dt) is proportional to the reaction rate ($d\alpha/dt$). Furthermore, the extent of conversion/cure (α_t) can be calculated from the integration of the heat flow (ΔH).

$$\frac{d\alpha}{dt} = \frac{dH/dt}{\Delta H_{Total}} \qquad \text{and} \qquad \alpha_t = \frac{\Delta H_t}{\Delta H_{Total}} \qquad\qquad (2.1 \text{ \& } 2.2)$$

Then, the reaction rate of epoxy-anhydride can be described by the Arrhenius equation, a formula for temperature-dependent reaction rate, such as follows:

$$\frac{d\alpha}{dt} = Ae^{-\frac{E_a}{RT}}f(\alpha) \qquad\qquad (2.3)$$

where $\frac{d\alpha}{dt}$ is the reaction rate, A is the exponential order, E_a is the activation energy, and $f(\alpha)$ is the function of cure. The overall activation energy can be calculated through the Kissinger methods from the heat flow curves using multiple heating rates:

$$\frac{d(\ln(\beta/T_p{}^2))}{d(1/T_p)} = -\frac{E_a}{R} \qquad\qquad (2.4)$$

where β is the heating rate in °C/min and T_p is the peak temperature [40]. Using this method, it is assumed that at the peak temperature, the extent of cure of the reaction is at a similar value. Then, the function of cure is often described with either a reaction order (RO) or an autocatalytic kinetic model:

$$\text{RO kinetic model: } f(\alpha) = (1-\alpha)^n \qquad\qquad (2.5)$$

$$\text{Autocatalytic kinetic model: } f(\alpha) = \alpha^m(1-\alpha)^n \qquad\qquad (2.6)$$

where n and m are the reaction orders. To determine whether a particular reaction would be appropriately modelled using an RO or autocatalytic kinetic model, a procedure described by Málek was followed; details of this procedure are provided in the literature [41]. In this literature, the calculations to obtain the kinetic parameters are also explained. Then, using iso-conversional Flynn-Ozawa-Wall kinetic methods, the activation energy as a function of cure was determined. The activation energy w

$$\frac{d(\ln(\beta))}{d(1/T_p)} = -\frac{E_a}{R}$$
(2.7)

where β is the heating rate in °C/min and T_p is the peak temperature.

However, the fastest and most efficient way to determine the kinetic parameters of a reaction from DSC experiments is through the TA Instruments Specialty Library with their Thermal Stability Analysis. This method is based on ASTM E698 and assumes that the reaction follows a first-order kinetic model ($n = 1$) [42]. Using this software, kinetic parameters can be obtained automatically. Kinetic parameters obtained using this method were compared with the values obtained using the RO and autocatalytic kinetic models.

2.4. Results and Discussion

2.4.1. Weight loss measurement by TGA

As an initial experiment, weight loss analysis was conducted to understand the volatility of the components during the curing process. Figure 2.2 shows the weight loss curves of the individual raw materials (ESS, MHHPA, and CXC-1765) in a dynamic scan. The ESS resin shows an insignificant weight loss up to 332 °C, and then starts to lose weight rapidly due the degradation of the resin. The MHHPA crosslinker starts to lose weight significantly at 126 °C, despite its high boiling point of 290 °C. Furthermore, MHHPA shows a complete weight loss before the boiling point was reached; this observation indicates that MHHPA has a high vapor pressure. The weight loss of the zinc complex catalyst CXC-1765 during the non-isothermal scan can be broken down into three regions: 126 – 175°C (R1), 175 – 235°C (R2), and 235 – 255°C (R3). According to the manufacturer's data sheet, the non-volatile content of CXC-1765 is 60% after 60 minutes heating at 110°C and the boiling point is around 250 °C. The catalyst loses weight rapidly in the first region (R1), followed by a slower rate in the second region (R2). The total weight loss during R1 and R2 combined is 45% of the initial weight; thus, this

weight loss is believed to be due to the evaporation of the carboxyl diluents. The weight loss during R2

occurs at a slower rate, which is anticipated since most of the volatile content has evaporated and the

viscosity of the chemicals is fairly high; thus limiting the mobility of the carboxyl diluents. The last weight

loss region (R3) shows a rapid decrease in the weight due to the boiling of the zinc catalyst, which may

indicate the dissociation of amino ligands from the zinc metal. The evaporation of carboxyl diluents and

ligand dissociation may also occur simultaneously in R2. At temperatures above 255 °C, the catalyst only

loses about 3% of its initial weight. The final weight of the catalyst at the end of the experiment is

observed to be 25%, while the CXC-1765 data sheet lists the metal content to be 7.5%. Therefore, it is

believed that not all of the ligands are dissociated from the zinc metals. Similar multi-step weight loss has

been observed with other organometallic compounds [43-45].
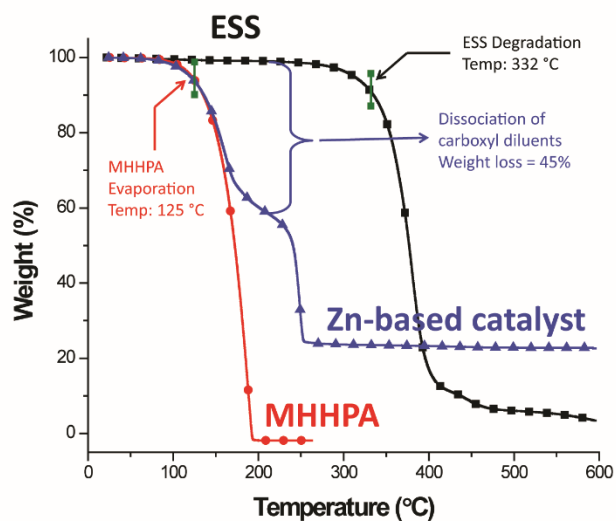
Figure 2.2. Weight loss curves of raw materials from TGA experiments

While understanding the volatility of the separate components is a necessary first step, in the

complete thermoset formulation, there is a competition between thermoset-forming reactions and the

volatilization of the components. The volatilization of components with anhydride-cured epoxidized

soybean oil thermoset curing has been observed by other researchers [46]. Figure 2.3 shows the results

of the TGA heating ramp experiments for the nine formulated samples. Overall, the samples undergo

multiple steps of weight loss: 100 – 175°C, 175 – 275°C, and above 275°C. The first weight loss is

observed at temperatures range of 100-175°C, indicating the evaporation of MHHPA and CXC-1765

32

carboxyl diluents. Then, the formulations show a steady weight at 175 – 275 °C. At this temperature range, the formulations may have reached the gel point or vitrification, where MHHPA has been incorporated into the network and thus can no longer evaporate. Samples with higher AE ratio tend to lose weight more rapidly due to the higher amount of anhydride crosslinker in the formulation mixture. Furthermore, higher crosslinker amounts translate to lower viscosity of the samples, leading to more chemical mobility. The amount of catalyst used in the formulation was expected to directly correlate to the amount of weight loss: as the amount of catalyst increases, reaction rates are expected to be higher and thermoset polymers may reach the gelation (and/or vitrification) point more rapidly, thus affecting the mobility and evaporation rate of the volatile components. However, the results show that there may be an interaction between the amount of catalyst and the AE molar ratio. When looking at samples with AE molar ratio = 0.5, the amount of catalyst did not affect the amount of weight loss significantly. The last region of the weight loss occurs above 275°C due to degradation of the thermoset network. One conclusion that can be drawn from these experiments is that anhydride curing is best used in applications done in a closed system, i.e. composites and adhesives, rather than in an open system, i.e. coatings, due to the potential volatility of the reagents.
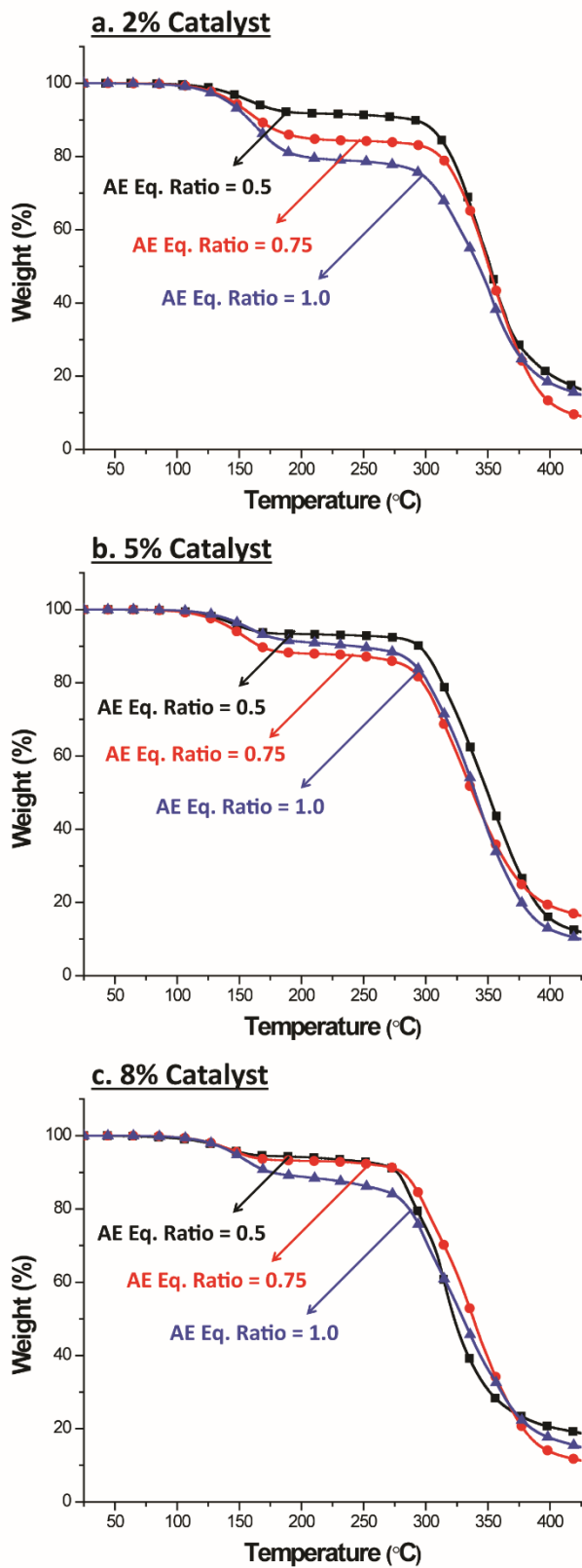
Figure 2.3. Weight loss curves of epoxy-anhydride samples

2.4.2. Curing kinetics by DSC

2.4.2.1. Heat flow curves

Differential scanning calorimetry was used to obtain the kinetic information of the epoxy-anhydride curing process. Non-isothermal curing of the epoxy-anhydride reaction shows a broad exothermic curve, spanning from 75 to 250 °C. Figure 2.4 shows representative heat flow curves with different heating rates; the curves shown are taken from Sample 5. The heat flows curves were then used to determine the total heat of polymerization, ΔH_{Tot}, by integrating the area under curves. As expected, the height intensity increases as the heating rate increases. Yet, the ΔH_{Tot} did not differ significantly between each heating rates. The values of the ΔH_{Tot} for the different samples are shown in Table 2.2.
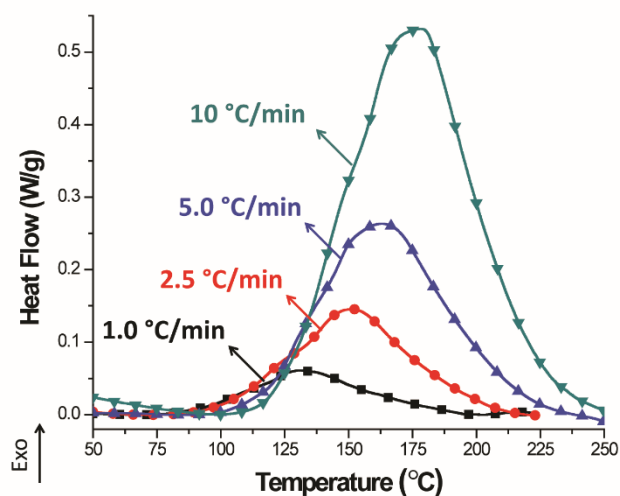
Figure 2.4. DSC curves of S5 at a series of heating rates: 1, 2.5, 5, 10 °C/min

Figure 2.5 shows representative heat flow curves of different samples using a 2.5 °C/min heating rate. Looking at this figure, multiple exothermic peaks are observed for every sample, and they are more pronounced for samples with 2% catalyst loading (S1, S2, and S3) as displayed in Figure 2.5a. For S1, the relative height of the maximum heat flow value from the first and second exothermic peaks are different as the heating rates were varied. As the heating rate was increased from 1 to 10 °C/min, the height of the maximum heat flow from the first exothermic peak is becoming lower than the value from the second exothermic peak. This observation may indicate the intrinsic nature of the epoxy-anhydride

35

reaction, which depends on the curing process and chemical composition. In addition to the two exothermic peaks, a shoulder peak was also observed at the very beginning of the exothermic peak. These observations of multiple exothermic peaks plus a shoulder peak may indicate that the curing process undergoes multiple reaction mechanisms, either sequentially, or simultaneously. Further discussion regarding this mechanism is presented in later section.
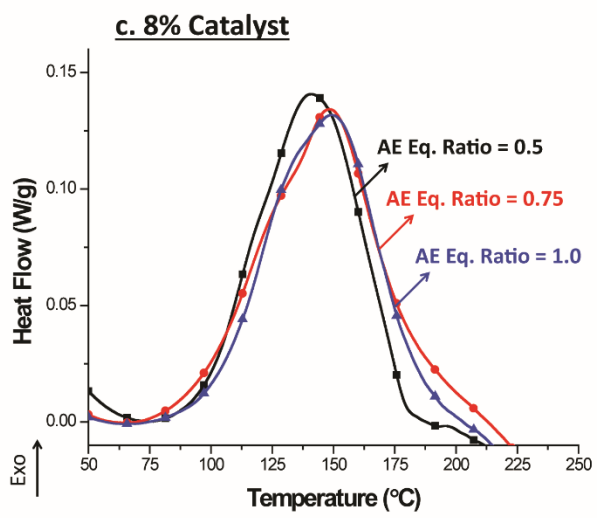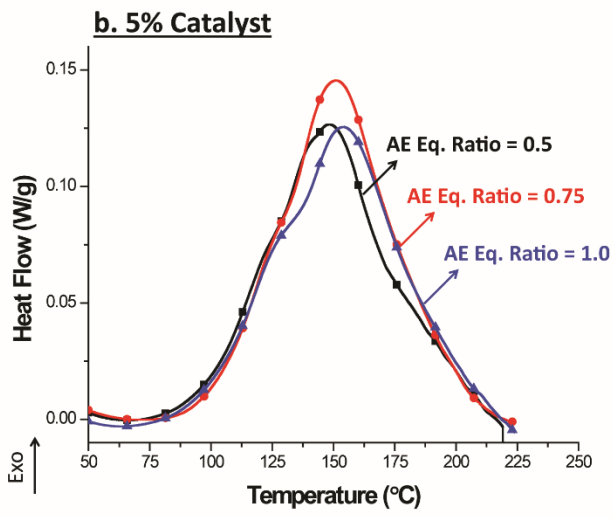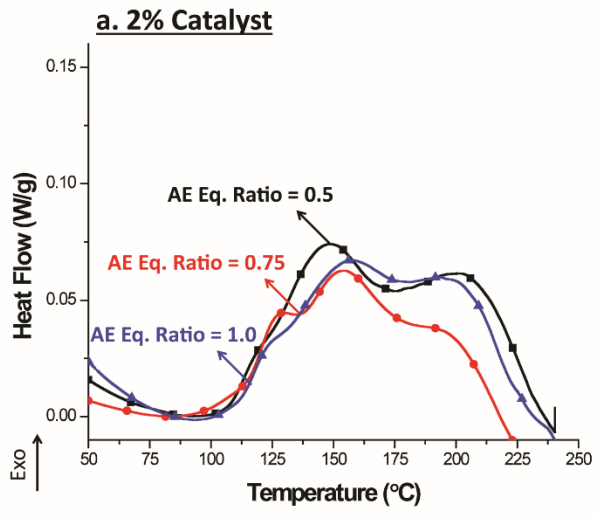
Figure 2.5. DSC curves of the samples at a heating rate of 2.5 °C/min

2.4.2.2. Activation energy

The reaction rate ($d\alpha/dt$) and the extent of cure (α_t) for the DSC non-isothermal scans was calculated using Equations 2.1 & 2.2. Then, using Equation 2.4, the overall activation energy was calculated through the Kissinger method at the maximum exothermic peak. The activation energy as a function of cure (from 0.01 – 0.99) was determined through iso-conversional Flynn-Ozawa-Wall method.. Also, the function of cure was determined through a procedure described by Malek [41]. The results are presented in Table 2.2. In this experiment, the activation energy was calculated in two ways: overall activation energy which is calculated from the degree of cure at maximum heating rate and activation energy as a function of degree of cure.

Table 2.2. Kinetic parameters determined from non-isothermal DSC scans

S #	ΔH_{Tot} (J/g)	E_a (kJ/mol)	α_{P1}	α_{P2}	α_S	α_M	Autocatalytic			RO α_P	RO
							n	m	n + m	n	n
1	150 ± 18	72.0	0.29 ± 0.03	0.80 ± 0.05	0.03 ± 0.01	0.03 ± 0.01	1.85 ± 0.4	0.07 ± 0.02	1.92 ± 0.4	3.66 ± 1.4	1.77 ± 0.4
2	106 ± 5	66.8	0.38 ± 0.05	0.85 ± 0.06	0.08 ± 0.03	0.09 ± 0.02	2.02 ± 0.4	0.19 ± 0.03	2.22 ± 0.4	3.02 ± 0.6	2.07 ± 0.6
3	132 ± 5	62.1	0.39 ± 0.05	0.79 ± 0.08	0.04 ± 0.01	0.06 ± 0.03	1.66 ± 0.4	0.11 ± 0.07	1.77 ± 0.4	2.66 ± 0.6	2.93 ± 0.4
4	178 ± 10	66.8	0.48 ± 0.04	-	0.10 ± 0.03	0.08 ± 0.01	1.74 ± 0.1	0.15 ± 0.02	1.90 ± 0.2	1.84 ± 0.4	1.60 ± 0.1
5	194 ± 3	66.7	0.49 ± 0.05	-	0.12 ± 0.01	0.09 ± 0.01	1.59 ± 0.1	0.16 ± 0.01	1.75 ± 0.1	1.76 ± 0.5	1.44 ± 0.1
6	173 ± 25	74.1	0.53 ± 0.05	-	0.13 ± 0.02	0.07 ± 0.02	1.53 ± 0.4	0.10 ± 0.01	1.63 ± 0.4	1.49 ± 0.4	1.49 ± 0.4
7	150 ± 13	78.3	0.55 ± 0.02	-	0.11 ± 0.03	0.09 ± 0.01	1.37 ± 0.1	0.14 ± 0.01	1.51 ± 0.1	1.33 ± 0.1	1.40 ± 0.4
8	182 ± 12	74.4	0.56 ± 0.01	-	0.19 ± 0.03	0.05 ± 0.03	1.42 ± 0.1	0.08 ± 0.03	1.50 ± 0.1	1.22 ± 0.1	1.22 ± 0.1
9	178 ± 5	80.2	0.58 ± 0.04	-	0.25 ± 0.02	0.08 ± 0.04	1.63 ± 0.2	0.14 ± 0.05	1.76 ± 0.3	1.16 ± 0.5	1.35 ± 0.2

First, the overall activation energy, E_a, of the reaction was calculated through the Kissinger method at temperatures where the maximum exothermic heat flow occurred. The results of the activation energy calculation from Equation 2.4 are listed in Table 2.2. The activation energy calculation through this method assumes that the degree of cure at the maximum exothermic peak is similar at different heating rates. Overall, the degree of cure at the maximum exothermic peaks ranges from 30 – 60%. Furthermore, samples with 2% catalyst loading possess multiple peaks; the second exothermic peaks were observed at approximately 80% degree of cure. It can be seen from Table 2.2 that the degree of cure values at the maximum exothermic peak at different heating rates can differ up to 10% conversion; the standard deviations for the four heating rates was found to be 1 – 7%. Using this method, the calculated activation energy was found to be between 60-80 kJ/mol, which is a typical range for common epoxy-anhydride polymerization.

The overall activation energy values can also be calculated using TA Specialty software. However, caution must be taken when using this software, especially when multiple peaks are present. The relative height of the multiple peaks may differ depending on the heating rates used, and the software may calculate the overall activation energy by using different exothermic peaks, i.e. first exothermic peak vs. second exothermic peak. This circumstance may happen because the software only determines one temperature where the maximum heat flow occurs, disregarding the fact that they may lie on different peak regions. As mentioned earlier, S1 has multiple peaks with different relative heights of its first vs. second exothermic peaks, which are dependent on the applied heating rate. Using the software, the activation energy is calculated using two degree of cure regions ($\alpha \approx 0.3$ and $\alpha \approx 0.8$). However, despite this occurrence, the linear fitting of $d(\ln(\beta/T_p{}^2))$ vs. $d(1/T_p)$ still shows an R^2 value of higher than 98%. This discrepancy can lead to misunderstanding on the assumption where the first-order reaction was still maintained. It will be shown in later section later that even though the R^2 value of the linear fitting is higher than 98%, the actual curve fitting itself does not represent the obtained data very well.

Using Equation 2.7, the activation energies of the reactions were also calculated as a function of cure, from $\alpha = 0.01$ through $\alpha = 0.99$ with 0.05 increments. The result is shown in Figure 2.6. It can be seen that the activation energy changes throughout the curing process. Significant changes are observed at the degree of cure where the shoulder and maximum exothermic peaks occurs. The samples

with 2% catalyst (S1, S2, and S3) show an initial decrease in the activation energy, but then the values start to increase at 0.4 degree of cure. In contrast, the activation energy value of samples with 5% and 8% catalyst (S4 – S9) showed an increasing value throughout the curing process. Interestingly, the activation energy of S9 showed a large increase at the beginning of the reaction up to $\alpha = 0.75$, followed by a large decrease at the end of the reaction. On the whole, the activation energy values are ranging from 60 – 120 kJ/mol which agrees with activation energy values found in the literature for both epoxy homopolymerization and epoxy-anhydride copolymerization with metal complex as the catalyst [31, 32, 47-50]. Overall, the amount of catalyst showed more of an effect on the curing reactions. Yet, the effect of AE molar ratio may depend on the catalyst content in the reaction, and thus the activation energy value depends on both the AE ratio and the catalyst amount.
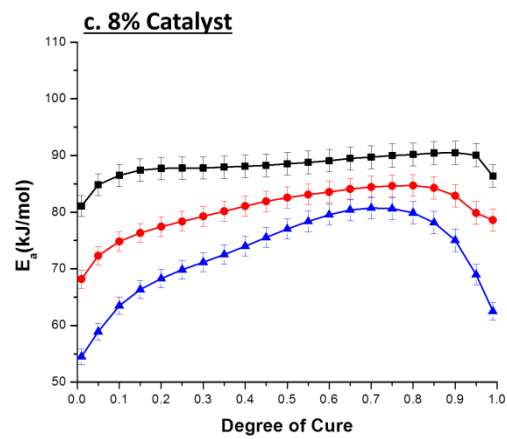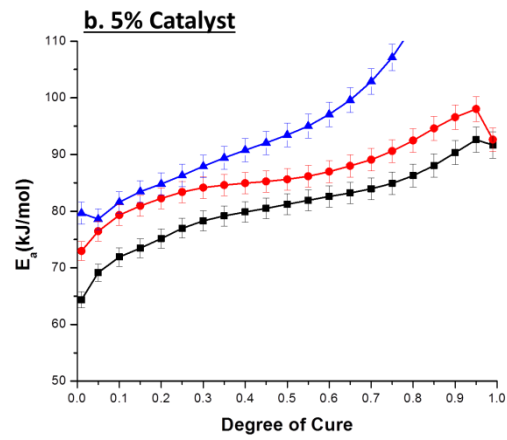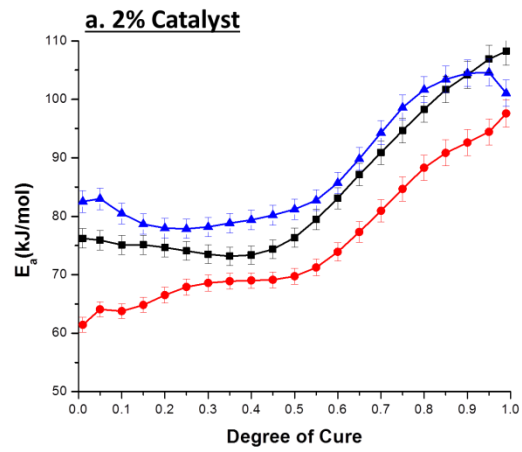
Figure 2.6. Activation energy of epoxy-anhydride reaction as function of cure

2.4.3. Possible curing mechanisms

Based on the observations above, it can be suggested that the reaction mechanism is influenced by both the catalyst amount and the AE molar ratio. The appearance of multiple exothermic peaks is believed to indicate different initiation mechanisms, instead of two types of polymerization reactions (polyesterification vs. polyetherification). The actual reaction mechanisms are hard to determine since the exact ligands of the metal complex are unknown. However, a Fourier-Transform infrared spectroscopy spectrum of the catalyst indicates the presence of amine-based ligands (1045 cm-1 C-N stretch and 3400-3300 cm-1 NH stretch) and carboxyl diluents (1699 cm-1 C=O stretch and broad 3300 – 2500 cm-1OH stretch) [51]. Therefore, the epoxy-anhydride reaction may be initiated through three possible reaction mechanisms: metal coordination, reaction with carboxylate diluents or reaction with amine-based ligands.

The first and the second mechanisms are believed to involve simultaneous initiation by carboxylate ligands and metal coordination. As energy is given to the system, the carboxylate ligands are released. Thus, the carboxylate ligands may initiate the reaction by ring-opening the epoxy functionalities and forming an alkoxide. The alkoxide then reacts with the cyclic anhydride to form carboxylate. Subsequently, the chain polymerization continues. The removal of carboxylate ligands may change the metal coordination of zinc complex from hexadentate to tetradentate, which allows anhydride and/or epoxy to complex with the metal atom. This coordination results in ring-opening of the anhydride and/or the epoxy, and re-conversion of tetradentate coordination into hexadentate [52].

The third mechanism is suggested from the reaction of anhydride and/or epoxy with the amine-based ligands. The ligands can be dissociated from the metal complex as more energy is given. The activation energy involving this initiation mechanism is predicted to be higher than the first one, therefore increasing the activation energy.

The dissociation of ligands in the zinc complex may happen in an equilibrium state, and a higher amount of catalyst shifts the equilibrium toward greater ligand dissociation. Consequently, there may be carboxylate ligands, tetradentate metal coordination, and loose amino ligands present right before the curing is started. Therefore, when a lower amount of catalyst is used, the three mechanisms may happen in different stages, thus multiple exothermic peaks in the heat flow curves were observed. In comparison,

when higher amount of catalyst used, the three initiation mechanisms may occur simultaneously and thus there was only one distinct exothermic peak observed.

2.4.4. Reaction kinetic model fitting

The rate of epoxy-anhydride reaction is often assumed to follow an Arrhenius temperature-dependent rate equation, and its function of cure can be fitted as either a reaction order (RO) or autocatalytic model (SB or Sestak-Berggren) [53, 54]. RO and SB models differ on when the maximum rate of heat evolution occurs. For the RO model, the maximum rate of heat evolution occurs at the beginning of a reaction, where $\alpha \approx 0$. In contrast, for an autocatalytic reaction, the maximum rate of heat evolution occurs at $\alpha > 0$ because one of the products is a reactant which can catalyze the reaction. In the case of the epoxy-anhydride reaction, one of the products is a hydroxyl functional group and this hydroxyl group may catalyze the reaction.

To determine whether the samples undergo RO or autocatalytic reaction, a procedure described by Malek was followed [41]. This procedure was used to find the α value where the maximum rate of heat evolution occurs. Table 2.2 shows that the average value for α ranges from 0.03 – 0.09, with standard deviation of 0.01 – 0.04. Malek suggested that a curing reaction can be considered to be an autocatalytic reaction if $0 < \alpha_M < \alpha_{P\infty}$; note that he also suggested the α_M to be equal or greater than 0.05 to anticipate the calculation error. For the samples described in this paper, the α_M values range from 0.03 – 0.09, making it borderline between the RO and autocatalytic process. Thus, the reaction rate of all of the samples will be fitted to both RO and autocatalytic process to obtain other kinetic parameters such as the reaction orders and pre-exponential factor. Following the Malek procedure, the reaction rate was fitted to an autocatalytic kinetic model at $\alpha = 0.2 – 0.8$, and to an RO kinetic model at $\alpha = \alpha_P$ ($RO_{\alpha P}$). For a fair comparison, the reaction rate was also fitted to an RO model at $\alpha = 0.2 – 0.8$ (RO_α). Please note that for samples with a 2% catalyst level (S1, S2, and S3), each exothermic peak was fitted individually. In addition to the autocatalytic and RO kinetic models, the reaction rate was also fitted to a first-order kinetic model obtained from the TA Specialty software. Table 2.2 lists the reaction kinetic order, while Figure 2.7 show the examples of how the obtained data fits the kinetic model.

First, as seen in Table 2.2, the values of reaction order n in the RO kinetic model and $m+n$ in the autocatalytic model are fairly similar, with the exception of samples with two exothermic peaks.

Furthermore, the values of reaction order m are moderately small, therefore the values of α^m are close to 1. This observation may indicate that the contribution of the autocatalytic reaction, i.e. the hydroxyl functional group catalyzing the epoxy-anhydride reaction, in the curing mechanism is fairly insignificant. That is also to say that the non-autocatalytic reaction, i.e. chain polymerization through alkoxide and carboxylate, dominates the curing process.

Figure 2.7 compares how well the different kinetic models fit with the original data from S5 (representing samples with catalyst amount of 5 & 8%, S4-S9). As seen in this figure, the autocatalytic and RO_α kinetic model fits the data well. In contrast, the results from $RO_{\alpha P}$ kinetic model deviate slightly from the original value: the reaction rate value is higher than original data before peak temperature, T_P, and lower than the original data after T_P. Figure 2.7 also shows that the first-order reaction model (RO, n = 1) calculation from the TA Specialty Software did not fit the original data well, where the calculated values are much higher than the original data.
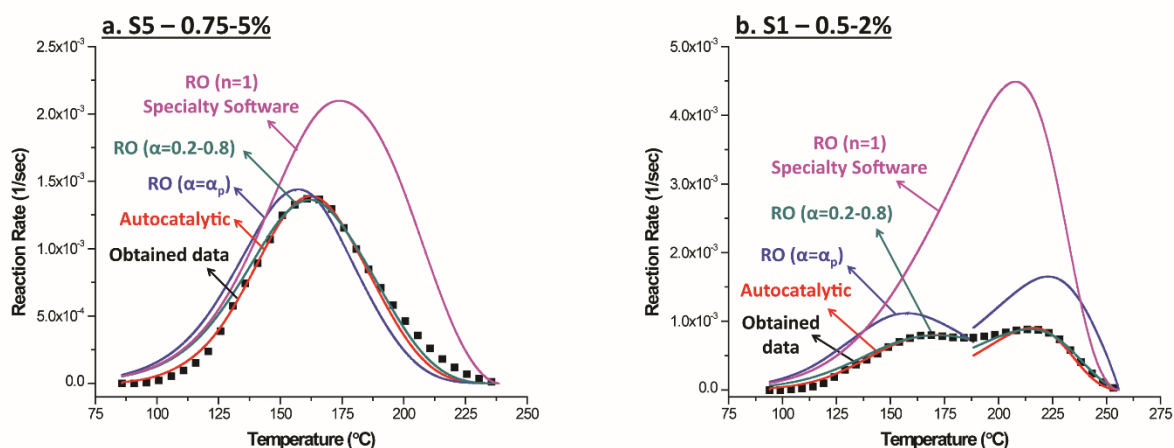
Figure 2.7. Reaction rate vs. temperature of S5 and S1: Obtained vs. fitted kinetic models

Similar observations are also noticed with reaction kinetic model fitting for samples with the 2% catalyst, shown in Figure 2.7 for S1. Two exothermic peaks were fitted individually using two different reaction kinetic models. The autocatalytic and RO_α kinetic models fit the data well with the exception of transition areas between the exothermic peaks. For these samples, the reaction order values for RO and autocatalytic models differ slightly, yet they are still within the standard deviations. However, note that the standard deviations for these samples are higher compared to samples with higher catalyst amount (S4-S9). Furthermore, Figure 2.7 shows that the first-order kinetic model did not fit the reaction rate data.

2.5.   Conclusion

Epoxidized sucrose soyate, a novel bio-based resin, was successfully crosslinked with methyl hexahydrophthalic anhydride with zinc catalyst to form a thermoset polymer. The curing kinetics of the thermoset system was studied as a function of composition variables, i.e. anhydride-to-epoxy molar ratio and catalyst amount. The kinetic parameters for the ESS-MHHPA reaction were obtained using differential scanning calorimetry. Based on the observation in the heat flow curves and activation energy values, the reaction mechanism may change as a function of the amount of catalyst, while the anhydride-to-epoxy molar ratio may have an insignificant influence. Furthermore, as with any other epoxy-anhydride reaction, the reaction kinetics was found to be fairly complex and does not follow a first-order reaction. Instead, the curves of reaction rate vs. temperature were fitted best to reaction order and autocatalytic kinetic model. Additionally, based on the reaction order values in the reaction order and autocatalytic kinetic model, it is suggested that epoxy-anhydride curing of ESS and MHHPA is dominated by the non-autocatalytic reaction (i.e. alternating addition of epoxy/anhydride through alkoxide/carboxylate end group) and the contribution of autocatalytic reaction (i.e. the reaction acceleration from hydroxyls or carboxylic acid formation) is minimal.

2.6.   Acknowledgements

2.7.   References

[1]   B.E. Dale, 'Greening' the chemical industry: research and development priorities for biobased industrial products, Journal of Chemical Technology & Biotechnology, 78 (2003) 1093-1103.

[2]   R. Hatti-Kaul, U. Törnvall, L. Gustafsson, P. Börjesson, Industrial biotechnology for the production of bio-based chemicals – a cradle-to-grave perspective, Trends in Biotechnology, 25 (2007) 119-124.

[3]   R. Auvergne, S. Caillol, G. David, B. Boutevin, J.-P. Pascault, Biobased Thermosetting Epoxy: Present and Future, Chemical Reviews, 114 (2013) 1082-1115.

[4]   J.M. Raquez, M. Deléglise, M.F. Lacrampe, P. Krawczak, Thermosetting (bio)materials derived from renewable resources: A critical review, Progress in Polymer Science, 35 (2010) 487-509.

[5]   S.G. Tan, W.S. Chow, Biobased Epoxidized Vegetable Oils and Its Greener Epoxy Blends: A

        Review, Polymer-Plastics Technology and Engineering, 49 (2010) 1581-1590.

[6]   S. Miao, P. Wang, Z. Su, S. Zhang, Vegetable-oil-based polymers as future polymeric

        biomaterials, Acta Biomaterialia, 10 (2014) 1692-1704.

[7]   C. Ding, A.S. Matharu, Recent Developments on Biobased Curing Agents: A Review of Their

        Preparation and Use, ACS Sustainable Chemistry & Engineering, 2 (2014) 2217-2236.

[8]   Z. Liu, G. Kraus, Green Materials from Plant Oils, RSC Green Chemistry ed., Royal Society of

        Chemistry, Cambridge, UK, 2014.

[9]   M.A. Mosiewicki, M.I. Aranguren, A short review on novel biocomposites based on plant oil

        precursors, European Polymer Journal, 49 (2013) 1243-1256.

[10]   Y. Xia, R.C. Larock, Vegetable oil-based polymeric materials: synthesis, properties, and

        applications, Green Chemistry, 12 (2010) 1893-1909.

[11]   G. Lligadas, J.C. Ronda, M. Galià, V. Cádiz, Renewable polymeric materials from vegetable oils:

        a perspective, Materials Today, 16 (2013) 337-343.

[12]   P. Mohan, A Critical Review: The Modification, Properties, and Applications of Epoxy Resins,

        Polymer-Plastics Technology and Engineering, 52 (2013) 107-125.

[13]   N.R. Paluvai, S. Mohanty, S.K. Nayak, Synthesis and Modifications of Epoxy Resins and Their

        Composites: A Review, Polymer-Plastics Technology and Engineering, 53 (2014) 1723-1758.

[14]   X. Pan, P. Sengupta, D.C. Webster, Novel biobased epoxy compounds: epoxidized sucrose

        esters of fatty acids, Green Chemistry, 13 (2011) 965-975.

[15]   X. Pan, P. Sengupta, D.C. Webster, High biobased content epoxy-anhydride thermosets from

        epoxidized sucrose ester of fatty acids, Biomacromolecules, 12 (2011) 2416-2428.

[16]   X. Pan, D.C. Webster, New Biobased High Functionality Polyols and Their Use in Polyurethane

        Coatings, ChemSusChem, 5 (2012) 419-429.

[17]   T. Nelson, T. Galhenage, D. Webster, Catalyzed crosslinking of highly functional biobased epoxy

        resins, J Coat Technol Res, 10 (2013) 589-600.

[18]   T. Nelson, B. Masaki, Z. Morseth, D. Webster, Highly functional biobased polyols and their use in

        melamine–formaldehyde coatings, J Coat Technol Res, 10 (2013) 757-767.

[19]   T.J. Nelson, L. Bultema, N. Eidenschink, D.C. Webster, Bio-Based High Functionality Polyols and Their Use in 1K Polyurethane Coatings, Journal of Renewable Materials, 1 (2013) 141-153.

[20]   X. Pan, D.C. Webster, Impact of Structure and Functionality of Core Polyol in Highly Functional Biobased Epoxy Resins, Macromolecular Rapid Communications, 32 (2011) 1324-1330.

[21]   C. Taylor, T. Krosbakken, C.A. Ulven, A. Paramarta, D.C. Webster, Structural quality biocomposites of treated flax fiber with epoxidized sucrose soyate resin, in: International Conference on Composite Materials, Montreal, Canada, 2013.

[22]   W. Fisch, W. Hofmann, J. Koskikallio, The curing mechanism of epoxy resins, Journal of Applied Polymer Science, 6 (1956).

[23]   E.C. Dearborn, R.M. Fuoss, A.K. MacKenzie, R.G. Shepherd, Epoxy resins from bis-, tris-, and tetrakisglycidyl etheres, Industrial and Engineering Chemistry, 45 (1953) 2715-2721.

[24]   L.A. O'Neill, C.P. Cole, Chemical and spectroscopic studies of epoxy resin reactions in the surface coating field, Journal of Applied Chemistry, 6 (1956) 356-364.

[25]   R. Wegler, Chemie der polyepoxyde, Angewandte Chemie, 67 (1955) 582-592.

[26]   R.F. Fischer, Polyesters from epoxides and anhydrides, Industrial and Engineering Chemistry, 52 (1960) 321-323.

[27]   Y. Tanaka, H. Kakiuchi, Study of epoxy compounds. Part VI. Curing reactions of epoxy resin and acid anhydride with amine, acid, alcohol and phenol as catalysts, Journal of Polymer Science: Part A, 2 (1964) 3405-3430.

[28]   Y. Tanaka, H. Kakiuchi, Study of epoxy compounds. Part I. Curing reactions of epoxy resin and acid anhydride with amine and alcohol as catalyst, Journal of Applied Polymer Science, 7 (1963) 1063-1081.

[29]   J. Luston, F. Vass, Anionic copolymerization of cyclic etehrs with cyclic anhydrides, Advances in Polymer Science, 56 (1984) 91-133.

[30]   H. Starck, F. Sclenker, Epoxy resin compositions cured with metalic salts of enol-keto tautomeric compounds, in: United States Patent Office, Chemische Werke Albert, Germany, 1957.

[31]   Z. Zhang, C.P. Wong, Study on the catalytic behavior of metal acetylacetonates for epoxy curing reactions, Journal of Applied Polymer Science, 86 (2002) 1572-1579.

[32]   Z. Zhang, C.P. Wong, Study on Metal Chelates as Catalysts of Epoxy and Anhydride Cure

Reactions for No-Flow Underfill Applications, in: Polymers for Microelectronics and

Nanoelectronics, American Chemical Society, 2004, pp. 264-278.

[33]   Z.Q. Zhang, S.H. Shi, C.P. Wong, Development of no-flow underfill materials for lead-free solder

bumped flip-chip applications, in: Advanced Packaging Materials: Processes, Properties

andInterfaces, 2000. Proceedings. International Symposium on, 2000, pp. 278-284.

[34]   J.D.B. Smith, R.N. Kaufmann, Fluid solventless epoxy-anhydride compositions containing metal

acetylacetonate accelerators and organic carboxilic acid co-accelerators, in: United States

Patent, Westinghouse Electric Corp., United States, 1978.

[35]   L.S. Frankel, Uses of chelated metal catalysts for acid/epoxy polymer system, in: U.S. Patent

(Ed.), Rohm and Hass Company, United States, 1980.

[36]   J.D.B. Smith, R.N. Kauffman, Carboxylic acid storage stabilizers for latent catalyst cured epoxy

resin, in: United States Patent, Westinghouse Electric Corporation, United States, 1977.

[37]   C.P. Wong, S.H. Shi, G. Jefferson, High performance no-flow underfills for low-cost flip-chip

applications: material characterization, Components, Packaging, and Manufacturing Technology,

Part A, IEEE Transactions on, 21 (1998) 450-458.

[38]   I. Hamerton, B.J. Howlin, P. Jepson, Metals and coordination compounds as modifiers for epoxy

resins, Coordination Chemistry Reviews, 224 (2002) 67-85.

[39]   E.M. Monono, D.C. Webster, D.P. Wiesenborn, Pilot scale (10 kg) production and

characterization of epoxidized sucrose soyate, Industrial Crops and Products, 74 (2015) 987-997.

[40]   H.E. Kissinger, Reaction Kinetics in Differential Thermal Analysis, Analytical Chemistry, 29 (1957)

1702-1706.

[41]   J. Málek, The kinetic analysis of non-isothermal data, Thermochimica Acta, 200 (1992) 257-269.

[42]   A Review of DSC Kinetics Method, in, TA Instrument, 2014.

[43]   A. Omrani, M. Ghaemy, A.A. Rostami, Curing Behavior of Epoxy Resin Using Controllable Curing

Agents Based on Nickel Complexes, Macromolecular Materials and Engineering, 291 (2006) 181-

193.

[44]   K. Mészáros Szécsényi, V.M. Leovac, Ž.K. Jaćimović, V.I. Češljević, A. Kovács, G. Pokol, S. Gál,
        Transition Metal Complexes with Pyrazole-based Ligands. Part 8. Characterization and thermal
        decomposition of zinc(II) complexes with di- and trisubstituted pyrazoles, Journal of Thermal
        Analysis and Calorimetry, 63 (2001) 723-732.

[45]   K. Mészáros Szécsényi, V.M. Leovac, Ž.K. Jaćimović, V.I. Češljević, A. Kovács, G. Pokol,
        Transition Metal Complexes with Pyrazole-based Ligands. Part 12. Characterisation and thermal
        decomposition of CuCl2 complexes with di- and trisubstituted pyrazoles, Journal of Thermal
        Analysis and Calorimetry, 66 (2001) 573-581.

[46]   A. Ručigaj, B. Alič, M. Krajnc, U. Šebenik, Investigation of cure kinetics in a system with reactant
        evaporation: Epoxidized soybean oil and maleic anhydride case study, European Polymer
        Journal, 52 (2014) 105-116.

[47]   M. Ghaemy, A. Omrani, A.A. Rostami, Study of reaction kinetics of epoxy and a nickel(II) complex
        using dynamic DSC technique, Journal of Applied Polymer Science, 97 (2005) 265-271.

[48]   A. Omrani, M. Ghaemy, A.A. Rostami, Thermosetting polymers from epoxy resin and a Nickel
        catalyst of diethylenetriamine, Journal of Thermal Analysis & Calorimetry, 98 (2009) 477-483.

[49]   A.A. Lugovaya, V.M. Mikhal'chuk, V.A. Beloshenko, D.V. Gurtovoi, Effect of Cr(III), Fe(III), Co(III),
        and Ni(II) acetylacetonates on the formation and thermal oxidative degradation of epoxy-
        anhydride polymers and composites, Russ J Appl Chem, 81 (2008) 2002-2007.

[50]   Y. Zheng, K. Chonung, X. Jin, P. Wei, P. Jiang, Study on the curing reaction, dielectric and
        thermal performances of epoxy impregnating resin with reactive silicon compounds as new
        diluents, Journal of Applied Polymer Science, 107 (2008) 3127-3136.

[51]   A.Paramarta, D.C. Webster, Bio-based high performance epoxy-anhydride thermosets for
        structural composites: The effect of composition variables, Reactive and Functional Polymers,
        105 (2016) 140-149.

[52]   N. Chantarasiri, N. Sutivisedsak, C. Pouyuan, Thermally stable metal-containing epoxy polymers
        from an epoxy resin-Schiff base metal complex-maleic anhydride system, European Polymer
        Journal, 37 (2001) 2031-2038.

[53]   J. Šesták, G. Berggren, Study of the kinetics of the mechanism of solid-state reactions at increasing temperatures, Thermochimica Acta, 3 (1971) 1-12.

[54]   J. Sestak, Science of Heat and Thermophysical Studies: A Generalized Approach to Thermal Analysis, Elsevier Science, 2005.

CHAPTER 3. BIO-BASED HIGH PERFORMANCE EPOXY-ANHYDRIDE THERMOSETS FOR STRUCTURAL COMPOSITES: THE EFFECT OF COMPOSITION VARIABLES

3.1. Abstract

The structure-property relationships of a designed series of anhydride-cured epoxidized sucrose soyate (ESS) thermosets were studied. Epoxidized sucrose soyate is a novel bio-based epoxy resin derived from sucrose and soybean oil fatty acids, and it contains an average of 12 epoxy functional groups per molecule. This epoxy resin was crosslinked with methyl hexahydrophthalic anhydride to form polyester thermosets with high crosslink density, and a zinc-complex catalyst was used. In this study, the impact of composition variables—anhydride-to-epoxy molar ratio and catalyst amount—on the chemical, mechanical, and thermal properties of the thermosets were examined. All of the thermoset samples had very high gel fraction, which indicated excellent network connectivity. Samples made using an equimolar ratio of anhydride-to-epoxy groups had lower conversion of functional groups as shown by the somewhat lower gel fraction and higher moisture absorption. Analysis of the thermomechanical and tensile properties of the thermosets suggests that there is a factor interaction between anhydride-to-epoxy molar ratio and catalyst amount. Furthermore, the results suggest that the molecular networks of the thermoset samples are fairly complex due to the simultaneous competing reactions between catalyst-initiated epoxy-anhydride, hydroxyl- initiated epo xy-anhydride, and epoxy homopolymerization.

3.2. Introduction

In the recent decade, due to the uncertainty of the cost and supply of petrochemicals, more and more research has been devoted to the development of vegetable oils as a chemical commodity [1-6]. Vegetable oils offer promising potential in replacing petrochemicals in some applications due to their relatively low cost, abundant availability, and greater sustainability. The use of vegetable oils as a chemical commodity is in fact not a new concept. Vegetable oils such as linseed oil, tung oil, and soybean oil have been used for centuries in paints and coatings applications, such as in atist's paints and varnishes. The application of these vegetable oils as coatings still exists until today. Currently, about 17 million tons of vegetable oils go toward the synthesis of chemicals and materials; this is about 15% by weight of the total annual production of vegetable oils, and the value is estimated to grow at about 3.3%

per year [7, 8]. Furthermore, the use of vegetable oils has been broadened to many more fields, such as

biofuels, lubricants, surfactants, and structural composites [1].

Chemically, vegetable oils are the triglycerides or glycerol esters of fatty acids. Vegetable oils

from different plant sources contain unique fatty acids compositions, with many vegetable oils containing

a significant fraction of unsaturated fatty acids. Polymerization of vegetable oils is possible through the

unsaturation in the fatty acid chains, and the degree of unsaturation dictates the reactivity of a particular

vegetable oil. The unsaturation can lead to polymerization through auto-oxidation using metal catalysts

[9]. However, this crosslinking route often takes an extensive period of time for the materials to fully cure.

One popular modification of vegetable oils is the epoxidation of the double bonds, which then provides

access to many crosslinking technologies, such as epoxy homo-polymerization and copolymerization with

amines or acid/anhydrides. Furthermore, the epoxy functionality can be ring opened with acids or

alcohols to introduce other functional groups. For example, epoxy groups can be reacted with acrylic or

methacrylic acid to provide terminal double bond functionality, which can then be polymerized under ultra-

violet light and/or thermal exposure to form crosslinked materials [10-13]. In addition, epoxy groups may

be reacted with alcohol to introduce hydroxyl functional groups, which then can be crosslinked with either

isocyanates to produce polyurethanes or with melamine formaldehyde resins [7, 8, 14-17].

As mentioned before, epoxy groups can be polymerized through crosslinking with either amines

or acid/anhydride groups. Between these two potential crosslinkers, the acid/anhydride hardener is the

main curing agent used for epoxidized vegetable oils for two reasons. First, epoxy groups in the fatty

acids are internal epoxides, and thus they are less reactive compared to terminal epoxides. This low

reactivity leads to low polymerization efficiency when crosslinked with amine hardeners. Second, during

the reaction between epoxidized vegetable oils with amine hardeners, there is possibility of de-

esterification of the fatty acid chain through an ester-aminolysis reaction to form amide bonds and

alcohols as a by-product [18].

The reaction of epoxides and anhydrides are known to be complex due to many simultaneous

reactions. The reaction can undergo both catalyzed and non-catalyzed processes. An uncatalyzed

reaction pathway may be possible due to the presence of hydroxyl groups on the epoxy resins or from

impurities in the raw materials. However, in most cases, the use of catalyst is necessary to ensure an

efficient polymerization [19-22]. Catalysis of epoxy-anhydride reactions is often performed with Lewis

base catalysts such as tertiary amines, amidines, quaternary onium salts, or metal salts. These catalysts

initiate the polymerization reaction through nucleophilic attack on the epoxy and/or anhydride, and then

form a zwitterionic alkoxide and/or carboxylate anion [23]. These anions then become the active group

and propagate the polymer chain by further reaction with anhydride and/or epoxy groups. Scheme 3.1

illustrates the two reaction mechanisms. The difference between these mechanisms lies in the initiation

mechanism and active end group of the polyester chain. For both mechanisms, the propagation

reactions have been suggested to occur in an alternating fashion, therefore the bulk of the thermoset

should contain polyester linkages. However, the polyetherification side reaction is possible due to

homopolymerization of epoxy groups; the extent of polyetherification that occurs depends on the type and

amount of catalyst used in the curing formulation.
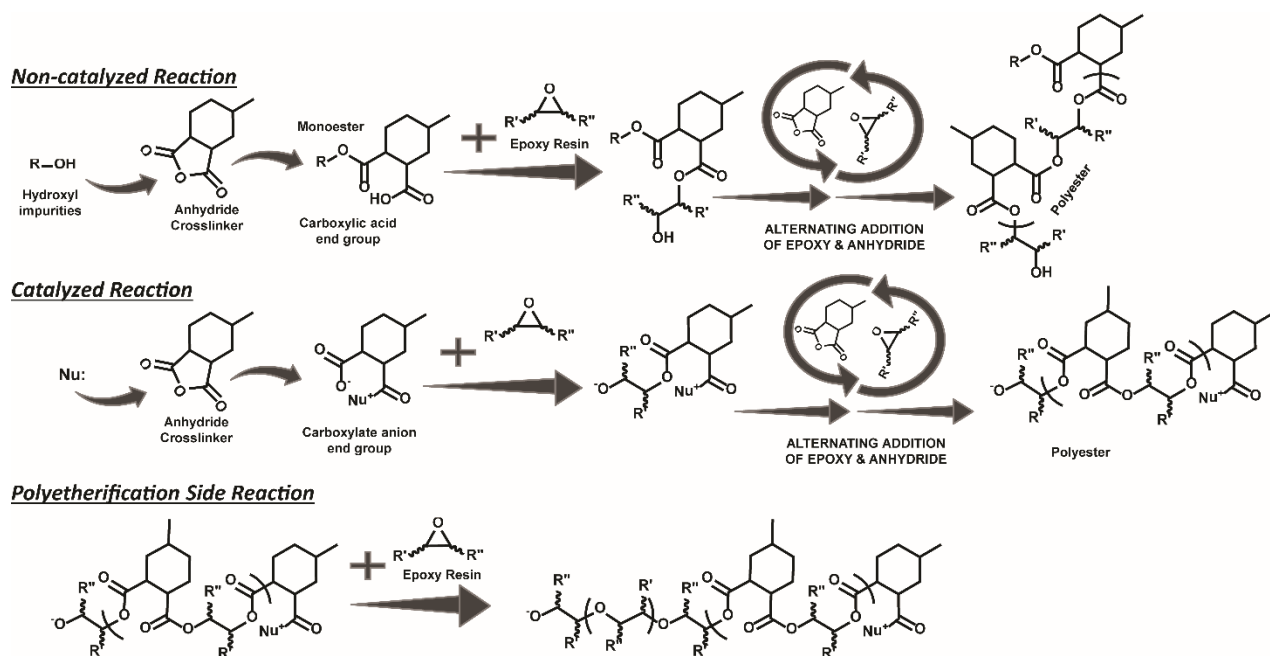
Scheme 3.1. Reaction mechanism of epoxy and anhydride curing

In the recent decade, there has been extensive research dedicated to the development of fiber

reinforced polymer (FRP) composites using bio-based thermosets as the matrix resin [24-29]. For an

application intended for structural parts that requires high performance properties, it is necessary that the

thermoset has high crosslink density and glass transition temperature (T_g) so that it can efficiently transfer

and distribute stress amongst the reinforcement without the initiation of cracks [30]. Unfortunately, most

of the thermosets based on anhydride-cured epoxidized vegetable oils (EVOs) generally have low crosslink density and T_g. Therefore, FRP composites based on pure anhydride-cured EVOs are typically employed for situations that do not require high performance [31-33]. For use in structural FRP composites, EVOs are often blended with petrochemical-based epoxy resins such as the diglycidyl ether of bisphenol A (DGEBA) to enhance the strength and toughness of the final product [30, 34]. In spite of this, the amount of DGEBA added to EVO must be carefully considered to ensure achieving optimum curing time, modulus, T_g, thermal stability, and chemical resistance. Often, DGEBA resin is used at concentrations of >60% of total weight, so that the final thermoset has comparable properties to the neat DGEBA polymers. Yet, at this concentration, the final product would have significantly lower bio-based content.

An improved bio-based epoxy resin derived from vegetable oil has recently been developed [35]. This epoxy resin is named epoxidized sucrose ester (ESE), and a representative chemical structure is shown in Figure 3.1. ESE resins are made by esterifying vegetable oil fatty acids onto the hydroxyl groups of sucrose, followed by epoxidation of the double bonds. Thermosets based on ESEs have significantly higher strength and T_g compared to EVO-based materials [36]. The improvement in the mechanical properties has been attributed to the rigidity of the sucrose core and the higher crosslink density due to more epoxy functional groups per molecule [36]. The number of the epoxy groups in the ESE depends on the type of fatty acids in the molecule. Anhydride-cured thermosets based on ESE have been shown to have good mechanical properties for coatings applications [24, 37]. Based on this result, therefore, the thermoset has excellent potential to be used as a matrix resin for FRP composites. Furthermore, in order to be able to achieve the best possible properties, it is important to understand the effect of composition variables of the matrix resin itself on the thermoset properties.
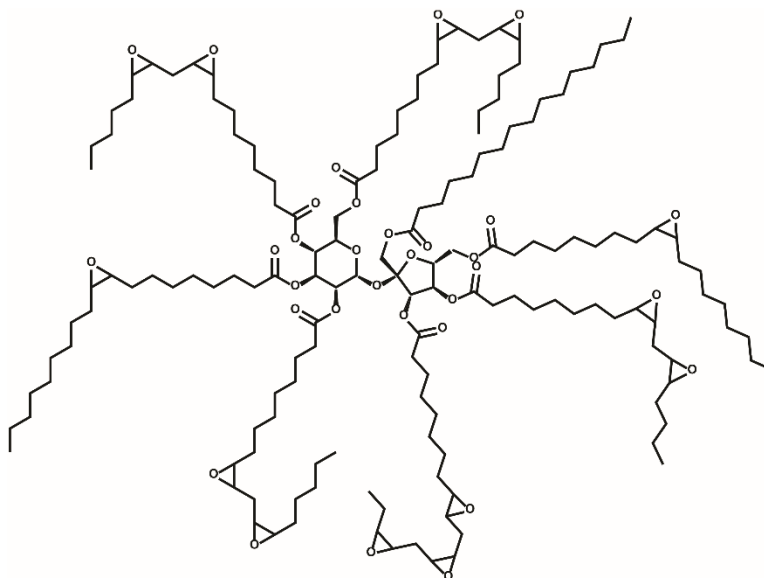
Figure 3.1. Representative chemical structure of epoxidized sucrose ester

In this study, the properties of anhydride-cured epoxidized sucrose soyate (ESS) are explored as a function of its composition variables, *i.e.* anhydride-to-epoxy equivalent ratio and catalyst amount. A good understanding of the structure-property relationships is critical when designing FRP composites for various applications. The properties assessed include sol/gel fraction, T_g and crosslink density, tensile properties, and moisture uptake.

3.3. Experimental

3.3.1. Materials, polymer composition, and cure procedure

Epoxidized sucrose soyate (ESS) was synthesized from sucrose soyate through the Prilezhaev reaction [35, 38]. The epoxy equivalent weight of the ESS resin was analyzed through hydrogen bromide titration, and the value was determined to be 250 g/mol. A liquid aliphatic anhydride, methyl hexahydrophthalic anhydride (MHHPA), was chosen as the crosslinker in this study; it was provided by Dixie Chemicals. The zinc-complex catalyst, CXC-1765®, was provided by King Industries. The thermoset polymer composition was varied based on the anhydride-to-epoxy (AE) molar ratio and the catalyst amount. The AE molar ratio was chosen to be 0.5, 0.75, and 1.0, while the catalyst amount was chosen to be 2, 5, and 8% of total weight of ESS and MHHPA; therefore, there is a total of nine formulations. The composition of these nine formulations is listed in Table 3.1.

To prepare the thermosets, first, ESS and MHHPA were mixed at 50 °C for 1 hour. Then, the catalyst was added gradually to the mixture over a 1-hour period. The epoxy-anhydride formulation mixtures were cured in a Teflon mold sandwiched between aluminum sheets. The formulation was cured in two stages: first stage involves curing at 120 °C for 1 hour, and then followed by curing at 150 °C for 3 hours.

Table 3.1. Polymer compositions

Sample #	AE Molar Ratio	AE Weight Ratio	Catalyst (% wt. total)
S1	0.5	0.32	2
S2	0.5	0.32	5
S3	0.5	0.32	8
S4	0.75	0.48	2
S5	0.75	0.48	5
S6	0.75	0.48	8
S7	1.0	0.65	2
S8	1.0	0.65	5
S9	1.0	0.65	8

3.3.2. Fourier-Transform infrared spectroscopy

FTIR analysis was performed using a Thermo Scientific Nicolet 8700 FTIR spectrometer using a potassium bromide crystal. The cured thermosets were characterized by Attenuated Total Reflectance-FTIR (ATR-FTIR) spectroscopy using a Bruker Vertex 70 HTS-XT equipped with Pike MiRacle (zinc selenide crystal plates). This crystal has a penetration depth of 2.00 µm at 45°. For both transmission and reflectance FTIR, the spectra acquisition was based on 32 scans with data spacing of 4.0 cm^{-1}.

3.3.3. Soxhlet extraction

Solvent extraction of the epoxy-anhydride thermosets was carried out using acetone (BP = 56 °C). Soxhlet extraction was conducted for partially and fully cured thermoset samples. For partially cured samples (cured at 120 °C for 1 hour), the samples were extracted for 6 hours. For fully cured samples, the samples were extracted for 17 hours. The gel content of the thermoset samples was calculated by the weight percentage of the remaining material compared to the total initial weight. Furthermore, chemical analysis of the sol content was conducted by transmission FTIR spectroscopy.

3.3.4. Moisture uptake

Water absorption measurements were conducted through a gravimetric process. The shape of the thermoset sample was a circular disk with 40 mm diameter × 2 mm thickness. The specimens were

fully immersed in deionized water at room temperature (19 °C). The weight of the specimens was

measured after 1 week and 1 month of immersion.

3.3.5. Dynamic mechanical analysis

Thermo-mechanical properties of the thermosets were characterized using dynamic mechanical

analysis (DMA) equipped with a 3-point bending clamp. The instrument used is a Q800 DMA from TA

Instruments. The sample size was 50 mm × 10 mm × 3 mm. The sample was heated from -100 °C –

200 °C at a heating rate of 5 °C/min and a frequency of 1 Hz. The glass transition temperature (T_g) was

determined as the temperature of the tan δ maximum.

3.3.6. Tensile testing

Tensile testing of the bio-based thermosets was conducted using an Instron 5567 load frame with

a 2 kN load cell at a rate of 5mm/min. The specimen shape is a dogbone style Type 1 based on ASTM

D638, with thickness of 3.4 mm and width of 10 mm. The grip separation distance of the tensile testing

was 115 mm, and the effective gauge length was 50 mm. The tensile properties of each sample are

reported as the average of five measurements of different specimens.

3.4. Results and Discussion

3.4.1. Epoxy-anhydride curing reaction

Epoxy-anhydride polymerization can undergo both a catalyzed and non-catalyzed reaction. The

uncatalyzed reaction of ESS and MHHPA may be possible through the presence of hydroxyl groups in

the sucrose ester (the sucrose is not fully esterified) and/or acid impurities in the anhydride crosslinker.

However, a previous study on the curing kinetics of the ESS/MHHPA reaction reveals that this

uncatalyzed reaction is minimal, and the curing process is dominated by a catalyzed reaction mechanism

[39].

Figure 3.2 shows the FTIR spectra of the raw materials and a cured thermoset sample. The

formation of polyester linkages is confirmed by the presence of carbonyl peaks at 1732 cm^{-1}. These

carbonyl ester linkages slightly overlap with the carbonyl ester peak of ESS at 1743 cm^{-1}. Furthermore,

the presence of anhydride carbonyl peaks at 1857 and 1780 cm^{-1} are no longer detected in the cured

material. Unfortunately, it is challenging to confirm and quantify the amount of polyether linkages in the

thermoset system through FTIR analysis, since the C-O ether peak may overlap with C-O of esters and carboxylic acids.
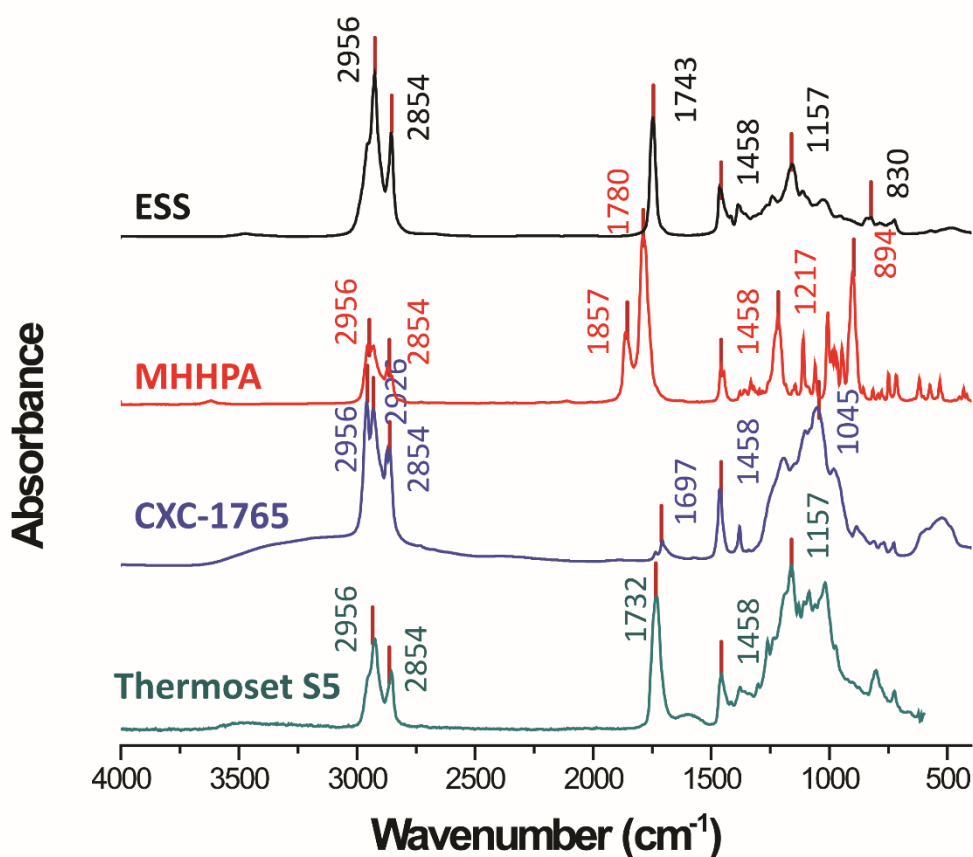
Figure 3.2. FTIR spectra of the raw materials and cured thermoset S5.

To form the thermosets, the first curing step is done in an open-face molding plate. Therefore, some of the anhydride and catalyst may evaporate due to their volatility at the curing temperature. Even after the second curing step in the closed mold system, further loss of material can occur. The amount of evaporation during the curing process is shown in Table 3.2; the listed value is the average and standard deviation of 3 samples. Overall, most of the samples retained 90%+ of their initial weight after the full curing process. The highest weight loss was observed for Sample 7, and the lowest was observed for Sample 3. This observation was not unexpected for two reasons: the viscosity of the formulation and the expected rate of polymerization. A high AE equivalent ratio means a high amount of anhydride in the formulation, thus leading to low viscosity and ability of the anhydride to diffuse through the system. Then, it is expected that with a high catalyst content, the polymerization reaction occurs faster, thus the

components are able to be incorporated into the network faster and the amount of evaporation is limited.

A previous study using thermogravimetric analysis of the raw materials indicated that MHHPA crosslinker

and CXC 1765 catalyst started to significantly lose its weight at 110 °C, while ESS started to decompose

at 332 °C [39]. Therefore, the weight loss observed in this experiment is likely to be due to the

evaporation of MHHPA crosslinker and dissociation of carboxyl diluents from the CXC 1765 catalyst.

Table 3.2. Weight retained during curing, gel fraction, and moisture uptake of the thermoset samples

Sample #	Weight Retained During Curing (%)		Gel Fraction (%)		Moisture Uptake (%)	
	Partially-cured*	Fully-cured**	Partially-cured*	Fully-cured**	1 week	1 month
S1	93.4 ± 0.6	92.5 ± 0.2	66.2 ± 0.6	98.3 ± 0.1	0.59 ± 0.03	0.69 ± 0.04
S2	93.3 ± 0.5	93.3 ± 0.3	71.2 ± 3.4	98.1 ± 0.3	0.61 ± 0.03	0.86 ± 0.13
S3	94.5 ± 0.2	95.8 ± 0.1	89.1 ± 1.9	97.5 ± 0.4	0.64 ± 0.02	1.10 ± 0.07
S4	89.1 ± 0.2	85.2 ± 0.8	68.1 ± 1.1	98.4 ± 0.3	0.92 ± 0.02	1.14 ± 0.03
S5	91.5 ± 0.3	91.4 ± 0.1	80.2 ± 0.9	98.7 ± 0.3	0.89 ± 0.06	1.15 ± 0.07
S6	93.3 ± 0.3	91.7 ± 0.9	87.1 ± 0.3	97.1 ± 0.6	0.84 ± 0.04	1.53 ± 0.20
S7	86.5 ± 0.3	81.8 ± 1.2	58.9 ± 1.8	95.6 ± 0.5	1.08 ± 0.04	1.50 ± 0.12
S8	89.0 ± 0.2	88.5 ± 0.3	74.0 ± 1.7	94.6 ± 0.4	1.11 ± 0.05	1.81 ± 0.02
S9	91.5 ± 0.6	90.6 ± 0.2	79.5 ± 0.8	95.0 ± 1.5	1.09 ± 0.02	1.62 ± 0.03

*Partially-cured samples: Samples that has been cured at 120 °C for 1 hour
**Fully-cured samples: Samples that has been cured at 120 °C for 1 hour + 150 °C for 3 hours

3.4.2. Gel content

Soxhlet extraction was conducted to determine the gel content of the epoxy-anhydride

thermosets, which may be related to the extent of cure. Table 3.2 list the gel content of the samples, after

the partial and full curing process. As expected, the gel content after partial curing is significantly lower

than the after the complete curing process. The gel contents of the partially-cured samples are fairly low;

samples containing 2%wt. catalyst loading only retain 60% of its weight after Soxhlet extraction. In

contrast, the gel content of all fully-cured samples are more than 94%, which indicates a high degree of

conversion of the components. It is very surprising that the gel content of partially-cured and fully-cured

samples can differ up to 37%, e.g. Sample 7; this observation indicates that significant additional curing

occurs during the second stage of the curing process. It can be clearly seen that the amount of gel in the

partially cured samples are affected by the catalyst amount; as the catalyst amount was increased, the

gel content significantly increased. The effect of AE molar ratio on the gel content of the fully cured resins

is more ambiguous, and there might be a cross interaction between the AE molar ratio and the catalyst

amount. This situation can be seen by comparing the increase in the gel content at a certain AE molar

ratio as the catalyst amount was increased. For example, when comparing Samples 1 and 2 (samples

with AE molar ratio = 0.5), as the catalyst amount was increased from 2 to 5 wt. %, the gel content only

differs by 5%. In contrast, when comparing Samples 7 and 8 (samples with AE molar ratio = 1.0),

increasing the catalyst amount from 2 to 5 wt. % results in 15% difference in the gel content. Unlike the

pattern seen in the partially-cured samples, the gel content in the fully-cured samples is more influenced

by the AE molar ratio; where the lowest gel content was observed for samples with AE molar ratio = 1.0.

Figure 3.3 shows the FTIR spectra of the sol content of the partially-cured samples. For all

samples, the spectra indicated that the sol contains the raw materials. Looking at the carbonyl region, the

anhydride peaks and the ester peaks from ESS (1857 and 1740 cm^{-1}) are still observed. As mentioned in

the previous section, the reaction between epoxy and anhydride results in ester linkages and carboxylate

end-groups. The FTIR peak corresponding to the newly formed ester peak may overlap with the one for

the ESS ester peak at 1740 cm^{-1}. Carboxylic acid end-groups can be observed at 1709 cm^{-1}. For

samples with an AE molar ratio = 0.5, the intensity of the hydroxyl region was not as strong.
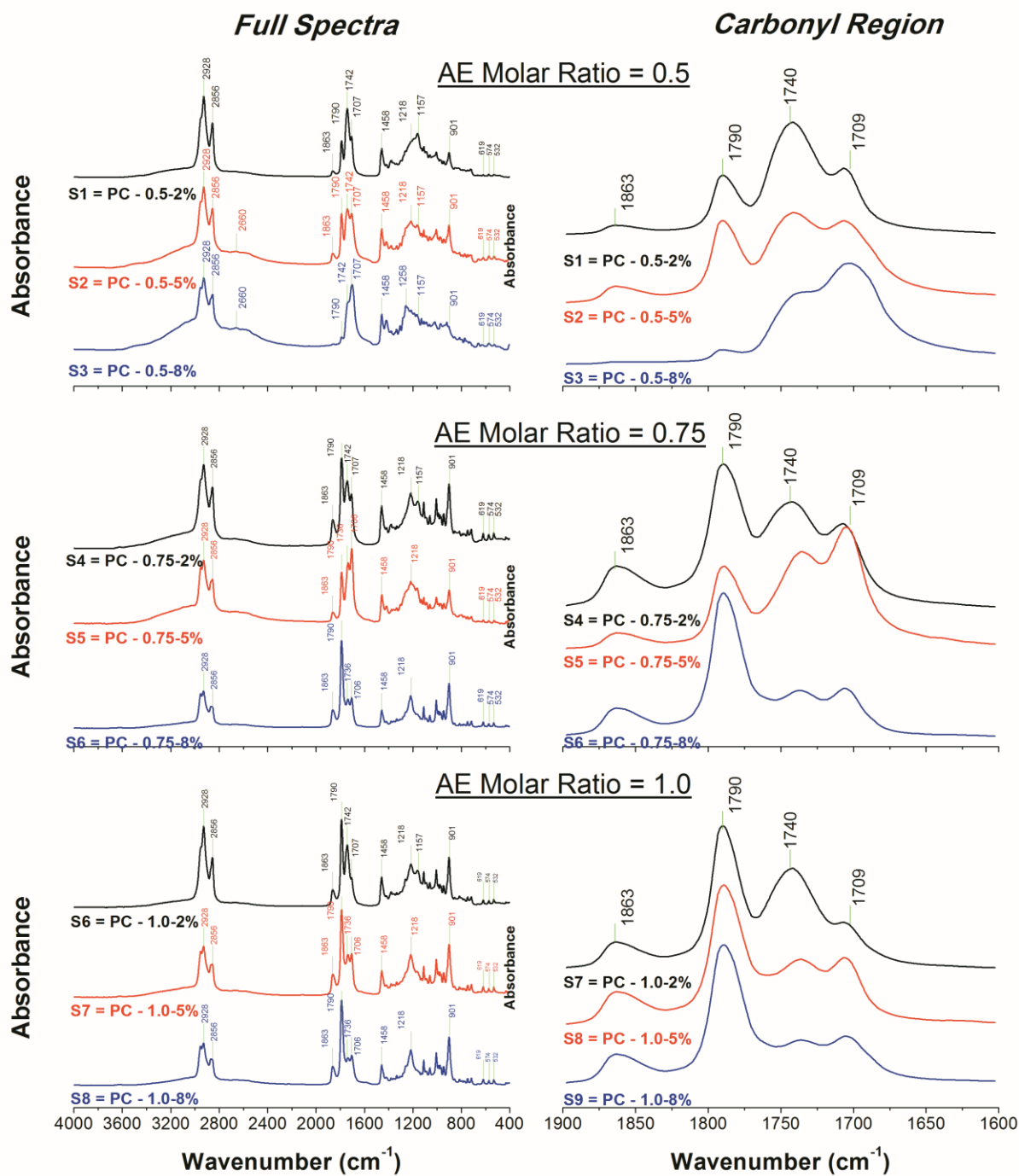
Figure 3.3. FTIR spectra of sol fraction for partially-cured system

Figure 3.4 shows the FTIR spectra for the sol content of the fully-cured samples. No anhydride was observed in the samples, except for Samples 7 and 8. However, for Samples 7 and 8, only shows trace amounts of anhydride are observed. Looking closely at the carbonyl peak region, the relative peak

intensity between the ester (1740 cm^{-1}) and carboxylate (1709 cm^{-}) are different for each sample. Samples with an AE molar ratio = 0.5 are dominated by the ester group. In contrast, samples with AE molar ratio = 0.75 and 1.0, are more dominated by pendant carboxylic acids indicated by the presence of an broad OH peak in the 2500 – 3000 cm^{-1} region.

The amount of sol in the partially-cured samples is predicted to correlate with the amount of initiated polymer chains. The FTIR spectra of the sol fraction show the presence of raw materials, in addition to newly formed functional groups. On the other hand, the amount of sol content in the fully-cured samples is predicted to correlate with the overall network of the final thermoset system. Samples with AE molar ratio 1.0 had the highest sol (lowest gel) content among all samples, and the FTIR spectra of the sol content indicates the presence of carboxylic acid/carboxylate pendant group. This observation suggests that there may be excess anhydride in the reaction through the carboxylate pendant group that cannot react with epoxy functionalities since the system has already vitrified.
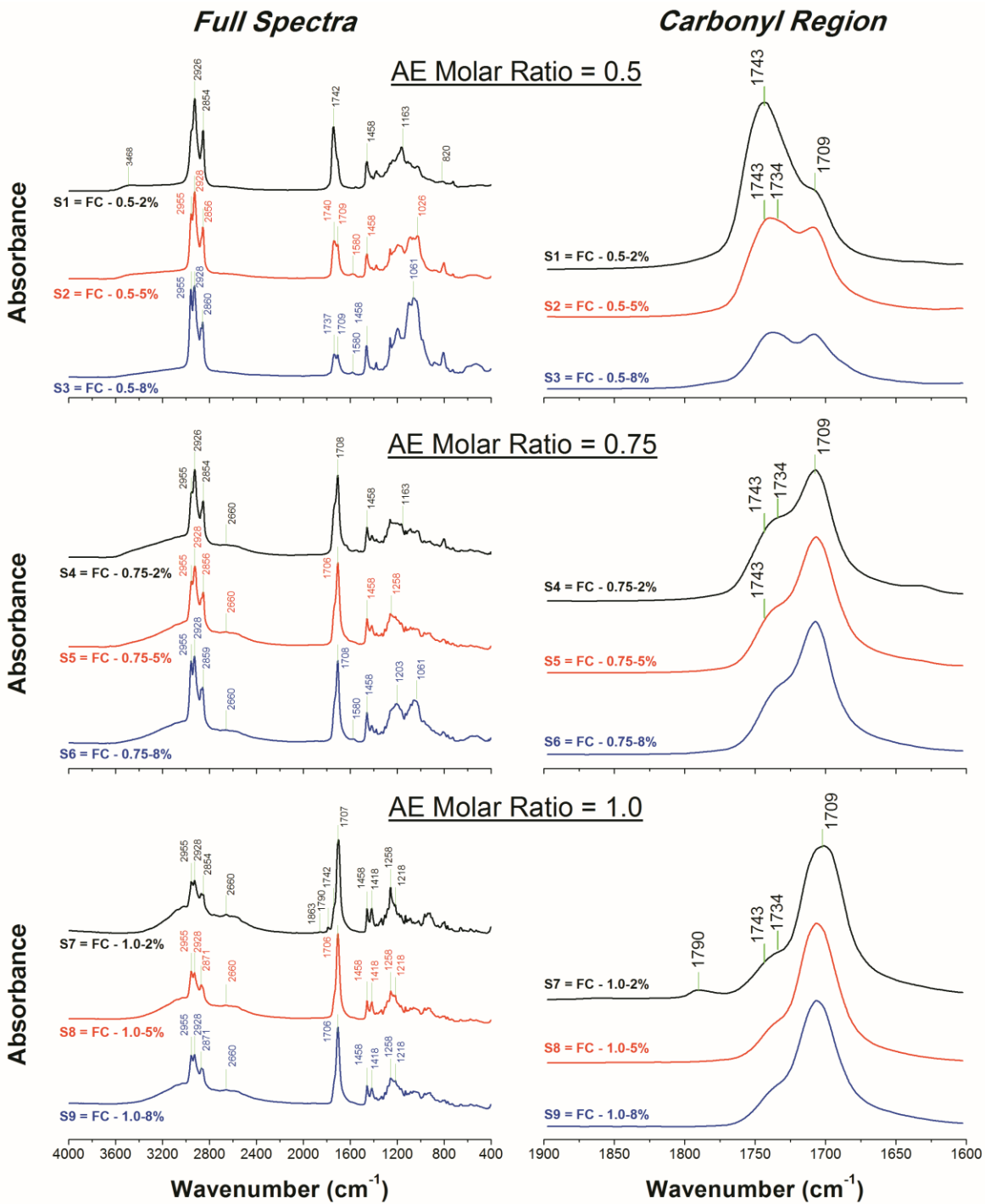
Figure 3.4. FTIR spectra of sol fraction of fully-cured samples

3.4.3. Moisture uptake

Determination of the amount of water absorption of the thermoset systems can indicate the hydrostability of the systems. Table 3.2 shows the weight gain after 1 week and 1 month of water immersion, and Figure 3.5 shows the appearance of the thermosets 1 month of immersion. As shown in Table 3.2, all of the samples have fairly low water absorption, less than 2%. Compared to a similar bio-based thermoset system based on epoxidized vegetable oil, most of the samples in this study show lower water absorption [40, 41]. The highest absorption is observed for the samples with AE molar ratio = 1.0. This observation is expected due to the presence of carboxylic acid and/or hydroxyl end groups in those thermosets; these functional groups are hydrophilic, thus able to attract and retain water. In contrast to the water absorption, the appearance of the thermoset samples appears to be related to the amount of catalyst used in the system. As can be seen in Figure 3.5, there are white blemishes observed on the surfaces of the samples. The amount of the blemishes increases with increasing catalyst amount and decreasing AE molar ratio. These white blemishes are attributed to the precipitation of the catalyst in the presence of water.
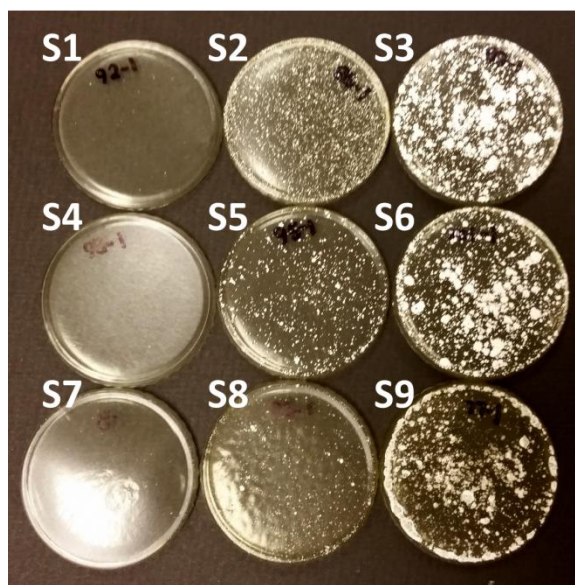
Figure 3.5. The appearance of the samples after 1 month water immersion

3.4.4. Viscoelastic properties

The goal of the study is to understand the molecular network structure by analyzing the dynamic mechanical properties of the thermosets, which includes the glass transition temperature, crosslink

density, and the temperature dependence of the storage modulus, loss modulus, and tan delta. Figures 3.6-3.8 show the temperature dependence of the storage modulus, loss modulus, and tan delta of the thermosets. The glass transition temperature can be determined through 3 different methods: the onset of the storage modulus drop ($T_{g, SM}$), the peak maximum of the loss modulus ($T_{g, LM}$), and the peak maximum of the tan delta ($T_{g, TD}$). Table 3.3 lists the T_g values of the thermosets derived from these three methods.

The storage modulus in the viscoelastic polymer represents the elastic portion, or solid-like behavior of the material. In Figure 3.6, the storage modulus can be divided to be 3 regions: glassy state, glass transition region, and rubbery state. In the glassy state, as the samples are heated, the storage modulus value is decreasing, indicating more movement in the polymer network. Looking at the shape of the curves, samples with lower AE molar ratio tend to experience a higher decrease rate of the storage modulus values. Then, samples with higher catalyst amount tend to have longer temperature range for its glassy state. The temperature at the onset of the rapid decrease in the storage modulus can be used to determine the glass transition temperature, T_g, of the materials ($T_{g, SM}$). Using this analysis, formulations with lower AE molar ratio and catalyst amount produce thermoset samples with lower $T_{g, SM}$. Based on the storage modulus of the thermosets in the glass transition state, the thermoset samples may undergo different stages of relaxation. For some samples, the storage modulus as a function of temperature does not undergo a constant decreasing rate. Sample 5 showed this occurrence more clearly than the other samples. The storage modulus in the rubbery region is used to analyze the crosslink density of the thermoset; this topic will be discussed in a later section.
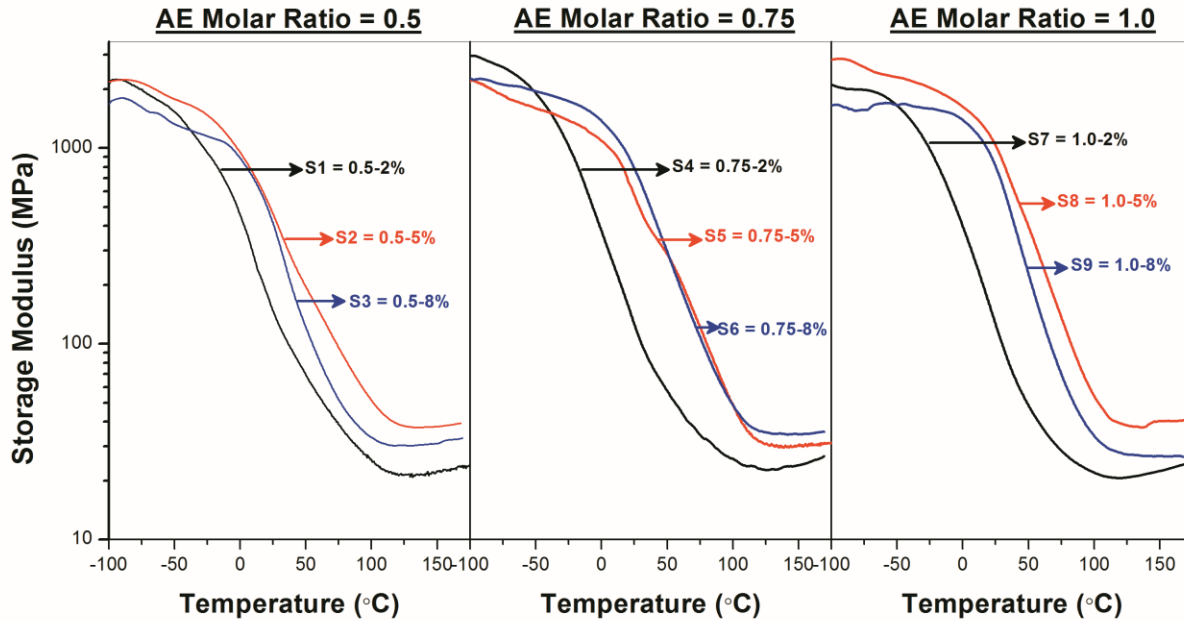
Figure 3.6. Storage modulus as function of temperatures of the thermoset samples

The loss modulus in the viscoelastic polymer represents the viscous portion, or liquid-like

behavior of the thermosets. Figure 3.7 shows the loss modulus curve as a function of temperature. For

the thermosets with 2% wt. catalyst, the loss modulus starts to increase significantly as soon as the

samples were heated. In contrast, the loss modulus did not increase immediately for other samples. This

observation has a similar pattern to what has been observed with the storage modulus, i.e. storage/loss

modulus changes significantly for samples with 2%wt. catalyst. Furthermore, the width of the loss

modulus curves for thermosets with 2 and 5% wt. catalyst is shown to be broader than the samples with

8% wt. catalyst amount. The peak maximum of the loss modulus curve can be used as another indication

for the T_g of the polymer ($T_{g, LM}$). Again, thermosets with 2% wt. catalyst showed significantly lower T_g

values compared to other samples. However, the effect of AE molar ratio is only observed with

thermosets having 8% wt. catalyst amount.
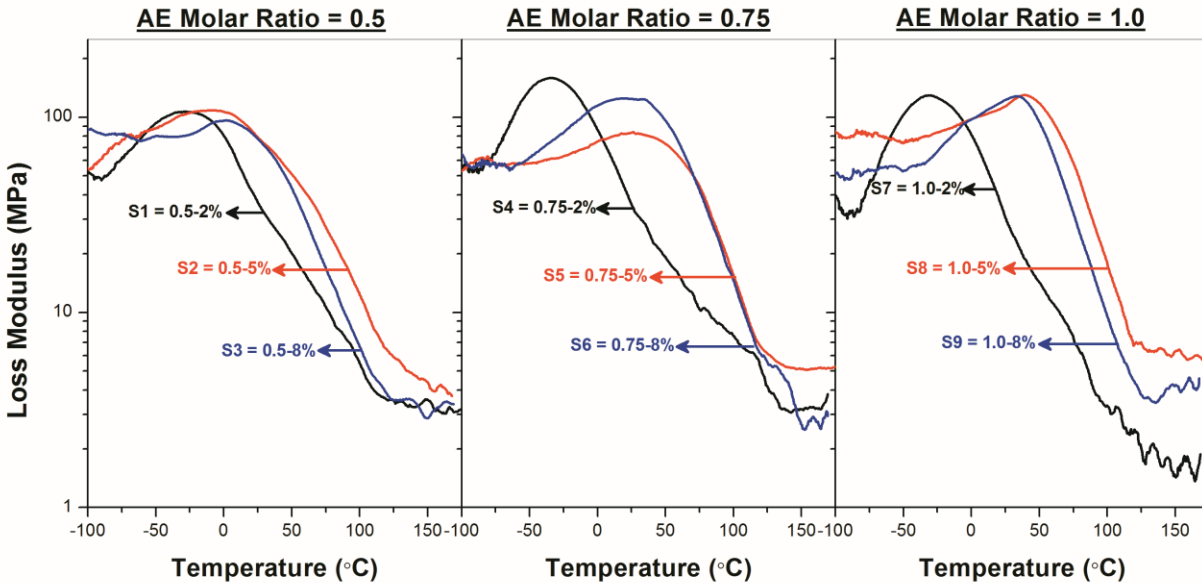
Figure 3.7. Loss modulus as function of temperatures of the thermoset samples

The ratio of loss modulus over the storage modulus is the tan delta. The peak maximum of the tan delta is commonly identified as the T_g of a polymer ($T_{g, TD}$). The tan delta curve of the thermoset samples is shown in Figure 3.8. The highest $T_{g, TD}$ was observed for S5 and S8, that is 79.1 °C and 78.8 °C, respectively. Furthermore, the width of the curve or the breadth of the tan delta peak may suggest the degree of homogeneity of the network. For all samples, the width of the peak is fairly broad, up to 100 °C; this observation is similar what has been seen with vegetable oil-based thermosets [37]. Narrow peak width and high peak intensity was observed for higher AE molar ratio and catalyst amount. Interestingly, samples with 2% catalyst (S1, S4, and S7) tend to have fairly broad tan delta peaks. Furthermore, the presence of multiple tan delta maxima may be observed for S4. This observation may indicate that samples made using low catalyst level have more heterogeneity in the polymer network structure.
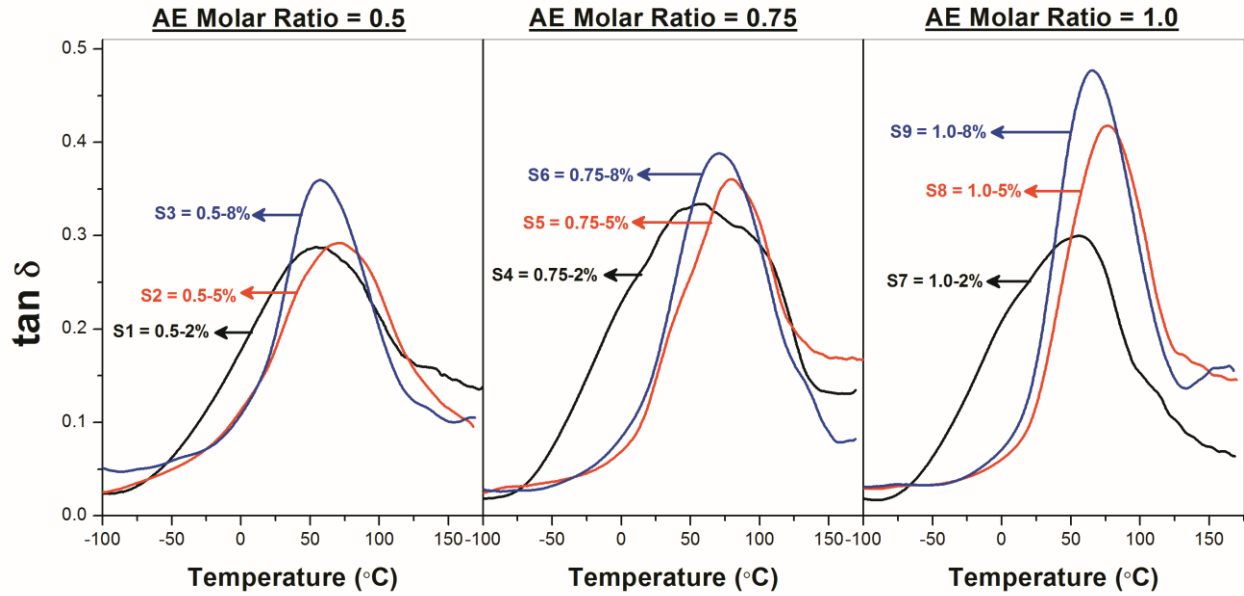
Figure 3.8. tan delta as function of temperatures of the thermoset samples

The molecular network structure of ESS-MHHPA can be characterized by the crosslink density and the molecular weight between crosslinks. This information can be calculated from the storage modulus in the rubbery region through rubber elasticity theory:

$$E' = 3\nu_e RT \tag{3.1}$$

where E' is the storage modulus, ν_e is the crosslink density, R is the gas constant, and T is the temperature [42]. For this equation to be valid, the temperature chosen should be well above the T_g of the thermosets. Often times, the crosslink density is calculated from the storage modulus at $T_{g, TD}$+ 60 °C. However, due to the width of the tan delta curves in this experiment, the chosen temperature is 150 °C, temperature above $T_{g, TD}$+ 60 °C where the storage modulus is in the plateau region. Table 3.3 shows the crosslink density values of the bio-based epoxy-anhydride thermosets.

Often, high crosslink density is believed to result in higher T_g values and vice versa, such as displayed for Sample 5 with the highest T_g and crosslink density. However, this assumption did not entirely hold true in this study. For example, Sample 7 shows lower T_g value compared to Sample 9; yet Sample 7 has comparatively lower crosslink density than Sample 9. This observation suggests that the mechanical properties of the thermoset do not only depend on the crosslink density of the network, but also on the composition of the polymer backbone.

69

Table 3.3. DMA analysis of thermoset samples

Sample #	Glass Transition Temperature (°C)			E' (MPa)		ν_e (mm^3/mol)
	$T_{g, SM}$	$T_{g, LM}$	$T_{g, TD}$	At 25 °C	At 150 °C	
S1	-56.9	-36.7	59.0	118	21.7	2.06
S2	-53.6	-34.2	57.0	126	23.9	2.27
S3	-42.7	-30.4	52.2	119	22.3	2.11
S4	-18.3	-3.7	68.5	423	37.8	3.59
S5	6.7	5.6	79.1	807	44.1	4.18
S6	13.9	21.0	69.2	788	34.5	3.27
S7	3.3	1.3	57.7	413	30.8	2.92
S8	18.1	41.4	78.8	1029	40.3	3.82
S9	12.2	24.6	61.3	712	25.6	2.42

3.4.5. Tensile testing

Tensile testing was conducted to determine the Young's modulus, tensile strength, elongation at break, and tensile toughness of the thermoset samples. Figure 3.9 shows representative stress-strain curves, and Table 3.4 provides the analysis values. Tensile toughness values were calculated from the area under stress-strain curve. The tensile properties of samples with 0.5 AE molar ratio and 2% catalyst amount (S1-S4 and S7) are significantly different than samples with higher AE molar ratio and catalyst amount. Looking at their stress-strain curves, S1-S3 and S7 behave more like rubbery materials, while the others tend to be more brittle. This observation is further confirmed by looking at the Young's modulus values. For the rubbery-like materials (S1-S3, S7), the Young's modulus values are fairly low, ≤ 300 MPa. In contrast, for brittle-like materials (S5, S6, S8, and S9), the Young's modulus values are close to 1 GPa. The tensile stress-strain curve for S4 is quite interesting; they have rubbery-like Young's modulus values at 260 MPa, yet brittle-like percent of elongation at 4.2%. Surprisingly, regardless of the shape of the stress-strain curve (rubbery vs. brittle), the toughness of most of the thermoset samples is fairly similar with values in the range of 800 – 1400 kJ/m^3.
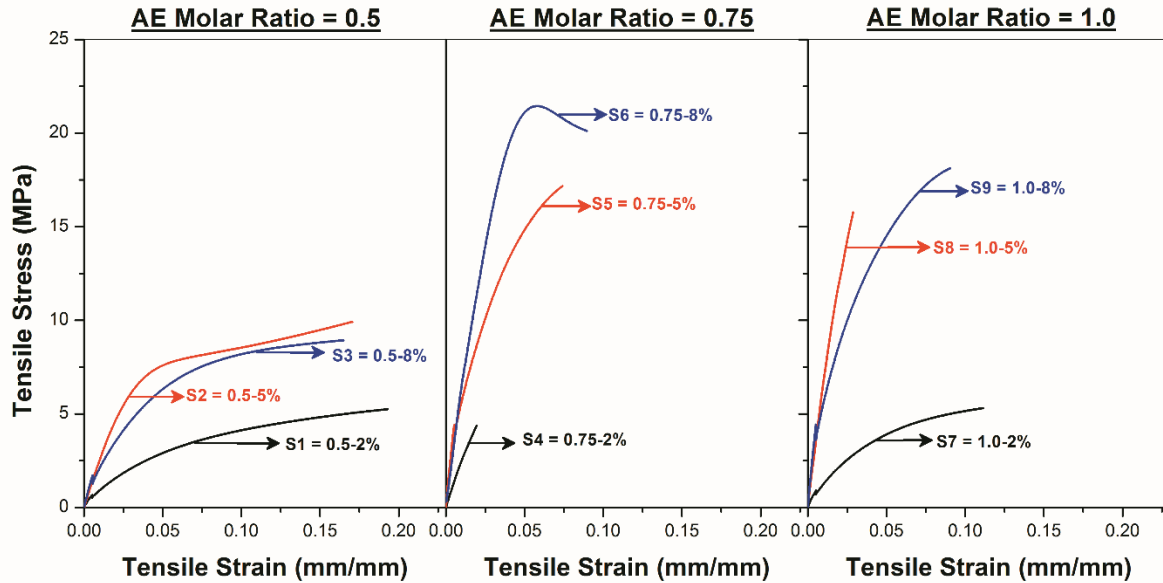
Figure 3.9. Representative stress-strain curves for the thermoset samples

Table 3.4. Tensile properties of the thermoset samples

Sample #	Young's Modulus (MPa)	Tensile Strength (MPa)	Elongation at Break (%)	Tensile Toughness (kJ/m^3)
S1	166 ± 43	5.9 ± 0.9	15.9 ± 1.4	731 ± 51
S2	283 ± 16	10.1 ± 0.3	19.5 ± 3.5	1320 ± 254
S3	333 ± 10	9.0 ± 0.3	14.9 ± 3.0	1193 ± 339
S4	263 ± 8	4.2 ± 0.3	2.3 ± 0.2	45 ± 8
S5	866 ± 39	17.5 ± 2.3	6.9 ± 3.1	1141 ± 535
S6	710 ± 43	21.6 ± 0.3	7.5 ± 0.9	1339 ± 320
S7	290 ± 108	6.9 ± 1.9	7.6 ± 2.5	377 ± 133
S8	717 ± 38	15.6 ± 0.4	2.9 ± 0.2	251 ± 25
S9	910 ± 75	17.2 ± 3.6	5.4 ± 1.7	789 ± 436

3.4.6. Structure-property relationships of ESS-MHHPA thermosets

Generally speaking, higher T_g and Young's modulus values are often caused by more highly crosslinked materials. However, this premise did not entirely hold true in this study. For example, S1 and S9 have fairly similar $T_{g,TD}$ and crosslink density values, yet their $T_{g,SM}$ and $T_{g,LM}$ values are quite different. Furthermore, the tensile properties also show a different failure behavior: S1 behaves more like a rubbery material, while S9 is more like a ductile material. It is widely known that the molecular network structures of epoxy-anhydride thermosets are fairly complex due to many possible reactions that can occur at the same time. In this study, the complexity is further enhanced when ESS was used, since ESS has a broad

range of functionalities [14]. Based on information above regarding the T_g, crosslink density and tensile properties, the molecular network of ESS-MHHPA is shown to be influenced by both the AE molar ratio and the catalyst amount; there may also be a synergistic effect between the AE molar ratio and the catalyst amount. The complexity of the molecular network may be due to the following factors: intermolecular vs. intramolecular linkages between ESS molecules, polyesterification vs. polyetherification, entanglements vs. actual crosslink of the ESS-MHHPA network, and dangling ends from unreacted functional groups. First, as the network is being formed, a carboxylic acid group can react with an epoxy group either on the same molecule or a different ESS molecule, leading to either an intra-molecular linkage or an inter-molecular linkage [43]. A higher fraction of intermolecular structures may result in a better network structure and higher modulus values. Second, due to the high number of epoxy functional groups and the complicated structure of ESS, the fatty acid chains between the same or different ESS molecules might entangle with each other [44]. When the epoxy groups subsequently react, a trapped entanglement network may form. This trapped entanglement can also act as a crosslink, and thus provide higher modulus. Furthermore, note that ν_e determined using Equation 3.1 does not separate trapped entanglements from actual crosslinks. Third, the epoxy-anhydride curing process may result in both polyesterification and polyetherification reactions; polyesterification occurs when epoxy groups react with anhydride, while polyetherification is produced when epoxy groups react with a hydroxyl group formed from another epoxy. It is expected that these two linkages have different bond strengths, and thus might result in different thermoset modulus. Finally, lower modulus and T_g of the thermoset may also be caused by the amount of dangling ends from unreacted functional groups.

3.5.   Conclusion

A series of novel bio-based thermosets were successfully prepared by reacting epoxidized sucrose soyate with cycloaliphatic anhydride crosslinker. It was found that the change in the compositional variables, such as anhydride-to-epoxy (AE) molar ratio and catalyst amount, results in unique chemical network and thus mechanical properties which include T_g, crosslink density, tensile properties, and moisture uptake. In other words, it is suggested that the mechanical properties of the thermoset depends not only on the crosslink density of the network, but also on the polymer backbone. This unique chemical network was predicted to be attributed from the following factors: intermolecular vs.

intramolecular linkages between ESS molecules, polyesterification vs. polyetherification, entanglements vs. actual crosslink of the ESS-MHHPA network, and dangling ends from unreacted functional groups. High T_g and Young's modulus values can be obtained with formulation containing less than equimolar ratio of anhydride-to-epoxy and higher catalyst amount. Yet, the tunability in the mechanical properties of these thermosets samples by changing its compositional variation is beneficial in producing composite materials for different applications with a broad range of properties.

3.6.   Acknowledgements

3.7.   References

[1]   Z. Liu, G. Kraus, Green Materials from Plant Oils, RSC Green Chemistry ed., Royal Society of Chemistry, Cambridge, UK, 2014.

[2]   Y. Xia, R.C. Larock, Vegetable oil-based polymeric materials: synthesis, properties, and applications, Green Chemistry, 12 (2010) 1893-1909.

[3]   S. Miao, P. Wang, Z. Su, S. Zhang, Vegetable-oil-based polymers as future polymeric biomaterials, Acta Biomaterialia, 10 (2014) 1692-1704.

[4]   R. Auvergne, S. Caillol, G. David, B. Boutevin, J.-P. Pascault, Biobased Thermosetting Epoxy: Present and Future, Chemical Reviews, 114 (2013) 1082-1115.

[5]   J.M. Raquez, M. Deléglise, M.F. Lacrampe, P. Krawczak, Thermosetting (bio)materials derived from renewable resources: A critical review, Progress in Polymer Science, 35 (2010) 487-509.

[6]   L. Montero de Espinosa, M.A.R. Meier, Plant oils: The perfect renewable resource for polymer science?!, European Polymer Journal, 47 (2011) 837-852.

[7]   D.P. Pfister, Y. Xia, R.C. Larock, Recent Advances in Vegetable Oil-Based Polyurethanes, ChemSusChem, 4 (2011) 703-717.

[8]   M. Desroches, M. Escouvois, R. Auvergne, S. Caillol, B. Boutevin, From Vegetable Oils to Polyurethanes: Synthetic Routes to Polyols and Main Industrial Products, Polymer Reviews, 52 (2012) 38-79.

[9]   M.D. Soucek, T. Khattab, J. Wu, Review of autoxidation and driers, Progress in Organic

        Coatings, 73 (2012) 435-454.

[10]   J.L. Scala, R.P. Wool, The effect of fatty acid composition on the acrylation kinetics of epoidized

        triacyclcerols, Journal of American Oil Chemists' Society, 79 (2002) 59-63.

[11]   M. Gonzalez-Lopez, J.T. Shaw, Cyclic anhydrides in formal cycloadditions and multicomponent

        reactions, Chemical Reviews, 109 (2009) 164-189.

[12]   A. Paramarta, X. Pan, D.C. Webster, Highly functional acrylated biobased resin system for uv-

        curable coatings, Radtech Report, (2013) 26-32.

[13]   H. Pelletier, N. Belgacem, A. Gandini, Acrylated vegetable oils as photocrosslinkable materials,

        Journal of Applied Polymer Science, 99 (2006) 3218-3221.

[14]   T. Nelson, B. Masaki, Z. Morseth, D. Webster, Highly functional biobased polyols and their use in

        melamine–formaldehyde coatings, J Coat Technol Res, 10 (2013) 757-767.

[15]   T.J. Nelson, L. Bultema, N. Eidenschink, D.C. Webster, Bio-Based High Functionality Polyols and

        Their Use in 1K Polyurethane Coatings, Journal of Renewable Materials, 1 (2013) 141-153.

[16]   T.J. Nelson, Novel bio-based resins for high-performance coatings, in, North Dakota State

        University, Ann Arbor, 2013, pp. 195.

[17]   X. Pan, D.C. Webster, New Biobased High Functionality Polyols and Their Use in Polyurethane

        Coatings, ChemSusChem, 5 (2012) 419-429.

[18]   A. Gandini, T.M. Lacerda, A.J.F. Carvalho, A straightforward double coupling of furan moieties

        onto epoxidized triglycerides: synthesis of monomers based on two renewable resources, Green

        Chemistry, 15 (2013) 1514-1519.

[19]   W. Fisch, W. Hofmann, J. Koskikallio, The curing mechanism of epoxy resins, Journal of Applied

        Polymer Science, 6 (1956).

[20]   E.C. Dearborn, R.M. Fuoss, A.K. MacKenzie, R.G. Shepherd, Epoxy resins from bis-, tris-, and

        tetrakisglycidyl etheres, Industrial and Engineering Chemistry, 45 (1953) 2715-2721.

[21]   L.A. O'Neill, C.P. Cole, Chemical and spectroscopic studies of epoxy resin reactions in the

        surface coating field, Journal of Applied Chemistry, 6 (1956) 356-364.

[22]   R. Wegler, Chemie der polyepoxyde, Angewandte Chemie, 67 (1955) 582-592.

[23] R.F. Fischer, Polyesters from epoxides and anhydrides, Industrial and Engineering Chemistry, 52 (1960) 321-323.

[24] C. Taylor, T. Krosbakken, C.A. Ulven, A. Paramarta, D.C. Webster, Structural quality biocomposites of treated flax fiber with epoxidized sucrose soyate resin, in: International Conference on Composite Materials, Montreal, Canada, 2013.

[25] N. Hosseini, C.A. Ulven, F. Azarmi, D.C. Webster, T.J. Nelson, Utilization of Flax Fibers and Glass Fibers in a Bio-Based Resin, in: ASME 2014 International Mechanical Engineering Congress and Exposition, The American Society of Mechanical Engineers, Montreal, Quebec, Canada, 2014.

[26] J.A. Foulk, M.A. Fuqua, C.A. Ulven, M.M. Alcock, Flax Fibre Quality and Influence on Interfacial Properties of Composites, International Journal of Sustainable Engineering, 3 (2010) 17-24.

[27] A. O'Donnell, M.A. Dweib, R.P. Wool, Natural fiber composites with plant oil-based resin, Composites Science and Technology, 64 (2004) 1135-1145.

[28] Y. Lu, R.C. Larock, Fabrication, Morphology and Properties of Soybean Oil-Based Composites Reinforced with Continuous Glass Fibers, Macromolecular Materials and Engineering, 292 (2007) 1085-1094.

[29] R.L. Quirino, J. Woodford, R.C. Larock, Soybean and linseed oil-based composites reinforced with wood flour and wood fibers, Journal of Applied Polymer Science, 124 (2012) 1520-1528.

[30] R. Wang, T. Schuman, CHAPTER 9 Towards Green: A Review of Recent Developments in Bio-renewable Epoxy Resins from Vegetable Oils, in: Green Materials from Plant Oils, The Royal Society of Chemistry, 2015, pp. 202-241.

[31] Z.S. Liu, S.Z. Erhan, P.D. Calvert, Solid freeform fabrication of epoxidized soybean oil/epoxy composite with bis or polyalkyleneamine curing agents, Composites Part A: Applied Science and Manufacturing, 38 (2007) 87-93.

[32] Z.S. Liu, S.Z. Erhan, J. Xu, P.D. Calvert, Development of soybean oil-based composites by solid freeform fabrication method: Epoxidized soybean oil with bis or polyalkyleneamine curing agents system, Journal of Applied Polymer Science, 85 (2002) 2100-2107.

[33]   J.V. Crivello, R. Narayan, S.S. Sternstein, Fabrication and mechanical characterization of glass
        fiber reinforced UV-cured composites from epoxidized vegetable oils, Journal of Applied Polymer
        Science, 64 (1997) 2073-2087.

[34]   S.G. Tan, W.S. Chow, Biobased Epoxidized Vegetable Oils and Its Greener Epoxy Blends: A
        Review, Polymer-Plastics Technology and Engineering, 49 (2010) 1581-1590.

[35]   X. Pan, P. Sengupta, D.C. Webster, Novel biobased epoxy compounds: epoxidized sucrose
        esters of fatty acids, Green Chemistry, 13 (2011) 965-975.

[36]   X. Pan, D.C. Webster, Impact of Structure and Functionality of Core Polyol in Highly Functional
        Biobased Epoxy Resins, Macromolecular Rapid Communications, 32 (2011) 1324-1330.

[37]   X. Pan, P. Sengupta, D.C. Webster, High biobased content epoxy-anhydride thermosets from
        epoxidized sucrose ester of fatty acids, Biomacromolecules, 12 (2011) 2416-2428.

[38]   E.M. Monono, D.C. Webster, D.P. Wiesenborn, Pilot scale (10 kg) production and
        characterization of epoxidized sucrose soyate, Industrial Crops and Products, 74 (2015) 987-997.

[39]   A. Paramarta, D.C. Webster, Curing Kinetics of Bio-based Epoxy-Anhydride Thermosets with
        Zinc Catalyst, Thermochimica Acta (In Revision).

[40]   S.G. Tan, W.S. Chow, Thermal Properties, Fracture Toughness and Water Absorption of Epoxy-
        Palm Oil Blends, Polymer-Plastics Technology and Engineering, 49 (2010) 900-907.

[41]   S.G. Tan, W.S. Chow, Thermal properties, curing characteristics and water absorption of
        soybean oil-based thermoset, eXPRESS Polymer Letters, 5 (2011) 480-492.

[42]   L.W. Hill, Calculation of crosslink density in short chain networks, Progress in Organic Coatings,
        31 (1997) 235-243.

[43]   S. Miao, S. Zhang, Z. Su, P. Wang, Chemoenzymatic synthesis of oleic acid-based polyesters for
        use as highly stable biomaterials, Journal of Polymer Science Part A: Polymer Chemistry, 46
        (2008) 4243-4248.

[44]   S. Miao, S. Zhang, Z. Su, P. Wang, Synthesis of bio-based polyurethanes from epoxidized
        soybean oil and isopropanolamine, Journal of Applied Polymer Science, 127 (2013) 1929-1936.

CHAPTER 4. IMPACT OF CATALYST ON THE CURING AND PROPERTIES OF BIO-BASED EPOXY ANHYDRIDE THERMOSETS

4.1. Abstract

While the non-catalyzed epoxy-anhydride reaction is feasible, a long polymerization time is required to achieve high conversion of functional groups. Thus, the use of an accelerator to catalyze the reaction is necessary to ensure efficient polymerization. Furthermore, the type of accelerator used in the reaction has been shown to affect the curing kinetics and reaction mechanism, which then determines the polymer network structure and properties of the material. This study explored many types of base catalysts used in the polymerization of cycloaliphatic anhydride and epoxidized sucrose soyate. These catalysts include tertiary amines, amidine, metal ligands, and onium salts. The optimum catalyst will provide low initiation temperature, minimum weight loss during the polymerization process, and excellent mechanical properties. Thermal analysis experiments such as thermogravimetric analysis (TGA), differential scanning calorimetry (DSC), and dynamic mechanical analysis (DMA) were conducted to evaluate the properties of the thermosets with different catalysts. Then, using the same experimental procedures, the effect of water in the catalyst on the thermoset properties was also studied.

4.2. Introduction

In the recent decade, there has been increasing interest in using renewable materials as chemical building blocks for structural materials. This interest is attributed to a higher awareness of future sustainability. Numerous epoxy resins from bio-based resources such as vegetable oils, polyphenols, tannins, cardanol, lignin, and starch have been developed [1-3]. Among these, vegetable oils are the most commonly used resources in the chemical industry due to their abundancy. Furthermore, the concept of using vegetable oils as a chemical commodity is actually not a new concept. Vegetable oils have been used for centuries in paints and coatings applications, owing to their ability to polymerize through autoxidation process of the olefin groups. To obtain epoxy functional groups, the olefins are reacted with a peracid. However, in order to be applied for structural applications requiring high performance, epoxidized vegetable oils are often mixed with a petroleum-based epoxy resin such as diglycidyl ether of bisphenol-A or diglycidyl ether of bisphenol-F. As a result, the bio-based content in the materials is reduced.

Recently, Webster et al. has developed a bio-based high performance epoxy thermoset technology based on epoxidized sucrose soyate (ESS). This epoxy resin is obtained from epoxidation of sucrose soyate (SS), sucrose ester of soybean oil fatty acid, through the Prilezhaev reaction [4-6]. This epoxy resin can be synthesized from 100% bio-based resources, and the viscosity is low regardless of the high epoxy group functionality. The representative structures for SS and ESS are shown in Scheme 4.1. With this resin system, many crosslinking routes have been explored which include homo-polymerization, acrylate/methacrylate grafting, carbonate grafting, hydroxyl functionalization and acid/anhydride crosslinking [2, 3, 7-17].
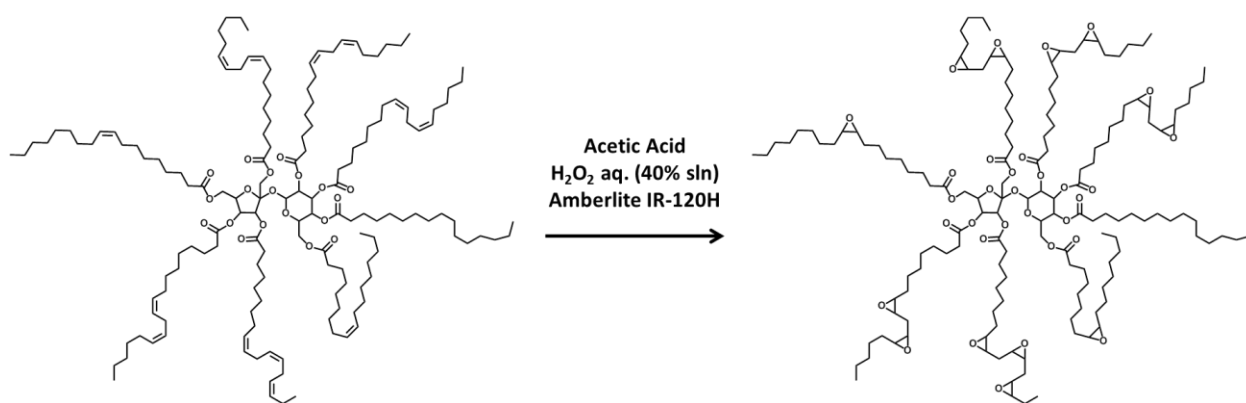
Scheme 4.1. Epoxidation reaction of sucrose soyate (SS) to yield epoxidized sucrose soyate (ESS).

One of the crosslinking technologies explored is the co-polymerization of epoxy and anhydride to produce polyester thermosets [2, 3, 17]. Structure-property relationship study from Chapter 3 has shown that the properties of the anhydride-cured ESS thermoset depend on the anhydride-to-epoxy molar ratio and catalyst amount [17]. It was observed that rubbery-like materials were produced with samples formulated with an anhydride-to-epoxy molar ratio of 0.5 and catalyst loading of 2%. In contrast, stiffer and more brittle materials were produced with samples formulated with an anhydride-to-epoxy molar ratio of 0.75-1.0 and catalyst loading of 5-8%. Overall, all of the samples had very high gel fraction, and glass transition temperature above 50 °C. Even though excellent mechanical properties were obtained from this study, it is necessary to minimize the amount of the catalyst in the formulation to reduce the overall cost.

Furthermore, it has been observed by many other researchers that the mechanical properties of anhydride-cured epoxies may depend on the type of the catalyst used [18-20].

The difference in the properties of the thermosets with variation in the catalyst is thought to be due to the different reaction mechanisms and kinetics. Overall, it is widely known that the epoxy-anhydride reaction can be fairly complex due to simultaneous initiation, propagation, and termination reactions. Trappe and Bhurchard studied the kinetics and conformational properties of anhydride-cured epoxies and found that the degree of polymerization depends on the molar ratio of the monomers and initiator [21]. Furthermore, they also found that the initiation rate constant of the reaction is 10-50 times smaller than the propagation rate constant. This finding was further confirmed by Leukel using matrix-assisted laser desorption ionization time-of-flight (MALDI-TOF) mass spectroscopy analysis [22].

The polymerization of epoxides and anhydrides itself has been thought to be able to be initiated with or without the presence of catalyst. Epoxy-anhydride polymerization is often catalyzed with Lewis base catalysts such as tertiary amines, amidines, imidazoles, quaternary onium salts, organometallic or metal salts. The main difference between the reaction pathways is the initiation mechanism and active propagating end-chain; Scheme 4.2 summarizes the reaction pathways with the non-catalyzed reaction and many types of catalysts. Without the presence of catalyst, the reaction can be self-catalyzed through hydroxyl impurities in the raw materials. Fisch et al. proposed that hydroxyl impurities can ring open the anhydride system to form mono-ester with a carboxyl group at the end of the chain, which then can further react to form polyester [23]. Based on the assumption that the epoxy and anhydride functional groups are added alternately, the consumption rate of the epoxy and anhydride groups should be similar to the formation of the diester. Yet, Fisch et al. observed the opposing case, where the consumption rate of epoxy groups is faster than the formation of diester. In other research, Dearborn et al. also observed unreacted anhydride when all of the epoxies were consumed, even at an equimolar ratio of epoxy to anhydride [24]. Therefore, it seems that the non-catalyzed reaction may lead to a significant amount of ether linkages due to homo-polymerization of epoxy functionalities.

Then, unlike the non-catalyzed reaction, when tertiary amine or amidine was used to catalyze the reaction, the active group is not the hydroxyl group, but a zwiterionic carboxylate and/or alkoxide group [23, 25]. Within this mechanism, there is a debate whether an active hydrogen atom should be present in the copolymerization system. This hydrogen active compound can be any proton donor such as acid, alocohol or phenol [26-28]. This hydrogen bounded complex has a higher reactivity to ring open either

79

anhydride or epoxy. The carboxyl group is able to auto-catalyze the reaction. The possibility of termination of the active propagating chain end was proposed through hydrogen abstraction from the ammonium salt [23].

One of the more popular catalyst systems for epoxy-anhydride reaction is imidazole. The initiation of the reaction involves nucleophilic ring opening of the anhydride or epoxide by the nitrogen atom to form anionic species of carboxylate or alkoxide, respectively. This anionic species then reacts subsequently with epoxide and anhydride [29, 30]. Using imidazole as catalyst for epoxy/anhydride reaction has been shown to result in materials with higher physical and chemical properties compared to networks formed when tertiary amine was used as catalyst [18]. Bouillon attributed this improved property due to the ability of the imidazole to act as a crosslinking agent and thus become incorporated into the network.

Non-catalyzed reaction

Hydroxyl initiated co-polymerization
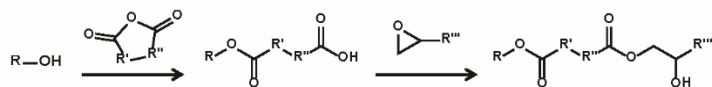
Initiating species = active hydrogen

Hydroxyl initiated epoxy homo-polymerization
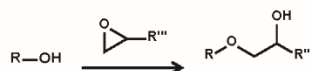
Imidazole-catalyzed reaction
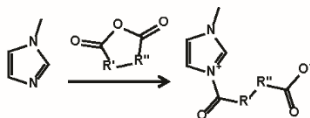
Initiation

Initiating species = carboxylate/alkoxide

Quaternary onium salts-catalyzed reaction
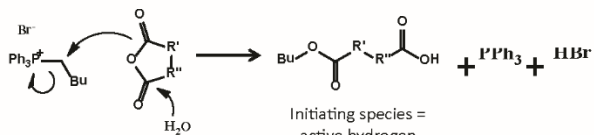
Initiating species = active hydrogen

Tertiary amine-catalyzed reaction

Initiation and Propagation
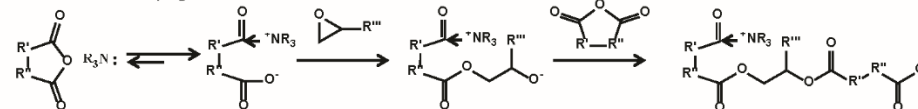
OR Activation through proton donor

$R_3N: \rightleftharpoons [R_3N \cdots HA]$
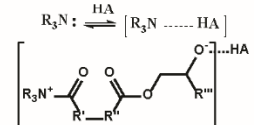
OR Activation through co-catalyst

$R_3N: \rightleftharpoons R_3N^+ H\ O^- H$
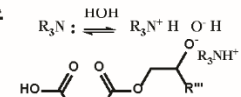
Termination
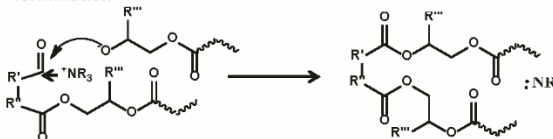
Organometallic-catalyzed reaction

Ligand dissociation
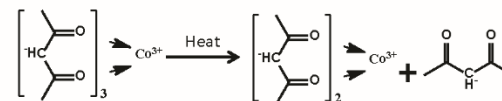
Initiation
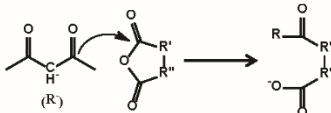
Initiating species = carboxylate/alkoxide

Scheme 4.2. Reaction mechanism of epoxy and anhydride curing using different catalysts

Another possible catalyst system for the epoxy/anhydride reaction are quaternary onium salts. This catalyst system has been widely used for hybrid powder coatings and step-growth acid/hydroxyl poly-condensation reactions [31-34]. The structure of cation and anion of the quaternary onium salts may affect the reactivity of the catalyst system [35]. For phosphonium salts-catalyzed reaction, Amirova et al. used electrospray mass-spectroscopy to analyze the initiation reaction mechanisms [36, 37]. They observed simultaneous reaction of nucleophilic substitution at the α-carbon atom of the phosphonium salt releasing triphenyl phosphine and nucleophilic attack of water to anhydride to form carboxylic acid groups. The active hydrogen in the carboxylic acid groups was then found to be the initiating species.

Another type of catalyst to accelerate the curing of epoxy-anhydride are organometallic compounds, which are mainly used for electronic applications [35, 38-42]. The initiation process can be started by either metal complexation and/or ligand dissociation in the catalyst system [43]. The type of metal, ligand, and anion type in the organometallic catalysts may affect the curing mechanisms and thus the properties. A review article regarding catalysis by coordination compounds with different ligands such as amino, acetylacetonate, imidazole, imidazolum, phthalocyanine, and Schiff's base has been published by Hamerton et al [44].

In this study, 11 possible catalysts with different chemistries (tertiary amine, imidazole, chromium-based, and quaternary ammonium salt) were selected to accelerate the crosslinking polymerization of ESS and MHHPA. For this catalyst screening study, anhydride-to-epoxy (AE) molar ratio was fixed to be 0.75 and catalyst was added at 2%wt. of the formulation. The effect of the catalyst was determined through many characterizations including studying the amount of volatilization by thermogravimetric analysis (TGA), heat of polymerization by differential scanning calorimetry (DSC), thermo-mechanical properties by dynamic mechanical analysis (DMA), gel fraction by Soxhlet extraction, and moisture uptake by water immersion.

4.3. Experimental
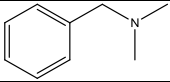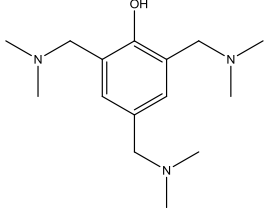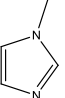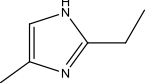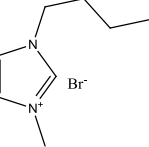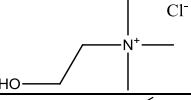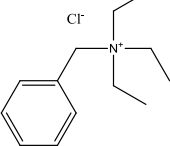
4.3.1. Materials, polymer composition and cure procedure

Epoxidized sucrose soyate was synthesized from sucrose soyate through the Prilezhaev reaction, and the detailed procedure is described previously [5, 6]. The epoxy equivalent weight was determined to be 250 g/mol by hydrogen bromide titration. A liquid aliphatic anhydride, methyl hexahydrophthalic

anhydride (MHHPA) was provided by Dixie Chemicals. The catalysts used in this study are shown in Table 4.1. Benzyldimethyleneamine (BDMA), 2-ethyl-4-methylimidazole (2E-4MI), 1-butyl-3-methylimidazolium bromide (1B-3MI Br), choline chloride (C Cl), benzyltriethylammonium chloride (BTEA Cl), tetrabutyl ammonium bromide (TBA Br), and chromium (III)-2-ethyl hexanoate (Cr-3) were purchased from Alfa-Aesar. 1-Methylimidazole (1-MI) was bought from TCI. BV-Cat 7 was given by Broadview Technologies, and 2,4,6-tris(dimethylaminoethyl) phenol (Ancamine K54) were provided by Air Products. The chemical and physical properties of the catalysts are shown in Table 4.1. In a later part of the study, a series of aqueous TBA Br catalysts were prepared and the properties of the thermosets were studied as a function of water content in the catalyst.
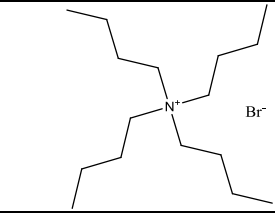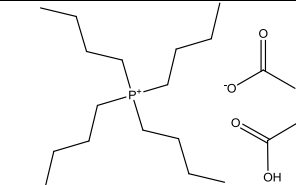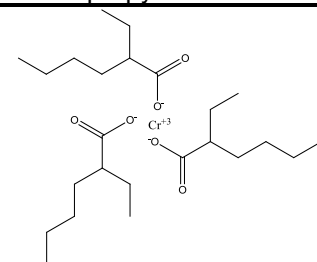
To prepare the thermosets, first, ESS and MHHPA were mixed at 50 °C for 1 hour; the anhydride-to-epoxy equivalent ratio was fixed at 0.75. Then, the catalyst was added to the mixture at 2%wt of total formulation, and the mixture was continued to be stirred for additional 30 minutes. The formulations were cured in either an aluminum weighing boat or silicone mold, depending on the sample format required for evaluation. The curing process consisted of two stages: 120 °C for 1 hour, followed by 150 °C for 3 hours. The amount of volatilization during curing was measured by comparing the weight of the materials before and after curing in the oven.

Table 4.1. Catalysts for epoxy-anhydride polymerization

#	Type	Catalyst	Structure	MW / (Active)	Appearance	BP/MP (°C)	Supplier	Purity (%)
1	**Tertiary amine**	Benzyldimethylamine (BDMA)		135.2 (1)	Colorless liquid	-75/180	Alfa-Aesar	98
2		2,4,6-tris(dimethylaminoethyl) phenol (Ancamine K54)		265.4 / (3) 88.5	Clear, light yellow viscous liquid	-20/130	Air Products	97
3	**Imidazole**	1-methylimidazole (1-MI)		82.1 (1)	Colorless liquid	-60/198	TCI	99
4		2-ethyl-4-methylimidazole (2E-4MI)		110.2 (1)	Light yellow crystalline	50/292	Alfa-Aesar	96
5		1-butyl-3-methylimidazolium bromide (1B-3MI Br)		219.1 (1)	Light brown crystalline	70	Alfa-Aesar	99
6	**Quaternary Onium Salts**	Choline chloride (C Cl)		139.6 (1)	White solid	Decompose at 302	Alfa-Aesar	98
7		Benzyltriethylammonium chloride (BTEA Cl)		227.8 (1)	White crystalline	190/450	Alfa-Aesar	99

(continues)

Table 4.1. Catalysts for epoxy-anhydride polymerization (continued)

#	Type	Catalyst	Structure	MW / (Active)	Appearance	BP/MP (°C)	Supplier	Purity (%)
8	**Quaternary Onium Salts**	Tetrabutylammonium bromide (TBA Br)		322.4 (1)	White solid	103	Alfa-Aesar	98
9		Tetrabutylphosphonium acetate acetic acid complex (TBP Ac)		318.5 (1 + 1) 159.3	Beige powder	72	Sachem	40% in water
10		BV-Cat 7	Quat ammonium salts in propyl alcohol	-	Liquid	-	Broadview Tech	-
11	**Chromium**	Chromium(III)-2-ethyl hexanoate (Cr-3)		481.6 (3 + 1) 120.4	Green viscous liquid	-	Alfa-Aesar	50 (in ethyl hexa-noate)
12	**Mixture**	Chromium (#11) + TBA Br (#8) (Cr-3+TBA Br)	#3 and #7	-	-	-	-	-

4.3.2.   Thermal analysis

4.3.2.1. Thermogravimetric analysis (TGA)

TGA experiments were conducted using a Q500 by TA Instruments, and the sample size used was 30-50 mg. During the dynamic scans, samples were heated from room temperature to 600 °C with 10 °C/min heating rate. Furthermore, the samples were purged with air at 60 mL/min flow rate, while the TGA balance was purged with nitrogen at 40 mL/min flow rate.

4.3.2.2. Differential scanning calorimetry (DSC)

The heat of polymerization and peak temperature of the curing was analyzed using a Q1000 differential scanning calorimetry (DSC) by TA Instrument. DSC dynamic scan was performed in which the samples (~10 mg) were heated from 0 to 275 °C at 5 °C/min heating rate. The experiment was conducted in modulated mode, where the modulated temperature is ±1.23 °C with a modulation period of 40 seconds. For selected samples, the glass transition temperature (T_g) of the thermosets was determined using modulated DSC. The samples were heated from -50 to 250 °C at 5 °C/min heating rate. The modulated temperature is ±3.18 °C and the modulation period is 60 seconds.

4.3.2.3. Dynamic mechanical analysis (DMA)

The thermo-mechanical properties of the thermosets were analyzed using a Q800 dynamic mechanical analysis (DMA) system by TA Instruments. The sample is a rectangular shape with size of 60 mm x 10 mm x 3.5 mm. Using 3 point-bending mode, the samples was heated from -100 to 175 °C at 3 °C/min heating rate. The sample was exposed to 15.0 µm oscillation with pre-load force of 0.075 N and the force track was set to 125%. The T_g was determined as the temperature of the tan delta maximum.

4.3.3.   Soxhlet extraction

The gel fraction of the sample was determined using Soxhlet extraction. Approximately 1 gram of sample was inserted in the extraction thimble of the Soxhlet apparatus. The extraction process was conducted using acetone as a solvent. Samples were extracted for 17 hours by warm acetone when acetone was heated to reflux. After the process is completed, wet residual samples were dried in the oven at 120 °C for 1 hour.

4.3.4. Moisture uptake

Moisture uptake of the thermosets was performed by immersing the sample in deionized water. A circular sample with 1.5" diameter x 2 mm was immersed in the water for 2 months. The weight of the sample was measured periodically, and the moisture uptake was determined by comparing the initial and final weights of the sample.

4.4.   Results and Discussion

4.4.1.   Appearance of the thermosets and volatilization during curing

4.4.1.1. Appearance of the thermoset

ESS was crosslinked with MHHPA to form a polyester thermoset, and the reaction was accelerated using the twelve catalysts shown in Table 4.1. First, looking at the appearance of the cured thermosets, shown in Figure 4.1, it can be clearly seen that the color of the samples depends on the catalyst used. Samples with tertiary amines (BDMA and K54) produced a light yellow color, while the ones with imidazole-based (1-MI, 2E-4MI, and 1B-3MI Br) catalysts gave a dark yellow, slightly amber color. This dark yellow, slightly amber color can be attributed to oxidation of amine during the curing reaction. The samples containing quaternary onium salts (C Cl, BTEA Cl, TBA Br, TBP Ac, BV-Cat 7) produced similar yellow color as tertiary amine samples. However, it is important to note that the catalysts with chloride ions could not be completely dissolved in the formulations, thus resulting in catalyst particles either dispersed in the sample or settled to the bottom of the pan. Then, as expected, samples with chromium-based (Cr3 and Cr3+TBA Br) catalyst had a green color. Among all of the samples, tacky surfaces after curing were observed for ESS/MHHPA mixture catalyzed by tertiary amine, choline chloride, and the chromium-based compounds.

Figure 4.1. Appearance of thermoset samples

4.4.1.2. Volatilization during curing by thermogravimetric analysis (TGA)

The high curing temperature may cause the raw materials in the liquid formulation to evaporate. An efficient catalyst should be able to initiate the reaction rapidly. For anhydride-cured epoxy, previous research has shown that the propagation rate is much faster than initiation rate [21, 26]. An efficient catalyst should be able to initiate the chain rapidly. Thus, more initiating chain ends would result in reaching the gel point faster, which then can reduce the evaporation of the raw materials. To study the evaporation of the raw materials in the liquid formulation, non-isothermal thermogravimetric analysis (TGA) experiments were conducted. In order to better analyze the formulation mixture, TGA analysis of ESS and MHHPA was first conducted, and the result is shown in Figure 4.2.

It is important to note that both chemicals are solvent-free and have >99% purity. It can be observed from Figure 4.2 that the ESS resin is thermally stable up to 345 °C, and then undergoes degradation rapidly. In contrast, the MHHPA crosslinker started to lose weight significantly at around 113 °C and no material remained after 200 °C. This result is surprising since the safety data sheet listed the boiling point of MHHPA at 290 °C. Thus, this observation suggests that MHHPA has a high vapor pressure. A similar experiment was then conducted with the uncatalyzed ESS/MHHPA mixture. Multiple stages of weight loss were observed with the uncatalyzed ESS/MHHPA mixture. Each stage is separated by an onset temperature. The first onset temperature occurs at 125 °C, which is in a similar range where MHHPA starts to evaporate. Therefore, it is suggested that MHHPA is evaporating at this onset temperature. The rate of weight loss of the MHHPA in the uncatalyzed mixture is slower than MHHPA itself due to higher viscosity of the mixture of MHHPA with ESS compared to MHHPA alone. This volatilization continues up to the second onset temperature which occurs at around 225 °C. At this temperature, the remaining weight is approximately ~70%. This mixture was formulated at 0.75 molar ratio of anhydride-to-epoxy molar ratio, or 32%wt. of anhydride in the mixture. Therefore, at this second onset temperature, most of the anhydride crosslinker has evaporated. The last observed temperature onset at 325 °C is suggested to be due to the degradation of ESS. This observation may indicate that there is minimal polymerization occurring with the uncatalyzed ESS/MHHPA mixture.
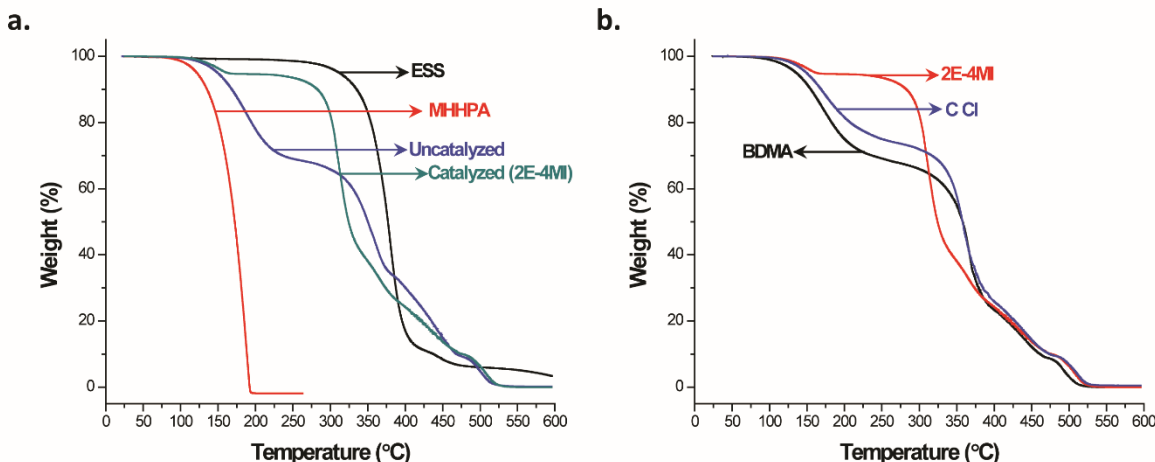
Figure 4.2. Weight loss curve as function of temperature: a. raw materials and liquid formulation, b. liquid formulation with different catalysts

In comparison, when a catalyst was added to the ESS/MHHPA mixture, the overall TGA curve shape is significantly different even though it still has similar weight loss stages: the MHHPA started to evaporate at ~125 °C and the materials started to degrade at ~325 °C. In contrast, the MHHPA volatilization is greatly reduced before the materials started to degrade. As seen in Figure 4.2b where several catalysts are used, the shape of the curves varies depending on the catalyst type. In order to compare the performance of the catalyst, the following criteria are used to compare the weight loss properties of samples with different catalysts. First, the temperature at which 2% weight loss occurred is used to signify the first onset temperature. As mentioned before, the first onset temperature may indicate the ability of the catalyst to initiate the reaction thus delaying the loss of anhydride. The second criterion used is the temperature at the second onset temperature at which the volatilization was significantly reduced, and may suggest the point where the matrix has gelled. A high temperature of the second onset indicates that the gelation of the bulk occurs more slowly. Other criterion being used is the total amount volatilization from 40-200 °C; an optimum catalyst would be one that can minimize the evaporation of MHHPA and thus have the lowest weight loss. The last criterion used to compare the properties of catalysts is the degradation temperature of the cured thermoset.

TGA analysis was carried out on systems containing each catalyst and the data analyzed based on the criteria above in Figure 4.3; this figure also contains the weight loss of materials during the curing process. Figure 4.3 indicates that the trend of the onset temperature and weight loss during curing is

89

fairly similar. ESS/MHHPA catalyzed with tertiary amines (BDMA and K54) shows the highest amount of weight loss, where MHHPA evaporation starts at a lower temperature and the evaporation rate slowed at higher temperature. Except for the 1-MI sample, other samples have 2% volatilization temperatures between 130-135 °C. TGA analysis of the 1-MI catalyst showed evaporation of the catalyst at ~100 °C. Therefore, it is expected that the lowest 2% volatilization temperature of the 1-MI catalyzed ESS/MHHA is due to evaporation of both MHHPA and the 1-MI catalyst. Comparing the second onset temperature, where the MHHPA evaporation slows down significantly, the lowest temperature was observed for 1-MI, 2E, 4MI, TBA Br, TBP Ac, BV-Cat 7 and the mixture of Cr3-TBA Br. These samples show a minimal weight loss (<3%) between the second onset temperature and the degradation temperature. In contrast, other samples which had higher second onset temperature (BDMA, K54, 1B-3MI Br, C Cl, BTEA Cl and Cr3) continue losing weight between the second onset temperature and the degradation temperature; in some samples, this is up to 10%. For this set of samples, the samples either initiate the reaction inefficiently and/or could not be dissolved in the ESS/MHHPA mixture. Then, comparing the degradation temperature of all of the systems, some of the highest degradation temperatures were obtained from the samples which have highest evaporation rate (BCMA, C Cl, Cr). The degradation temperature of these samples is similar to the degradation temperature of the ESS, which is indicated by the horizontal line on Figure 4.3c. It is observed that the polyester thermoset crosslinked systems are less thermally stable than the ESS itself. The total amount of weight loss during TGA at 40 – 200 °C is presented on Figure 4.3d. A total weight loss of 5-25% was observed, and the trend is similar to what is observed for the second temperature onset. The highest amount of volatilization was observed for ESS/MHHPA catalyzed by tertiary amine, and the lowest amount of volatilization was observed for 2E-4MI and soluble onium salt.
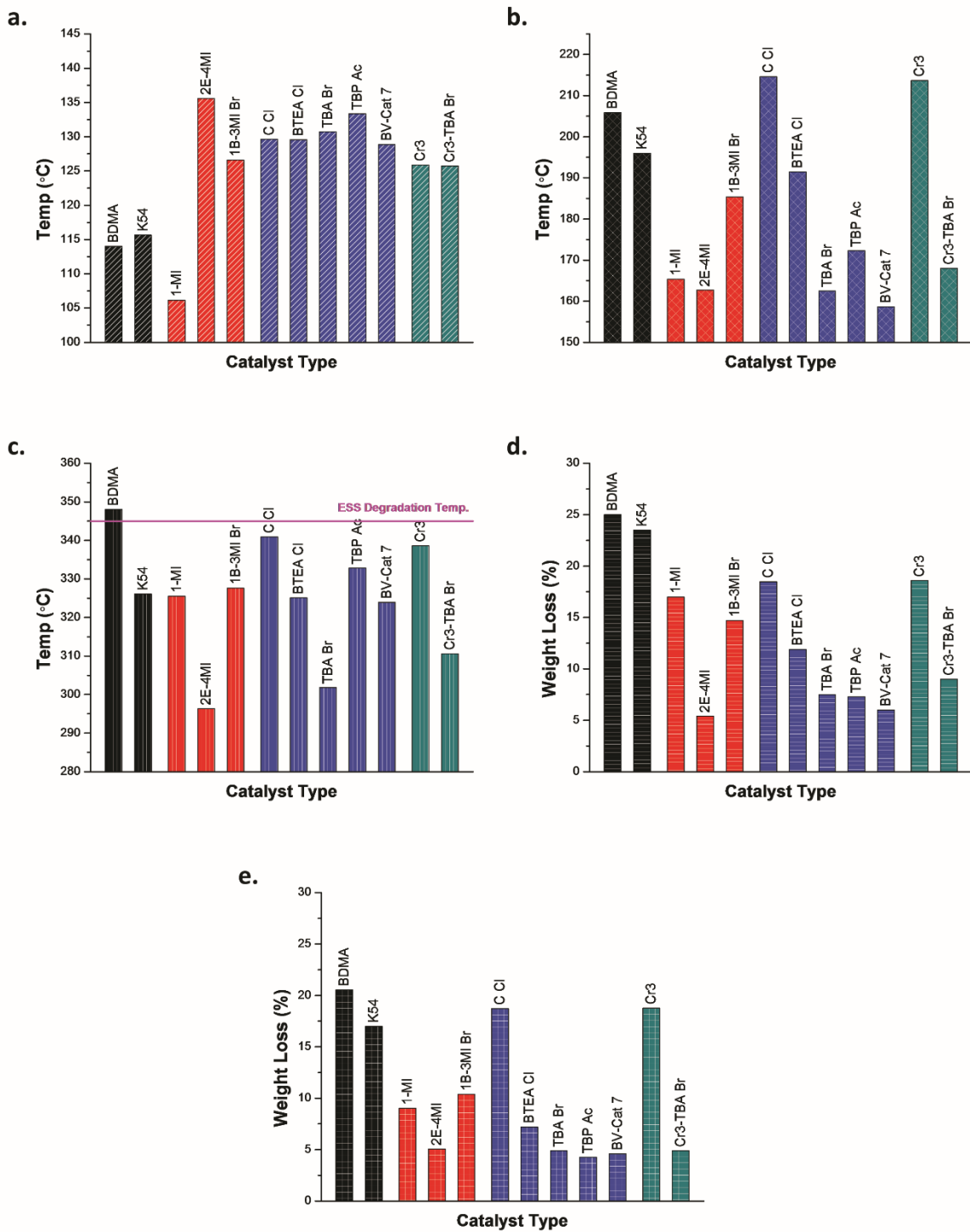
Figure 4.3. TGA analysis for curing of ESS/MHHPA as a function of catalyst type: a. Temperature at which 2% weight loss occurs, b. Temperature at which 2nd onset temperature (possibly gelation) occurs, c. Degradation temperature, d. Total amount of weight loss at 40-200 °C; e. Total amount of weight loss during oven curing

4.4.1.3. Volatilization during curing in the oven

Although a TGA non-isothermal experiment can indicate the weight loss during the curing process, it is also necessary to measure the weight loss of materials that occurs during curing in the oven. The weight of the samples is measured gravimetrically using an analytical balance before and after curing. The amount of weight loss during curing is shown in Figure 4.3e. The results from this measurement showed similar trends compared to what was observed from the TGA experiments. When ESS/MHHPA mixture was catalyzed using 2E-4MI or soluble quaternary onium salts, less than 5% of materials were lost. Overall, the TGA measurement tends to produce higher weight loss than the gravimetric measurement; it is believed that this occurrence was caused by the air flow purge used in the TGA experiment.

4.4.2. Soxhlet extraction

Soxhlet extraction was conducted to determine the gel content of the cured epoxy-anhydride thermosets, which may indicate the network connectivity of the cured thermoset. Table 4.2 lists the gel content of the thermoset samples made using the series of catalysts. Most of the samples have very high gel fractions, >95%, with the exception of samples made using the chromium-3 based catalysts. This observation was a result of the lower reactivity of the chromium-3 catalyst in catalyzing the reaction, as shown in the TGA analysis and later in the differential scanning calorimetry (DSC) analysis.

Table 4.2. Gel fraction and moisture uptake of thermoset samples cured with the catalysts

#	Type	Catalyst	Gel Fraction (%)	Moisture Uptake (%)	
				1-week	1-month
1	**Tertiary**	BDMA	95.83 ± 0.49	0.63 ± 0.08	0.67 ± 0.05
2	**amine**	K54	98.05 ± 0.11	0.70 ± 0.08	0.90 ± 0.13
3		1-MI	99.21 ± 0.35	0.97 ± 0.02	1.05 ± 0.02
4	**Imidazole**	2E-4MI	99.05 ± 0.14	0.73 ± 0.05	0.61 ± 0.14
5		1B-3MI Br	98.17 ± 0.13	1.07 ± 0.04	1.32 ± 0.02
6		C Cl	99.45 ± 0.03	-2.20 ± 0.25	-1.58 ± 0.38
7	**Quaternary**	BTEA Cl	97.91 ± 0.2	2.18 ± 0.55	5.10 ± 0.94
8	**Onium**	TBA Br	98.49 ± 0.08	0.53 ± 0.05	0.53 ± 0.12
9	**Salts**	TBP Ac	99.19 ± 0.1	0.74 ± 0.01	0.97 ± 0.00
10		BV-Cat 7	98.92 ± 0.19	0.56 ± 0.03	0.53 ± 0.01
11	**Chromium**	Cr-3	87.78 ± 0.32	0.93 ± 0.04	0.78 ± 0.04
12	**Mixture**	Cr3-TBA Br	99.45 ± 0.03	0.49 ± 0.09	0.83 ± 0.39

4.4.3. Moisture uptake

The moisture uptake experiment was conducted to give insight into the hydrophilicity of the cured systems. Table 4.2 shows the weight gain after 1-week and 1-month of full immersion in deionized water. As shown in Table 4.2, most of the samples have low moisture uptake, with less than 2% after 1-month immersion. The highest water uptake was observed for the BTEA Cl samples with up to 5% weight gain. BTEA Cl thermoset samples have undissolved catalyst within the thermoset system, and it is expected that this undissolved catalyst is able to attract and retain water. An interesting observation was found with samples with C Cl, where the samples actually lost weight after water immersion. Similar to BTEA Cl, C Cl catalyst could not be dissolved well in the thermoset system. Yet, in contrast to BTEA Cl, it is predicted that the samples were solubilized in the water, thus decreasing its weight.

4.4.4. Heat of polymerization by differential scanning calorimetry (DSC)

4.4.4.1. Theoretical heat of polymerization

Chemically, the heat released during polymerization arises from the ring opening of epoxy and anhydride functional group. Thus, theoretically, the total enthalpy of polymerization (ΔH_{pzn}) can be calculated based on the total heat released for ring opening of epoxy and anhydride functional group. The ring opening of both epoxy and anhydride by hydroxyl end is shown Scheme 4.3. It has been reported in many literature that the heat released from epoxy ring opening in epoxy homo-polymerization is ~94 kJ/mol, and the heat released from hydrolysis of phthalic anhydride is ~32 kJ/mol [10, 45].

a. Ring opening of epoxy

$\Delta H = 94$ kJ/mol

b. Ring opening of anhydride

$\Delta H = 32$ kJ/mol
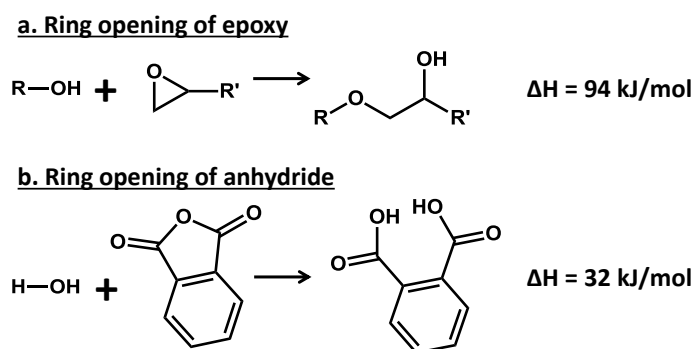
Scheme 4.3. Ring opening of epoxy and anhydride

In this experiment, the system was formulated with anhydride-to-epoxy molar ratio of 0.75. Using the heat released value above, the theoretical enthalpy of polymerization is calculated to be 305 kJ/mol. Then, considering the molecular weight of ESS (~2500-2600 g/mol) and MHHPA (168 g/mol), the

theoretical $\Delta Hpzn$ is equal to be 335 J/g. The experimental $\Delta Hpzn$ can be obtained from differential scanning calorimetry (DSC) experiments.

4.4.4.2. DSC peak analysis

Modulated differential scanning calorimetry (DSC) non-isothermal experiments were conducted to study the exothermic reaction of epoxy-anhydride polymerization, where the enthalpy of polymerization and temperature at maximum heat flow was compared between the catalysts. The samples were loaded into hermetic pans and were heated from 0-275 °C at 5 °C/min heating rate. Figure 4.5a-e shows the DSC non-reversible heat flow curves of epoxy-anhydride polymerization using different catalysts, and Figure 4.5f shows an example of the peak analysis that was used to compare the performance of the catalysts. The result of the peak analysis is then shown in Table 4.3.
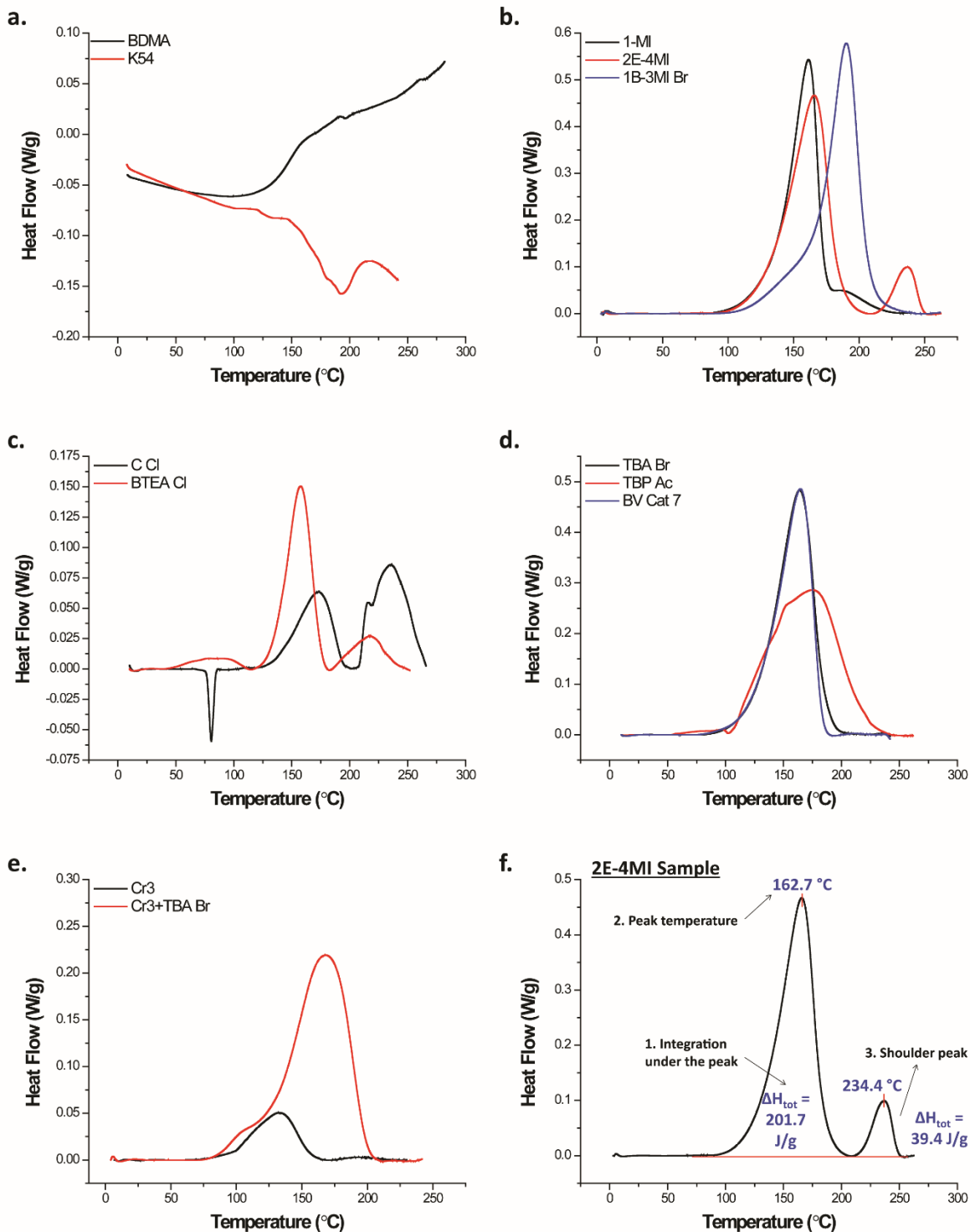
Figure 4.4. DSC curves of samples with different catalysts: a. tertiary amine, b. imidazole, c. quaternary ammonium salt containing chloride ion, d. quaternary onium salt, e. chromium-based, f. example of peak analysis

First, it is necessary to note the shape of the curves. All of the samples, except the one catalyzed with a tertiary amine possess exothermic non-reversible heat flow. For these samples, peak integration was not able to be obtained. Furthermore, as listed in Table 4.3, the heat of polymerization (ΔH_{pzn}) of all samples was less than the theoretical value of 355 J/g. In fact, only TBP Ac sample was able to reach enthalpy of polymerization of 300 J/g. The observed median value was found to be around 200 J/g. Therefore, the theoretical functional group conversion for the samples can be assumed to be between 70 – 90%. Based on this observation and results from volatilization study, it is expected that two competing events occur simultaneously: epoxy/anhydride polymerization (exothermic process) and volatilization of anhydride (endothermic process). These simultaneous events are therefore reducing the overall observed heat released. Furthermore, it is predicted that not all of the functional groups were indeed reacted. It may be quite difficult to reach 100% functional group conversion due to the thermoset reaching the vitrification point. Finally, ring-opening process may have occurred during mixing procedure and thus not being recorded by DSC experiment, thus also reducing the observed ΔH_{pzn}.

The temperature at where the maximum in the heat flow curves occurs is often associated with the activation energy of the reaction [46]. The Borchardt and Daniels approach assumes that the reaction follows nth order reaction and obeys Arrhenius temperature-dependence behavior. However, it is necessary to note that the activation energy of epoxy-anhydride polymerization can involve both initiation and propagation since propagation steps has been reported to occur at much faster rate than initiation [21, 22]. The peak temperature of exothermic heat flow curves of anhydride-cured ESS ranges from 155 – 190 °C. It is commonly thought that lower peak temperature can indicate lower activation energy. However, it will be shown later that lower peak temperature does not necessarily indicate lower activation energy.

Table 4.3. DSC peak analysis of samples with different catalysts

#	Type	Catalyst	ΔH$_{tot}$ (J/g)	T$_p$ (°C)	Shoulder ΔH$_{tot}$ (J/g)	Shoulder T$_p$ (°C)	Ea (kJ/mol)
1	**Tertiary amine**	BDMA	N/A	N/A	N/A	N/A	N/A
2		K54	N/A	N/A	N/A	N/A	N/A
3		1-MI	193.8	161.4	N/A	185.4	89.6
4	**Imidazole**	2E-4MI	201.7	165.7	39.5	236.4	79.4
5		1B-3MI Br	236.6	190.2	N/A	N/A	79.4
6		C Cl	26.43	173.7	34.6	235.3	N/A
-7	**Quaternary**	BTEA Cl	55.3	157.7	16.1	216.9	N/A
8	**Onium**	TBA Br	218.5	164.0	N/A	N/A	75.7
9	**Salts**	TBP Ac	300.6	175.2	N/A	N/A	93.5
10		BV-Cat 7	219.5	164.6	N/A	N/A	82.5
11	**Chromium**	Cr-3	21.3	133.2	N/A	N/A	N/A
12	**Mixture**	Cr3-TBA Br	142.6	168.1	102.7	N/A	N/A

The activation energy values calculated from peak temperature can be obtained more accurately by using a multiple heating rate method. Using the Kissinger method, the activation energy values can be obtained through following equations:

$$\frac{d(\ln(\beta/T_p{}^2))}{d(1/T_p)} = -\frac{E_a}{R} \tag{4.1}$$

where β is the heating rate in °C/min and T_p is the peak temperature [47]. Using this method, it is assumed that at the peak temperature using different heating rates, the extent of cure of the reaction is at a similar value. For this experiment, the activation energy of selected samples was determined. The samples include 1-MI, 2E-4MI, TBA Br, TBP Ac, 1B-3MI Br, BV-Cat 7. These samples were selected due to considerably lower volatilization amount and fairly high enthalpy of polymerization. With these samples, multiple DSC heating rate experiments (5, 10, and 20 °C/min) were conducted to determine the activation energy of the reaction. Using Equation 4.1, the calculated activation energy is listed in Table 4.3. The value of activation energy ranges from 67 – 90 kJ/mol, which is similar to what has been reported in the literature [18, 19, 48]. The lowest value was obtained for samples catalyzed with TBP Ac, while the highest is with TBA Br. Observing the peak temperatures, the samples catalyzed with TBA Br have a relatively lower peak temperature. The opposite is true with the 1B-MI Br sample, where it has the highest peak temperature, yet relatively low activation energy.

4.4.5.   Thermo-mechanical properties by dynamic mechanical analysis (DMA)

The viscoelastic properties of the thermoset samples were analyzed using dynamic mechanical analysis (DMA). Unfortunately, not all samples were able to be prepared successfully; some samples contain bubbles throughout the samples and thus could not be tested. Figures 4.5 and 4.6 show the storage modulus and tan delta curves of the tested samples, respectively; while Table 4.4 lists the detailed analysis of the DMA curves. These samples include BDMA, K54, 1-MI, 2E-4MI, C Cl, TBP Ac, BV Cat 7, Cr3 and Cr3 + TBA Br. Glass transition temperature, T_g, of the samples is determined as the temperature where the tan delta maximum occurs, and the values range from 20 to 100 °C. Overall, the T_g value and shape of the storage modulus and tan delta curves depends on the type of the catalyst used.
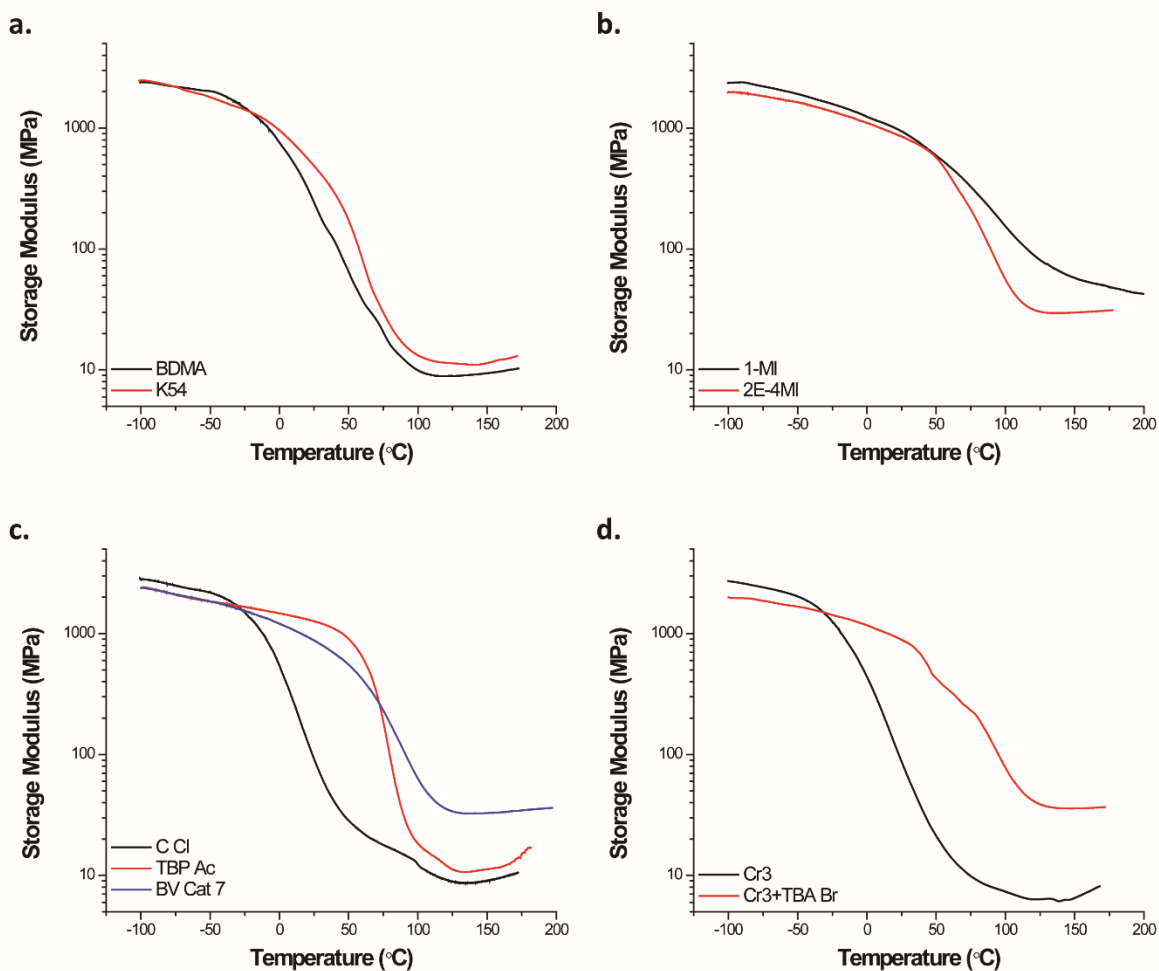
Figure 4.5. Storage modulus of anhydride-cured ESS thermoset with different catalysts: a. tertiary amine, b. imidazole, c. quaternary onium salt, d. chromium-based
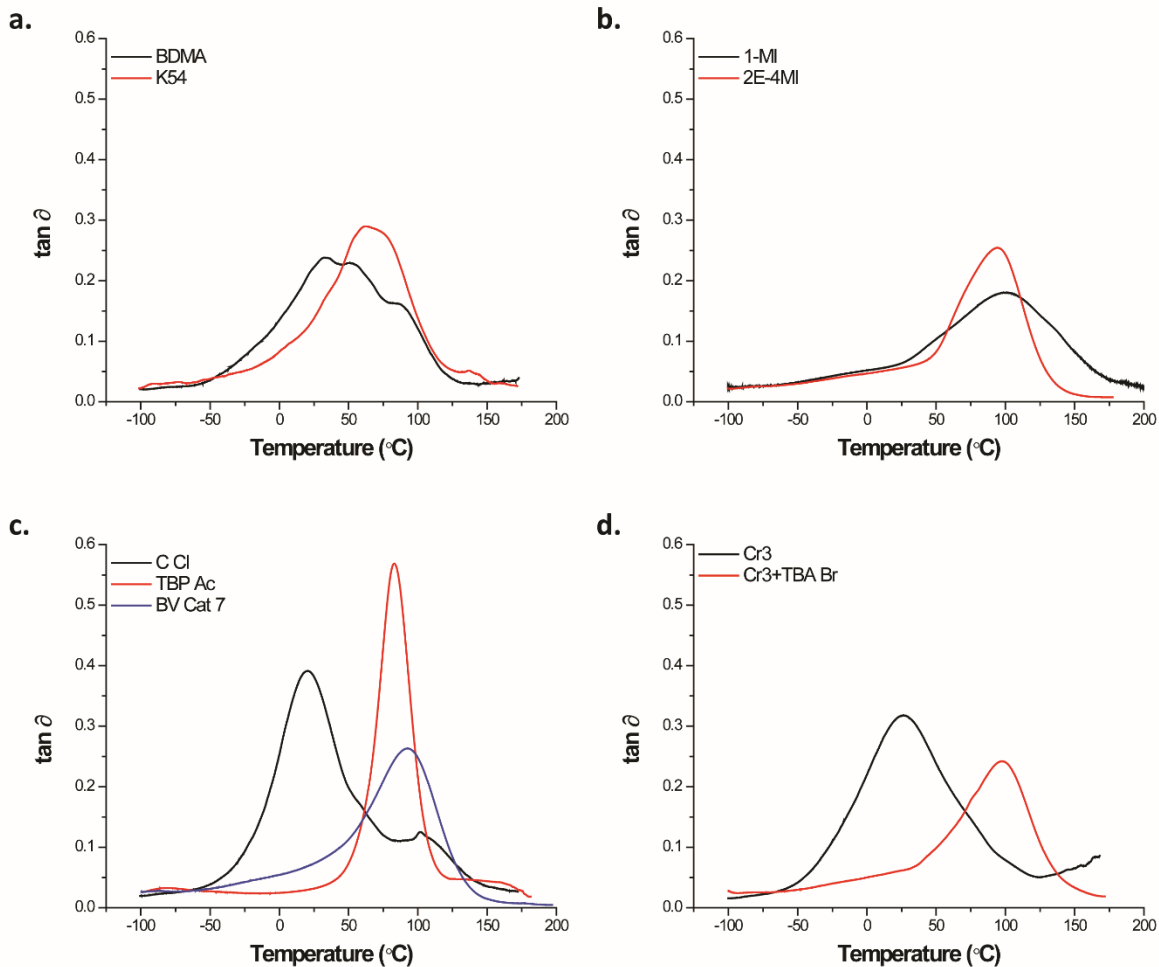
Figure 4.6. tan delta of anhydride-cured ESS thermoset with different catalysts: a. tertiary amine, b. imidazole, c. quaternary onium salt, d. chromium-based

Table 4.4. DMA peak analysis

#	Type	Catalyst	T_g by tan δ (°C)	tan δ Peak		Storage Modulus (MPa)		XLD at 150 °C
				Width (°C)	Height	At 25 °C	At 150 °C	
1	**Tertiary**	BDMA	32.6	104.4	0.24	243.2	9.41	0.89
2	**amine**	K54	64.8	70.1	0.29	487.7	11.4	1.08
3		1-MI	100.9	94.9	0.16	940.2	57.6	5.46
4	**Imidazole**	2E-4MI	94.1	54.4	0.24	850.9	29.8	2.88
5		1B-3MI Br	N/A	N/A	N/A	N/A	N/A	N/A
6		C Cl	20.3	52.6	0.36	92.2	9.03	0.86
7	**Quaternary**	BTEA Cl	N/A	N/A	N/A	N/A	N/A	N/A
8	**Onium**	TBA Br	N/A	N/A	N/A	N/A	N/A	N/A
9	**Salts**	TBP Ac	83.1	26.4	0.53	1266	11.3	1.07
10		BV-Cat 7	92.6	57.8	0.25	878.4	32.81	3.11
11	**Chromium**	Cr-3	26.1	73.6	0.28	87.7	6.52	0.62
12	**Mixture**	Cr3-TBA Br	97.6	58.2	0.22	889.5	35.8	3.39

The lowest T_g of ESS-MHHPA thermosets was observed for the C Cl-catalyzed sample, while the highest value was observed for the 1-MI catalyzed sample. Samples catalyzed using tertiary amines and imidazoles tend to have very broad tan delta peaks. Furthermore, for certain samples, multiple peaks were observed in the tan delta curves. Broad and multiple peaks in tan delta curves are often associated with the heterogeneity of the network system and the associated temperature where the polymer chain relaxation occurs. It is suggested that the high T_g value and the broad tan delta peak of the 1-MI catalyzed sample is attributed to its ability to be incorporated in the network system as a crosslinking agent. It was originally expected that the presence of water in the TBP Ac catalyst results in two types of initiation and/or propagation mechanisms, and thus lead to a more heterogeneous network. Yet, surprisingly, the tan delta curve of TBP Ac-catalyzed sample shows a comparatively narrow peak, which may indicate a homogenious network. One of the highest T_g values was obtained with samples catalyzed with Cr3+TBA Br, that is 97.6 °C. This result is quite unexpected since the T_g value is higher than any of the T_g value observed for quaternary-onium salt samples, and the T_g of the Cr3-catalyzed sample itself is fairly low at 26.1 °C.

The crosslink density (v_e) of the polymer network can be estimated using the storage modulus value in the rubbery plate region using rubber elasticity theory as follows:

$$E' = 3v_e RT \qquad\qquad (4.2)$$

where E' is the storage modulus, v_e is the crosslink density, R is the gas constant, and T is the temperature. For this experiment, the v_e is calculated at 150°C; and the result is shown in Table 4.4. The v_e of the network is relatively proportional to the T_g of the samples: higher T_g samples have higher v_e. However, the relationship between T_g and v_e is not quite linearly correlated due to following reason. The shape of the tan delta curves of the thermoset samples with different catalysts are quite unique, which indicates that the molecular network structure of the polymers are likewise unique. A linear correlation between T_g and v_e can be obtained only if the molecular network structure and the backbone of the polymers are relatively similar. The dissimilarity of the molecular network structure of the anhydride-cured ESS thermoset may be caused by possible side reactions occurring, amount of polymer dangling end chains from unreacted functional group, and different amount of intermolecular vs. intramolecular linkages between ESS molecules (intramolecular ESS linkages are when the epoxy in an ESS molecule is

connected with another epoxy within the same molecule, while intermolecular linkages are when the epoxy is connected with another epoxy of different ESS molecule). Furthermore, the polymer backbone and v_e of the ESS-MHHPA thermosets may differ due to the volatilization of MHHPA during curing. As shown in the previous section, the amount of MHHPA volatilization depends on the type of the catalyst used in the formulation. In this project, the anhydride-to-epoxy molar ratio of the formulation was fixed to 0.75 or 32% by wt. of anhydride in the formulation. The amount of anhydride left in thermoset can then be calculated from the difference of the initial concentration and the amount of volatilization. Figure 8 compares the amount of anhydride leftover in the thermoset after curing in the oven and the v_e. There seems to be a correlation between the amount of anhydride leftover after curing and the v_e of the thermosets.   Samples that has <15% anhydride content (BDMA, K54, C Cl, and Cr3), the v_e is approximately 1.0 mm^3/mol; while samples that has >15% anhydride content (2E-4MI, BV-Cat 7, and Cr3+TBA Br), the v_e is approximately 3.0 mm^3/mol. The exception to this observation occurs for 1-MI and TBP-Ac, where 1-MI sample has comparatively higher v_e and TBP-Ac sample has comparatively lower v_e.
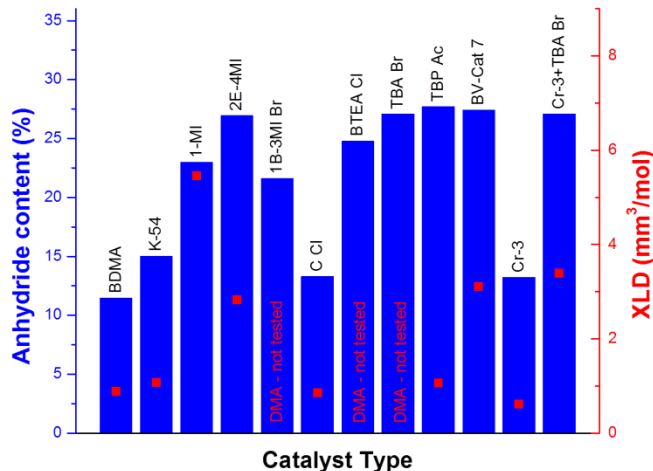
Figure 4.7. The amount of anhydride after curing process and the crosslink density of the cured thermosets

4.4.6.   Effect of water in the catalyst

One of the catalysts that performed well in catalyzing ESS/MHHHPA polymerization is tetrabutyl phosphonium acetate (40% aqueous solution). Previous research has shown that the presence of hydroxyl functionalities and/or impurities in the system can affect the reaction mechanisms, and may

promote polyetherification reactions [23, 24]. Here, the impact of the water in the catalyst system on the curing process and thermoset properties was evaluated. To accomplish this, a series of tetrabutyl ammonium bromide (TBA Br) aqueous solution catalyst systems (25, 50, and 75% wt. TBA Br) were prepared. Two sets of experiments were conducted. First, thermoset systems with 2% wt. loading of TBA Br catalyst solution were prepared; this set of experiments will be referred as "Set A". Second, the amount of pure TBA Br catalyst in formulation is fixed to 2% wt., therefore the TBA Br catalyst solution was added at 2-8% wt; this set will be referred as "Set B". The same series of experiments was conducted on both sets to evaluate the properties of the thermosets.

4.4.6.1. Volatilization during curing

Similar to the previous approach described above, the volatilization during curing was analyzed gravimetrically while curing in the oven and using non-isothermal TGA. The amount of volatilization during curing in the oven is presented in Table 4.5. All of the formulations only loss a total of 5% or less of its weight after the complete curing schedule. This volatilization is suggested due to the evaporation of raw materials and the water in the catalyst. There is no significant difference in the weight loss amount observed between the samples. However, in contrast, a difference between samples was detected through TGA experiment. Figure 4.7 shows the TGA curves of curing formulations heated from 23 to 600 °C at 10 °C/min heating rate; while Table 4.5 listed the results of TGA experiments.
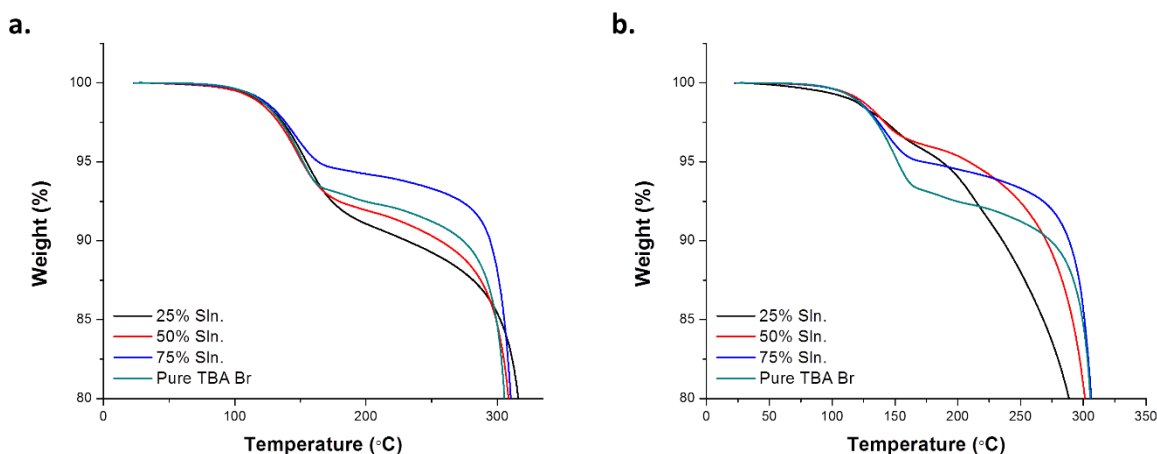
Figure 4.8. TGA curves of thermosets catalyzed with TBA Br solution: a. Set A, b. Set B

Table 4.5. TGA curves analysis and amount of volatilization

#	Type	Catalyst (% Aq. Solution)	Temp. at 2% wt. loss (°C)	Temp. at 2nd onset (°C)	Degradation Temp. (°C)	Weight loss at 40-200 °C (%)	Weight loss oven curing (%)
13	**Set A –**	25	131.7	174.4	310.4	8.9%	4.71%
14	**2%wt.**	50	128.7	166.8	306.2	8.0%	5.40%
15	**solution**	75	133.7	162.5	303.5	5.8%	4.44%
8	**loading**	Pure TBA Br	130.8	162.5	301.8	7.5%	4.15%
16	**Set B –**	25	134.4	158.3	288.4	5.9%	4.21%
17	**2%wt.**	50	135.9	153.6	292.7	4.6%	2.61%
18	**active**	75	131.9	156.4	298.5	5.5%	3.51%
8	**loading**	Pure TBA Br	130.8	162.5	301.8	7.5%	4.15%

The presence of water in the catalyst did not affect the weight loss during curing up to 130 °C. However, as the temperature was further heated, the weight loss curve of the samples is dependent on the amount of catalyst and water that are added in the formulation. Samples with 75% aqueous solution tend to perform better in minimizing anhydride volatilization. In contrast, samples with 25 and 50% aqueous solutions performed poorer than if no water were added to TBA Br. Comparing the two sets of samples, there are differences in the shapes of the TGA curves. For the 2% active TBA Br or Set B, the formulation continued to lose its weight as the temperature was increased. Furthermore, for these formulations, little or minimal gelation occurred to minimize the weight loss. The amount of volatilization during curing in the oven was found to be less than 6%, and the values are less than the weight loss during TGA experiment at 40 – 200 °C.

4.4.6.2. Soxhlet extraction and moisture uptake study

Gel fraction and water uptake of the samples was obtained through Soxhlet extraction and moisture uptake experiments, respectively; the result is shown in Table 4.6. The gel fractions of most of the samples are very high at >97%, while the moisture uptake after 1-month water immersion are very low at <2%. The exception of this observation is the sample catalyzed with 25% TBA Br solution of Set B, where the gel fraction is only 58% and the 1-month moisture uptake is 7%. It is expected that this sample has a high amount of carboxylic acid end groups in the network, which then caused poor hydrostability of the thermoset.

Table 4.6. Moisture uptake and gel content of thermosets catalyzed with TBA Br solution

#	Type	Catalyst	Gel Fraction (%)	Moisture Uptake (%)	
				1-week	1-month
13	**Set A –** 2%wt. solution loading	25% Sln.	99.13 ± 0.03	0.92 ± 0.03	1.25 ± 0.06
14		50% Sln.	99.06 ± 0.09	0.78 ± 0.03	0.92 ± 0.01
15		75% Sln.	99.02 ± 0.03	0.59 ± 0.03	0.70 ± 0.01
8		Pure TBA Br	98.49 ± 0.08	0.53 ± 0.05	0.53 ± 0.12
16	**Set B –** 2%wt. active loading	25% Sln.	58.14 ± 0.49	3.68 ± 0.10	7.15 ± 0.01
17		50% Sln.	97.05 ± 0.12	1.18 ± 0.02	1.78 ± 0.02
18		75% Sln.	98.32 ± 0.05	0.74 ± 0.03	0.91 ± 0.05
8		Pure TBA Br	98.49 ± 0.08	0.53 ± 0.05	0.53 ± 0.12

4.4.6.3. DSC results

Differential scanning calorimetry experiments were conducted to analyze the exothermic profile of the formulations during curing. Figure 4.8 shows the non-reversible heat flow curves of samples when heated from 25 to 250 °C at 5 °C/min, while Table 4.7 shows the detailed data analysis. For Set A samples, as the amount of water in the catalyst system was increased, the peak width at half height was broadened from 35 to 70 °C. Despite the broadening of the curve, the peak temperature did not shift significantly. In contrast, for Set B samples, the temperature at the maximum exothermic peak shifted to lower temperature as the amount of water was increased. The temperature at the maximum exothermic peak of 25% TBA Br solution occurs at 134 °C, that is 30 °C lower than if no water was added to the catalyst. For samples containing 50 and 75% TBA Br solution, the appearance of multiple peaks seems to be observed. It is thought that the first peak correlates to the polymerization when pure TBA Br (no water added), while the other one correlates to the polymerization when water is added to the catalyst. For all of the samples, no additional shoulder peak was observed in the heat flow curves.
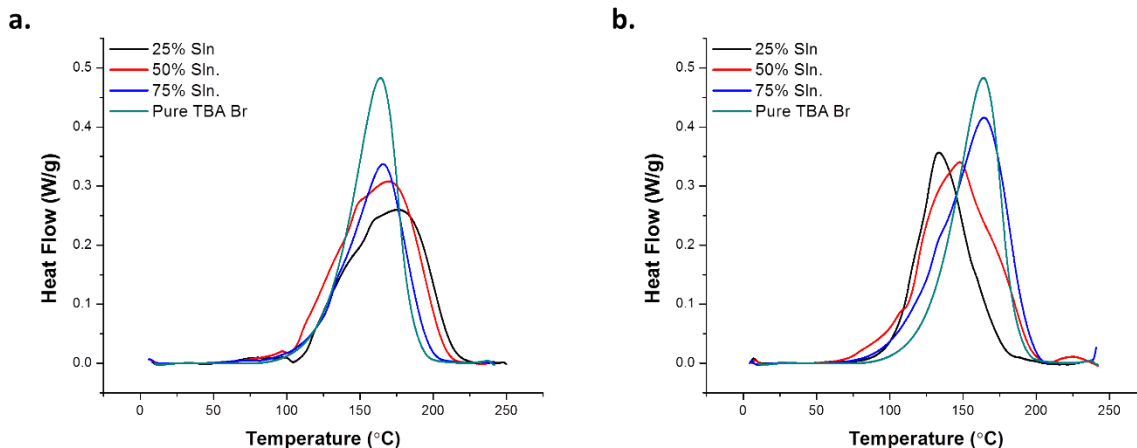
Figure 4.9. DSC curves of thermoset catalyzed with TBA Br solution: a. Set A, b. Set B

Table 4.7. DSC peak analysis

#	Type	Catalyst	ΔH_{tot} (J/g)	T_p (°C)	Ea (kJ/mol)
13	**Set A –**	25% Sln.	210.4	175.75	77.1
14	**2%wt.**	50% Sln.	241.4	169.19	80.8
15	**solution**	75% Sln.	192.8	165.7	N/A
8	**loading**	Pure TBA Br	218.5	164.0	66.3
16	**Set B –**	25% Sln.	205.6	133.59	N/A
17	**2%wt.**	50% Sln.	247.5	147.64	71.8
18	**active**	75% Sln.	265.2	164.3	N/A
8	**loading**	Pure TBA Br	218.5	164.0	66.3

Integration of the heat flow curves results in the enthalpy of polymerization (ΔH_{pzn}). The ΔH_{pzn} values for these formulations were determined to be 180 – 280 J/g, which is similar to what has been previously observed. Note that the standard deviation of ΔH_{pzn} is about 20%, thus it can be thought that there was no significant difference in the ΔH_{pzn} values for Set A samples. Furthermore, it is suggested that TBA Br and water works synergistically to ring open the epoxy/anhydride groups. In comparison, for Set B samples, the ΔH_{pzn} produced samples catalyzed with 25% solution and pure TBA Br (no water added), is less than the one catalyzed with 75% TBA Br solution.

Then, the effect of water in the catalyst system on the activation energy is studied by comparing samples catalyzed by pure TBA Br and 50% TBA Br solution from Set A and Set B. Samples catalyzed with 50% TBA Br solution for both sets indicates lower activation energy compared to the one catalyzed by pure TBA Br. Based on this observation, lower activation energy may be caused by following

explanation. First, at the same weight amount of TBA Br in the samples, the presence of water

decreases the activation energy by 20 kJ/mol. Second, as expected, increasing the amount of

catalyst/water in the samples results in a lower activation energy. Then, at the same weight amount of

catalysts, decreased in the activation energy can be obtained by partially substituting TBA Br in the water.

4.4.6.4. DMA results

The viscoelastic property of the thermosets was analyzed using dynamic mechanical analysis.

Unfortunately, only few samples were successfully prepared and examined; while other samples

contained many trapped bubbles within the samples and thus cannot be tested. The samples being

tested include Set A: 25%, 50%, and 75% TBA Br solution and Set B: 50% and 75% TBA Br solution.

Figure 4.9 display the storage modulus and tan delta curves of the samples, while Table 4.8 lists the

detailed analysis of the curves.
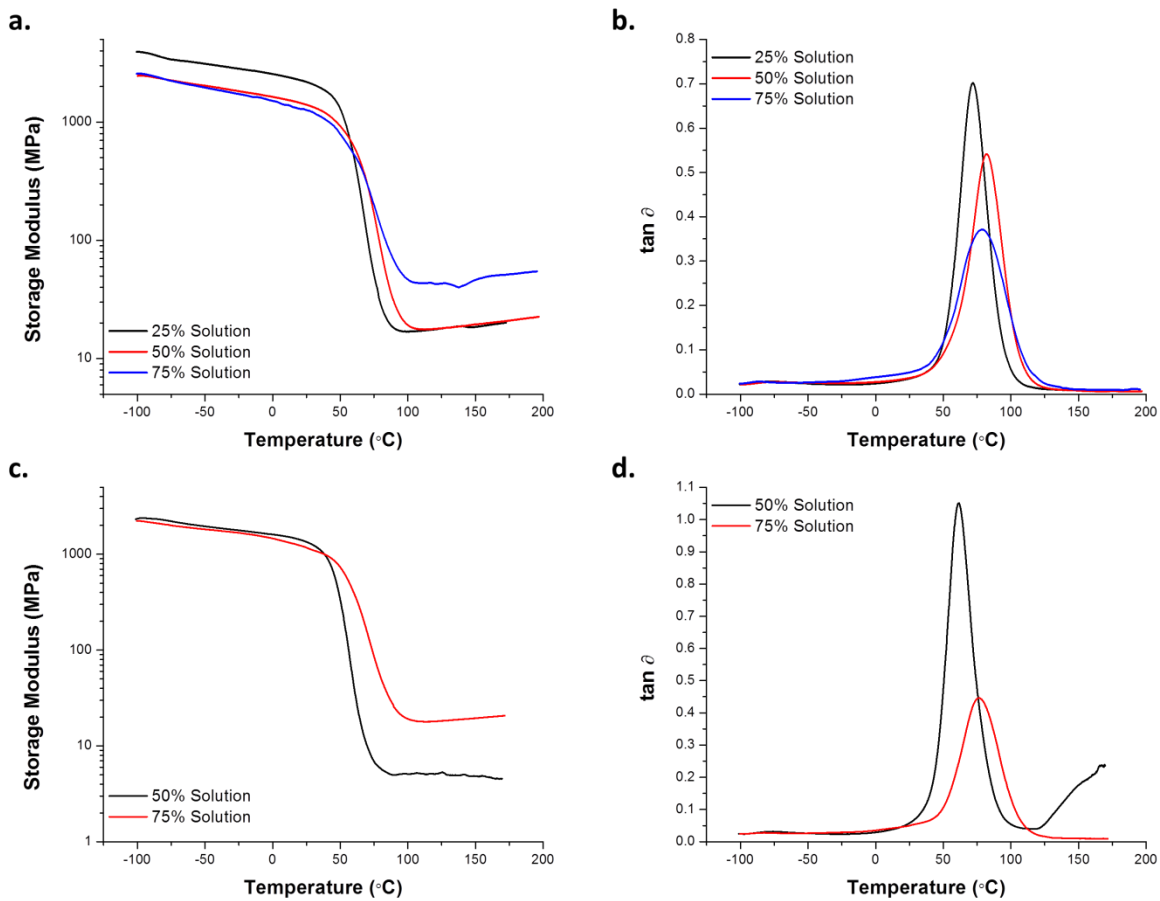
Figure 4.10. Storage modulus and tan delta curve of thermosets catalyzed with TBA Br solution: a-b. Set A, c-d. Set B

106

Table 4.8. DMA analysis of samples catalyzed with TBA Br solution

#	Type	Catalyst	T_g by tan δ (°C)	tan δ Peak		Storage Modulus (MPa)		XLD at 150 °C (mol/mL)
				Width (°C)	Height	At 25 °C	At 150 °C	
13	**Set A –**	25% Sln.	71.7	24.1	0.69	2184	18.52	1.76
14	**2%wt.**	50% Sln.	82.1	27.7	0.53	1402	19.48	1.84
15	**solution**	75% Sln.	80.0	29.6	0.35	1266	46.27	4.38
8	**loading**	Pure TBA Br	N/A	N/A	N/A	N/A	N/A	N/A
16	**Set B –**	25% Sln.	N/A	N/A	N/A	N/A	N/A	N/A
17	**2%wt.**	50% Sln.	61.5	22.0	1.02	1349	4.847	0.46
18	**active**	75% Sln.	76.5	33.0	0.43	1174	19.48	1.846
8	**loading**	Pure TBA Br	N/A	N/A	N/A	N/A	N/A	N/A

The tan delta curves of these samples indicate that increased amounts of water in the catalysts result in narrower and more intense peaks, which is similar to what has been observed with TBP Ac-catalyzed sample. The glass transition temperature of the thermoset samples was determined at the temperature at maximum tan delta peak. The highest T_g was observed with samples catalyzed by 50% and 75% TBA Br solution from Set A: 82.1 and 80.0 °C, respectively. Even though their T_g values are fairly similar, the approximate crosslink density of 75% solution was observed to be higher than 50% solution. This disparity is possible due to similar reasons explained in previous section, where their molecular network chain structures are quite different.

4.5. Conclusion

The structure-property relationships of ESS-MHHPA thermosets were studied as a function of the type of curing catalyst. An optimum catalyst is determined to be one that can initiate the reaction efficiently at a relatively low temperature, minimizing the amount volatilization during curing, and yielding networks having a high glass transition temperature, high gel fraction, and good hydrostability. Based on a series of experiments, it is believed that the nucelophilicity of the catalyst influences the reaction mechanism, and thus the materials properties, where the chromium-3 tris-2-ethylhexanoate shows the least efficiency, while quaternary onium salts shows the highest efficiency. However, it was also observed that the structure of the cation/anion in the quaternary onium salts affect the catalyst efficiency. The poor dispersity/solubility of the chloride anion in the formulation results in the inefficiency of the catalyst. Then, it was shown that moisture does play role in the catalysis of the epoxy-anhydride reaction.

However, there seems to be an optimum or threshold concentration before the effect of moisture in the catalyst becomes detrimental, resulting in lower T_g and poor hydrostability.

4.6. Acknowledgements

4.7. References

[1]   R. Auvergne, S. Caillol, G. David, B. Boutevin, J.-P. Pascault, Biobased Thermosetting Epoxy: Present and Future, Chemical Reviews, 114 (2013) 1082-1115.

[2]   X. Pan, P. Sengupta, D.C. Webster, High biobased content epoxy-anhydride thermosets from epoxidized sucrose ester of fatty acids, Biomacromolecules, 12 (2011) 2416-2428.

[3]   X. Pan, D.C. Webster, Impact of Structure and Functionality of Core Polyol in Highly Functional Biobased Epoxy Resins, Macromolecular Rapid Communications, 32 (2011) 1324-1330.

[4]   D.C. Webster, P.P. Sengupta, Z. Chen, X. Pan, A. Paramarta, Highly functional epoxidized resins and coatings, in: United States Patent Office, NDSU Research Foundation, US, 2015.

[5]   X. Pan, P. Sengupta, D.C. Webster, Novel biobased epoxy compounds: epoxidized sucrose esters of fatty acids, Green Chemistry, 13 (2011) 965-975.

[6]   E.M. Monono, D.C. Webster, D.P. Wiesenborn, Pilot scale (10 kg) production and characterization of epoxidized sucrose soyate, Industrial Crops and Products, 74 (2015) 987-997.

[7]   P.P. Sengupta, X. Pan, T.J. Nelson, A. Paramarta, D.C. Webster, Cationic UV curing characteristics of epoxidized sucrose esters, in: American Coatings Society National Meeting, PMSE, 2010, pp. 888-889.

[8]   X. Pan, D.C. Webster, New Biobased High Functionality Polyols and Their Use in Polyurethane Coatings, ChemSusChem, 5 (2012) 419-429.

[9]   A. Paramarta, X. Pan, D.C. Webster, Highly functional acrylated biobased resin system for uv-curable coatings, Radtech Report, (2013) 26-32.

[10]   T. Nelson, T. Galhenage, D. Webster, Catalyzed crosslinking of highly functional biobased epoxy resins, J Coat Technol Res, 10 (2013) 589-600.

[11]   T. Nelson, B. Masaki, Z. Morseth, D. Webster, Highly functional biobased polyols and their use in melamine–formaldehyde coatings, J Coat Technol Res, 10 (2013) 757-767.

[12]   T.J. Nelson, L. Bultema, N. Eidenschink, D.C. Webster, Bio-Based High Functionality Polyols and Their Use in 1K Polyurethane Coatings, Journal of Renewable Materials, 1 (2013) 141-153.

[13]   C.S. Kovash, E. Pavlacky, S. Selvakumar, M.P. Sibi, D.C. Webster, Thermoset Coatings from Epoxidized Sucrose Soyate and Blocked, Bio-Based Dicarboxylic Acids, ChemSusChem, 7 (2014) 2289-2294.

[14]   J. Yan, D.C. Webster, Thermosets from highly functional methacrylated epoxidized sucrose soyate, Green Materials, 2 (2014) 132-143.

[15]   S. Ma, D.C. Webster, Naturally Occurring Acids as Cross-Linkers To Yield VOC-Free, High-Performance, Fully Bio-Based, Degradable Thermosets, Macromolecules, 48 (2015) 7127-7137.

[16]   S. Ma, D.C. Webster, F. Jabeen, Hard and Flexible, Degradable Thermosets from Renewable Bioresources with the Assistance of Water and Ethanol, Macromolecules, 49 (2016) 3780-3788.

[17]   A. Paramarta, D.C. Webster, Bio-based high performance epoxy-anhydride thermosets for structural composites: The effect of composition variables, Reactive and Functional Polymers, 105 (2016) 140-149.

[18]   N. Bouillon, J.-P. Pascault, L. Tighzert, Influence of different imidazole catalysts on epoxy-anhydride copolymerization and on their network properties, Journal of Applied Polymer Science, 38 (1989) 2103-2113.

[19]   N. Boquillon, C. Fringant, Polymer networks derived from curing of epoxidised linseed oil: influence of different catalysts and anhydride hardeners, Polymer, 41 (2000) 8603-8613.

[20]   W.J. Blank, Z.A. He, M. Picci, Catalysis of the epoxy-carboxyl reaction, Journal of Coatings Technology, 74 (2002) 33-41.

[21]   V. Trappe, W. Burchard, B. Steinmann, Anhydride-cured epoxies via chain reaction. 1. The phenyl glycidyl ether/phthalic acid anhydride system, Macromolecules, 24 (1991) 4738-4744.

[22]   J. Leukel, W. Burchard, R.-P. Krüger, H. Much, G. Schulz, Mechanism of the anionic copolymerization of anhydride-cured epoxies – analyzed by matrix-assisted laser desorption

ionization time-of-flight mass spectrometry (MALDI-TOF-MS), Macromolecular Rapid Communications, 17 (1996) 359-366.

[23]   R.F. Fischer, Polyesters from epoxides and anhydrides, Industrial and Engineering Chemistry, 52 (1960) 321-323.

[24]   E.C. Dearborn, R.M. Fuoss, A.K. MacKenzie, R.G. Shepherd, Epoxy resins from bis-, tris-, and tetrakisglycidyl etheres, Industrial and Engineering Chemistry, 45 (1953) 2715-2721.

[25]   L. Matějka, J. Lövy, S. Pokorný, K. Bouchal, K. Dušek, Curing epoxy resins with anhydrides. Model reactions and reaction mechanism, Journal of Polymer Science: Polymer Chemistry Edition, 21 (1983) 2873-2885.

[26]   Y. Tanaka, H. Kakiuchi, Study of epoxy compounds. Part I. Curing reactions of epoxy resin and acid anhydride with amine and alcohol as catalyst, Journal of Applied Polymer Science, 7 (1963) 1063-1081.

[27]   Y. Tanaka, H. Kakiuchi, Study of epoxy compounds. Part VI. Curing reactions of epoxy resin and acid anhydride with amine, acid, alcohol and phenol as catalysts, Journal of Polymer Science: Part A, 2 (1964) 3405-3430.

[28]   J. Feltzin, M.K. Barsh, E.J. Peer, I. Petker, The Kinetics of Epoxy Polymerization, Journal of Macromolecular Science: Part A - Chemistry, 3 (1969) 261-274.

[29]   J. Rocks, L. Rintoul, F. Vohwinkel, G. George, The kinetics and mechanism of cure of an amino-glycidyl epoxy resin by a co-anhydride as studied by FT-Raman spectroscopy, Polymer, 45 (2004) 6799-6811.

[30]   M.S. Heise, G.C. Martin, Curing mechanism and thermal properties of epoxy-imidazole systems, Macromolecules, 22 (1989) 99-104.

[31]   J.D.B. Smith, Latent organic phosphonium salt catalysts for curing glycidyl ether epoxy resins, in: US Patent Office, Westinghouse Electric Corporation, 1974.

[32]   L.L. Bott, M. Helvey, Thermosetting powder coating compositions, in: US Patent Office, Eastman Kodak Company, 1993.

[33]   G.E. Meyer, Carboxyl terminated polydienes, in: US Patent Office, The Goodyear Tire and Rubber, United States, 1978.

[34]   R.L. De Hoff, Process for curing epoxy resin anhydride blends at moderately elevated

         temperatures, in: US Patent Office, United States, 1990.

[35]   J.D.B. Smith, R.N. Kauffman, Carboxylic acid storage stabilizers for latent catalyst cured epoxy

         resin, in: United States Patent, Westinghouse Electric Corporation, United States, 1977.

[36]   L.R. Amirova, A.R. Burilov, L.M. Amirova, I. Bauer, W.D. Habicher, Kinetics and mechanistic

         investigation of epoxy–anhydride compositions cured with quaternary phosphonium salts as

         accelerators, Journal of Polymer Science Part A: Polymer Chemistry, 54 (2016) 1088-1097.

[37]   R.O. De Jongh, A. Visser, R. van der Linde, Powder coating, in: United States Patent Office,

         Internationale Octrooi Maatschappij "octropa" B.V., 1982.

[38]   Z. Zhang, C.P. Wong, Study on the catalytic behavior of metal acetylacetonates for epoxy curing

         reactions, Journal of Applied Polymer Science, 86 (2002) 1572-1579.

[39]   Z. Zhang, C.P. Wong, Study on Metal Chelates as Catalysts of Epoxy and Anhydride Cure

         Reactions for No-Flow Underfill Applications, in: Polymers for Microelectronics and

         Nanoelectronics, American Chemical Society, 2004, pp. 264-278.

[40]   Z.Q. Zhang, S.H. Shi, C.P. Wong, Development of no-flow underfill materials for lead-free solder

         bumped flip-chip applications, in: Advanced Packaging Materials: Processes, Properties

         andInterfaces, 2000. Proceedings. International Symposium on, 2000, pp. 278-284.

[41]   J.D.B. Smith, R.N. Kaufmann, Fluid solventless epoxy-anhydride compositions containing metal

         acetylacetonate accelerators and organic carboxilic acid co-accelerators, in: United States

         Patent, Westinghouse Electric Corp., United States, 1978.

[42]   C.P. Wong, S.H. Shi, G. Jefferson, High performance no-flow underfills for low-cost flip-chip

         applications: material characterization, Components, Packaging, and Manufacturing Technology,

         Part A, IEEE Transactions on, 21 (1998) 450-458.

[43]   A.V. Kurnoskin, Reaction mechanisms of the metal chelates with epoxy oligomers and the

         structures of the epoxy—chelate metal-containing matrixes, Journal of Applied Polymer Science,

         46 (1992) 1509-1530.

[44]   Hamerton, B.J. Howlin, P. Jepson, Metals and coordination compounds as modifiers for epoxy

         resins, Coordination Chemistry Reviews, 224 (2002) 67-85.

[45]   V.G. Alekseev, V.D. Kizaev, N.V. Fedyainov, V.I. Bushinskii, Standard enthalpies of

         anhydridisation of phthalic and pyromellitic acids, Russian Journal of Physical Chemistry (English

         Translated), 63 (1989) 1280-1282.

[46]   H.J. Borchardt, F. Daniels, The Application of Differential Thermal Analysis to the Study of

         Reaction Kinetics1, Journal of the American Chemical Society, 79 (1957) 41-46.

[47]   H.E. Kissinger, Reaction Kinetics in Differential Thermal Analysis, Analytical Chemistry, 29 (1957)

         1702-1706.

[48]   N. Sbirrazzuoli, S. Vyazovkin, Learning about epoxy cure mechanisms from isoconversional

         analysis of DSC data, Thermochemica Acta, 388 (2002) 289-298.

CHAPTER 5. TOUGHENING OF BIO-BASED ANHYDRODE-CURED EPOXY THERMOSETS MADE FROM EPOXIDIZED SUCROSE SOYATE

5.1. Abstract

Several methods to improve the toughness of anhydride-cured epoxidized sucrose soyate thermosets were explored. These included flexibilization via the addition of a secondary crosslinker and the introduction of a secondary phase rubbery polymer. The addition of these toughening agents resulted in the tensile failure mode changing from brittle to ductile; yet the degree of toughness improvement was dependent on the nature of the toughening agents. Overall, using a secondary crosslinker to flexibilize the polymer network resulted in a lower increase in the tensile strain, yet did not compromise the Young's modulus and tensile strength. In contrast, using a secondary phase rubbery polymer resulted in a greater increase in tensile strain, yet compromised the Young's modulus. The secondary phase network in the thermosets is well incorporated and is nanoscale sized based on results obtained from dynamic mechanical analysis, as well as visual and electron microscopy imaging.

5.2. Introduction

Epoxy resins are one of the most versatile chemical building blocks for thermoset materials, and have been used extensively for a wide range of applications including composites, coatings, adhesives, laminates, tooling, molding, and many more. The versatility of epoxy resins can be attributed to their reactivity and numerous options for crosslinking. Epoxy resins were first commercialized in the 1940s, and since then, a wide range of epoxy resins with different backbones and the number of functionalities per molecule have been introduced. Epoxy resins are often prepared by glycidylation of hydroxyl groups using epichlorohydrin or via epoxidation of olefins using peracids. The majority of the commercially available epoxy resins today are derived from petrochemicals, with one of the most commonly used classes of epoxy resins being the diglycidyl ethers of bisphenol-A (DGEBA). However, in the recent decade, there has been an ongoing movement to promote future sustainability by using renewable materials as chemical commodities. For epoxy thermosets, there has been an extensive research in creating building blocks—both epoxy resins and crosslinkers—and then exploring their applications in many fields. These building blocks include renewable materials from polyphenols, tannins, cardanol, woody biomass, lignin, starch and vegetable oils [1-9]. The use of these renewable-based sources is

explored as either a full replacement or partial substitution of the petrochemical based systems depending on the desired target properties of the final application.

One of the recently explored bio-based epoxy resin systems that shows promise as a replacement for the DGEBA epoxy system is epoxidized sucrose soyate crosslinked with a cyclic anhydride [10-12]. The epoxy resin is comprised of the sucrose ester of vegetable oil fatty acids, and named epoxidized sucrose ester (ESE); a representative chemical structure is shown in Figure 5.1. The number of epoxy functional group in the ESE can be controlled by modifying the degree of esterification in the sucrose and/or changing the type of vegetable oil used. For example, epoxidized sucrose soyate, ESS, can have an average of 12-13 epoxy functional groups per molecule. Thermosets based on ESE have been shown to have significantly higher strength, modulus and Tg compared to comparable thermosets based on epoxidized vegetable oils. The improvements observed in the mechanical properties of the thermosets has been attributed to both the rigidity of the sucrose core and the higher crosslink density obtained due to the high number of epoxy functional groups per molecule [13]. Many crosslinking technologies using this epoxy resin have been explored: epoxy homopolymerization (cationic UV and thermally cured) and epoxy-acid/anhydride curing [9, 13-18]. In addition, (meth)acrylated derivatives have been cured thermally and using UV and polyols derived from ESEs have been cured using either polyisocyanates to form polyurethanes and also melamine-formaldehyde resins [19-23]. Furthermore, the use of this thermoset system based on ESE as a matrix resin for composite applications has been explored [24-28]. Even though composites comprising ESE resin have excellent flexural and tensile strengths, the ESE-based thermosets suffer a similar issue that is commonly encountered with petroleum-based epoxy resins; the thermosets tend to be brittle and thus require modification to yield an improvement in toughness.

Epoxidized Sucrose Soyate (ESS)
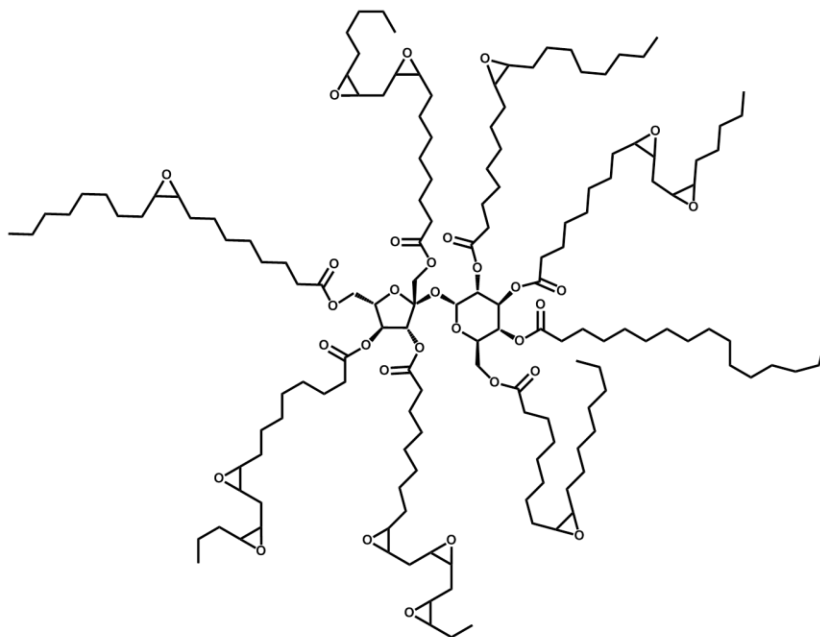
Anhydride Crosslinker
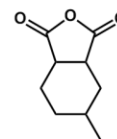
Methylhexahydrophthalic anhydride

Catalyst
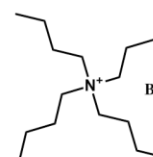
Tetrabutylammonium bromide (75% aq. Sln)

REACTIVE DILUENTS
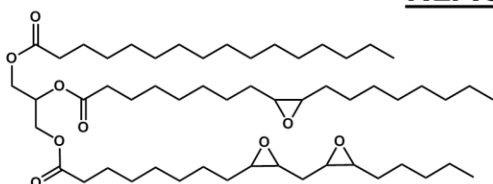
Epoxidized Soybean Oil (ESO)
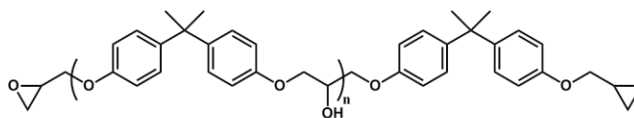
Bisphenol-A Diglycidyl Ether (EPON 828)
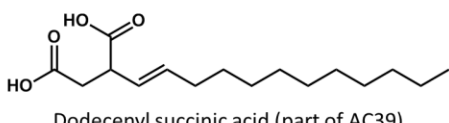
Dodecenyl succinic acid (part of AC39)

R = soybean oil fatty acids
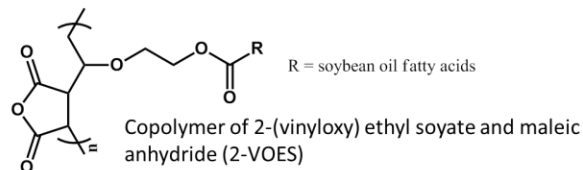
Copolymer of 2-(vinyloxy) ethyl soyate and maleic anhydride (2-VOES)

SECONDARY PHASE ADDITIVE

x=0.67, y=0.15, z=0.18
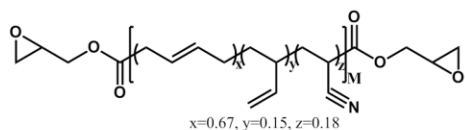
Epoxy terminated poly(butadiene-acrylonitrile) (ETBN)

x=0.67, y=0.15, z=0.18
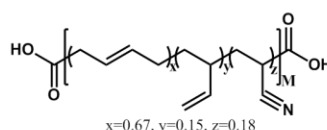
Carboxy terminated poly(butadiene-acrylonitrile) (CTBN)
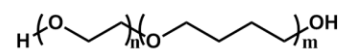
Copolymer of ethylene oxide and butylene oxide (Fortegra 100)

Figure 5.1. Chemicals used in this study which include epoxidized sucrose soyate, anhydride crosslinkers and toughening agents

Figure 5.2 illustrates the various methods that are used to modify epoxy thermosets to improve their toughness. First, the toughness can be improved by a flexibilization method, which works based on modification of the structure of the polymer backbone [29-32]. The flexibilization may involve incorporation of a more flexible backbone structure and/or decrease in the network crosslink density by either increasing the molecular weight between chains or decreasing the functionality of the crosslinker. The other common approach for epoxy toughening involves the incorporation of a dispersed secondary phase in the cured epoxy resin. This secondary phase may include soft materials (i.e. rubber, reactive liquid polymer, and thermoplastic) or hard materials (i.e. silica, metal oxide, ceramic, clay, small molecular rigid molecule such as lignin). These secondary phase materials are often chemically functionalized to minimize the aggregation of the particles, to improve the interaction between particles and polymer network, and to further reinforce the polymer network. One of the most commonly used functionalized rubbers or reactive liquid polymers is a copolymer of butadiene and acrylonitrile. This copolymer is miscible in the liquid formulation, yet undergoes phase separation during the curing process. The degree of phase separation and type of morphology in the cured matrix has been shown to depend on the curing temperature, loading amount, type of reactive functionalities, and ratio between acrylonitrile and butadiene. Another type of rubbery polymer often used as toughening agents is amphiphilic block copolymers. Similar to reactive liquid polymers, this block copolymers phase separate during the curing process. However, in contrast to acrylonitrile-butadiene copolymer, the phase separation occurs at the nanoscale, and is thus expected to improve the toughness more efficiently [33, 34]. Many literature review articles regarding rubber-toughened epoxy thermosets have been published [30, 35, 36].
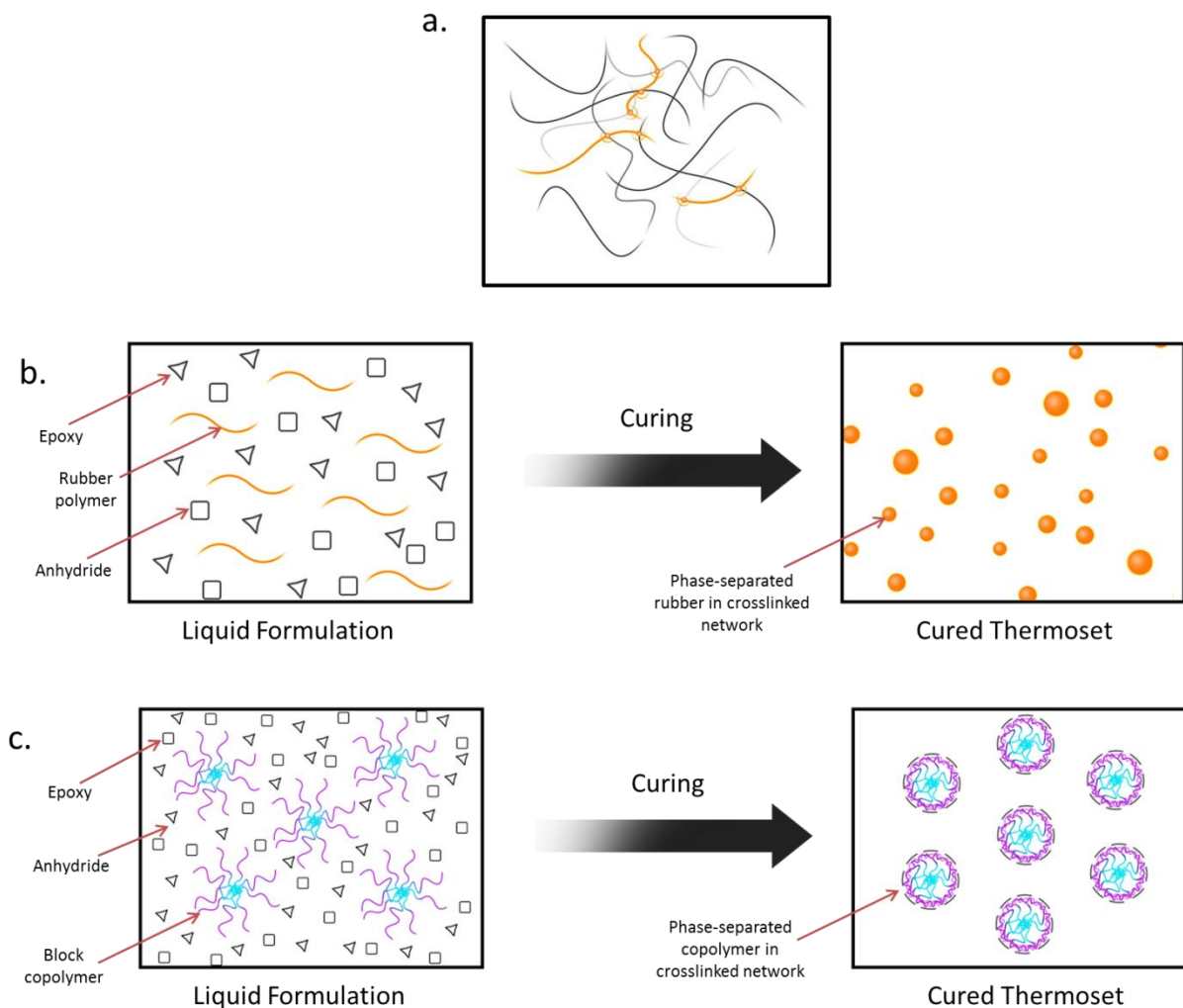
Figure 5.2. Methods of epoxy toughening: a. flexibilization through secondary crosslinker, b. secondary phase through reactive functionalized rubber, c. secondary phase through block copolymers

In this study, the toughness improvement of the ESS-anhydride thermoset system was explored. Two methods of toughening were evaluated. The first approach involved the addition of a secondary crosslinker or reactive diluents; this secondary epoxy resin or anhydride crosslinker was predicted to act as a flexibilizing agent by modifying the rigidity of the polymer chain and the crosslinking density. The second approach involved adding a secondary phase rubbery polymer; this rubbery polymer was predicted to phase separate during the curing process and then form a secondary phase in the thermoset network. Viscoelastic properties, tensile properties, impact toughness, and fracture toughness were assessed. Morphology of the fractured surface was studied using electron microscopy. As a control

system, thermosets materials comprised of DGEBA, epoxidized soybean oil (ESO), and polyanhydride AC39 were also prepared.

5.3. Experimental

5.3.1. Material and formulation composition

Epoxidized sucrose soyate (ESS) was synthesized from sucrose soyate (Sefose 1618U from Procter and Gamble Chemicals) via the Prilezhaev reaction; the detailed synthesis process used is described in the literature [10, 11]. The epoxy equivalent weight of ESS was analyzed through hydrogen bromide titration, and the value was determined to be 246 g/eq. The crosslinker used in the study is methyl hexahydrophthalic anhydride (MHHPA), provided by Dixie Chemicals. MHHPA is liquid at room temperature, thus providing for easy mixing. Tetrabutyl ammonium bromide aqueous solution (75% concentration) was used to catalyze the epoxy-anhydride reaction; it was purchased from Sigma Aldrich. Epoxy and carboxy terminated polybutadiene acrylonitrile copolymer (ETBN X63, ETBN X68, CTBN X8, CTBN X13, CTBN X31) was provided by Emerald Performance Materials, while copolymer of ethylene oxide and butylene oxide (Fortegra 100) was given by Dow Chemicals.

5.3.2. Formulation compositions, mixing and curing procedures

5.3.2.1. Formulation compositions

In this study, 3 sets of formulations were prepared: control (C), secondary crosslinker-modified (SC), and secondary phase-modified (SP). Secondary crosslinkers used in this experiment include epoxidized soybean oil (supplied by Arkema), bisphenol-A diglycidyl ether or EPON 828 (supplied by Momentive), polypropylene glycol di-dodecenyl succinate or AC 39 (supplied by Broadview Technology), and 2-(vinyloxy) ethyl soyate and maleic anhydride copolymer in 50% toluene or 2-VOES. The synthesis of 2-VOES crosslinker is described by Chisholm et al [37]. The secondary phase used in this experiment includes epoxy or carboxy terminated poly-butadiene acrylonitrile (ETBN and CTBN) and copolymer of ethylene oxide and butylene oxide (Fortegra 100). Many types of the ETBN and CTBN with variation in the acrylonitrile content were explored: ETBN X68, ETBN X63, CTBN X8, CTBN X31, and CTBN X13. ETBN polymer has an epoxy groups as its end chain, while CTBN polymer carboxylic acid groups as its end chain. The amount of acrylonitrile in the polymer is as follow: 10% for CTBN X31, 18% for CTBN X8 and ETBN X68, and 26% for CTBN X13 and ETBN X63. Figure 5.1 shows the chemical structures of the

materials used in this study, while Table 5.1 lists the composition of the formulations that were prepared. The control formulations contain one primary epoxy resin (either ESS or secondary crosslinker epoxy resin) and one anhydride crosslinker (either MHHPA or seondary anhydride crosslinker). The secondary crosslinker-modified (SC) formulations contain ESS, MHHPA and a secondary epoxy/anhydride crosslinker. Then, the secondary phase-modified (SP) formulations contain ESS, MHHPA and a reactive liquid block copolymer. For all of the systems, the thermoset polymer was formulated at an anhydride-to-epoxy equivalent ratio of 0.75, catalyst amount of 2% by total weight, and toughening agents at 15% by weight relative to the epoxy resin or approximately 9% by weight of the total formulation.

Table 5.1. Formulation compositions

#	Type	Sample	Epoxy Resin	Anhydride/Carboxylic Acid Crosslinker	Toughening Agent
1		ESS	ESS	MHHPA	-
2	**Controls (C)**	ESO	ESO	MHHPA	-
3		EPON 828	EPON 828	MHHPA	-
4		AC39	ESS	AC39	-
5		ESS & ESO	ESS + ESO	MHHPA	ESO
6	**Secondary Crosslinker (SC)**	ESS & EPON 828	ESS + EPON 828	MHHPA	EPON 828
7		MHHPA & AC39	ESS	MHHPA + AC39	AC39
8		MHHPA & 2-VOES	ESS	MHHPA + 2-VOES	2-VOES
9		ETBN X68	ESS + ETBN X68	MHHPA	ETBN X68
10		ETBN X63	ESS + ETBN X63	MHHPA	ETBN X63
11	**Secondary phase (SP)**	CTBN X31	ESS	MHHPA + CTBN X31	CTBN X31
12		CTBN X8	ESS	MHHPA CTBN X8	CTBN X8
13		CTBN X13	ESS	MHHPA CTBN X13	CTBN X13
14		Fortegra 100	ESS	MHHPA	Fortegra 100

5.3.2.2. Mixing procedure

The addition of some toughening agents to the formulation requires pre-reaction of the functional groups. This pre-reaction ensures a higher degree of conversion of the functional groups of the toughening agents and promotes the incorporation of the toughening agents into the thermoset networks. This step is important especially for lower reactive functionalities such as carboxyl groups in CTBN or internal epoxy groups in ESO. ETBN toughening agents do not necessarily require pre-reaction since they contain terminal epoxy groups, which are more reactive than the internal epoxy of ESS.

For the controls (#1-4), ETBN-containing formulations (#9-10) and Fortegra 100 (#16), the epoxy resin and anhydride crosslinker were first mixed at 50 °C for 1 hour. Catalyst at 2% wt. of epoxy resin

and crosslinker was then added and the mixture was further mixed at 50 °C for 30 minutes, and then was cured in the oven.

For the other formulations, pre-polymer mixing of the toughening agents and resin/crosslinker is required, and the mixing procedure varied based on the type of the toughening agents. For formulations containing secondary epoxy crosslinker (ESO-#5 and EPON 828-#6), the epoxy was first mixed with MHHPA crosslinker at 10:1 equivalent ratio, while for formulations containing anhydride diluents (AC39-#7, 2-VOES-#8, and CTBN-#11-13), the anhydride crosslinker was first mixed with ESS resin at 40:60 weight ratio. To catalyze the pre-polymer mixing, TBA Br catalyst was added at 1%wt total of the pre-polymer and the reaction was stirred at 90 °C for 2 hours. Then, the remainder of the ESS resin and/or MHHPA crosslinker was added to the mixture and the formulation was stirred at 50 °C for 1 hour. Finally, the remaining TBA Br catalyst was added to the mixture, and the formulation was continued to be stirred at 50 °C for 30 minutes, and then ready to be cured in the oven.

5.3.2.3. Curing procedure

All of the formulations are cured in an RTV-11 silicone mold. The formulations were cured at 120 °C for 1 hour, followed by 150 °C for 3 hours.

5.3.3. Dynamic mechanical analysis

Viscoelastic properties of the thermoset systems were characterized using dynamic mechanical analysis (DMA) using a Q800 DMA from TA Instruments. The experiment was conducted using a 3-point bending clamp, and the sample size was 50 mm x 10 mm x 4mm. The sample was heated from -100 to 180 °C at a heating rate of 3 °C/min and a frequency of 1 Hz. The glass transition temperature (T_g) was determined as the temperature of the tan δ maximum. The crosslink density (ν_e) was calculated using rubber elasticity theory as shown in Equation 5.1:

$$E' = 3\nu_e RT \qquad (5.1)$$

where E' is the storage modulus at the plateau region, R is the gas constant, and T is the absolute temperature. In this experiment, the ν_e is calculated at temperature T_g+ 60 °C.

5.3.4. Tensile test

Tensile properties of the thermosets were characterized using an Instron 5567 load frame with a 2kN load cell. The tests were conducted following ASTM D638. The specimen shape is a dogbone style

Type 1, with thickness of 3.4 mm and width of 10 mm. The grip separation distance of the tensile testing was 115 mm, and the effective gauge length was 50 mm. The strain rate was 5 mm/min. The tensile properties of each sample are reported as the average of measurements five specimens.

5.3.5. Izod impact tests

Izod impact tests were performed using a Tinius Olsen Izod impact pendulum tester with no additional weight attachment. The test was conducted following ASTM D256. The samples were rectangular specimens with dimension of 60 mm x 11 mm x 3.8 mm. The depth of the notch was approximately 1mm. The reported value is an average of 6 different specimens.

5.3.6. Atomic Force Microscopy imaging

Atomic force microscopy (AFM) imaging of selected samples (CTBN X8 and Fortegra 100) was conducted using a Veeco Digital Instrument Dimension^{TM} 3100 equipped with a Nanoscope IIIa ADC5 controller. The surface being analyzed was the fractured surface from the tensile test specimen. The surface was analyzed through tapping contact mode using an FMG01 tip and the image analysis was conducted using Veeco Nanoscope. For each sample, two scan sizes were performed: 20 μm × 20 μm and 4 μm × 4 μm (for CTBN X8) or 3 μm × 3 μm (for Fortegra 100).

5.3.7. Scanning Electron Microscopy imaging

Scanning electron microscopy (SEM) imaging of the same selected samples was observed using a JEOL JSM-7600F field-emission scanning electron microscopy (JEOL USA Inc., Peabody MA). Fractured samples were mounted on aluminum blocks with silver paste to view the fractured surface, and then the surface was coated with a conductive layer of carbon in a high-vacuum evaporative coater (Cressington 208C, Ted Pella Inc., Redding CA). Energy-dispersive x-ray spectroscopy information was acquired using an UltraDry silicon drift X-ray detector and NSS-212e NORAN System 7 X-ray Microanalysis System (ThermoFisher Scientific, Madison WI).

5.3.8. Transmission Electron Microscopy imaging

In addition to AFM and SEM, TEM was also performed to analyze the samples. First, samples were sectioned to 60-80 nm thickness using a RMC PowerTome XL ultramicrotome and then picked up on 2 mm slot grids with a carbon-coated Formvar film. Sections on grids were placed in an enclosed petri dish on dental wax and 1-2 drops of ruthenium tetroxide, 0.5% stabilized aqueous solution or 2% osmium

tetroxide was placed near the grids. The samples were subjected to the vapor for periods of 3-10 minutes. Images were acquired using a JEOL JEM-2100 LaB$_6$ transmission electron microscope equipped with a Gatan Orius CCD camera at 200 kV.

5.4.   Results and Discussion

5.4.1.   Appearance of the thermosets

In this study, two different approaches to improving the toughness of ESS-based thermosets were explored: the addition of secondary crosslinkers and incorporation of secondary phase rubbery materials. The secondary crosslinkers chosen for the study included the diglycidyl ether of bisphenol-A (EPON 828), epoxidized soybean oil (ESO), AC39 polyanhydride, and copolymer of 2-(vinyloxy) ethyl soyate and maleic anhydride (2-VOES). The addition of the secondary crosslinker is expected to act as a flexibilizer by modifying the rigidity of the polymer backbone and/or the crosslinking density. Further, two types of rubbery polymers selected as secondary phases were poly-butadiene-acrylonitrile copolymers (CTBN and ETBN) and an amphiphilic polyethylene block copolymer (Fortegra 100). These secondary phase agents are designed to be miscible in the liquid formulation and then undergo phase separationduring the curing process. For the poly-butadiene-acrylonitrile copolymer system, the degree of phase separation and type of morphology has been shown to depend on the curing temperature, molecular weight of the thermoplastic, butadiene-acrylonitrile ratio, catalyst time, and gelation rate of the thermoset system [36]. In this study, 5 different poly-butadiene-acrylonitrile copolymers were selected for evaluation

The toughening agents were added at 15% wt. of ESS resin or approximately 9%wt. of the total formulation. The first step in preparing the thermoset samples is pre-reacting the functional groups of the toughening agents with either ESS or MHHPA. This step was carried out since some of the functional groups have lower reactivity than the main crosslinker. Furthermore, pre-reaction of the functional groups of the rubbery polymer has been suggested to lead to better control over the particle size of the secondary phase in the cured thermoset. After this pre-polymer was made, the rest of the formulation ingredients were added. The formulation was then cured in a silicone mold at 120 °C for 1 hour, followed by 150 °C for 3 hours.

First, it is necessary to note the visual appearance of the thermoset samples which is shown in Figure 5.3 since it may indicate the presence of a secondary phase in the cured thermoset. All of the modified toughened samples are transparent. This observation is particularly surprising, especially the ones modified with the secondary phase rubbery polymer. The secondary phase particles in the cured thermosets were initially expected to have an approximate size of 1-2 µm, thus creating a hazy appearance. Since all of the samples are transparent, the actual size of the secondary phase may be in the nanoscale range (<700 nm or below the visible light spectrum wavelength). This observation will be further discussed in a later section through microscopy imaging.
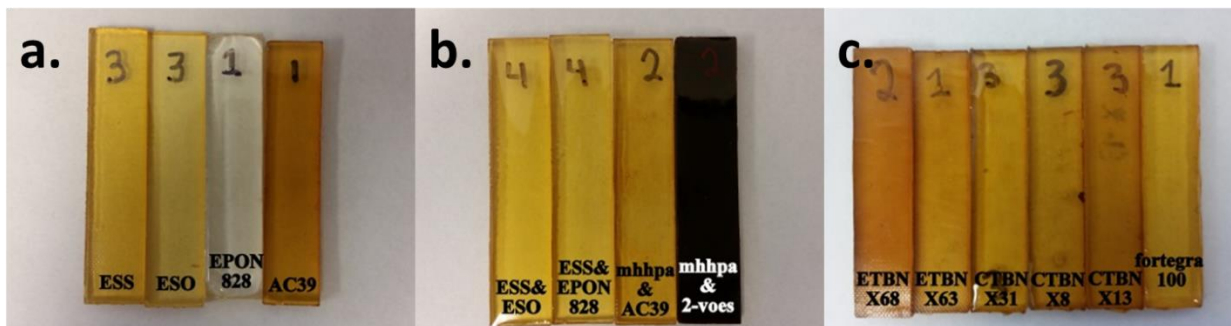
Figure 5.3. Appearance of thermosets after curing: a. control, b. secondary crosslinker modified, c. secondary phase modified

5.4.2. Tensile test

One of the simple, but necessary methods to evaluate the toughness improvement is through tensile testing. Figure 5.4 shows representative stress-strain curves for the thermoset samples. Table 5.2 lists the data from the stress-strain experiments which includes Young's modulus (E), ultimate tensile strength (UTS), and tensile toughness (U_T).
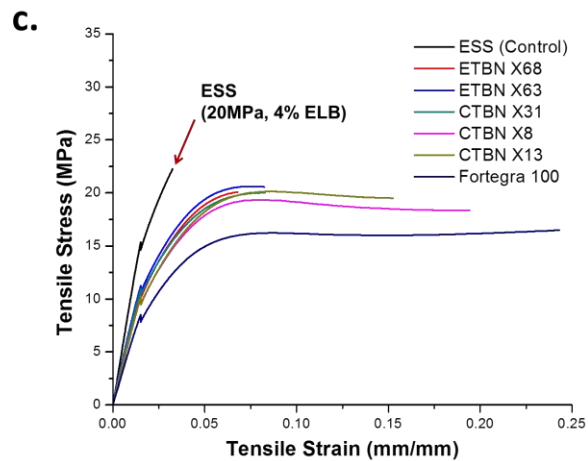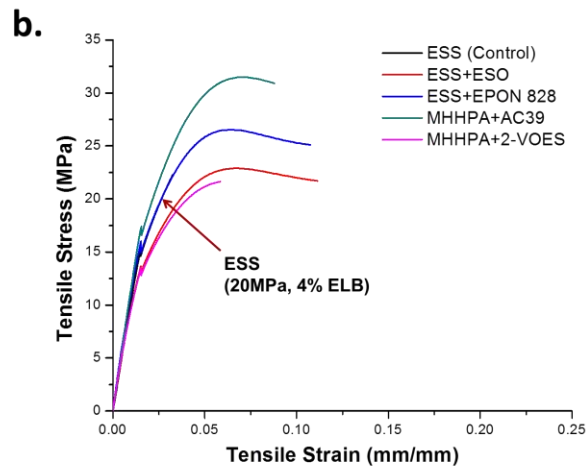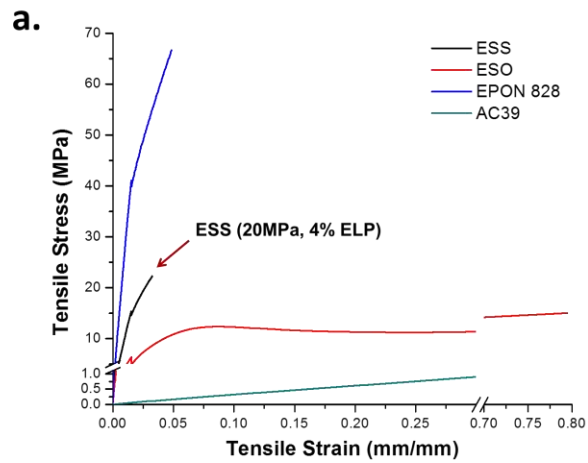
Figure 5.4. Representative stress-strain curves of the thermosets: a. controls, b. secondary crosslinker (SC) modified systems, c. secondary phase (SP) modified systems

The tensile behavior of the control samples will be discussed first. The stress-strain data for ESS and EPON 828 samples indicates that the materials are brittle, with less than 5% elongation at break. In contrast, the ESO thermoset shows a much more rubbery behavior. It has the highest elongation with up to 80% strain at break. Meanwhile, the AC 39 sample shows a unique stress-strain behavior. The materials are very flexible and elastic, and show a linear stress-strain curve. The AC39 thermoset failed at 35% elongation at break, yet the stress-strain curve indicates that the materials did not undergo plastic deformation. After the AC39 sample broke, the thermoset actually went back to its original shape without any changes in dimension or shape. In contrast, when the ESO sample failed, the specimen underwent plastic deformation, and the broken specimens buckled.

Comparing the stress-strain curves of the modified vs. unmodified ESS-thermosets, there is clearly a difference in the shape of the curves. In general, the addition of toughening agents causes a change in the failure type from brittle to ductile, with an exception of the 2-VOES sample. However, it is important to note that the 2-VOES sample contained bubbles throughout which were thought to be from the evaporation of solvent (toluene) contained in the 2-VOES material. For all of the modified samples, the strain at break is observed to be higher and necking formation or plastic deformation were observed. Furthermore, strain hardening of the thermosets was observed with CTBN X8 and Fortegra 100 samples. From these stress-strain curves, tensile toughness of the materials was calculated by determining the area under the curve. The addition of the toughening agents resulted in up to a 5 times increase in the tensile toughness compared to the unmodified thermosets. The highest increase is observed with the addition of CTBN X8 and Fortegra 100, where the samples underwent strain hardening.

Table 5.2. Results from tensile and Izod impact tests

#	Type	Sample	Tensile Test			Izod Impact
			E (MPa)	UTS (MPa)	U_T (J)	Toughness (kJ/m^2)
1	Controls (C)	ESS	1068 ± 69	22.9 ± 4.2	1.86 ± 1.12	0.88 ± 0.01
2		ESO	456 ± 17	15.1 ± 1.1	25.21 ± 3.70	1.12 ± 0.27
3		EPON 828	2760 ± 83	67.7 ± 10.8	8.56 ± 3.64	2.80 ± 0.31
4		AC39	3.14 ± 0.1	0.95 ± 0.1	0.69 ± 0.11	3.98 ± 0.46
5	Secondary Crosslinker (SC)	ESS & ESO	1057 ± 46	22.40 ± 0.8	5.85 ± 1.19	0.89 ± 0.05
6		ESS & EPON 828	1211 ± 59	26.2 ± 0.4	5.81 ± 1.40	0.92 ± 0.10
7		MHHPA & AC39	1158 ± 44	31.2 ± 0.7	5.78 1.00	0.83 ± 0.09
8		MHHPA & 2-VOES	982 ± 164	20.4 ± 1.8	1.93 ± 0.71	0.89 ± 0.05
9	Secondary phase (SP)	ETBN X68	775 ± 36	19.5 ± 1.1	2.65 ± 1.14	0.85 ± 0.05
10		ETBN X63	821 ± 26	20.4 ± 0.7	3.80 ± 2.46	0.80 ± 0.07
11		CTBN X31	853 ± 58	20.4 ± 1.3	3.46 ± 1.22	0.88 ± 0.07
12		CTBN X8	721 ± 31	19.4 ± 0.2	9.31 ± 2.19	0.81 ± 0.10
13		CTBN X13	707 ± 25	19.9 ± 0.4	6.03 ± 1.55	0.84 ± 0.07
14		Fortegra 100	584 ± 15	16.6 ± 0.7	9.76 ± 3.36	0.79 ± 0.06

First of all, for the Young's modulus (*E*) and ultimate tensile strength (UTS) data, it is no surprise that EPON 828 control thermoset sample (#3) shows the highest value among all of the samples which is predicted due to the presence of the aromatic groups in the polymer backbone. Then, the addition of the secondary crosslinker-type toughening agents to the ESS system do not significantly affect either the Young's modulus or UTS values, while the addition of the secondary phase-type toughening agents lead to a reduction of these values by approximately 25%. The exception to this observation is with the MHHPA & AC39 samples(#7), where the UTS is slightly improved. AC39 is a polyanhydride molecule based on dodecenyl succinate, which has a long dangling aliphatic chain, and its functional equivalent weight is higher than the ESS epoxy equivalent weight. As seen in the stress-strain curve, the ESS-thermoset crosslinked with AC39 crosslinker (#4) itself shows elastic behavior with very low strength. Then, when AC39 added as a secondary crosslinker to the ESS/MHHPA thermoset, the UTS was improved by approximately 50%. It is predicted that the addition of AC39 alters the ESS/MHHPA thermoset network structure by modifying the crosslink density of the network and by increasing the amount of ESS intermolecular crosslinking, where epoxy groups in an ESS molecule are connected to another ESS molecule instead of an epoxy group from the same molecule.

5.4.3. Izod impact test

Another method that was used to evaluate the toughness of the modified thermosets is the Izod impact pendulum test. Impact toughness is determined from the energy needed to create a new surface area. A notched sample is put on the holder, and when the latch is released, the pendulum swings and breaks the sample at the notch. The Izod impact pendulum tester measures the energy absorbed, which then can be used to calculate the impact toughness. The impact toughness values listed in Table 5.2 are an average value for 7 measurements. The highest Izod impact value observed is for the AC39 sample (#4). This sample did not fully break after the pendulum swing. For other samples, there is no difference in the observed impact toughness values between the toughening agents. This observation may indicate one of the following. First, the results may indicate that there is truly no significant difference in the toughness properties between the unmodified and modified samples. Second, the impact test conducted in this experiment could not sufficiently discriminate the differences in the impact toughness, and modification of the test method maybe necessary in order to observe the differences.

5.4.4. Viscoelastic properties by DMA

Dynamic mechanical analysis was performed to evaluate the viscoelastic properties of the thermosets and also to determine the glass transition temperature, T_g, and approximate crosslink density (XLD). Figure 5.5 shows the tan delta curves of the thermoset samples as a function of temperature. The glass transition temperature of the thermosets was determined as the temperature at tan delta peak, while the XLD was calculated from storage modulus values at rubbery region (T_g + 60°C). The observed T_g and XLD values of the thermoset samples are shown in Table 5.3.
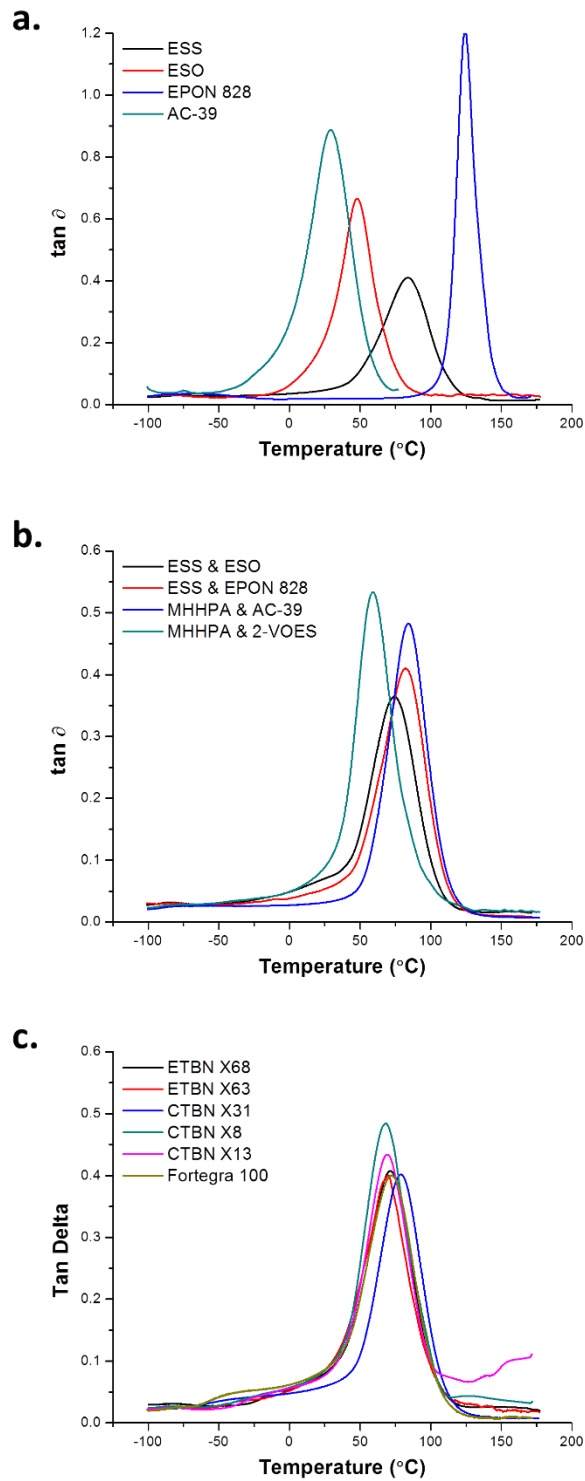
Figure 5.5. tan delta curves of the thermoset samples: a. control (C), b. secondary crosslinker (SC) modified systems, c. secondary phase (SP) modified systems

The impact of toughening agents on the T_g of a thermoset is dependent on the modification method. Yet, first, it is important to note the T_g values of the control samples: ESS, ESO, and EPON 828. ESS and ESO have fairly similar chemical structures and epoxy equivalent weight, yet their T_g (83.8 vs 48.9 °C, respectively) and XLD (2.21 vs. 0.67 mol/ml, respectively) are significantly different. This observation is expected due to the greater number functional groups per ESS molecule compared to ESO which then leads to higher XLD values. The presence of the sucrose moiety in the ESS molecule has also been shown to contribute to the T_g of the networks [13]. Then, the T_g of the EPON 828 (124.4 °C) sample is higher than that of the ESS network, yet the XLD (0.92 mol/ml) is relatively low. This observation thus suggests that the T_g of the EPON 828 network is primarily derived from the rigid aromatic backbone structure and less dependent on the XLD of the polymer network. Comparing the T_g and XLD of the secondary crosslinker-modified samples, even though the samples have lower crosslink density compared to the ESS control (XLD ≤ 2.21 mol/ml), the T_g values are not necessarily lower, specifically for samples modified with the addition of EPON 828 (T_g = 82.0°C) and AC39 polyanhydride (T_g = 84.1°C). This observation is expected due to the modification in the rigidity of the backbone and the type of intermolecular/intramolecular network of the system. Then, for the secondary phase modified systems, a decrease in both T_g and XLD of the thermosets was observed. Overall, the amount of decrease for these secondary phase modified systems is independent of the type of the toughening agents.

Table 5.3. Results from the DMA experiments

#	Type	Sample	T_g (°C)	SM at 25 °C (MPa)	XLD (mol/ml)
1	**Controls (C)**	ESS	83.8	1251	2.21
2		ESO	48.9	612	0.67
3		EPON 828	124.4	2527	0.92
4		AC39	29.1	74	0.47
5	**Secondary Crosslinker (SC)**	ESS & ESO	73.6	914	2.07
6		ESS & EPON 828	82.0	1217	1.91
7		MHHPA & AC39	84.1	1357	2.01
8		MHHPA & 2-VOES	59.3	948	1.04
9	**Secondary phase (SP)**	ETBN X68	72.5	901	1.51
10		ETBN X63	69.7	941	1.06
11		CTBN X31	78.1	823	1.62
12		CTBN X8	68.1	885	0.72
13		CTBN X13	69.4	826	1.20
14		Fortegra 100	72.4	761	1.49

In addition to determining glass transition temperature (T_g) values, analysis of the tan delta curves can be used to determine the presence of different phases present in the networks and identify β-relaxations of the thermosets. If multiple phases in the thermoset network are present, a shoulder or secondary peak would be observed. The peak temperature of this shoulder peak can then be correlated to the T_g values of the secondary phase. Figure 5.6 shows the tan delta curves of the secondary phase modified samples in the low temperature region, and the observed T_g values Figure 5.6 indicates the presence of multiple shoulder peaks in the tan delta curves. The peaks at the lowest temperature range of -100 to -60 °C in Region 1 are thought to indicate the β-relaxation of the ESS thermoset, since they occur at similar temperature range for all networks. Furthermore, this peak was also observed in the control ESS sample. Then, the peaks in the temperature range of -60 to 15 °C in Region 2 are believed to indicate the presence of secondary phases within the modified systems. It is important to note that these peaks were not observed in the ESS control samples or the secondary crosslinker-modified samples, and they are only observed for the secondary-phase modified samples. For all of the samples, the observed T_g temperatures (at maximum tan delta peak) are slightly higher than the reported T_g values for the pure toughening agents. For example, the T_g for ETBN X8 phase in ESS thermoset (#9) is observed at -13.3 °C, while the reported T_g of ETBN X8 copolymer is -66 °C. This occurrence can be attributed to the phase mixing between ESS thermoset and rubbery polymer due to the chemical bonding of the ESS and toughening agents from the pre-polymer reaction. The difference between the observed T_g of the secondary phase and T_g of the toughening agent may indicate the extent of phase mixing and connectivity of the ESS/MHHPA thermoset phase and the toughening agent phase.
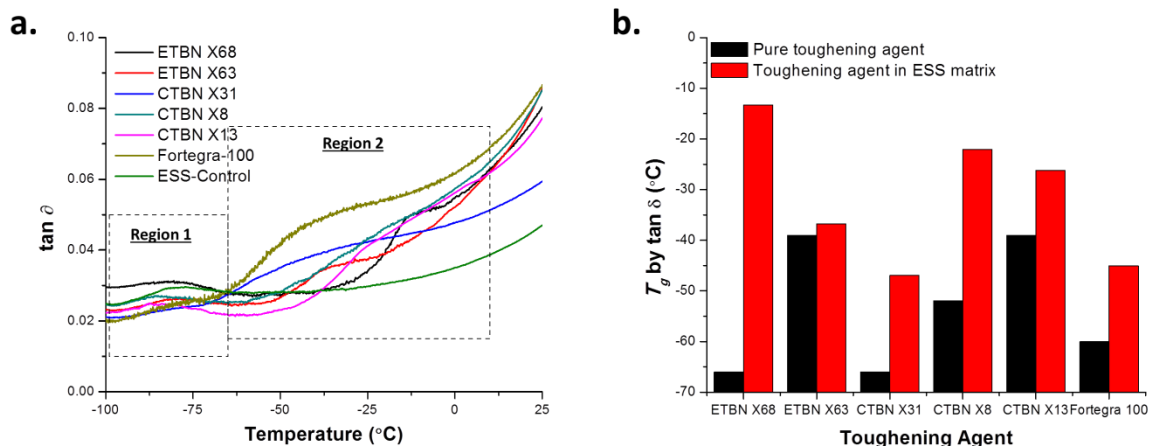
Figure 5.6. DMA tan delta curve analysis: a. tan delta curve of secondary phase modified samples at lower temperature region, b. T_g comparison of pure thermoplastic polymer and observed peak temperature

5.4.5. Cross-section imaging of fractured samples

Atomic force microscopy (AFM), scanning electron microscopy (SEM), and transmission electron microscopy (TEM) were used to visually analyze the secondary phase of selected modified samples. The samples investigated include the CTBN X8 and Fortegra 100 modified samples. These two samples were chosen since they showed the greatest improvement in the tensile toughness. Figure 5.7 shows AFM scan of fractured surface of CTBN X8 and Fortegra 100 samples with 3 µm and 4 µm scan size, respectively; while Figure 5.8 shows AFM scan of the fractured surface with 20 µm scan size.

Using AFM imaging, it was expected that the height and phase images would show the presence of the secondary phase in the thermoset samples. Based on other literature articles, using bisphenol-A based thermoset system, the size of this spherical secondary phase can be expected to be approximately 1-2 µm for CTBN X8 and 100 nm for Fortegra 100 [32]. Therefore, the height image was expected to show either a spherical valley and/or ridge, which indicates the fractured regions from the secondary phase. However, as shown in Figure 5.7a, 5.7c, 5.8a, and 5.8c, the height image of the fractured surface shows a fairly smooth surface, only with <100 nm features. Then, the phase image was expected to show two regions of different modulus: more rigid ESS thermoset phase (lighter color) and rubbery thermoplastic secondary phase (darker color). Similar to the height image, the phase image of the fractured surface shown in Figure 5.7b, 5.7d, 5.8b, and 5.8d, indicates fairly homogenous appearance of the materials with little separation between the rigid ESS-thermoset phase and the rubbery secondary

131

phase. From these images, it is expected that rubbery thermoplastic copolymer did not fully separate into

a secondary phase, and was well incorporated into the ESS-thermoset network.
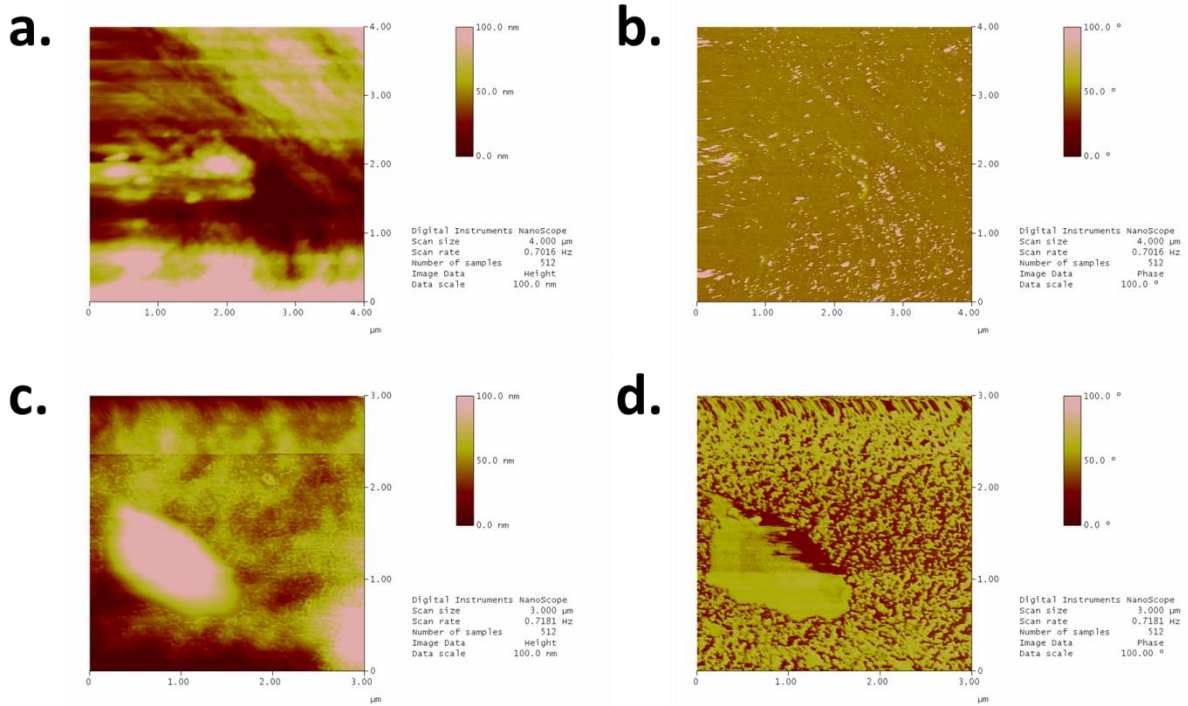
Figure 5.7. AFM imaging of fracture surfaces 3 x 3 or 4 x 4 μm scan size: a. height image of CTBN X8 (#12), b. phase image of CTBN X8 (#12), c. height image of Fortegra 100 (#14), d. phase image of Fortegra 100 (#14)
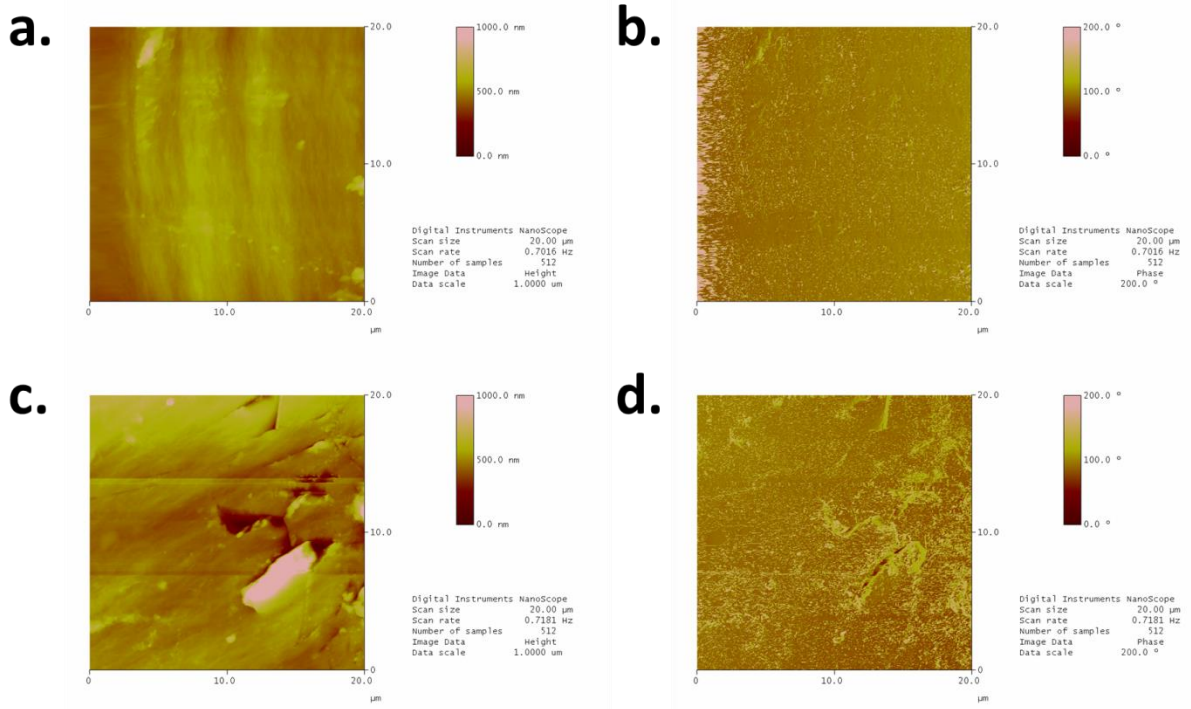
Figure 5.8. AFM imaging of fracture surfaces with a20 x 20 μm scan size: a. height image of CTBN X8 (#12), b. phase image of CTBN X8 (#12), c. height image of Fortegra 100 (#14), d. phase image of Fortegra 100 (#14)

SEM imaging of the samples was also used to investigate the morphology of the thermosets, shown in Figure 5.9. Similar results to the AFM was observed; the size of the particles was detected at much smaller size than what was originally expected at 1-2 μm. SEM images of CTBN X8 (#12) shows spherical particles dispersed throughout the samples; the size of these particles is approximately 100 nm. Meanwhile, the appearance of a secondary phase within Fortegra 100 sample (#14) is barely seen.
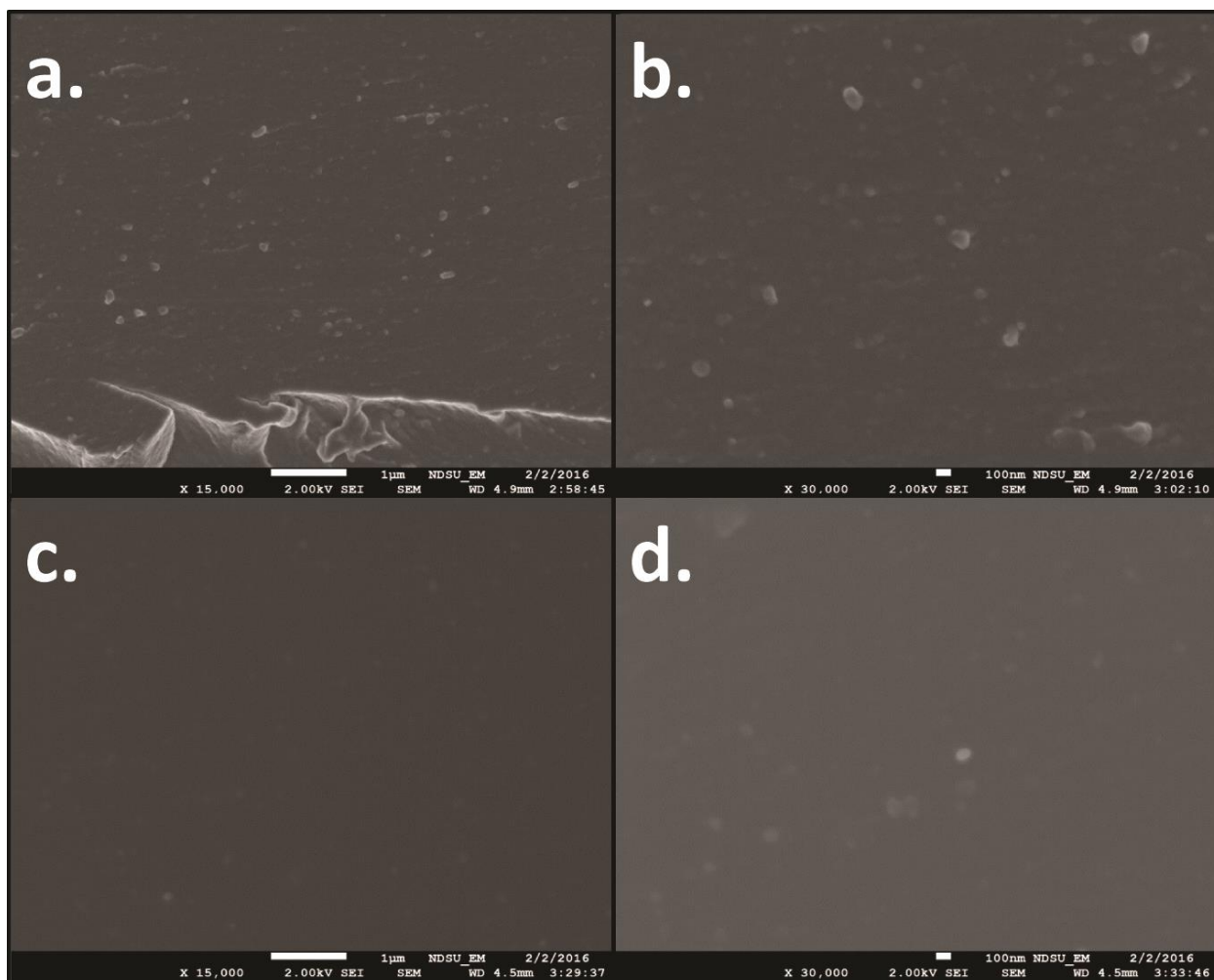
Figure 5.9. SEM imaging of cross-sectioned samples: a. CTBN X8 (#12) with 15K magnification, b. CTBN X8 (#12) with 30K magnification, c. Fortegra 100 (#14) with 15K magnification, d. Fortegra 100 (#14) with 30K magnification

Energy dispersive x-ray spectroscopy (EDX) was conducted to further analyze the composition of the networks. The samples were treated with osmium tetroxide to provide staining since it reacts with the unsaturation in the CTBN X8. Figure 5.10 shows the SEM/EDX results of the CTBN X8 and Fortegra 100 sample. The nitrogen in the polybutadiene-acrylonitrile copolymers was expected to be detected within the CTBN X8 samples (#12). However, area analysis showed only the presence of carbon, oxygen, and osmium atom. Furthermore, point analysis of the particles vs. the bulk material showed that there is no significant difference in the elemental analysis. With the Fortegra 100 modified sample (#14), it was expected that the point analysis of the particles would show a higher carbon-to-oxygen atom ratio than the bulk particles since Fortegra 100 is a copolymer of ethylene oxide and butylene oxide. Yet, there was

no significant difference in the atom count. With no difference detected within the particles and the bulk materials, it is expected that the toughening agents are well incorporated and mixed with the ESS-thermoset and the difference in the atom count might be beyond the detection limit of the instrument.
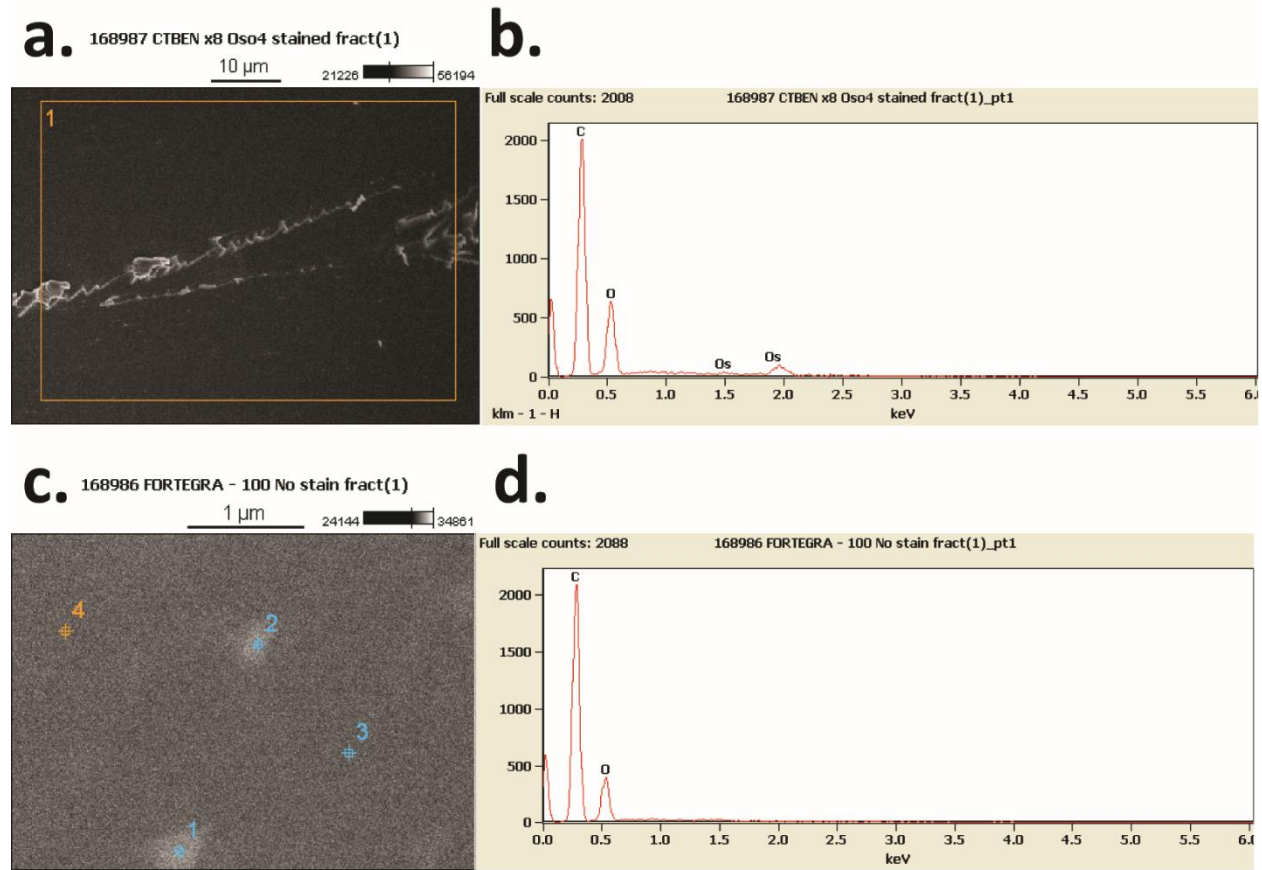
Figure 5.10. SEM/EDX imaging of cross-sectioned samples: a. SEM imaging of CTBN X8 (#12), b. EDX atom count of area displayed in Figure 5.10a, c. SEM imaging of Fortegra 100 (#14), d. EDX atom count of point 1 displayed in Figure 5.10c

Figure 4.11 shows the TEM images of the cross sections of the ESS Control (#1) and CTBN X8 (#12) samples. As clearly seen in these images, the samples of non-toughened (control ESS) thermoset vs. CTBN-toughened thermoset are different in appearance; the toughened thermoset appears to have more texture of darker/lighter areas compared to the control sample. The appearance of the darker spot areas is distributed fairly uniformly across the samples. The darker field in the TEM represents regions that are able to absorb more electrons, signifying regions with higher atomic number. It is believed that these darker spots corresponded to the CTBN X8 particles, which has higher electron density due to the staining with osmium tetroxide.
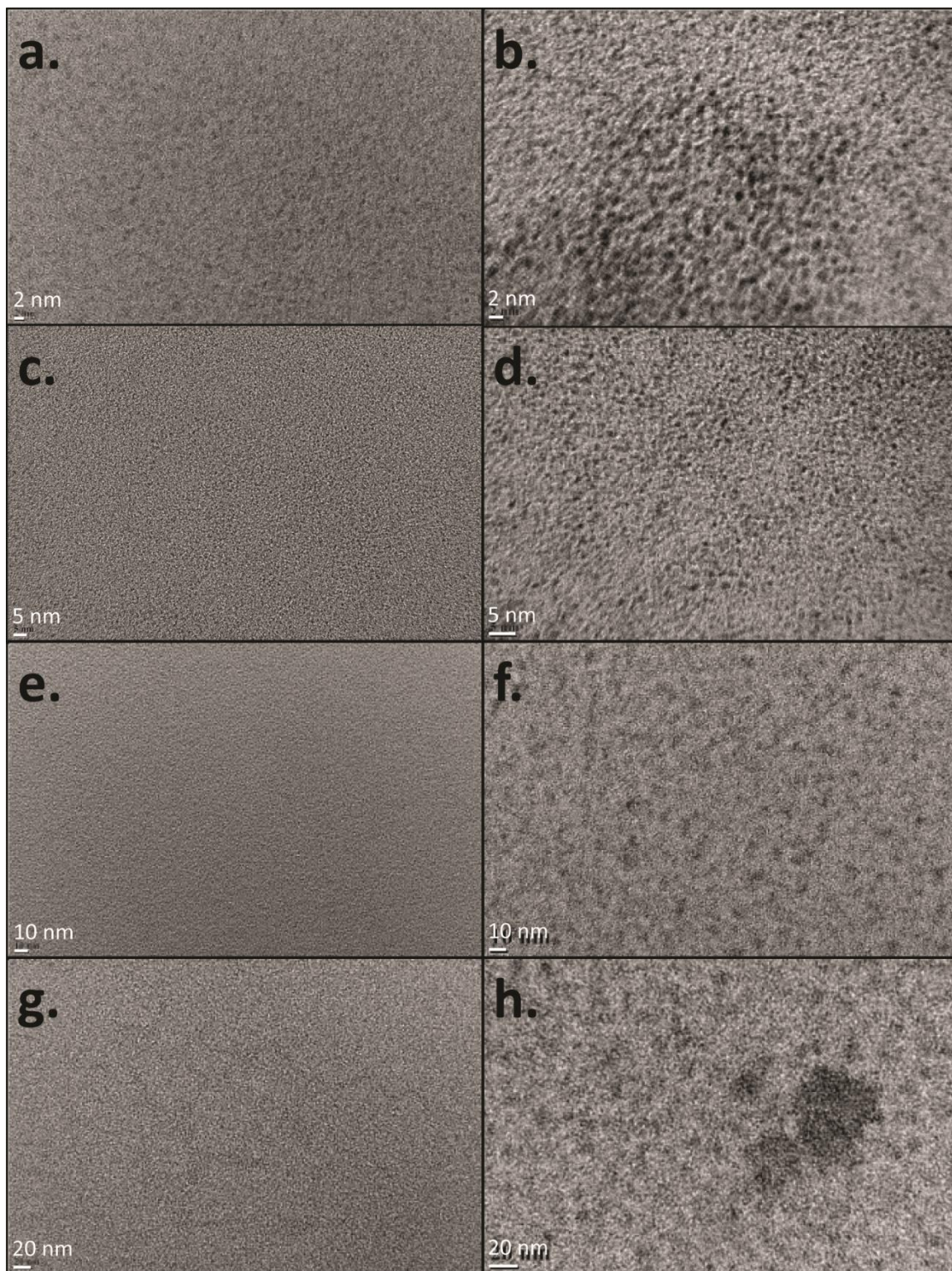
Figure 5.11. TEM imaging of cross sectioned samples: a. ESS with 2 nm bar scale, b. CTBN X8 with 2 nm bar scale, c. ESS with 5nm bar scale, d. CTBN X8 with 5 nm bar scale, e. ESS with 10 nm bar scale, f. CTBN X8 with 10 nm bar scale, g. ESS with 20 nm bar scale, h. CTBN X8 with 20 nm bar scale

5.5. Conclusions

Different methods were explored in order to improve the toughness of the ESS-MHHPA thermoset system including the use of flexibilizing curing agents and use of secondary phase rubbery polymers. The improvement in the tensile toughness was observed to be dependent on the specific type of toughening agent used. Using secondary crosslinkers as toughening agents for ESS/MHHPA thermoset resulted in more ductile behavior without compromising the Young's modulus and tensile strength of the thermosets. In contrast, using reactive liquid polymers for toughening resulted in higher elongation at break materials, yet led to a compromise in the Young's modulus. With these promising results, it will be worthwhile to explore the properties of ESS/MHHPA thermosets with the addition of both types of toughening agents. With a more ductile primary bulk phase due to addition of secondary crosslinker, the toughness improvement due to incorporation of secondary phase is predicted to be significantly intensified. This intensified improvement can be expected due to the role of matrix ductility in influencing the toughness of multiphase network. The ductility of the bulk matrix system reduces the stress needed for localized shear yielding that is initiated by the secondary rubber polymer, and thus inducing plastic deformation to a far lesser extent and much greater improvement in the toughness properties. Furthermore, exploration in the amount of toughening agents, miscibility additive, mixing and curing process is valuable to ensure defined phase separation between the rubbery thermoplastic phase and rigid ESS-thermoset phase, which can ultimately lead to further optimization of the toughness improvement.

5.6. Acknowledgements

5.7. References

[1]   R. Auvergne, S. Caillol, G. David, B. Boutevin, J.-P. Pascault, Biobased Thermosetting Epoxy: Present and Future, Chemical Reviews, 114 (2013) 1082-1115.

[2]   C. Aouf, C. Le Guernevé, S. Caillol, H. Fulcrand, Study of the O-glycidylation of natural phenolic compounds. The relationship between the phenolic structure and the reaction mechanism, Tetrahedron, 69 (2013) 1345-1353.

[3]   Y.H. Kim, E.S. An, S.Y. Park, B.K. Song, Enzymatic epoxidation and polymerization of cardanol obtained from a renewable resource and curing of epoxide-containing polycardanol, Journal of Molecular Catalysis B: Enzymatic, 45 (2007) 39-44.

[4]   W.O.S. Doherty, P. Mousavioun, C.M. Fellows, Value-adding to cellulosic ethanol: Lignin polymers, Industrial Crops and Products, 33 (2011) 259-276.

[5]   C.I. Simionescu, V. Rusan, M.M. Macoveanu, G. Cazacu, R. Lipsa, C. Vasile, A. Stoleriu, A. Ioanid, Lignin/epoxy composites, Composites Science and Technology, 48 (1993) 317-323.

[6]   M. Shibata, K. Nakai, Preparation and properties of biocomposites composed of bio-based epoxy resin, tannic acid, and microfibrillated cellulose, Journal of Polymer Science Part B: Polymer Physics, 48 (2010) 425-433.

[7]   Y. Takada, K. Shinbo, Y. Someya, M. Shibata, Preparation and properties of bio-based epoxy montomorillonite nanocomposites derived from polyglycerol polyglycidyl ether and ε-polylysine, Journal of Applied Polymer Science, 113 (2009) 479-484.

[8]   J.O. Metzger, Fats and oils as renewable feedstock for chemistry, European Journal of Lipid Science and Technology, 111 (2009) 865-876.

[9]   X. Pan, P. Sengupta, D.C. Webster, High biobased content epoxy-anhydride thermosets from epoxidized sucrose ester of fatty acids, Biomacromolecules, 12 (2011) 2416-2428.

[10]   D.C. Webster, P.P. Sengupta, Z. Chen, X. Pan, A. Paramarta, Highly functional epoxidized resins and coatings, in: United States Patent Office, NDSU Research Foundation, US, 2015.

[11]   E.M. Monono, D.C. Webster, D.P. Wiesenborn, Pilot scale (10 kg) production and characterization of epoxidized sucrose soyate, Industrial Crops and Products, 74 (2015) 987-997.

[12]   X. Pan, P. Sengupta, D.C. Webster, Novel biobased epoxy compounds: epoxidized sucrose esters of fatty acids, Green Chemistry, 13 (2011) 965-975.

[13]   X. Pan, D.C. Webster, Impact of Structure and Functionality of Core Polyol in Highly Functional Biobased Epoxy Resins, Macromolecular Rapid Communications, 32 (2011) 1324-1330.

[14] T. Nelson, T. Galhenage, D. Webster, Catalyzed crosslinking of highly functional biobased epoxy resins, J Coat Technol Res, 10 (2013) 589-600.

[15] P.P. Sengupta, X. Pan, T.J. Nelson, A. Paramarta, D.C. Webster, Cationic UV curing characteristics of epoxidized sucrose esters, in: American Coatings Society National Meeting, PMSE, 2010, pp. 888-889.

[16] C.S. Kovash, E. Pavlacky, S. Selvakumar, M.P. Sibi, D.C. Webster, Thermoset Coatings from Epoxidized Sucrose Soyate and Blocked, Bio-Based Dicarboxylic Acids, ChemSusChem, 7 (2014) 2289-2294.

[17] S. Ma, D.C. Webster, Naturally Occurring Acids as Cross-Linkers To Yield VOC-Free, High-Performance, Fully Bio-Based, Degradable Thermosets, Macromolecules, 48 (2015) 7127-7137.

[18] S. Ma, D.C. Webster, F. Jabeen, Hard and Flexible, Degradable Thermosets from Renewable Bioresources with the Assistance of Water and Ethanol, Macromolecules, 49 (2016) 3780-3788.

[19] A. Paramarta, X. Pan, D.C. Webster, Highly functional acrylated biobased resin system for uv-curable coatings, Radtech Report, (2013) 26-32.

[20] J. Yan, D.C. Webster, Thermosets from highly functional methacrylated epoxidized sucrose soyate, Green Materials, 2 (2014) 132-143.

[21] T. Nelson, B. Masaki, Z. Morseth, D. Webster, Highly functional biobased polyols and their use in melamine–formaldehyde coatings, J Coat Technol Res, 10 (2013) 757-767.

[22] T.J. Nelson, L. Bultema, N. Eidenschink, D.C. Webster, Bio-Based High Functionality Polyols and Their Use in 1K Polyurethane Coatings, Journal of Renewable Materials, 1 (2013) 141-153.

[23] X. Pan, D.C. Webster, New Biobased High Functionality Polyols and Their Use in Polyurethane Coatings, ChemSusChem, 5 (2012) 419-429.

[24] N. Hosseini, S. Javid, A. Amiri, C. Ulven, D.C. Webster, G. Karami, Micromechanical viscoelastic analysis of flax fiber reinforced bio-based polyurethane composites, Journal of Renewable Materials, 3 (2015) 205-2015.

[25] N. Hosseini, C.A. Ulven, F. Azarmi, D.C. Webster, T.J. Nelson, Utilization of Flax Fibers and Glass Fibers in a Bio-Based Resin, in: ASME 2014 International Mechanical Engineering

Congress and Exposition, The American Society of Mechanical Engineers, Montreal, Quebec, Canada, 2014.

[26]   N. Hosseini, D.C. Webster, C. Ulven, Advanced biocomposite from highly functional methacrylated epoxidized sucrose soyate (MAESS) resin derived from vegetable oil and fiberglass fabric for composite applications, European Polymer Journal, 79 (2016) 63-71.

[27]   A. Amiri, A. Yu, D. Webster, C. Ulven, Bio-Based Resin Reinforced with Flax Fiber as Thermorheologically Complex Materials, Polymers, 8 (2016) 153.

[28]   C.A. Taylor, Development of Biobased Composites of Structural Quality, in: Mechanical Engineering, North Dakota State University, Ann Arbor, 2015.

[29]   J.N. Sultan, F.J. McGarry, Effect of rubber particle size on deformation mechanisms in glassy epoxy, Polymer Engineering & Science, 13 (1973) 29-34.

[30]   K.P. Unnikrishnan, E.T. Thachil, Toughening of epoxy resins, Designed Monomers and Polymers, 9 (2006) 129-152.

[31]   R.J. Varley, W. Tian, Toughening of an epoxy anhydride resin system using an epoxidized hyperbranched polymer, Polymer International, 53 (2004) 69-77.

[32]   O.L. Shaffer, R. Bagheri, J.Y. Qian, V. Dimonie, R.A. Pearson, M.S. El-Aasser, Characterization of the particle–matrix interface in rubber-modified epoxy by atomic force microscopy, Journal of Applied Polymer Science, 58 (1995) 465-484.

[33]   R. Turakhia, G. Jacob, M. Dettloff, H. Pham, Novel Epoxy Toughening for Coatings and Composites Applications, in: Thermoset Resin Formulators Association Meeting, Thermoset Resin Formulators Association Chicago, IL, 2008.

[34]   R. Karunakaran, N. E-Verghese, Curable Composition, in: U.S.P. Office (Ed.), Dow Global Technologies LLC, United States, 2014.

[35]   D. Ratna, A. Banthia, Rubber toughened epoxy, Macromol. Res., 12 (2004) 11-21.

[36]   R. Bagheri, B.T. Marouf, R.A. Pearson, Rubber-Toughened Epoxies: A Critical Review, Polymer Reviews, 49 (2009) 201-225.

[37]   S. Alam, H. Kalita, A. Jayasooriya, S. Samanta, J. Bahr, A. Chernykh, M. Weisz, B.J. Chisholm, 2-(Vinyloxy)ethyl soyate as a versatile platform chemical for coatings: An overview, European Journal of Lipid Science and Technology, 116 (2014) 2-15.

CHAPTER 6. THE EXPLORATION OF MICHAEL-ADDITION REACTION CHEMISTRY TO CREATE HIGH PERFORMANCE, AMBIENT CURE THERMOSET COATINGS BASED ON SOYBEAN OIL

6.1.   Abstract

Utilizing Michael addition crosslinking technology, thermoset coatings were prepared from acrylated epoxidized sucrose soyate (AESS) resin and amine crosslinkers. AESS was synthesized from sucrose soyate, which is the sucrose ester of soybean oil fatty acids and has an average of about 12 functionalities per molecule. Due to the high functionality of AESS and fast reactivity of the amine crosslinkers, the coatings can be cured at ambient temperature (21 °C) in a relatively short period of time yielding good coatings properties. When AESS was reacted with 4'4'-methylene bis(cyclohexylamine), the acrylate group conversion was determined by FTIR to be up to 90%. It was also found that the type of solvent used in the coatings formulation affected the film formation and thus the coatings properties. The addition of 1,6-hexanediol diacrylate diluent in the formulation resulted in softer and lower T_g coatings. Using a trifunctional amine such as diethylene triamine, coatings could be prepared without the addition of any catalyst. Overall, thermosets made from AESS Michael crosslinking technology provide a highly bio-based coating system with good hardness and chemical resistance.

6.2.   Introduction

Michael addition is reaction between nucelophiles (Michael donors) and activated olefins (Michael acceptors) to produce covalent bonds between Michael donors and acceptors. The general reaction scheme is shown in Scheme 6.1. The Michael addition reaction has been employed as a versatile tool in the synthesis of linear, graft, hyperbranched, dendritic and network polymers for a wide range of applications such as coatings, adhesives, bio-medical/pharmaceutical, and specialty chemicals [1-11].

Scheme 6.1. General reaction mechanism of Michael addition

The use of the Michael addition reaction for crosslinking in the coatings industry has been gaining more attention recently. This popularity is motivated by the following benefits. First, the reaction only requires mild conditions to achieve high conversion with favorable reaction rates, and thus coatings can

be cured at ambient temperature. The reaction rates can be controlled by the selection of monomer precursor, catalyst system, and solvent [12-15]. Second, there are no volatile by-products of the reaction, thus eliminating or minimizing the amount of volatile organic compounds (VOCs). Lastly, there are a wide range of varieties of commercially available chemicals that can be used as reactants and catalysts. Common functional groups used as Michael donors include acetoacetates, amines, thiols and phosphines. There are more options of functional groups that can be used as Michael acceptors, which include acrylate esters, acrylonitrile, acrylamides, maleimides, alkyl methacrylate, and α,β-unsaturated aldehydes. Even though it is not necessary to add catalyst to accelerate the reaction, catalyst is often added to ensure the reaction reaches high conversion; the catalyst can be either base (hydroxide, amine, alcohol, etc) or acid (p-toluene sulfonic acid, sulfuric acid, bis(trifluoromethanesulfon)imide, etc. Mather et al. presented a thorough review discussing the use of a wide variety of those precursors for polymer macromolecular design for many applications [12].

The use of Michael addition technology for coatings application has been explored since the 1980s [1, 13, 16-19]. Yet, there are many concerns to be addressed in order for this reaction to be widely applied for coatings applications. First, this reaction can proceed fairly fast at room temperature and thus has a somewhat short pot life or working time. Recently, Brinkhuis et al. address this concern by using a novel blocked catalyst and kinetic control additive system [20]. The system consists of the reversible blocking of a strong base catalyst with dialkylcarbonate. The strong base reacts with the carbonate to form carbonate anions, which have low reactivity to initiate the Michael addition reaction and thus results in a long pot life in the container. Upon application, the large surface area shifts the equilibrium to trigger the catalyst de-blocking and thus initiates the reaction. Unfortunately, this reversible catalyst blocking system produces alcohol as a by-product. Another cause of the limited use of the Michael addition reaction in the coatings industry is due to limited options for highly functionalized resins and/or crosslinkers to create thermoset coatings with good hardness and chemical resistance. The most commonly used functional groups reported for Michael addition curing are acetoacetate and acrylate esters. Often, appropriate blends of di-, tri-, and tetra- acrylates must be used to achieve good performance [8, 10, 19]. Recently, Webster et al. invented a highly functionalized acrylate resin based on epoxidized sucrose soyate (ESS) [21]. Epoxidized sucrose soyate is an epoxy resin derived from the

sucrose ester of soybean oil fatty acids. This epoxy resin has an average of 12 functional groups per molecule, and has been shown to offer excellent mechanical properties in coatings and composites applications [22-32]. The ESS resin can be modified into an acrylate resin through ring opening of the epoxy using acrylic acid; the reaction is shown in Scheme 6.2. The synthesis of AESS resin is a fairly straightforward, one-pot synthesis process with very high conversion and no further purification is needed. The number of acrylate groups can be tuned by controlling the amount of acrylic acid used during the synthesis process. The use of this highly functionalized acrylate resin for UV-curable coatings has been shown to have improved performance compared to an acrylate resin based on soybean oil [25]. Using this AESS resin for Michael addition crosslinking can be beneficial due to its high functionality which can lead to a high crosslink density. Furthermore, the use of AESS will also potentially increase the sustainability of the materials since it is a 75+% bio-based resin.
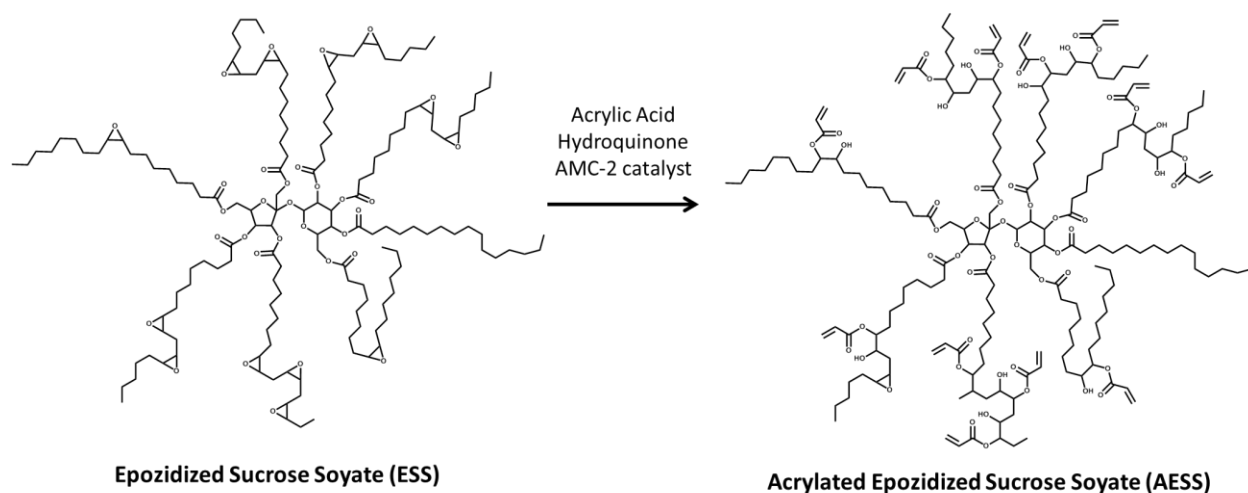
Scheme 6.2. Acrylation of epoxidized sucrose soyate

Thus, the goal of this work was to explore the feasibility of using the AESS resin to produce high performance, ambient cured coatings using Michael addition crosslinking. Structure-property relationships of the coatings system were studied based on the variation in the acrylate-to-amine ratio, type of amine crosslinker used, and the amount of reactive diluent used. The properties evaluated include mechanical coatings properties and thermal properties. As a comparison, a coatings system derived from acrylated epoxidized soybean oil (AESO) was also prepared.

6.3. Experimental

6.3.1. Raw materials

Acrylated epoxidized sucrose soyate (AESS) resin was synthesized from epoxidized sucrose soyate (ESS), with 90% of the epoxy groups being converted into acrylate groups. The synthesis and characterization of ESS and AESS resin is presented in previous publications [25, 33]. Ethyl 3-ethoxypropionate (EEP) solvent was provided by Eastman Chemical Co. 4'4'-Methylene bis(cyclohexylamine) (PACM) was provided by Air Products. Diethylene triamine (DETA), m-xylylyne diamine (MXDA), and p-toluene sulfonic acid monohydrate (pTSA) were obtained from Sigma Aldrich. 1,6-Hexanediol diacrylate was provided by Sartomer. Ethanol was obtained from Alfa-Aesar. The structure of the chemicals used in this work is illustrated in Figure 6.1.
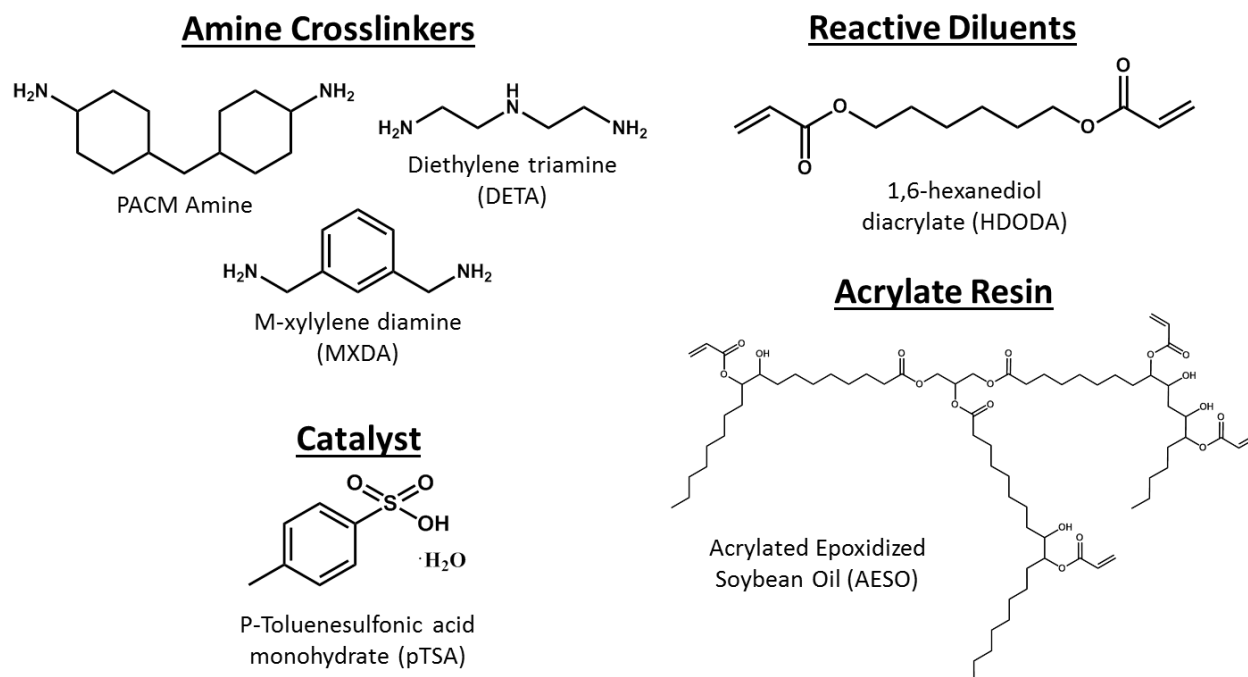
Figure 6.1. Structures of the chemicals used in this work

6.3.2. Coatings formulation

AESS was first dissolved in a variety of solvent solvents, and then air bubbles in the mixture were removed by sonication. Then, amine crosslinker and pTSA catalyst was added to the mixture. The mixture was stirred using a spatula for 1 minute, and then applied onto 3 x 6 x 0.020 in. Q-panel cold rolled steel panels pretreated with iron phosphate (Bonderite 1000 ™ obtained from Q-panel) and 4 x 6 x

0.032 in. glass panels using a draw down bar at 6 mils wet film thickness. The panels were then forced-cured in the oven at 80°C for 45 minutes. For ambient-cured coatings, the coatings were set aside on the laboratory bench at 21°C. Coatings properties were measured 1 week after the coatings were cured.

6.3.3. Viscosity and gel-time study using rheometer

An ARES Series Rheometer was used to measure the viscosity of the resin system and determine the gel time of the coatings formulation. Parallel plate geometry was used and the gap between the plates was set to be 1 mm. For viscosity measurement, the sample shear rate was 0.1 to 100 Hz, and the reported value was taken from an average of 3 measurements at 10 Hz. Then, for gel time determination, the coatings formulations was sheared at 0.1 Hz, and storage modulus, loss modulus, and viscosity values were monitored. Gel time was determined when storage modulus value was equal to loss modulus value or when the viscosity value increased dramatically.

6.3.4. Drying time determination

The drying times of the coatings were determined using a BK Drying Recorder. The results were analyzed using ASTM D5895. Four stages were determined: Stage 1 corresponds to set-to-touch time, stage 2 corresponds to tack-free time, stage 3 corresponds to dry-hard time, and stage 4 corresponds to dry-through time.

6.3.5. Chemical analysis using FTIR spectroscopy

Fourier-transform infrared (FTIR) spectroscopy was performed using a Thermo Scientific Nicolet 8700 FTIR spectrometer using a potassium bromide salt crystal. FTIR analysis was used to determine the conversion of the acrylate group in the AESS after the curing process. The conversion is determined from the decrease in the area of three peaks that correspond to the unsaturation of the functional groups: 810 cm^{-1} (C=C out of plane deformation), 1407 cm^{-1} (C=C scissoring of $HC=CH_2$ (medium) in-plane CH_2 deformation 1637 cm^{-1} (C=C stretching for $HC=CH_2$).

6.3.6. Coatings characterization

The dry film thickness on steel substrates was measured using a Byko-Test 8500 coatings thickness gauge; the reported value is the average and standard deviation of 10 points of measurement on the panel. The hardness of the coatings was determined using König pendulum hardness and pencil hardness following ASTM D4366 and ASTM D3363, respectively. Flexibility was measured using conical

mandrel bend test (ASTM D522) which indicates a slow deformation and reverse impact (ASTM D3794) which indicates a rapid deformation. Adhesion was measured using cross-hatch adhesion method of ASTM D3359. Solvent resistance was determined through the methyl ethyl ketone (MEK) double rubs test, where a MEK-saturated cheese cloth was wrapped on a hammerhead and then rubbed against the coatings surface back and forth until coatings failure was observed. Solvent resistance may indicate the degree of crosslinking of the thermoset. The specular gloss was measured using BYK Gardner Micro-Tri-Gloss 20/60/85 degree Gloss Meter at 20°, 60° and 85° following ASTM D523.

6.3.7. Thermal analysis

Thermal properties of the cured coatings were analyzed through differential scanning calorimetry (DSC) and dynamic mechanical analysis (DMA). DSC experiments were performed using a TA Instruments Q2000 DSC. The glass transition temperature, T_g, of free films were determined using a heat-cool-heat method, and the reported value was taken from the inflection point during the heating cycle. 10 mg free film samples were exposed to heat-cool-heat cycle from -80 to 250 °C with 30 °C/min heating (or cooling) ramp. DMA experiments were performed using a TA Instruments Q800 DMA. Coatings films were cut to have a width of 5 mm and was loaded at 15 mm in length. The sample was heated from -50 to 150 °C with 3 °C/min heating ramp at 1Hz frequency and 0.1% strain. Furthermore, a preload force of 0.01 N was used and force track was set to 125%.

6.3.8. Soxhlet extraction

Soxhlet extraction of the coatings was performed to determine the gel fraction of the thermoset network. About 0.3 g of cured samples was folded inside filter paper, which then was inserted into an extraction thimble in the Soxhlet extraction apparatus. The extraction process was conducted with acetone as a solvent, and samples were extracted for 17 hours by acetone at reflux. After the process was completed, the wet residual samples were dried in the oven at 120 °C for 1 hour. The gel fraction was calculated from the ratio of sample weight after and before the Soxhlet extraction.

6.4.   Results and Discussion

6.4.1. Aza-Michael addition reaction overview

A Michael addition reaction involving nitrogen-donor functionality is often referred as an aza-Michael addition. Since amine can act as both the donor agent and base, the addition of catalyst is often

not necessary. In this research, highly functionalized AESS resin was reacted with an amine crosslinker

to form a thermoset network, and the reaction is catalyzed using Bronsted acid p-toluene sulfonic acid

monohydrate in ethanol. Catalyst was added in the formulation to ensure high conversion of functional

groups. In the case of an acid-catalyzed reaction, the acid coordinates with the unsaturated olefin and

activates the receptor. This coordination increases the reactivity of the acrylate by increasing its

electrophilicity [34-37]. The reaction mechanism and chemical structures of the raw materials are

depicted in Scheme 6.3.
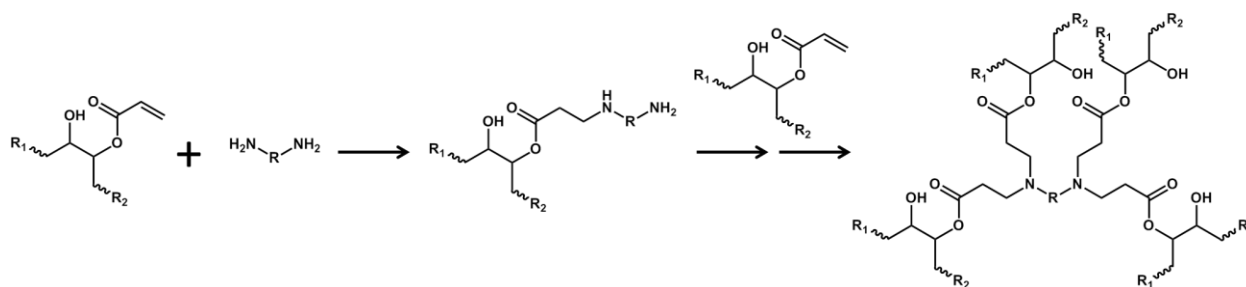
R_1, R_2 = highly functionalized acrylate resin
R = aliphatic, cycloaliphatic and aromatic crosslinker

Scheme 6.3. Reaction between acrylate groups in AESS and amine

As shown in Scheme 6.3, primary amines can react with two equivalents of acrylate to form

tertiary amines. The reaction of amine hydrogen with the acrylate functionality tends to follow second

order kinetics based on the concentration. Yet, the addition of acrylate to the formed secondary amine

may affect the overall reaction kinetics as the reaction proceeds. The reactivity of 1° amine vs. 2° amine

is highly dependent on the electronic and steric environment of the amine [38]. Generally, 2° amines are

more nucleophilic than 1° amines and are therefore more reactive, yet the steric hindrance of the

surrounding environment often causes the slow addition of 2° amines. In the case of linear aliphatic

amines having low steric hindrance on the 2° amine such as n-methylenediamine, the reactivity sequence

of multi-functional amines was observed to be 2° amines (original) > 1° amine >> 2° amines (formed).

Yet, for linear aliphatic amines having high steric hindrance on the 2° amine such as n-

hexylethylenediamine, the reactivity sequence changed to 1° amine > 2° amine (original) > 2° amine

(formed). For a similar reason, the addition to the 2° amine (formed) tends to be significantly slower due

to high steric hindrance of the polymer backbone [38].

6.4.2. Solvent selection

Before going into more detail into the Michael reaction between AESS resin and amine croslinker, it is important to mention that AESS resin has an extremely high viscosity (1.30×10^6 mPa.s due to the high number of hydroxyl groups in the resin. Thus, in order to be easily applied as coatings, the resin viscosity must be reduced by the addition solvent and/or diluents. The solvent or diluent should be compatible with the formulation components. Furthermore, if using solvent, the solvent should evaporate at an appropriate rate during the curing process. If diluents are used, the addition of diluents should not affect the mechanical properties dramatically. The range of the viscosity for easy application was targeted to be below 1000 mPa.s.

Several solvents were screened to determine their suitability in reducing the viscosity of the AESS resin as well as their influence on coatings properties. Solvents were added at 40% wt. of AESS to produce 75% solids coatings formulations. The solvents evaluated included methyl ethyl ketone (MEK), methyl iso-butyl ketone (MIBK), tert-butyl acetate (TBA), ethyl-3-ethoxypropionate (EEP), hexane (HEX) and cyclohexanone (CHX). These solvents were selected based on the following criteria: polarity, boiling point, and regulatory issues (i.e., VOC exempt). In this experiment, 4'4'-methylene bis(cyclohexylamine) (PACM) was used as the crosslinker. Coatings formulations were prepared with acrylate to primary amine equivalent ratio of 1.5:1, and pTSA catalyst at 5% by mole of 1° amine. To form coatings, the formulations were applied on cleaned and degreased Bonderite steel panels using a drawdown film applicator at 6 mils wet film thickness. The coatings were cured in the oven at 80 °C for 45 minutes. Coatings characterization was performed one week after being cured.

Table 6.1. Effect of solvent on coatings made using AESS cured with PACM.

Solvent	AESS + Solvent Properties		Coatings Properties		
	Soluble	Viscosity (mPa.s)	Appearance	König Hardness (s)	MEK double rubs
MEK	Yes	770	Trapped bubbles (small size)	75	200
MIBK	Yes	660	Trapped bubbles (small size)	48	325
CHX	Yes	2940	Defects throughout	20	75
TBA	Yes	1260	Trapped bubbles (bigger size)	50	325
EEP	Yes	790	Minimal amount of bubbles	109	>400
HEX	No	-	-	-	-

The addition of solvent decreases the viscosity of the resin due to a decrease in the polymer-polymer interaction forces, dominated by the hydrogen bonding, which was overcome by the polymer-solvent interactions. As expected, AESS was not soluble in non-polar solvents such as hexane; and thus the AESS-HEX coatings formulation was not prepared. AESS is miscible fairly well in ketone- and ester-based solvents. The amount of decrease in the viscosity depends on the polarity of the solvent. With the ketone-based solvent, due to similar structures of MEK and MIBK, the decrease in the viscosity is similar. The symmetrical chemical structure of the CHX causes the molecule to be less polar than MEK and MIBK, and thus the viscosity of the AESS-CHX system is higher. Then, comparing TBA and EEP solvents, EEP is more polar than TBA due to its ethoxy group and thus the decrease in the viscosity was observed to be higher. Even though the viscosity of AESS-CHX and AESS-TBA was out of the target range, coatings formulations were still prepared.

Initially, it was thought that the addition of PACM to the formulation would reduce the viscosity further since its viscosity is fairly low (80 mPa.s @25 °C). However, after the addition of amine and catalyst, the viscosity increases immediately to the range of 2000+ mPa.s for MIBK and EEP. This increase in the viscosity thus did not allow air bubbles introduced in the mixing process to escape quickly enough during application, and thus resulted in trapped bubbles in the cured coatings. The size of the bubbles in the cured coatings is affected by the boiling point and the solubility of the solvent. For the TBA system, the size of the bubbles was observed to be the largest compared to the other systems. It is thought that the solvent was not quite miscible in the AESS-PACM mixture, and thus tended to result in larger trapped bubbles in the cured coatings.

As seen in Table 6.1, the coatings properties based on AESS-PACM with different solvents are fairly good with the exception of the CHX system. The CHX-containing coating is fairly soft and not well crosslinked as indicated by MEK double rubs. Furthermore, this coating formulation had a longer pot-life than the other systems. Typically, the formulations would gel in the vial an hour after mixing, yet the CHX system did not. It is known that ketones may react with primary amines to form imine and water, and this reaction is reversible. Since CHX has a comparatively higher boiling point compared to MEK and MIBK, it does not evaporate as quickly and is expected to bind more with amine as an imine. Thus, there are less amine functionalities available to react with AESS, resulting in poor MEK double rubs for the coating.

Overall, the most optimum coatings were obtained with EEP with excellent pendulum hardness and MEK double rubs. The slow evaporation rate of EEP balances the quick reactivity of the AESS-amine reaction, resulting in a minimal amount of bubbles trapped in the cured coatings. Based on these observations, EEP was chosen to be the solvent for further exploration.

6.4.3. Effect of stiochiometry

As shown in the previous section, initial thermoset coatings made from AESS-PACM were successfully prepared and the excellent MEK double rubs data is an indication that the coatings are cured and have good solvent resistance. To confirm that the reaction did occur at the molecular level, FTIR spectroscopy analysis of the coatings formulations and cured coatings was carried out. Furthermore, it is necessary to study the impact of the molar ratio of acrylate to 1° amine on the properties of the materials. In this part of the study, AESS was crosslinked with PACM and the reaction was catalyzed using pTSA catalyst. Mixing and curing processes are conducted following previously described procedures.

6.4.3.1. Functional group conversion

Figure 6.2 shows the FTIR spectra of 2 different coating systems before and after curing: AESS-PACM with a range of acrylate to 1° amine ratios and AESS with pTSA catalyst without any PACM. It can be observed in the spectra that there is a decrease in the acrylate group concentration shown by a decrease in the intensity of the C=C bond at 1637 cm-1 (C=C stretching for HC=CH2), 1406 cm-1 (C=C scissoring for HC=CH2), and 810 cm-1 (C=C out of plane deformation). By calculating the change in the peak area of those C=C peaks before and after curing, the acrylate group conversion can be estimated. It is important to note that peak deconvolution was performed to obtain a more accurate determination of the peak area. For liquid coatings formulation, peak fitting was carried out using Voight calculation, while a Gaussian peak fit calculation was used for the solid cured coatings. The results of the calculations are shown in Table 6.2.

As seen in Table 6.2, the acrylate conversion decreases as the acrylate-to-1°amine molar ratio is increased, and the pattern can be observed with every C=C peak. The conversion ranges from 90% to 40%, which seems to be fairly low for a thermoset system. However, it is important to note also that even though complete conversion was not achieved after curing at 80 °C for 45 minutes, the coated surfaces were tack-free.
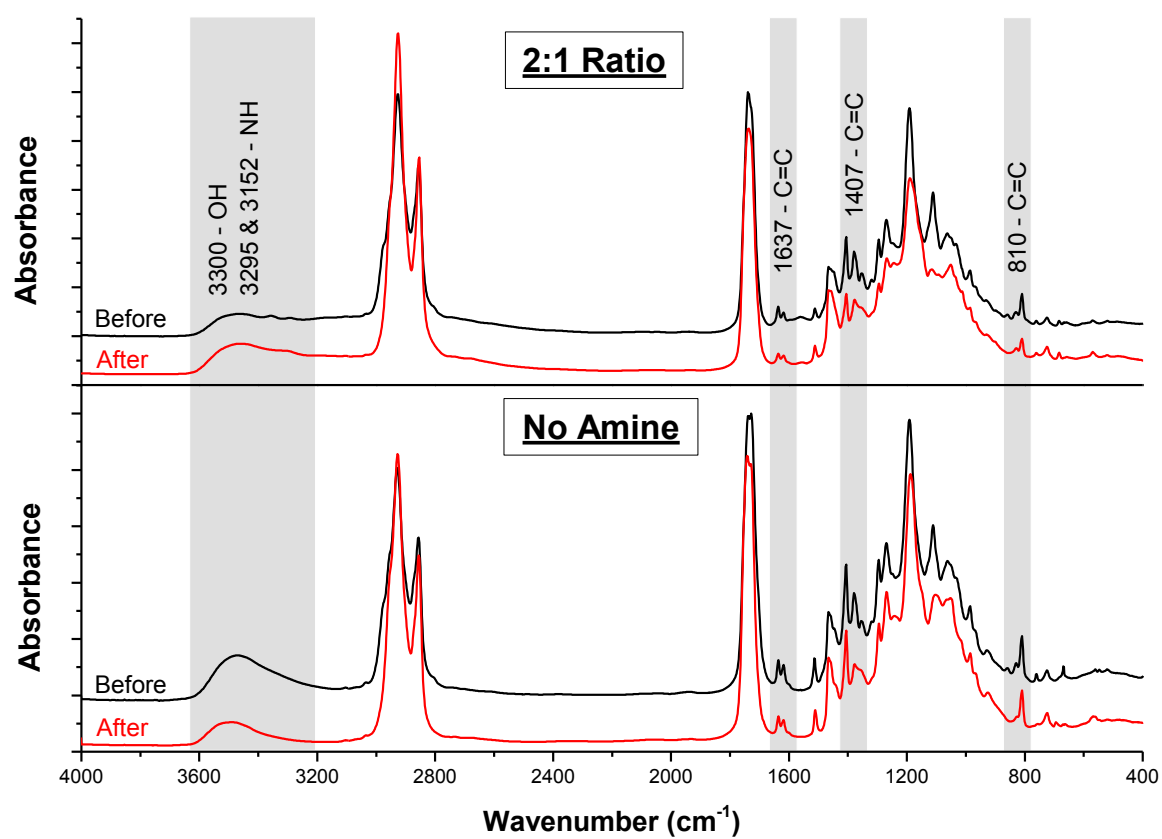
Figure 6.2. FTIR spectroscopy of coatings with 2:1 molar ratio of acrylate to 1° amine (using PACM amine) and coatings with no PACM amine (AESS+pTSA catalyst)

Table 6.2. Acrylate conversion by FTIR spectroscopy with different equivalent ratios

Acrylate-to- 1° Amine	Decrease in the peak area (%)		
	1637 cm^{-1}	1406 cm^{-1}	810 cm^{-1}
1 : 1	86.4	96.6	93.0
1.5 : 1	67.5	87.0	82.3
2 : 1	53.6	71.5	69.3
3 : 1	63.8	50.2	44.5
No Amine	32.1	50.1	17.6

Coatings were prepared using PACM

While preparing the formulations, it was found that the mixture of AESS and pTSA catalyst, without the presence of PACM amine, gelled in the container 6 hours after it was mixed. This unexpected observation suggests that the hydroxyl groups in the AESS resin might be able to react with the acrylate groups. To verify this hypothesis, AESS resin was mixed with pTSA catalyst (2.45%wt.) and then cured in the oven at 80 °C for 45 minutes. Then, the same FTIR analysis was conducted. As shown in Figure 6.2 and Table 6.2, characterization by FTIR spectroscopy further showed that the hydroxyl and acrylate

groups decreased after curing at 80 °C for 45 minutes. Furthermore, the coating film from the AESS-pTSA system was found to have 100 MEK double rubs, which shows that the coating was fairly crosslinked. The crosslinking between acrylate and 2° hydroxyl in the AESS resin may signify two possible scenarios. First, without the presence of amine or other crosslinker, the AESS resin may react with itself to form a polymer network as shown in Scheme 6.4. Then, in the presence of amine or other crosslinker, this reaction becomes a side reaction. Looking back at Figure 6.2, it can be observed that there were no changes in the area of the OH peak at 3300 cm^{-1}, which indicates that the amount of this side reaction maybe very minimal.
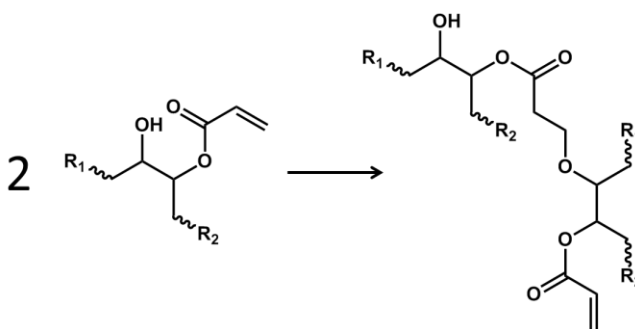
Scheme 6.4. Possible reaction of AESS self-crosslinking

6.4.3.2. Gel time and dry time

In the previous experiment, AESS-PACM coatings formulations were cured at an elevated temperature to accelerate the curing reaction. However, these systems have sufficient reactivity to be cured at ambient temperature, and it will be shown later that the properties of the oven-cured and room temperature-cured coatings do not differ significantly. In this section, the gel time and dry time of the AESS-PACM coatings at ambient temperature (~23 °C) were studied as a function of the acrylate to 1° amine molar ratio and the results are shown in Figure 6.3 and Table 6.3.

The gel time of the coatings was determined using a rheometer at 23 °C. At the gel point, the molecular network is undergoing a transition from liquid to solid, and thus the storage modulus value (G') is equal to the loss modulus value (G") and the viscosity (η) increases dramatically. As seen in Figure 6.3 and Table 6.3, the gel time increased as the acrylate to 1° amine molar ratio was increased. The results from G'=G" value and η agree with each other as they follow the same pattern, and the gel time values are in the same range. It is interesting to observe that despite the fact that the gel times of the four

formulations were different, the G' or G" values at the gel point are approximately the same at 2.32 kPa. Then, as expected, the viscosities of the formulations at 90 minutes are very different; they increased as the molar ratio was increased.
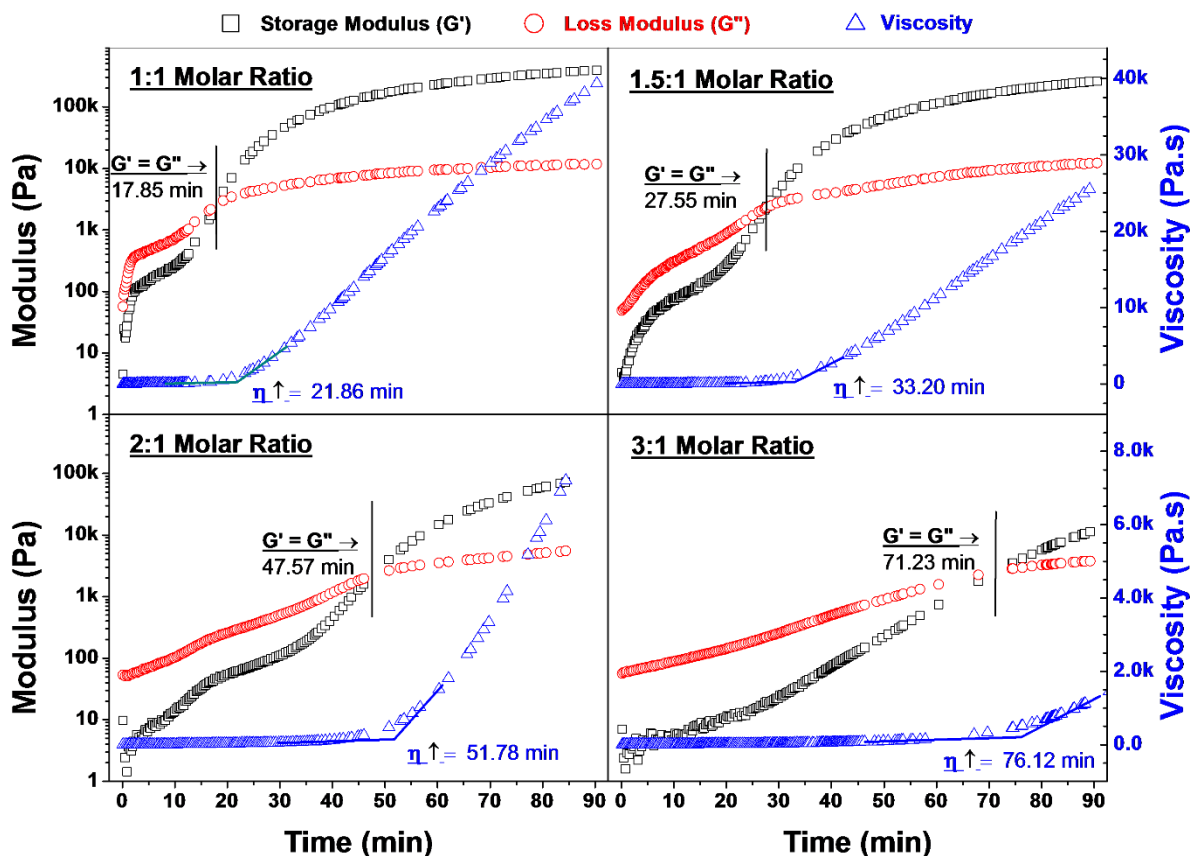
Figure 6.3. Rheological properties of AESS-PACM with different acrylate to 1° amine molar ratios

Table 6.3. Gel time and dry time of thermoset coatings with different equivalent ratios

Acrylate-to-1° Amine	Gel Time (min)		Dry Time (hour:min)			
	G' = G"	η increase	Set-to-touch	Tack free	Dry-hard	Dry-through
1 : 1	17.85	21.86	0:20	0:30	5:30	>12:00
1.5 : 1	27.55	33.20	0:35	0:50	2:00	5:25
2 : 1	47.57	51.78	1:05	1:25	2:45	5:50
3 : 1	71.23	76.12	1:30	1:45	3:45	6:10

Coatings formulations were prepared using PACM

The dry times of the coatings formulations of AESS-PACM with different molar ratio were also determined using a BK drying time recorder, where a stylus was moved across a 12" glass strip which was applied with liquid formulation at a rate of 1"/hour. The recorded drying behavior values listed in Table 6.3 are an average of 6 different measurements. As observed with the gel time values, increasing

the molar ratio resulted in slower drying times up to the tack free time. Yet, surprisingly, the dry-hard and dry-through times of the 1:1 coatings system were much slower compared to the other coatings system, which implies that the molecular network was built up at a slower rate after a certain point. Furthermore, after 12 hours, the 1:1 coatings are still soft and can be easily scratched. Overall, this observation indicates that fast tack-free time or gel time does not necessarily imply a fast dry-through time.

6.4.4. Coatings properties

In order to further understand the impact of the acrylate-to-amine molar ratio on the AESS-PACM coatings, it is important to conduct thermal and mechanical coatings characterization. Thermal characterization was conducted using differential scanning calorimetry (DSC) to obtain the glass transition temperature, T_g and residual heat of polymerization. Dynamic mechanical analysis (DMA) was used to obtain the T_g and storage modulus values. Mechanical coatings characterization includes determinations of hardness, solvent resistance, adhesion, and flexibility. These characterizations were determined 7 days after application process to ensure a high level of conversion, and the results are shown in Figure 6.4 and Tables 6.4 and 6.5.

First, in the DSC curves in Figure 6.4, the T_g of the coatings obtained from the first heating cycle is lower than that obtained in second heating cycle. However, a small exothermic peak in the first heating cycle was observed, indicating the occurrence of some additional curing. It is predicted that during the first heating cycle, polymer network rearrangement and further curing occur simultaneously, thus causing the increase in the observed T_g in the second heating cycle. The T_g by DMA was determined at the temperature where tan delta maximum occurred. The obtained T_g value from both DSC and DMA show a similar pattern. The T_g value of coatings with acrylate to 1° amine molar ratio of 1:1 and 1.5:1 are fairly similar. Increasing the molar ratio results in a decrease in the T_g value. The storage modulus values at 25 °C values decrease as the acrylate to 1° amine was increased, which indicates that the coatings became softer and more flexible. The storage modulus value in the rubbery region at T_g+60°C is often used to indicate the crosslink density of the coatings. The highest modulus was obtained for coatings with acrylate to 1° amine molar ratio of 1.5:1.

Coatings mechanical properties in Table 6.5 show that there is no significant difference in the hardness and T_g of the coatings with 1:1 and 1.5:1 molar ratio, similar to what was observed with the T_g

values. Yet, surprisingly, the chemical resistance of the 1:1 molar ratio system is lower compared to 1.5:1. This observation was predicted due to the the cracking defects that appeared in the 1:1 system, which was caused by fast gelation at the surface. Furthermore, this cracking appearance caused the coatings to have lower specular gloss. Increasing the molar ratio resulted in softer coatings, which agrees to what was observed with the findings in thermal analysis.

To summarize, the system with 1.5:1 molar ratio showed good properties compare to other molar ratios with fairly high conversion, good gel time thus workable condition, excellent hardness, flexibility and chemical resistance. Thus, this formulation was chosen as a control system for further study involving variation in the diluents, amine crosslinker, acrylate resin, and curing process.
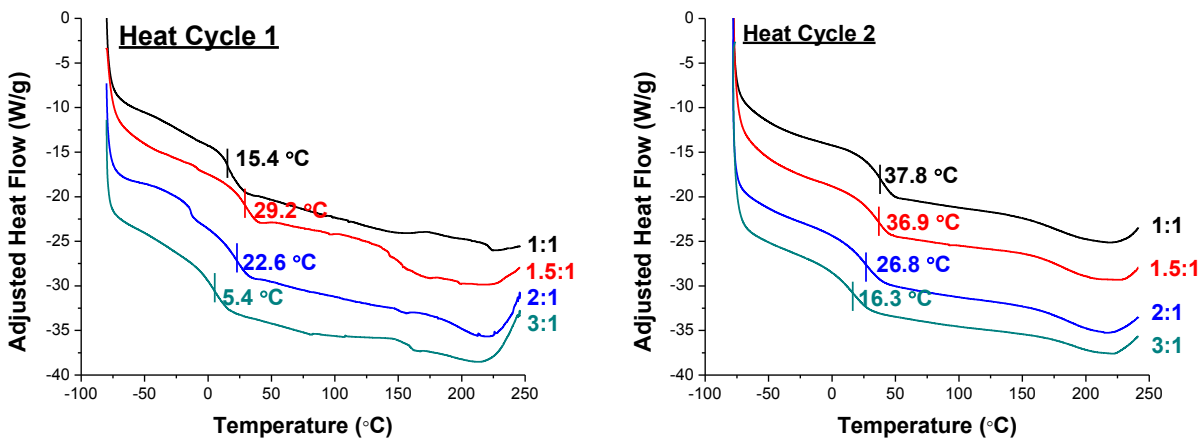
Figure 6.4. The DSC first and second heating cycle of coatings with different acrylate to 1° amine ratios

Table 6.4. Thermal properties of the coatings

System	No.	Sample	DSC analysis		DMA analysis		
			T_g Cycle 1 (°C)	T_g Cycle 2 (°C)	T_g by tan δ (°C)	E' @ 25°C (MPa)	E' @ T_g+60°C (MPa)
Acrylate-to-Amine Ratio*	1	1:1	15.4	37.8	45.8	1037	5.87
	2†	1.5:1	29.2	36.9	43.4	714	6.28
	3	2:1	22.6	26.8	35.9	304	4.62
	4	3:1	5.4	16.3	28.5	92	4.35
HDDA Amount*	2†	0%	29.2	36.9	43.4	714	6.28
	5	25%	26.6	26.7	33.1	298	4.40
	6	50%	15.3	15.3	19.1	21	4.54
	7	75%	-0.8	2.4	16.0	13	6.31
Amine X-linker	2†	PACM	29.2	36.9	43.4	714	6.28
	8‡	DETA	21.4	28.4	39.9	489	15.74
	9	MXDA	20.8	20.6	38.2	516	11.78
Acrylate Resin*	2*	AESS	29.2	36.9	43.4	714	6.28
	10	AESO	-2.7	1.1	13.8	8	2.94
Cure Process*	2*	Forced	29.2	36.9	43.4	714	6.28
	11	RT	39.3	36.6	38.6	581	8.65

*Coatings were formulated using PACM crosslinker and pTSA catalyst
†Formulation used as control: using PACM crosslinker (1.5:1 molar ratio)
‡No catalyst was added

Table 6.5. Mechanical coatings properties

System	No.	Sample	DFT μm	König (sec)	Pencil Hardness Gouge	Pencil Hardness Scratch	MEK Double Rubs	Reverse Impact (inch/lb)	Adhesion	Mandrel Bend	Gloss 20°	Gloss 60°	Gloss 85°	Gel Fraction (%)
Acrylate-to-Amine Ratio	1	1:1	64±17	108	6H	3B	250	100	2B	>28%	85	123	81	93.6
	2†	1.5:1	62±14	105	9H	B	>400	80	2B	>28%	109	132	100	91.6
	3	2:1	57±9	52	7H	2B	275	100	3B	>28%	120	135	100	92.9
	4	3:1	58±11	21	7H	4B	100	80	3B	>28%	116	128	101	92.5
HDDA Amount	2†	0%	62±14	105	9H	B	>400	80	2B	>28%	109	132	100	91.6
	5	25%	53±8	59	8H	2B	175	40	0B	28%	88	113	97	92.2
	6	50%	44±11	20	3H	4B	50	80	3B	>28%	107	139	98	93.7
	7	75%	48±10	14	2H	4H	100	100	4B	>28%	77	133	85	95.3
Amine X-linker	2†	PACM	62±14	105	9H	B	>400	80	2B	>28%	109	132	100	91.6
	8‡	DETA	52±5	56	5H	HB	225	100	2B	28%	64	109	77	98.0
	9	MXDA	50±4	82	9H	B	>400	120	4B	>28%	88	117	86	94.1
Acrylate Resin	2*	AESS	62±14	105	9H	B	>400	80	2B	>28%	109	132	100	91.6
	10	AESO	43±8	12	B	8B	75	100	4B	>28%	143	149	97	93.2
Cure Process	2*	Forced	62±14	105	9H	B	>400	80	2B	>28%	109	132	100	91.6
	11	RT	57±10	107	8H	F	>400	60	0B	>28%	88	113	97	90.4

*Coatings were formulated using PACM crosslinker and pTSA catalyst
†Formulation used as control: using PACM crosslinker (1.5:1 molar ratio)
‡No catalyst was added

6.4.5.   Structure-property relationships

Further studies were then carried out to explore the properties of coatings made using reactive diluents and different amines. Then, the obtained properties were compared with a system derived from a similar, but much lower functionality, bio-based acrylate resin, acrylated epoxidized sucrose soyate (AESO). It is important to note that all of the coatings were cured at 80 °C for 45 minutes to accelerate the experimental time. Therefore, it is also necessary to compare the properties of oven-cured coatings with ambient-cured coatings. The complete thermal and mechanical coatings properties are listed in Tables 6.4 and 6.5. Overall, all of the coatings were observed to have good flexibility with >28% elongation and highly crosslinked with >90% gel fraction.

One method to adjust the viscosity of the formulations is by blending the AESS resin with a reactive diluent such as 1,6-hexanediol diacrylate (HDDA). Therefore, a series of AESS-HDDA blends was prepared and coatings formulations were made. Adding low molecular weight difunctional acrylate into the formulation may cause plasticization as observed in the lower hardness and T_g of the thermoset networks. Furthermore, looking at the DMA results, the storage modulus values at temperatures well above T_g for systems with 75% of HDDA and without HDDA are fairly similar. This observation indicates that the approximate crosslink density of the network system is fairly similar, and thus the properties of the networks are largely dependent on the backbone of the network rather than on the crosslink density.

Variation in the amine crosslinker composition results in different coatings properties. First, it is important to mention that catalyst was not added to the formulation with diethylene triamine (DETA). It was found that if catalyst was added to the formulation, the system gelled within a few minutes of mixing and thus making the application process difficult. This rapid gelation was predicted due to the presence of the 2° amine. Recall in the previous section, unhindered 2° amine is more reactive than a 1° amine. The order of reaction rate was predicted to be 1° amine > 2° amine > 2° amine (formed). Since gelation was obtained very quickly, it is expected that high conversion of functional groups might be limited as the network is locked in place, and thus inferior MEK double rubs were observed. However, surprisingly, the storage modulus values of the DETA system at a temperature well above T_g is comparatively higher than PACM system.

Comparing coatings derived from AESS and AESO, it can be clearly seen that the AESO-based coating is significantly softer and has a lower T_g despite a similar acrylate equivalent weight between AESS and AESO at 310g/mol. However, the key difference between the resins is the much higher number of functional groups per molecule in the AESS. This higher functionality leads to a higher crosslink density resulting in higher T_g and hardness.

Finally, coatings properties for the system cured at ambient temperature are compared with those cured at elevated temperature. It was found that the properties are not significantly different with similar values of hardness, flexibility and T_g.

6.5.   Conclusion

The Michael addition reaction was successfully utilized to produce thermoset coatings derived from AESS and amine crosslinker. FTIR spectroscopy of the coatings before and after curing indicates that the reaction is capable of reaching up to 90+% conversion of acrylate. Furthermore, it is suggested that AESS is able to undergo self-crosslinking polymerization from the reaction of acrylate and hydroxyl groups. Yet, in the presence of amine crosslinker, this reaction might be occurring, but to a minimal extent. A fast gelation time can be reached with a formulation having a 1:1 molar ratio of acrylate to 1° amine, and it can be prolonged by increasing the molar ratio. However, fast gelation times can cause cracking and incomplete reaction and thus lead to inferior chemical resistance. The thermal and mechanical coatings properties with different amounts of diluents and different amine crosslinkers were also evaluated. The addition of diluents into the system resulted in coatings that are softer, while the presence of 2° amine in the DETA causing the system to gel very fast and thus did not require the addition of catalyst. In sum, this preliminary study has shown that the aza-Michael reaction of a highly functional acrylated resin can be used as a viable coating binder system that cures rapidly at ambient conditions and can yield coatings having good solvent resistance, as well as good hardness and flexibility.

6.6.   Acknowledgements

6.7. References

[1]   Noomen, Applications of Michael addition chemistry in coatings technology, Progress in Organic Coatings, 32 (1997) 137-142.

[2]   F.D. Rector, W.W. Blount, D.R. Leonard, Applications for Acetoacetyl Chemistry in Thermoset Coatings, Journal of Coatings Technology, 61 (1989) 31-37.

[3]   B.D. Mather, K.M. Miller, T.E. Long, Novel Michael Addition Networks Containing Poly(propylene glycol) Telechelic Oligomers, Macromolecular Chemistry and Physics, 207 (2006) 1324-1333.

[4]   P. Ferruti, M.A. Marchisio, R. Duncan, Poly(amido-amine)s: Biomedical Applications, Macromolecular Rapid Communications, 23 (2002) 332-355.

[5]   D.A. Tomalia, A.M. Naylor, W.A. Goddard, Starburst Dendrimers: Molecular-Level Control of Size, Shape, Surface Chemistry, Topology, and Flexibility from Atoms to Macroscopic Matter, Angewandte Chemie International Edition in English, 29 (1990) 138-175.

[6]   A. Bielinska, J.F. Kukowska-Latallo, J. Johnson, D.A. Tomalia, J.R. Baker, Regulation of in vitro Gene Expression Using Antisense Oligonucleotides or Antisense Expression Plasmids Transfected Using Starburst PAMAM Dendrimers, Nucleic Acids Research, 24 (1996) 2176-2182.

[7]   D.A. Tomalia, H. Baker, J. Dewald, M. Hall, G. Kallos, S. Martin, J. Roeck, J. Ryder, P. Smith, Dendritic macromolecules: synthesis of starburst dendrimers, Macromolecules, 19 (1986) 2466-2468.

[8]   N. Moszner, V. Rheinberger, Reaction behaviour of monomeric β-ketoesters, 4. Polymer network formation by Michael reaction of multifunctional acetoacetates with multifunctional acrylates, Macromolecular Rapid Communications, 16 (1995) 135-138.

[9]   J.E. Klee, F. Neidhart, H.-J. Flammersheim, R. Mülhaupt, Monomers for low shrinking composites, 2. Synthesis of branched methacrylates and their application in dental composites, Macromolecular Chemistry and Physics, 200 (1999) 517-523.

[10]   L.G. Dammann, M.L. Gould, Liquid uncrosslinked Michael addition oligomers prepared in the presence of a catalyst having both an epoxy moiety and a quaternary salt in, Ashland Inc, United States, 2004.

[11]   R. Roy, C.A. Laferriere, Michael addition as the key step in the syntheses of sialyloligosaccharide-protein conjugates from N-acryloylated glycopyranosylamines, Journal of the Chemical Society, Chemical Communications, (1990) 1709-1711.

[12]   B.D. Mather, K. Viswanathan, K.M. Miller, T.E. Long, Michael addition reactions in macromolecular design for emerging technologies, Progress in Polymer Science, 31 (2006) 487.

[13]   R.J. Clemens, F.D. Rector, A comparison of catalysts for crosslinking acetoacetylated resins via the Michael reaction, Journal of Coatings Technology, 61 (1989) 83-91.

[14]   C.L. Bickel, The Addition of Malonic Esters to an Acetylenic Ketone, Journal of the American Chemical Society, 72 (1950) 1022-1023.

[15]   R. Connor, W.R. McClellan, THE MICHAEL CONDENSATION. V*. THE INFLUENCE OF THE EXPERIMENTAL CONDITIONS AND THE STRUCTURE OF THE ACCEPTOR UPON THE CONDENSATION, The Journal of Organic Chemistry, 3 (1939) 570-577.

[16]   J.S. Witzeman, W.D. Nottingham, Transacetoacetylation with tert-butyl acetoacetate: synthetic applications, The Journal of Organic Chemistry, 56 (1991) 1713-1718.

[17]   S.J. Marsh, Acetoacetate chemistry—crosslinking versatility for high-solids coatings resins, in: American Chemical Society Division of Polymer Chemistry, American Chemical Society, 2003, pp. 52-53.

[18]   R.J. Clemens, J.A. Hyatt, Acetoacetylation with 2,2,6-trimethyl-4H-1,3-dioxin-4-one: a convenient alternative to diketene, The Journal of Organic Chemistry, 50 (1985) 2431-2435.

[19]   C.C. Tung, Recent advances in isocyanate free coatings, Surface Coatings Australia, (1999) 10-15.

[20]   R. Brinkhuis, J. Schutyer, F. Thys, E.D. Wolf, T. Buser, J. Kalis, N. Mangnus, F.V. Wijk, Taming the Michael Addition reaction, European Coatings Journal, (2015) 34-40.

[21]   D.C. Webster, P.P. Sengupta, Z. Chen, X. Pan, A. Paramarta, Highly functional epoxidized resins and coatings, in: United States Patent Office, NDSU Research Foundation, US, 2015.

[22]   X. Pan, P. Sengupta, D.C. Webster, High biobased content epoxy-anhydride thermosets from epoxidized sucrose ester of fatty acids, Biomacromolecules, 12 (2011) 2416-2428.

[23] X. Pan, D.C. Webster, Impact of Structure and Functionality of Core Polyol in Highly Functional Biobased Epoxy Resins, Macromolecular Rapid Communications, 32 (2011) 1324-1330.

[24] X. Pan, D.C. Webster, New Biobased High Functionality Polyols and Their Use in Polyurethane Coatings, ChemSusChem, 5 (2012) 419-429.

[25] A. Paramarta, X. Pan, D.C. Webster, Highly functional acrylated biobased resin system for uv-curable coatings, Radtech Report, (2013) 26-32.

[26] T. Nelson, T. Galhenage, D. Webster, Catalyzed crosslinking of highly functional biobased epoxy resins, J Coat Technol Res, 10 (2013) 589-600.

[27] T. Nelson, B. Masaki, Z. Morseth, D. Webster, Highly functional biobased polyols and their use in melamine–formaldehyde coatings, J Coat Technol Res, 10 (2013) 757-767.

[28] T.J. Nelson, L. Bultema, N. Eidenschink, D.C. Webster, Bio-Based High Functionality Polyols and Their Use in 1K Polyurethane Coatings, Journal of Renewable Materials, 1 (2013) 141-153.

[29] C.S. Kovash, E. Pavlacky, S. Selvakumar, M.P. Sibi, D.C. Webster, Thermoset Coatings from Epoxidized Sucrose Soyate and Blocked, Bio-Based Dicarboxylic Acids, ChemSusChem, 7 (2014) 2289-2294.

[30] S. Ma, D.C. Webster, Naturally Occurring Acids as Cross-Linkers To Yield VOC-Free, High-Performance, Fully Bio-Based, Degradable Thermosets, Macromolecules, 48 (2015) 7127-7137.

[31] S. Ma, D.C. Webster, F. Jabeen, Hard and Flexible, Degradable Thermosets from Renewable Bioresources with the Assistance of Water and Ethanol, Macromolecules, 49 (2016) 3780-3788.

[32] A. Paramarta, D.C. Webster, Bio-based high performance epoxy-anhydride thermosets for structural composites: The effect of composition variables, Reactive and Functional Polymers, 105 (2016) 140-149.

[33] X. Pan, P. Sengupta, D.C. Webster, Novel biobased epoxy compounds: epoxidized sucrose esters of fatty acids, Green Chemistry, 13 (2011) 965-975.

[34] T.C. Wabnitz, J.B. Spencer, A General, Brønsted Acid-Catalyzed Hetero-Michael Addition of Nitrogen, Oxygen, and Sulfur Nucleophiles, Organic Letters, 5 (2003) 2141-2144.

[35]   T.C. Wabnitz, J.-Q. Yu, J.B. Spencer, Evidence That Protons Can Be the Active Catalysts in Lewis Acid Mediated Hetero-Michael Addition Reactions, Chemistry – A European Journal, 10 (2004) 484-493.

[36]   T.C. Wabnitz, J.-Q. Yu, J.B. Spencer, A General, Polymer-Supported Acid Catalyzed Hetero-Michael Addition, Synlett, (2003) 1070-1072.

[37]   E. Vedejs, M. Gingras, Aza-Claisen Rearrangements Initiated by Acid-Catalyzed Michael Addition, Journal of the American Chemical Society, 116 (1994) 579-588.

[38]   Wu, Y. Liu, He, Chung, Goh, Effects of Chemistries of Trifunctional Amines on Mechanisms of Michael Addition Polymerizations with Diacrylates, Macromolecules, 37 (2004) 6763-6770.

CHAPTER 7. OVERALL CONCLUSION

The overall objective of this study was to explore the design of high performance thermosets systems derived from highly functionalized epoxidized sucrose ester of soybean oil (ESS). Two crosslinking methods were explored: direct polymerization of epoxy with anhydride moieties and crosslinking of acrylate-derivative of ESS (AESS) resin through the Michael-addition reaction. Anhydride-cured ESS thermoset are intended for structural composite applications, while AESS Michael-addition reaction is intended for coatings applications.

In developing thermoset systems for structural composite applications, it is critical to understand the reaction kinetics and structure-property relationships of the thermosets with variation in the composition variables such as molar ratio of the reagents, type and amount of catalyst, and presence of moisture in the reaction. Overall, the change in the compositional variables resulted in unique reaction kinetics behavior and chemical network, and thus unique mechanical properties. Thermoset samples from this experiment possesses either rubbery or brittle properties, depending on the compositional variations. The tunability of the mechanical properties of these thermoset samples is beneficial in producing composite materials for different applications with a broad range of properties. However, interestingly, despite the long linear chain of fatty acid chains, some of the anhydride-cured ESS thermoset systems possessed quite brittle properties and therefore an improvement in toughness is necessary. Improvement in the toughness properties of the materials was achieved by the addition of flexible crosslinkers and secondary phase rubbery materials. Through this method, the toughness was shown to be increased up-to 5-fold depending on the materials used.

Acrylated epoxidized sucrose soyate (AESS) resin was obtained by reacting the epoxy functionalities with acrylic acids. Thermoset coatings were then prepared by crosslinking the acrylate with amine compounds. Structure-property relationships of the thermoset coatings based on the molar ratio between acrylate to amine, type of amine, and addition of diluents was also explored. Due to the high functionality of the resin and high reactivity of the resin, the coatings can be cured at room temperature, while still providing excellent coatings hardness and chemical resistance. In comparison, a similar coatings system based on epoxidized soybean oil was observed to have lower glass transition

temperature and inferior chemical resistance. This observation shows the potential of AESS as a

coatings binder system that can be cured rapidly at ambient temperature.

CHAPTER 8. FUTURE WORKS

8.1.   Reaction kinetics of anhydride-cured ESS thermosets

The curing kinetics of anhydride-cured ESS was studied using differential scanning calorimetry (DSC). The reaction parameter values (reaction order, activation energy, and pre-exponential factor) were established with variation in the compositional variables (anhydride-to-epoxy molar ratio and catalyst amount). Using these values, it is beneficial to obtain a time-temperature curve to provide a general guideline of curing schedule. Also, this value can then be used in computational polymer molecular modeling software such DryAdd, which is capable of simulating reaction condition and provide an overview of the thermoset networks.

8.2.   Structure-property relationship of anhydride-cured ESS thermosets

The structure-property relationship studied in this work was limited to the variation in the anhydride-to-epoxy molar ratio, catalyst amount, and catalyst type. Further exploration can be made by blending methyl-hexahydrophthalic anhydride (MHHPA) crosslinker with other types of anhydride or acid-functionalized crosslinkers. Another useful study to be conducted may include the study of durability performance of the thermoset using accelerated weathering testing such as QUV, prohesion chamber, moisture uptake, and thermal aging.

8.3.   Impact of catalyst on anhydride-cured ESS thermosets

Many types of base catalysts were explored in the polymerization of ESS with methyl-hexahydropthalic anhydride. The results showed that the type of catalyst used in the reaction affects the curing kinetics and reaction mechanism. It woud be interesting to create a mixture of catalysts and assess the thermoset properties. The results also indicated that there seems to be an optimum concentration or threshold concentration before the effect of moisture in the catalyst becomes detrimental. The presence of water in the system can acts as catalyst and hydrolyzing agent. Therefore, it will be advantageous to understand the role of water in the polymerization process from molecular structure at various degree of conversion.

8.4.   Toughness improvement of anhydride-cured ESS thermosets

The study found that the addition of both a flexibilizing secondary crosslinker and secondary phase rubbery material can improve the toughness of ESS-thermosets. Yet, both methods showed

opposing behavior: the secondary crosslinker resulted in lower improvement in tensile strain and no compromise on the Young's modulus and tensile strength, while secondary phase materials resulted in higher improvement in tensile strain and decrease in the Young's modulus and tensile strengh. Therefore, it would be interesting to combine both methods and explore the materials properties as the blend ratio was varied. The toughening agents that would be recommended for this study are AC39 polyanhydride and HYPRO CTBN X8 rubber. With this blend, it can be expected that toughness can be further improved. Furthermore, other reported studies have shown that the impact of secondary phase rubbery material is larger in ductile environment compared to brittle materials.

8.5. Michael-addition crosslinking coatings

In this dissertation, it was shown that the Michael-addition reaction can indeed be used as one of the crosslinking technoligies of epoxidized sucrose soyate (ESS). This represents a significant potential in broadening the research scope to further explore this crosslinking technology and optimize the thermoset properties. First, it is necessary to further explore the compositional variables in the coatings formulation such as type of crosslinkers and catalyst. Few examples of the crosslinkers include acetoacetate, bis-maleimide, and thiols; while an example of catalyst may include strong amines such as 1,8-diazabicyclo-5.4.0-unde-7-ene (1,8-DBU). Second, further optimization in the formulation pot life without compromising the coatings hardness can be carried out. One method to accomplish this goal can be by blending the AESS resin with methacrylated-epoxidized sucrose soyate (MAESS); MAESS is a methacrylated version of AESS. Since methacrylate groups have lower reactivity than acrylate groups, they will react more slowly and result in longer pot life. Yet, since MAESS has same backbone with AESS, no decrease in the mechanical properties should be expected. Third, it is important to study the weathering performance of this technology since coatings based on acrylic system are often used as a top-coat due to its excellent UV-stability. Fourth, da ual-cure system of AESS resin can be explored. An oligomer can be first prepared by using a Michael addition reaction. Then, this oligomer can be further crosslinked by the use of UV light. Finally, due its fast reaction and no-byproduct, Michael-addition AESS crosslinking can be used not only for coatings application, but also for composite and rigid foams application. For composite applications, exploration of the fiber type, loading and treatment can be

explored. Meanwhile, for rigid foams application, it is necessary to study the impact of compositional

variables such as blowing agent, catalyst, and surfactant on the properties of the foam.